Analysis and Optimization of a New Family of Parallel Manipulators with Decoupled Motions

Sébastien Briot

THESE

Présentée le 20 juin 2007

Devant l'Institut National des Sciences Appliquées de Rennes

En vue de l'obtention du

Doctorat de **GENIE MECANIQUE**

Par : **Sébastien BRIOT**

N° d'ordre : D-07-07

Analyse et Optimisation d'une Nouvelle Famille de Manipulateurs Parallèles aux Mouvements Découplés

Directeur de Thèse : Vigen ARAKELYAN

Membres du jury :

BIDAUD Philippe	Professeur des Universités	Président
GOGU Grigore	Professeur des Universités	Rapporteur
WENGER Philippe	Directeur de Recherche CNRS	Rapporteur
ARAKELYAN Vigen	Professeur des Universités	Examinateur
CHABLAT Damien	Chargé de Recherche CNRS	Examinateur
GLAZUNOV Victor	Professeur à l'Académie des Sciences de Russie	Examinateur
GUEGAN Sylvain	Maître de Conférences	Examinateur

Abstract

It is well known that, amongst the numerous advantages of parallel manipulators when compared with their serial counterparts, one can notice better velocities and dynamic characteristics, as well as higher payload capacities. However, there are some drawbacks, such as a smaller workspace, a high coupling in the kinematic relationships and more constraining singularities. In order to overcome these disadvantages, the decoupling of the movements of parallel robots has been proposed.

Thus, the research project deals with the design, the optimization and the improvement of a new family of parallel manipulators from 3 to 6 degrees of freedom named PAMINSA (**PA**rallel **M**anipulator of the **I.N.S.A.**). The second part of this manuscript presents the characteristics of these architectures, namely the decoupling between the movements of the platform in the horizontal plane from its translations along the vertical axis.

In a third section, we analyse the singular configurations of these manipulators. This analysis is necessary in order to choose the manipulator which has the largest singularity-free workspace.

In sections 4 and 5, we propose novel methods allowing an increase in the size of their singularity-free workspace. The first solution is based on the use of mechanisms with variable structures, i.e. mechanisms of which structural parameters can be altered. Such a solution makes it possible to increase the singularity-free workspace to 100% of the maximal workspace. The second solution deals with the optimization of the dynamic parameters of the manipulators, which makes it possible to pass through the singularities during the displacements of the manipulator.

Finally, in a sixth section, a new, fast and efficient method of computing the accuracy of PAMINSA manipulators is described. In addition, solutions for the improvement of functional characteristics of PAMINSA manipulators are proposed.

Foreword

Before beginning this manuscript, I would like to say a few words for people who have shared time with me and supported me during these past three years.

Firstly, I am very much obliged to my research supervisor, the Prof. Vigen Arakelian, for his tremendous support and his unfailing faith in me. With his comprehensive experience in mechanism and machine theory, he has been a mentor and a great source of ideas. His quiet leadership, a perfect balance between providing direction and encouraging independence, has been a guiding inspiration for me.

I am also grateful to Prof. Victor Glazunov of the Russian Academy of Science. During the three months he passed in Rennes, he helped me understand the screw theory concept. Without this knowledge, I would not have been able to complete some important parts of my thesis. His kindness, patience and our shared affinity for music have left me with wonderful memories.

I would like to thank Dr. Ilian Bonev who supervised me during a three-month visit to his laboratory in Montreal. This stay was very important for me and, through our long discussions, Ilian contributed to my better understanding of certain kinematic concepts. I would also like to thank Prof. Philippe Wenger and Dr. Damien Chablat of the IRCCyN of Nantes for the time they have spent with me and their wise advice during the editing of several articles.

I would like to express my gratitude to Dr. Sylvain Guegan who completed the electronics and the control of the prototype. He also supported me during the experimental validations of my theoretical results, which would never have been completed without his help.

I would like to acknowledge Dr. Eric Courteille for his useful comments and advice during the edition of this dissertation, as well as for his participation in experimental tests.

Special thanks are also due Prof. Jean Le Flecher and to all the members of the C.C.M. (Manufacturing Centre of Mechanics) of I.N.S.A. Without them, and their wonderful and meticulous work, the prototype would never have been so perfectly accomplished.

I would like to thank the English teachers (Mr. Garrett Moran and Mrs. Ann Cochennec) who voluntarily improved the quality of several papers and parts of this dissertation by their judicious advice and comments.

I also wish to express my gratitude to my thesis defence committee and especially to Profs. Grigore Gogu and Philippe Wenger. Their detailed comments and valuable suggestions have contributed to the quality of this manuscript.

I would like to address a particular acknowledgment to my friend Cedric Baradat, who is finishing its Ph. D. thesis at this time. We have spent very good moments together. I hope that he will enjoy his new life in Montpellier and will have more time to devote to his wife Morgane and their baby Leo. I would also like to address special thanks to the other (current or past) Ph. D. students of our research team (Amine, Behnam, Cunsheng, Dominique, Galou, Mathieu and Sarik). Without them, the work atmosphere would not have been so good. Not forgetting my friend Benjamin Fuchs with whom I have had long discussions about our respective job problems and career projects. I wish him good luck for the future.

I address a special thank to Veronique Martin, Simon Lessard and to Dr. Stephane Caro who made my stay in Montreal one of the greatest memories I will have from this past three years.

I would like to thank the secretaries (Alex, Lily and Vero) of the G.M.A. department and the G.C.G.M. laboratory of I.N.S.A. for their efficiency, kindness and for the good times we have spent during coffee breaks. Thank you to the other technical employees and the teaching team.

Last, but not least, I would like to express all my gratitude and my love to my family and to my girlfriend Sylvie. I am not sure this thesis would have been a success if their patience, comprehension and love had not always been there for me. With these few lines, I would like to express to them how much their presence is necessary to my happiness. Thank you very much.

To the woman I love,
To my parents.

Contents

List of Figures

List of Tables

Nomenclature

This nomenclature references the principal variables and abbreviations used in this manuscript. The used conventions are the followings:

- vectors and matrices in bold style;
- axes names in bold italic style;
- scalar variables and names of points in italic style;
- abbreviations of terms in regular style.

$\mathbf{A}$	a matrix characterizing the velocity equation of a mechanical system.
$\mathbf{B}$	a matrix characterizing the velocity equation of a mechanical system.
DOF	degree(s) of freedom.
g	the gravitational acceleration.
i	an integer; $i = 1, 2, 3$.
$\mathbf{I}_{Bj}$	the inertia matrix of the j-th limb of the pantograph linkage.
I_j	the axial moment of inertia of the j-th link of the 5R planar parallel manipulator.
I_{pl}	the axial moment of inertia of the platform about the $\boldsymbol{z}$-axis.
$I_{XX}^{(Bj)}$	the axial moment of inertia about the $\boldsymbol{x}$-axis of the j-th limb of the pantograph linkage.
$I_{YY}^{(Bj)}$	the axial moment of inertia about the $\boldsymbol{y}$-axis of the j-th limb of the pantograph linkage.
$I_{ZZ}^{(Bj)}$	the axial moment of inertia about the $\boldsymbol{z}$-axis of the j-th limb of the pantograph linkage.
j	an integer.
$\mathbf{J}$	the global kinematic Jacobian matrix of a mechanical system.
jDnL	references a PAMINSA manipulator with j degrees of freedom and n legs ($j =$ 3 to 6, $n = 2, 3$).
k	the magnification factor of the pantograph linkage.
L_{Bj}	the length of the j-th limb of the pantograph linkage.

L_j	the length of the j-th link of the 5R planar parallel manipulator.
l_i	a geometric offset for the design of PAMINSA manipulators.
m	an integer; $m = 0, 1, 2, ...$
m_{Bj}	the mass of the j-th limb of the pantograph linkage.
m_j	the mass of the j-th axis of the pantograph linkage or of the j-th link of the 5R planar parallel manipulator.
m_{pl}	the mass of the platform.
n	an integer; $n = 0, 1, 2, ...$
P, $\underline{\text{P}}$	a passive/actuated prismatic joint.
p	an integer.
$\mathbf{q}$	the vector of the active-joints variables.
q_j	the j-th active-joint variable for the planar displacements of the PAMINSA manipulators or for the 5R robot.
q_v	the active-joint variable for the vertical translations of the PAMINSA-4D3L.
q_{vi}	the active-joint variable for the vertical translations of points B_i of pantograph linkages.
R, $\underline{\text{R}}$	a passive/actuated rotoid joint.
R_b	the radius of the circumscribed circle of the base triangle.
$\mathbf{R}_i$	a wrench applied on the platform by the i-th leg.
r_j	the relative position of the centers of masses of the j-th limb of the 5R parallel robot.
R_{pl}	the radius of the circumscribed circle of the platform triangle.
S	a passive spherical joint.
T	the kinetic energy of a mechanical system.
$\mathbf{t}$	a twist.
V	the potential energy of a mechanical system.
$\mathbf{W}$	a wrench.
x	the position of the platform along the $\boldsymbol{x}$-axis of the base frame.
$\boldsymbol{x}$	an axis.
$\mathbf{x}$	the vector of the coordinates of the platform.
y	the position of the platform along the $\boldsymbol{y}$-axis of the base frame.
$\boldsymbol{y}$	an axis.
z	the position of the platform along the $\boldsymbol{z}$-axis of the base frame.
$\boldsymbol{z}$	an axis.
α	an angle.

α_b an angle characterizing the base triangle.

α_{pl} an angle characterizing the platform triangle.

β_b an angle characterizing the base triangle.

β_{pl} an angle characterizing the platform triangle.

δ_{ij} the Kronecker symbol; $\delta_{ij} = 1$ if $j = i$ and $\delta_{ij} = 0$ if $j \neq i$

δ_{pl} an angle; $\delta_{pl} = \beta_{pl}/2 + n\pi$ $(n = 0, 1, 2, \ldots)$.

δx the position error of the platform along the $\boldsymbol{x}$-axis of the base frame.

$\delta \mathbf{x}$ the vector of the errors of the platform.

δy the position error of the platform along the $\boldsymbol{y}$-axis of the base frame.

δz the position error of the platform along the $\boldsymbol{z}$-axis of the base frame.

$\delta \phi_x$ the orientation error of the platform around the $\boldsymbol{x}$-axis of the base frame.

$\delta \phi_y$ the orientation error of the platform around the $\boldsymbol{y}$-axis of the base frame.

$\delta \phi_z$ the orientation error of the platform around the $\boldsymbol{z}$-axis of the base frame.

ΔX the norm of the vector of position error due to active-joints errors.

$\Delta \phi$ the orientation error due to active-joints errors.

ε the error bound on the active-joint variables

ε_i an angle for the kinematic description of the i-th pantograph linkage.

ε_{pl} an angle; $\varepsilon_{pl} = \alpha_{pl} \pm \pi/2$.

ϕ the orientation of the platform around the $\boldsymbol{z}$-axis of the base frame.

γ_i an angle; $\gamma_i = -5\pi/6, -\pi/6, \pi/2$.

$\boldsymbol{\lambda}$ the vector of the Lagrange multipliers.

θ the orientation of the platform around the $\boldsymbol{z}$-axis of the second intermediary moving frame (Euler angles description).

ρ_i the length of the i-th passive prismatic joint of the PAMINSA manipulators.

$\boldsymbol{\tau}$ the vector of the actuators torques/efforts.

ψ the orientation of the platform around the $\boldsymbol{x}$-axis of the first intermediary moving frame (Euler angles description).

ζ_i an angle for the kinematic description of the i-th pantograph linkage.

Introduction

Context of the thesis.

Over the last decades, researchers and companies have been attracted by the idea of creating new parallel manipulators. Such a mechanical architecture divides the manipulated load between the several legs of the system and, as a result, each kinematic chain carries only a fraction of the total load. Thus, it makes it possible the creation of mechanical structures with higher rigidity, containing movable links having relatively small masses. Many industrial applications of these manipulators in the electronics, food and pharmaceutical sectors, or in aeronautics or medical devices are well-known.

However, parallel manipulators have also some drawbacks, such as a limited workspace, more constraining singularity loci or a high coupling of kinematics and dynamics.

This non-linearity of the kinematic and dynamic models of parallel manipulators is not attractive for industrial applications. In order to solve this problem, over the last few years, new structures have been developed. The literature review of previous research on decoupling of the kinematic and dynamic input/output relationships of parallel manipulators shows that, in most of the cases, two approaches are developed (see chapter 1):

- decoupling between position and orientation;
- full-decoupling, i.e. the decoupling of the displacements in relation to all the degrees of freedom of the platform.

Our observations show that, despite rather encouraging results, it is not easy to develop a simple parallel architecture with fully-decoupled motions whilst conserving its principal advantages: a greater rigidity of the structure with light links.

In order to solve this problem, we have tried to find a compromise between the decoupling of the movements and the architectural characteristics of parallel structures. In other words, we have changed the statement of problem: it is not essential that

parallel architecture be fully decoupled, it can also be partially decoupled but it is important to obtain a mechanical architecture with important payload. This problematic has led to the creation of a new family of decoupled parallel manipulators, which is the main topic of this thesis.

Contributions of the thesis.

This manuscript presents several major contributions which are listed below:

- **the creation of a new family of decoupled parallel manipulators:** the non-linearity of the kinematic and dynamic models of parallel manipulators is not attractive for industrial applications. In order to solve this problem, decoupled structures have been proposed. It appears in chapter 1 that, in order to decouple the kinematic and dynamic input/output relationships of parallel manipulators, two approaches are developed in most of the cases: (i) decoupling between position and orientation; (ii) full-decoupling, i.e. the decoupling of the displacements about all the degrees of freedom of the platform. Despite rather encouraging results, the fully-decoupled manipulators have drawbacks also, such as a lack of rigidity or the increase in the number of joints. This is the reason why we have tried to find a compromise between the decoupling of the movements and the architectural characteristics of parallel structures. In chapter 2, a new design approach is proposed and a family of new parallel manipulators, of which displacements in the horizontal plane are decoupled from the other movements, is developed. These manipulators are called PAMINSA (**PA**rallel **M**anipulators of the **I.N.S.A.**);
- **the singularity analysis of PAMINSA manipulators:** one of the most important drawbacks of parallel manipulators is their singular configurations. Therefore, the chapter 3 analyses the singularities of PAMINSA manipulators. It is shown that one particular case of singularity corresponds to an unusual type of self motion. Thus, the geometric conditions for such a type of self motion are derived and the global behaviour of the manipulators inside the gained degree of freedom is kinematically interpreted. The obtained results can be used to design manipulators without self motions, to optimize the singularity-free workspace of this type of robots and to choose the optimal architectures of PAMINSA manipulators;

- **the increase of singularity-free zones by the use of mechanisms of variable structures:** the closed-loop of parallel manipulators limits the motion of the platform and creates special singular zones inside the workspace. The workspace of parallel manipulators, which is less than that of serial manipulators, is reduced and limits their functional performances. Therefore, solutions for enlarging the workspace of parallel manipulators are needed. One possible solution consists of using mechanisms with variable structure, i.e. mechanisms of which structure parameters can be altered. This solution is developed in chapter 4. For this purpose, the pressure angle is used as an indicator of force transmission. The optimal control of the pressure angle for a given trajectory of the manipulator is obtained by means of legs with variable structure. The suggested procedure used to determine the optimal structure of PAMINSA manipulators is performed and illustrated by two numerical simulations. Such a solution can be easily extended to other type of parallel structures, such as Gough-Stewart platforms;
- **the optimal dynamic conditions for passing through the Type 2 singular configurations:** the chapter 5 presents another method, based on the optimization of the dynamic parameters of parallel manipulators, which makes it possible to pass through the Type 2 singular configurations (see chapter 3), and as a result, to enlarge the workspace of parallel mechanisms. The principal contribution of this chapter is the presentation, for the first time, of the general definition of the condition for passing through the singular position which can be formulated as the following: in the presence of Type 2 singular configurations, the platform of a parallel manipulator can pass through the singular positions without perturbation of motion if the wrench applied on the platform by the legs and the external loads is orthogonal to the direction of the uncontrollable motion (in other terms, if the work of applied forces and moments on the platform along the uncontrollable motion is equal to zero). An example of this approach is treated on a PAMINSA manipulator and experimental validations are shown;
- **the proposition of a simple method for the accuracy analysis of PAMINSA manipulators:** simple and fast methods for computing the accuracy of a given robot design are needed in order to use them in design optimization procedures which seek maximum accuracy. Several performance indices have been developed and used to roughly evaluate the accuracy of serial and parallel robots. However, none of them deal with robot accuracy.

Therefore, in chapter 6, a simple method for the accuracy analysis of PAMINSA manipulators is presented. This method is achieved by following a detailed mathematical proof that gives important insight into the accuracy of planar parallel robots. The method is illustrated on two practical designs;

- **the improvement of the performances of PAMINSA manipulators:** in chapter 6, we also propose new compensation schemes, which consist of the introduction into the initial system of complementary units making it possible to cancel the positioning errors. Two different approaches are proposed and the performances of such designs are shown. The reduction of the input torques is also studied. It is shown in simulation and by experimental tests that, for a dynamic mode of operation, the complete static balancing may be ineffective in terms of input torques. In the case of accelerated motions, it is proposed to carry out an optimal redistribution of the movable masses and to achieve a partial mass balancing.

Let us now begin with a short overview of the development of parallel robots.

Chapter 1

Parallel Robots: from the Gwinnett Platform to the Tripteron

This chapter is devoted to the historical evolution of parallel manipulators. First of all, a review of the well-known parallel structures which are applied in industry, patented or prototyped, is presented. The efficiency of such structures is shown and their advantages and drawbacks are discussed.

It is well-known that parallel manipulators have attracted several manufacturers because it was promised, they would have greater rigidity and better dynamic characteristics compared with their serial counterparts. However, despite these very attractive advantages, they also have some drawbacks, as for example, a small workspace, the presence of singular positions and nonlinear coupled kinematics and dynamics. It is obvious that a parallel structure with linear input-output equations is more appealing than a nonlinear one. A literature review shows the principal solutions for motion decoupling of parallel manipulators: (i) decoupling between position and orientation; (ii) full-decoupling, i.e. the decoupling of the displacements around all the degrees of freedom of the platform.

Finally, it is proposed to find a new kind of decoupling, which could be used for the development of new architectures of parallel manipulators with high-load carrying capacity.

1.1. The historical evolution of parallel robots.

In this chapter, we propose to make a short presentation of the expansion of parallel structures. However, please note that we do not want to make an exhaustive list of all the existing parallel machines, but to give some key points in the development of these structures.

1.1.1. At the beginnings.

Mechanisms known as parallel manipulators are defined in the terminology for the mechanism and machine science [IFToMM 2003] as manipulators that control the motion of their end-effector by means of at least two kinematic chains going from the end-effector towards the frame.

There exist numerous texts which deal with the true origins of parallel robots, such as [Bonev 2003a] and [Merlet 2006a]. Accordingly to Dr. Bonev, it seems that, the history of parallel kinematic began in 1928 when James E. Gwinnett thought of building a motion platform for the entertainment industry and applied for a patent which presents a device based on a spherical parallel mechanism [Gwinnett 1931] (Fig. 1.1).

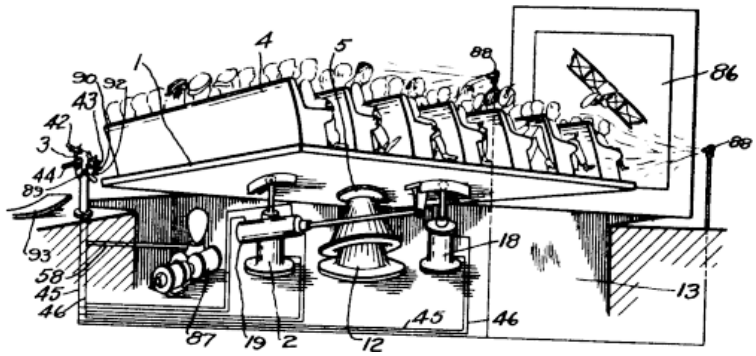

Figure 1.1. – Possibly the first spatial parallel mechanism [Gwinnett 1931].

However, the industrial development of parallel structures really began with the development of the Gough platform [Gough 1962]. Dr. Eric Gough is the person who built the first octahedral hexapod, which is probably the most popular parallel robot

(Fig. 1.2). This parallel mechanism was invented in 1947 to respond to problems of aero-landing loads. A universal machine was needed in order to determine the properties of tires under combined loads.

This robot probably has the simplest structure a parallel manipulator can have. It is composed of six legs. Each leg is made of a jack which is connected to both the base and the platform by spherical joints located at the end of each leg. The actuation is achieved by changing the length of the legs.

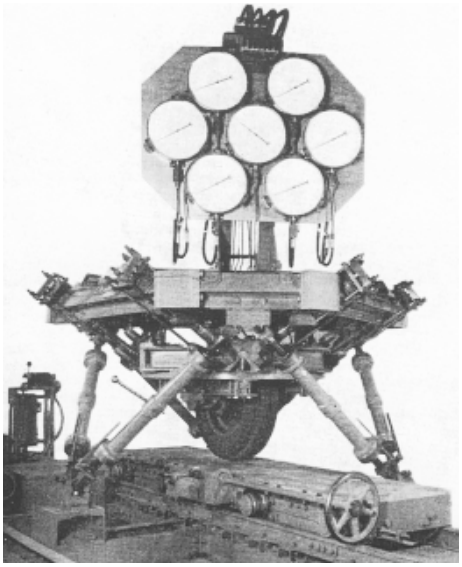

Figure 1.2. – The first octahedral hexapod [Gough 1962].

The idea of using hexapods for aeronautics appeared only twenty years later when Dr. Stewart described a 6-degrees-of-freedom (DOF) manipulator for use as a flight simulator [Stewart 1965] (Fig. 1.3). In the 1960's, the expansion of the aeronautic industry, the increasing costs for the training of pilots and the necessity of testing new aircrafts led to the creation of new mechanical structures able to move a platform with a very high payload (which can carry aircraft cockpits for example). The aim of such systems is to create manipulators with high rotational acceleration capacities. For this purpose, hexapods are well suited because they have a high ratio payload/mass-of-the-structure.

Nowadays, thanks to its attractive characteristics, the industrial applications of the Gough-Stewart platform have been diversified (surgical operations, assembling, etc. – see Fig. 1.4).

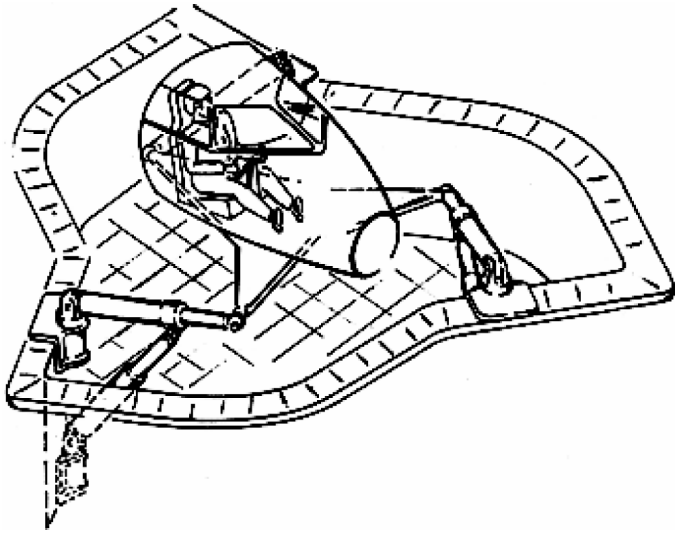

Figure 1.3. – The Stewart platform [Stewart 1965].

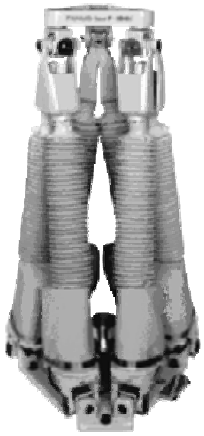

(a) Fanuc F-100 robot for assembling applications.

(b) Motorized manipulator for surgery. [Lazarevic 1997]

Figure 1.4. – Various applications of the Gough-Stewart platform.

The evolution of parallel manipulators continued with the creation of the Delta robot by Prof. Raymond Clavel in 1986 [Clavel 1990]. The creation of this robot resulted from a simple observation.

During a visit to a chocolate factory, Prof. Clavel noticed that the manual conditioning of the chocolates was a monotone and boring activity for the operators. Moreover, there was a lack of hygiene during the manipulation of the products.

However, he also noticed that the existing industrial robots were not well suited to replacing the operators because of their poor dynamic capabilities which would have resulted in to a poor productivity.

Thus, Prof. Clavel suggested a new original device for positioning and orienting an element in space (Fig. 1.5).

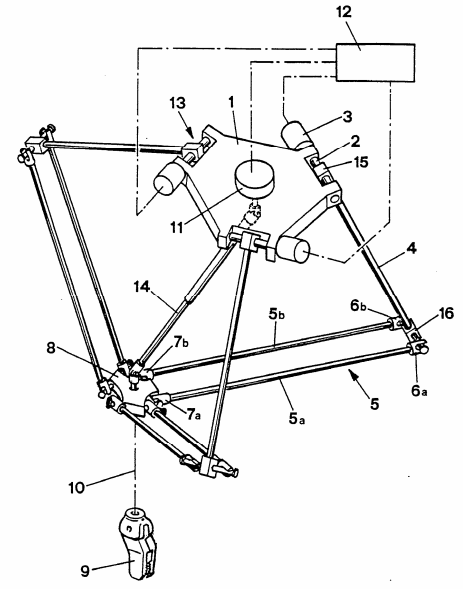

Figure 1.5. – Schematic of the Delta parallel robot from Prof. Clavel's patent [Clavel 1990].

The displacement of the platform (8) of the Delta robot is the result of the movement of the three articulated arms (4) mounted on the base (1), each of which is connected to a pair of parallel rods (5). The three orientations are eliminated by joining the rods in a common termination and the three parallelograms ensure the stability of the platform (8). This configuration of the robot has three degrees of freedom. The platform (8) stays constantly parallel to the base (1) and cannot rotate about the axis perpendicular to this plane. The platform (8) supports a working element (9) the rotation of which is controlled by a fixed actuator (11) situated on the base (1) by means of the slider (14). Thus, taking into account this supplementary rotation, the Delta robot has four degrees of freedom.

It should be noted that the Delta robot was developed for high-speed manipulations (Fig. 1.6.a) and it is well known in the electronics, food and pharmaceutical sectors as a reliable system for the fast execution of light-duty tasks. However, in recent years,

more attention has been paid to the increasing number of possible industrial applications, such as the manipulation of medical devices (Fig. 1.6.b).

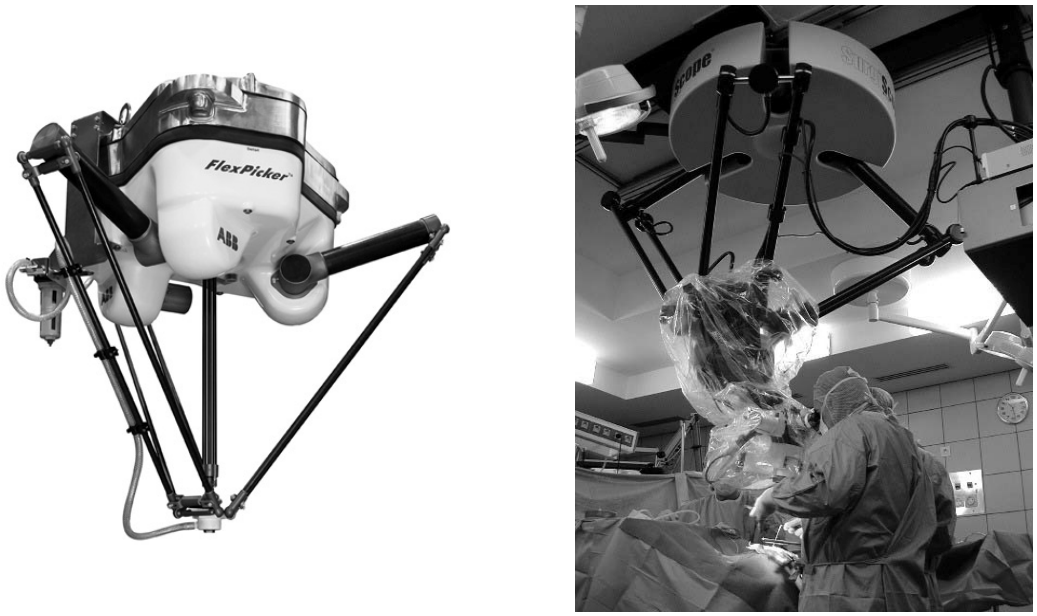

(a) the FlexPicker by ABB. (b) the SurgiScope by ISIS.

Figure 1.6. – Various applications of the Delta robot.

1.1.2. Prototypes and industrial applications of parallel manipulators.

Nowadays, parallel structures are well known and widely developed, mainly for machining applications. While the number of DOF can vary, the actuated systems can be linear or rotary and the number of legs can change, their structures are mostly some declinations of the Gough-Stewart platform and of the Delta robot.

Parallel robots are very attractive for several industrial applications because such mechanical architectures divide the manipulated load between the several legs of the system and, as a result, each kinematic chain carries only a fraction of the total load, which allows the creation of more rigid robots. Such structural architectures also make it possible to reduce the mass of the movable links (all the actuators are mainly fixed on the base and many legs are stressed by traction/compression efforts) and, as a result, make it possible to use less powerful actuators. Moreover, compared with the errors of serial manipulators which are accumulated, it seems the errors of parallel

manipulators are averaged out. Such characteristics promise to create structures with high payload, high dynamic capacities and high accuracy.

These appealing characteristics have attracted the attention of several researchers and companies, and many of them have begun to patent and to build new machines based on parallel structures. Among several examples, we can notice:

- the *Variax* (Fig. 1.7.a): this machine with 6 DOF, commercialized by Giddings and Lewis, is typically based on an hexapod structure. It has got a large workspace (700 mm × 700 mm × 750 mm). However, the performances of this machine are not equivalent wherever in its workspace;
- the *Tricept* (Fig. 1.7.b): Neos Robotics has developed a machine tool with 5 DOF based on a serial wrist with two rotary DOF mounted on a tripod which allows one translation and two rotations. The Tricept is mainly used for welding operations and is one of the most successful parallel machines with more than 200 units sold;
- the *Sprint Z3* (Fig. 1.7.c): this machine tool, developed by DS Technologies, has 3 DOF (two rotations and one translation) and is mounted on a serial structure with two translatory DOF, one of which can translate along 60 m. Its use is foreseen for the aeronautic industry.
- the *double Scara robot* (Fig. 1.7.d): probably one of the most popular structures with 4 DOF (with the FlexPicker). It can place components with a precision of 0.005 mm in a workspace around the size of a DIN A6 sheet of paper (150 mm × 105 mm). Its dynamic properties are very appealing (its cycle period for pick-and-place is inferior to 0.5 s);
- the *FlexPicker* (Fig. 1.6.a): the FlexPicker from ABB, which is an industrial version of the Delta robot with 4 DOF, can produce accelerations and velocities superior to 10 G and 10 m/s respectively (its cycle period is inferior to 0.4 s);
- the *Quattro* (Fig. 1.7.e): based on the Delta robot concept [Nabat 2005], but having four legs instead of three (the rotation of the end-effector is induced by the shearing of the platform), the Quattro from Adept is specifically designed for high-speed packaging and material handling. Its dynamic properties are better than for the previous manipulators (its cycle period is inferior to 0.25 s).
- the *QuickStep* (Fig. 1.7.f): the QuickStep (from Krause & Mauser) has been developed for high speed cutting operations. It is a Delta like robot with 3 DOF which is actuated by means of linear motors mounted in parallel (not in

the same plane). Its workspace is quite significant (630 mm × 630 mm × 500 mm) and it can reach velocities about 200 m/min and accelerations superior to 2 G;

- the *UraneSX* (Fig. 1.7.g): the UraneSX, from Renault Automation, has been designed on the same structure as the QuickStep. It can reach velocities about 150 m/min and accelerations from 3.5 up to 5 G;
- the *XYθ stage NAF 3* (Fig. 1.7.h): it is a planar parallel manipulator with 2 translations and one rotation developed by Seiko. This robot has been designed for positioning operations requiring high rigidity and high accuracy in a small workspace (repeatability: 0.7 μm; workspace: 3 × 3 mm for 3 deg. of orientation).
- the *Orthoglide* (Fig. 1.7.i): this mechanism with 3 translatory DOF was developed at the IRCCyN of Nantes (France) [Chablat 2000] [Chablat 2003]. The use of this robot is foreseen for high-speed machining applications (workspace: 200 mm × 200 mm × 200 mm; velocity of 1.2 m/s and acceleration of 20 m/s^2).
- the *Schoenflies Motion Generator* (SMG – Fig. 1.7.j): the SMG of McGill University (Montreal, Canada) [Angeles 2006] has 3 translatory DOF and one motion of rotation. It is designed for pick-and-place operations. Its cycle period is about 0.5 s.
- the *Isoglide* (Fig. 1.7.k): this mechanism with 4 DOF [Gogu 2007] (3 translations and one rotation) was developed at the LAMI of Clermont-Ferrand (France). This manipulator is decoupled (see section 1.2.2) and can be used in machining applications where great accuracy is necessary.
- the *CaPaMan* (Cassino Parallel Manipulator – Fig. 1.7.l): this family of spatial parallel manipulators with 3 controlled DOF was developed in the LARM of Cassino (Italy) [Ottaviano 2001]. Several prototypes have been completed for different types of applications, such as earthquake simulations.

Surprisingly, despite numerous promises of parallel structures, companies such as Giddings & Lewis and Ingersoll with long-standing expertise in machining have failed with their hexapods even though they were the first to deliver them to the market. Why did have they met such a defeat? Were the promises of high payload capacity, high velocities and high accuracy too ambitious?

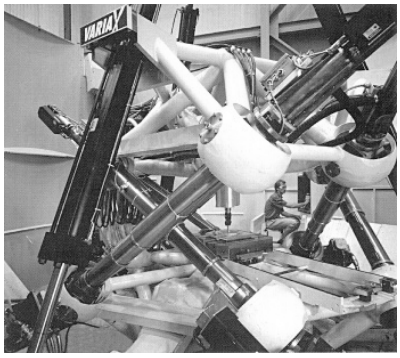

(a) the Variax by Giddings and Lewis.

(b) the Tricept by Neos Robotics.

(c) the Sprint Z3 by DS Technologies.

(d) the Scara robot from Mitsubishi.

(e) the Quattro from Adept.

(g) the QuickStep by Krause & Mauser.

Figure 1.7. – Examples of parallel manipulators.

(g) the UraneSX by Renault Automation.

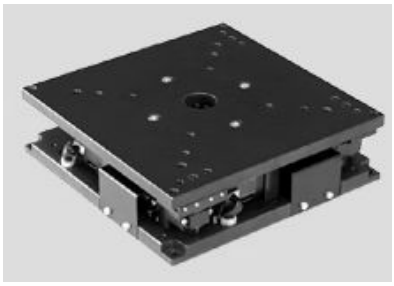

(h) the XYθ stage NAF 3 by Seiko.

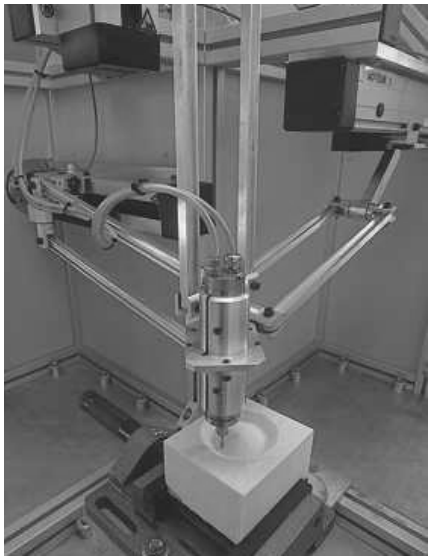

(i) the Orthoglide of the IRCCyN.

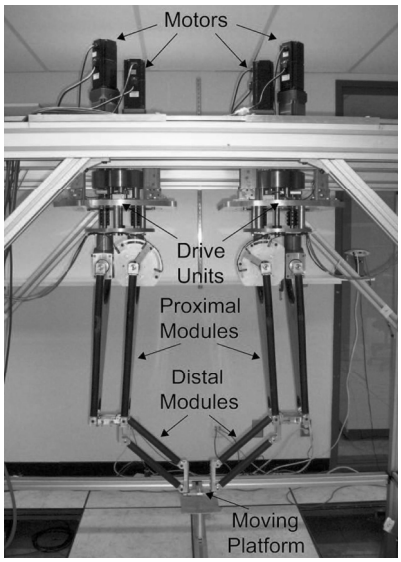

(j) the SMG of McGill University.

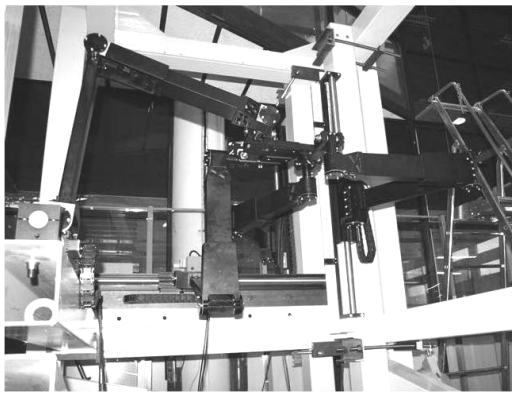

(k) the Isoglide of the LAMI.

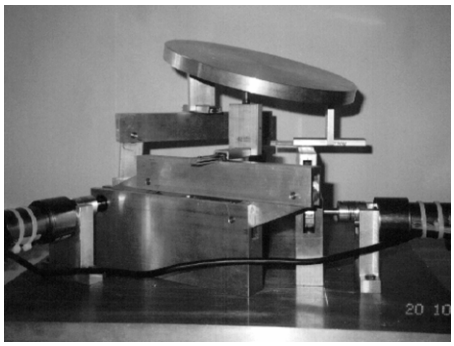

(l) the CaPaMan of the LARM.

Figure 1.7. – Examples of parallel manipulators (continued).

Indeed, the fact that virtually all the hundreds, or even thousands, of motion simulators with load capacities of up to several tons are based on parallel robots (mostly hexapods), compared with serial robots, which are able to carry at most five hundred kilograms, unquestionably demonstrates that the promise of high payload capacities has been fulfilled. The commercial success of the Delta parallel robot and the performance of the recently launched Quattro confirms the fulfillment of the promise of high productivity, though serial robots are not far behind (Scara serial robots can operate at up to 140 cycles per minute and cheaper linear motors make Cartesian robots operate even faster). But the promise of high accuracy has not been fulfilled yet. Among several factors which may lead to the poor accuracy of these mechanisms, we may note:

- the presence of singularities in the workspace, some of them leading to huge positioning errors (the Type 2 singularities – see chapters 3 and 6); such a problem may however be avoided by the use of actuation redundancy (which is a costly solution) or by reducing the size of the workspace (which is already smaller than for their serial counterparts);
- the use of links with lighter masses which leads to a loss of rigidity of the structure; such a problem may be easily avoided by the use of more rigid links;
- manufacturing errors and joint clearances, which can be rectified by calibration and an appropriate design;
- the non-linearity and the complexity of the kinematic and dynamic models of the parallel manipulators which leads to positioning errors. It seems obvious that if the position (or the orientation) of a manipulator depends on fewer input parameters, it will be less sensitive to input errors.

The non-linearity of the static and dynamic models of parallel manipulators is really not attractive for industrial applications and leads to insurmountable problems of accuracy. This is the reason why, over the last few years, new structures of parallel architectures have been developed in order to simplify and linearize the kinematic and dynamic input/output relationships.

1.2. Towards the kinematic decoupling of parallel structures.

In order to improve the accuracy of the parallel structures, researchers have thought of decoupling/simplifying the control laws of such structures. This is an interesting point of view because:

- decoupling the control laws implies decreasing the number of error parameters able to influence the accuracy of a parallel manipulator;
- decoupling makes it possible to improve the dynamic performances of parallel manipulators because there is no need to synchronize the different actuators.

Several approaches of decoupling the control laws have been proposed in the literature. Let us consider these approaches.

1.2.1. From the decoupling between position and orientation...

Designing for decoupled parallel manipulators began when Prof. Clavel developed the 4-DOF Delta robot (Fig. 1.5), of which position is decoupled from its orientation. However, it seems decoupling really started to attract the interest in the 90's. One of the first works on this subject was proposed in [Patarinski 1993].

In this paper, the authors proposed four new manipulators with 6 DOF derived from the Gough-Stewart platforms, in which the laws controlling the position of the end-effector are decoupled from the laws controlling its orientation (Fig. 1.8). For each of them, three legs control the position P of the moving platform while the orientation is controlled by the actuation of the six legs.

In this article, the authors also present the kinematic analysis of such manipulators. It is shown that their Jacobian matrices (which make it possible to obtain the twist of the platform as a function of the velocities of the articulated joints) have a block triangular structure, which simplifies the kinematic control laws.

The principal drawback of such structures is the necessity of using a triple spherical joint at point P. The use of such a triple spherical joint complicates the design and can create serious technological problems. However, such design conditions are improved in the works [Di Gregorio 2001] and [Legnani 2005].

In 1995, Prof. Min Ki Lee presented a new decoupled structure [Lee 1995] that he named the *double parallel manipulator* (Fig. 1.9).

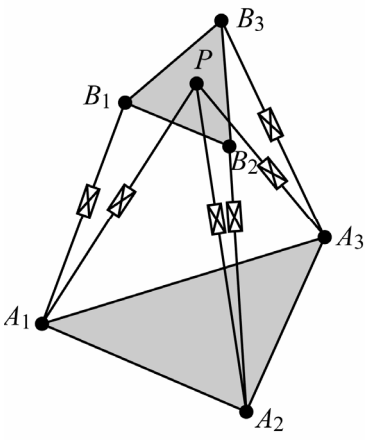

(a) basic structure.

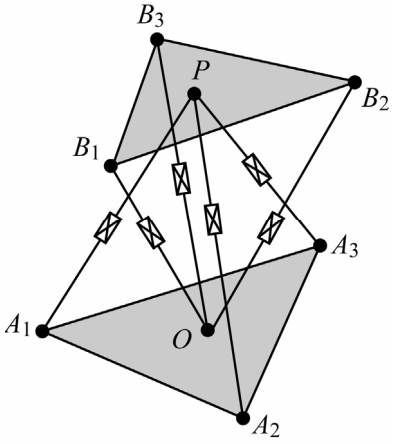

(b) double tetrahedron.

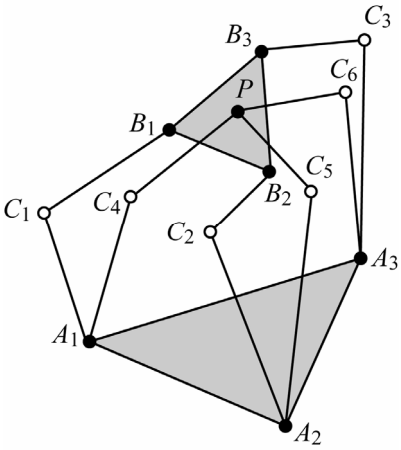

(c) decoupled parallel manipulator with R[1] joints (at C_j, $j = 1$ to 6).

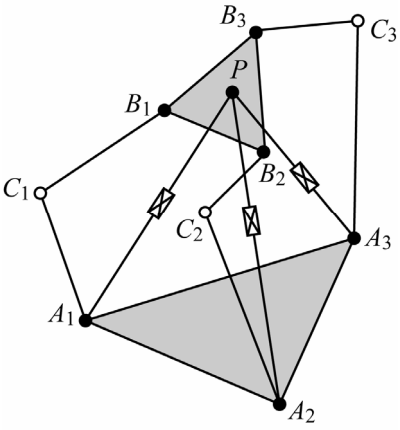

(d) decoupled parallel manipulator with both P and R joints (at C_j, $j = 1, 2, 3$).

Figure 1.8. – The decoupled parallel manipulators proposed in [Patarinski 1993].

This manipulator is made up of two parallel manipulators with a common central axis. The first manipulator with three linear actuators places a movable platform-1 at the desired position. In the second manipulator, two linear actuators tilt the platform-2 to the desired orientation with respect to the base-2 which is rigidly located above platform-1. Linear actuators are attached to base-1 and base-2 via universal joints and connected to platform-1 and platform-2 via spherical joints. The purpose of the

[1] In the remainder of this manuscript, R, P and S will stand for passive rotoid, prismatic and spherical joints, respectively, and R and P for actuated rotoid and prismatic joints, respectively.

common central axis is to constrain each parallel manipulator in order to have respectively 3 and 2 DOF. Adding a rotary actuator on platform-2 allows the decoupled parallel manipulator to have 6 DOF.

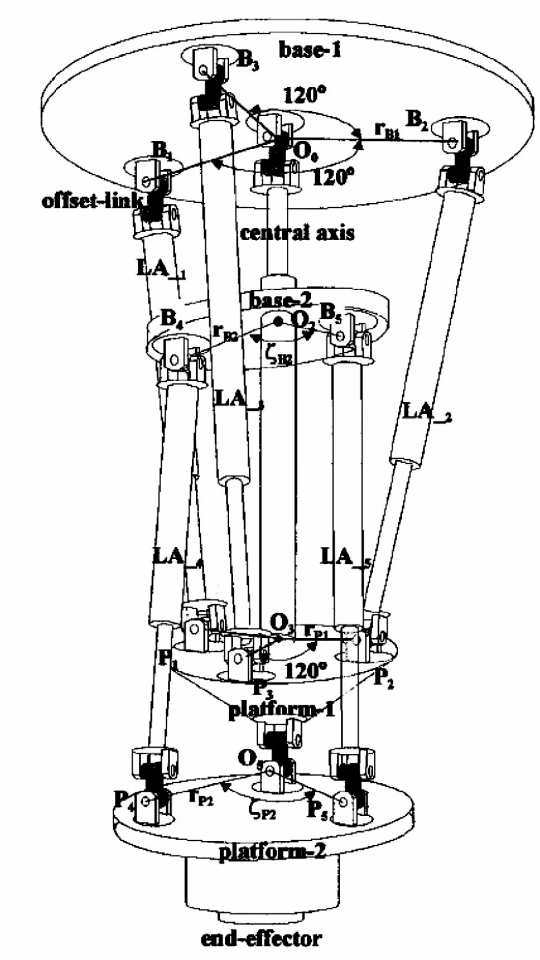

Figure 1.9. – The double parallel manipulators proposed in [Lee 1995].

The same design approach is applied by Prof. Lallemand in the *double-Delta parallel robot* [Lallemand 1997]. The first Delta manipulator places a movable platform at the desired position. The second Delta robot makes it possible to orient the end-effector with respect to the base frame.

Obviously, the control laws of such structures are simplified because one manipulator makes it possible to position the end-effector and the other makes it possible to orientate it. However, their major drawback is their design complexity.

In 1995 again, the *Nabla 6* was presented in [Bernier 1995]. This manipulator is a spatial robot with 6 DOF actuated by six linear motors (Fig. 1.10). The centre of the platform is linked to the extremity of three rods via a triple spherical joint. The other extremity of each rod is linked via spherical joints to a moving solid (B_1, B_2 and B_3 respectively) which has a linear movement along a linear guide. The three guiding axes lie on a same plane and intersect at point G. The angle between the axes is equal to 120 deg. Three other rods are connected via spherical joints to the platform and to the moving solids (B_4, B_5 and B_6). The orientation of the platform is controlled by the displacement of the six linear actuators.

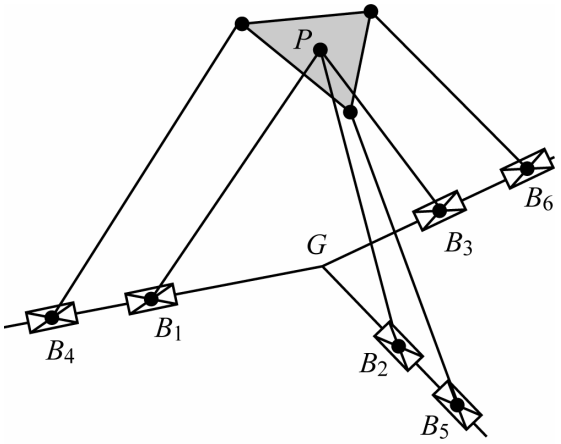

Figure 1.10. – Architecture of the Nabla 6.

As for the manipulators of [Patarinski 1993], the Jacobian matrix has a block triangular structure, which simplifies the kinematic control laws.

Three years later, in the study [Mianowski 1998] the *Polman-6* (Fig. 1.11) was developed. This manipulator consists of three identical driving mechanisms in the form of 2-DOF five bar planar parallelograms mounted in the base in such a way that their axes are situated in the lines parallel to ***x***, ***y*** and ***z***-axes of the Cartesian coordinate system. The moving platform has a form of a half spatial cross with spherical joints and is connected to driving mechanisms by the way of three identical parallelograms similar to those used in the Delta robot. With such a structure, the position of the end-effector is controlled by the rotation of the rods (1), (2) and (3) while the orientation is controlled by the rotation of the rods (4), (5) and (6). This time, the position of the end-effector is totally independent on its position, which implies that the laws are much more simplified than for the previous manipulators.

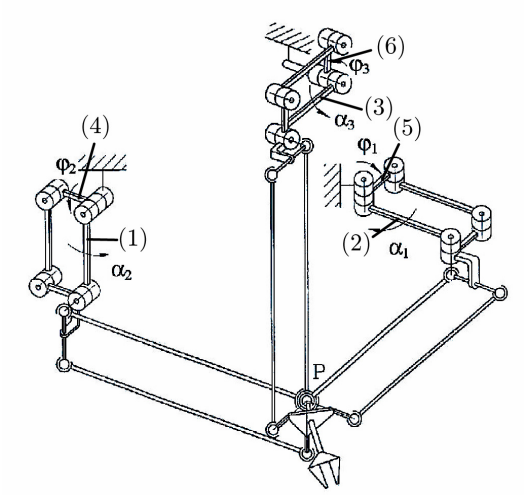

Figure 1.11. – Architecture of the Polman-6.

All the presented works dealt with the decoupling between the position and the orientation of the parallel manipulators with 6 DOF. However, the robots with 6 DOF are not the only manipulators of which control laws can be simplified. The decoupling between position and orientation can also be obtained on structures with different DOF. As examples, we can notice:

- spatial structures with two translations and one rotation (Fig. 1.12.a): some examples of such structures have been presented in [Chablat 2003]. The position of the point P in the ***xOy*** plane is controlled by the displacement of one planar mechanism controlled by prismatic joints of which direction are $\mathbf{e_1}$ and $\mathbf{e_2}$, and the orientation is given by the displacement of the link B_3P which is actuated through a prismatic joint of which direction is $\mathbf{e_3}$.
- spatial structures with two translations and two rotations (Fig. 1.12.b): the example we present for such structures is based on the previous manipulator. While the position is controlled by the displacement of one planar mechanism, the orientations are obtained by the displacement of the link CP. The position of point C is controlled by the simultaneous displacement of linear actuators of which directions are $\mathbf{e_3}$ and $\mathbf{e_4}$;
- spatial structures with one translation and two rotations (Fig. 1.12.c, d, e): presented in [Jin 2004], it is specified that, for all these manipulators, the position (S_2/R_2) is controlled by the displacement of one leg and the orientations are given by the simultaneous displacement of the three legs;

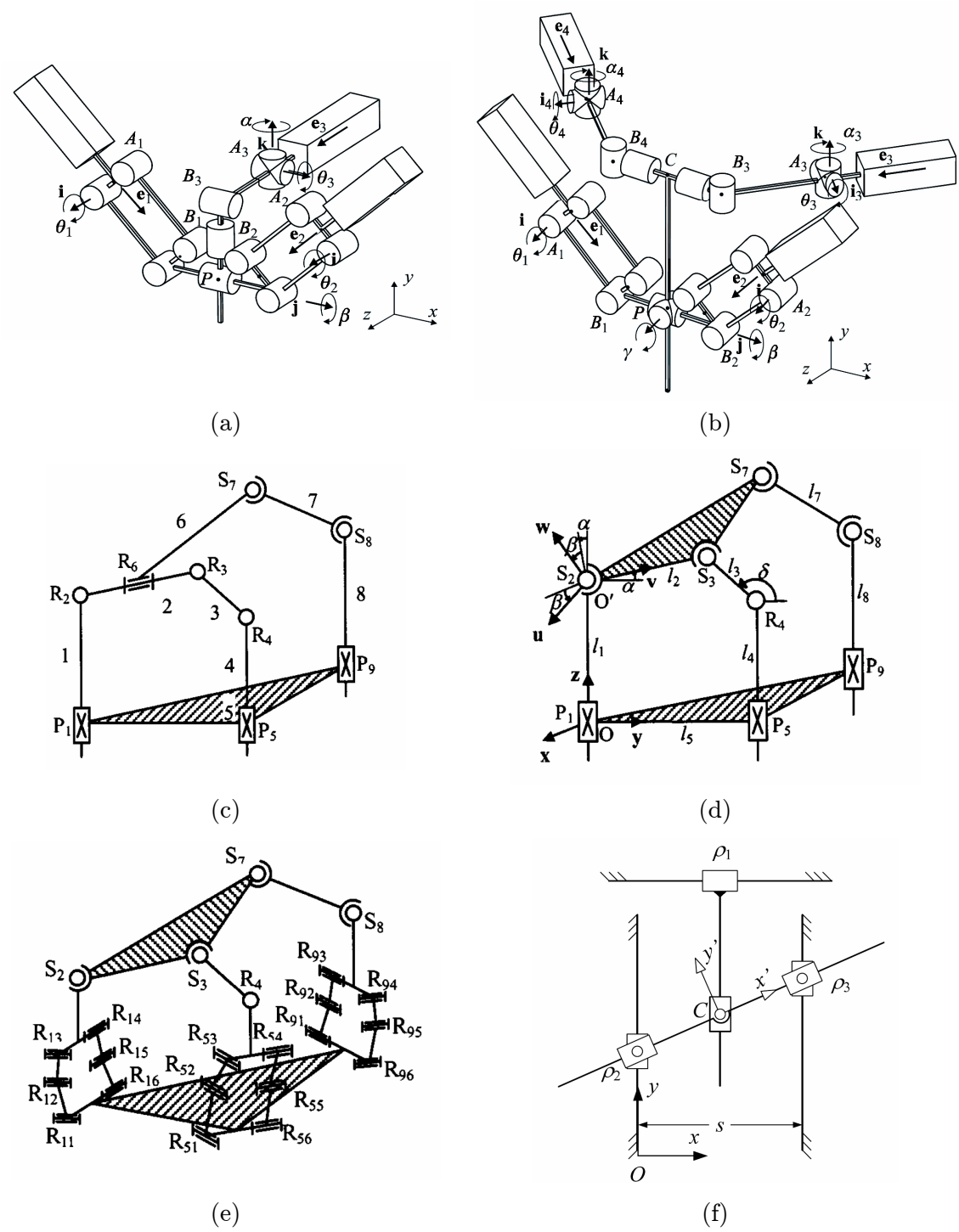

Figure 1.12. – Structures decoupled between position/orientation with various DOF.

- planar structures with three translations and one rotation (Fig. 1.12.f): for this manipulator presented in [Yu 2006], the displacement along the ***x***-axis is fully independent. The translation along the ***y***-axis is allowed by the simultaneous displacements of the prismatic pairs ρ_2 and ρ_3 and the orientation is obtained by their antagonistic displacements.

It should be noted that the decoupling between position and orientation is not the only case of partial decoupling of parallel structures. There are also other kinds of simplification of the control laws, as for example the partial decoupling between the DOF of manipulators with only translatory movements (Fig. 1.13). For the presented mechanism, the translation along the ***x***-axis is decoupled from the translations along the other axes.

Thus, the control laws of the manipulators of which positions are decoupled from their orientations have evolved in order to be dependent on fewer parameters, and, as a result, to become simpler. However, even if the simplification is already tangible, the kinematics relationships are still coupled. Therefore, researchers have continued to seek architectures with the simplest control law possible.

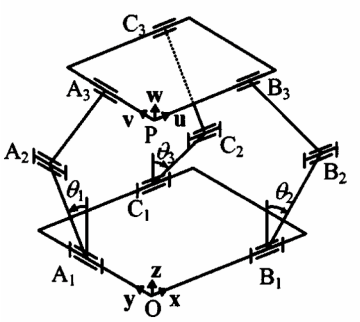

Figure 1.13. – Other kind of partial decoupling [Jin 2004].

1.2.2. ... to the full-decoupling of the movements.

The next step of the simplification of the control laws of the manipulators is the apparition of fully-isotropic manipulators.

Isotropicity of a robotic manipulator is related to the condition number of its Jacobian matrix, which can be calculated as the ratio of the largest and smallest singular value. A robotic manipulator is fully-isotropic if its Jacobian matrix is isotropic

throughout the entire workspace, i.e. the condition number of the Jacobian matrix is equal to one. The condition number is an interesting index characterizing the distortion of a unit hypersphere under the linear mapping [Angeles 2003]. It has been developed as a kinetostatic performance index of robotic mechanical systems [Merlet 2006b]. Thus, the isotropic design aims at ideal kinematic and dynamic performance of the manipulator [Fattah 2002].

Several works have dealt with the synthesis of fully-isotropic parallel manipulators [Bouzgarrou 2004] [Carricato 2002] [Carricato 2004a] [Carricato 2004b] [Gogu 2004] [Gogu 2005a] [Gogu 2005b] [Gogu 2005c] [Gogu 2005d] [Gogu 2006a] [Gogu 2006b] [Gogu 2006c] [Gogu 2007] [Gosselin 2004] [Gosselin 2007] [Kong 2002a] [Kong 2002b] [Li 2004] [Richard 2007]. An analysis of these works shows that the Jacobian matrix **J** of such structures *mostly* corresponds to the identity matrix. Thus the kinematic control laws are very simple:

$$\begin{bmatrix} \mathbf{V} \\ \boldsymbol{\omega} \end{bmatrix} = \dot{\mathbf{q}} \tag{1.1}$$

where $\mathbf{V}$ corresponds to the Cartesian velocity of the platform, $\boldsymbol{\omega}$ to its rotational velocity and $\dot{\mathbf{q}}$ is the vector of the articular velocities. Thus these architectures are fully-decoupled, i.e. the displacements around all the degrees of freedom of the platform are decoupled.

The figure 1.14 presents several examples of fully-isotropic manipulators. The manipulator of figure 1.14.a is a manipulator with one translation and two rotations. The translational displacement of the end-effector along the ***x***-axis is directly obtained by the movement of the prismatic pair (2_A). One rotation of the platform is performed by the displacement of one rotating actuator (2_B) and the rotation about the other axis is given by the displacement of a second rotating actuator (2_C).

Figure 1.14.b presents a manipulator with two translations and two rotations. The laws controlling the position and orientation of the end-effector are fully-decoupled, i.e. the displacement of the controlled point along the ***x*** and ***z***-axes are respectively obtained by the actuation of the prismatic guides (2_A) and (2_B) and the two orientations of the platform are obtained by the rotation of actuators (2_C) and (2_D) respectively.

The architecture of figure 1.14.c represents a fully-isotropic manipulator with 3 translations and 1 rotation. Once again, the position and orientation of the end-effector are fully-decoupled, i.e. the displacement of the controlled point along the ***x***, ***y*** and ***z***-

axes are respectively obtained by the actuation of the prismatic guides (2_A), (2_B) and (2_C) and the rotation of the platform is given by the rotation of link (2_D). The same design concept is proposed in the manipulator of figure 1.14.d.

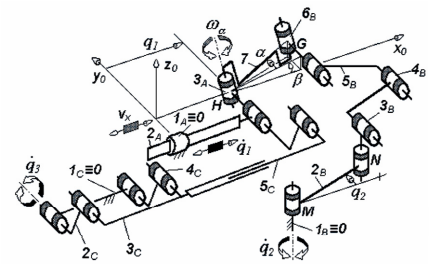

(a) 1 translation and 2 rotations.

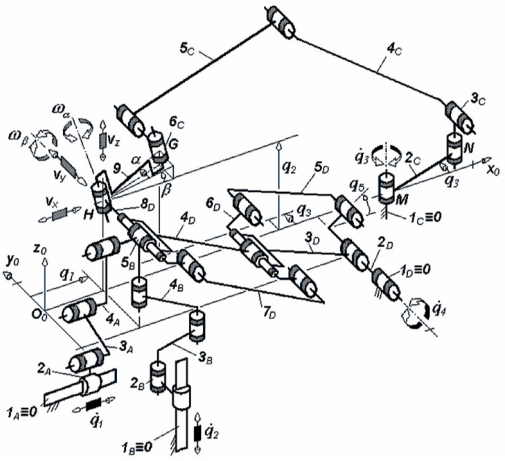

(b) 2 translations and 2 rotations.

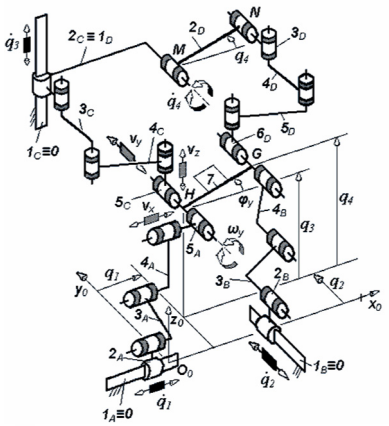

(c) 3 translations and 1 rotation.

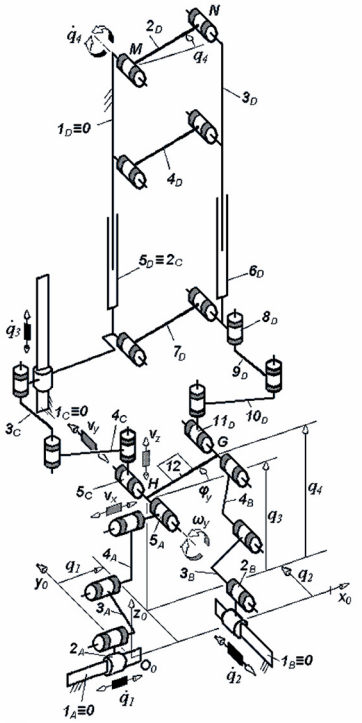

(d) 3 translations and 1 rotation.

Figure 1.14. – Examples of uncoupled manipulators proposed by Prof. Gogu.

It may be mentioned that many works on full-decoupling of the movements deal with manipulators with translatory motions. Such a result has been obtained in publications as [Carricato 2002] [Carricato 2004b] [Gosselin 2004] [Kong 2002a] [Kong 2002b] [Li 2004]. Some examples of such structures are presented in figure 1.15. For all these manipulators, it is possible to see that the displacement of only one actuator controls the translation of the platform along one direction.

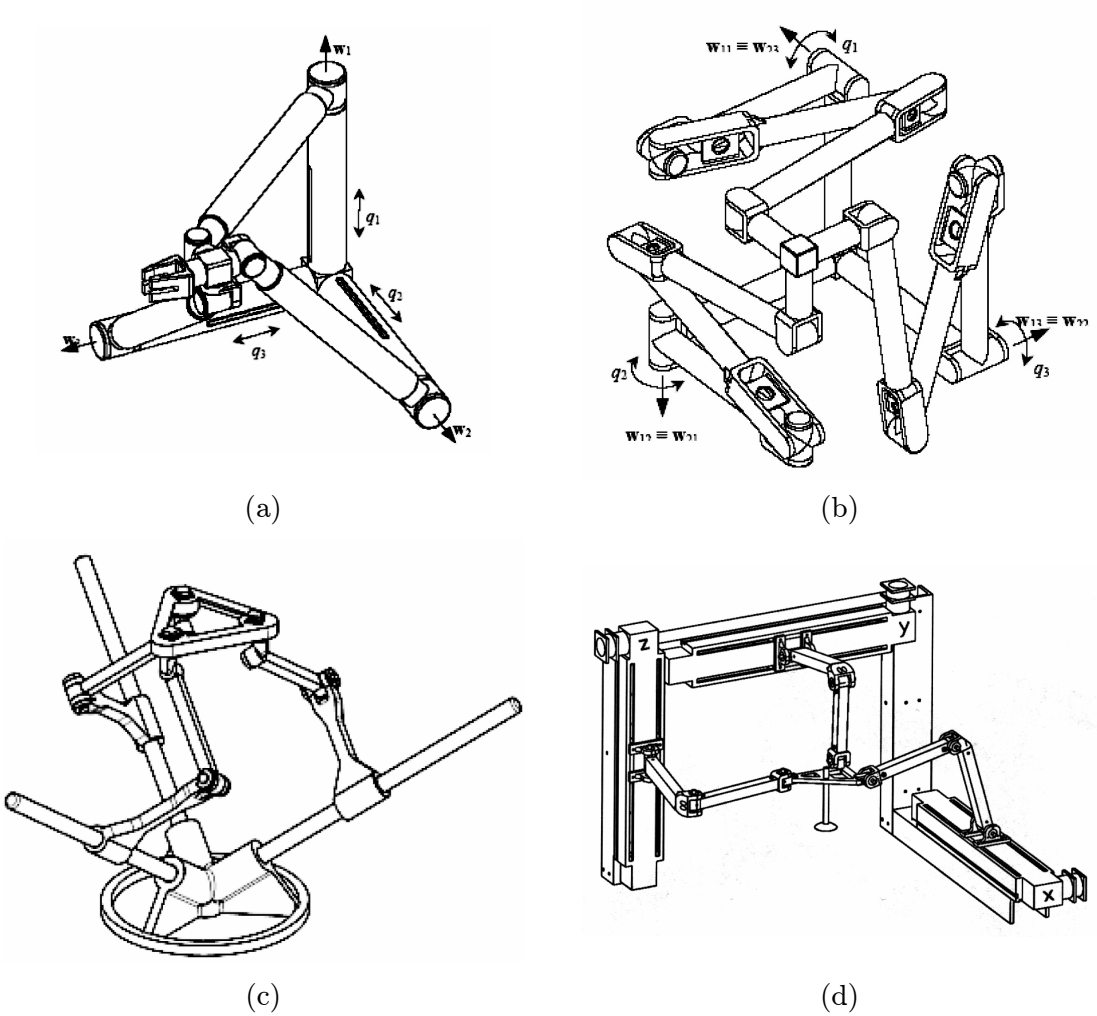

Figure 1.15. – Examples of fully-decoupled manipulators with 3 translatory DOF: (a) and (b), two manipulators designed in [Carricato 2004b], (c) and (d), two possible arrangements of manipulators called Tripteron presented in [Gosselin 2004] and [Kong 2002].

Obviously, the most important advantage of such fully-decoupled manipulators is their very simple input/output kinematic relationships (and as a result their input/output dynamic equations).

However, despite these very encouraging results, fully-decoupled structures have also many drawbacks, such as:

- the increase in the number of joints, which multiplies the number of parameters which can induce errors during the manufacturing stage;
- the loss of rigidity of the structures; on figures 1.15.a, b and d, one can see that the payload is only supported by one leg. This is in contradiction with one of the main advantages of the parallel manipulators (each kinematic chain carries only a fraction of the total load, which leads to the creation of more rigid robots).

It seems obvious that trying to simplify the control laws of parallel structures and conserving their principal advantages is a complicated problem. This is the reason why we have tried to find a compromise between the decoupling of the movements and the architectural characteristics of the parallel structures, i.e. to find a new kind of decoupling which makes it possible to develop parallel manipulators with high-load carrying capacities.

1.3. Summary.

In this chapter, we have presented a short review of the well known parallel structures which were patented and developed for industry. Parallel manipulators have attracted several manufacturers because it was promised, they would have greater rigidity, better velocities and dynamic characteristics and greater accuracy compared with their serial counterparts. However, despite these very attractive advantages, companies have mostly failed to deliver parallel structures to the market.

While the promises of great rigidity and high velocities have already been obtained on several structures, the promise of a high degree of accuracy has not been fulfilled yet, which can explain the industrial defeat of parallel manipulators.

Among several factors which may lead to the poor accuracy of the mechanisms, we may note:

- the presence of singularities in the workspace, some of them leading to huge positioning errors; however, solutions have already been proposed and validated;

- the use of links with lighter masses which leads to a loss of rigidity of the structure; such a problem may be easily avoided by the use of more rigid links;
- manufacturing errors and joint clearances, which can be rectified by calibration and an appropriate design;
- the non-linearity of the kinematic and dynamic models of the parallel manipulators which leads to tracking errors.

In order to solve the problem of the poor accuracy of the parallel structures, several researchers have thought of decoupling/simplifying the control laws of such structures. Our literature review shows that, in most of the cases, two approaches are developed:

- decoupling between position and orientation;
- full-decoupling, i.e. the decoupling of the displacements around all the degrees of freedom of the platform.

Despite these rather encouraging results, the fully-decoupled manipulators have drawbacks also, such as a lack of rigidity or the increase in the number of joint.

In the following chapter, a new approach to the decoupling of parallel structures is presented. This approach seeks to find a compromise between the decoupling of the movements and the architectural characteristics of the parallel structures.

Chapter 2

PAMINSA: A New Family of Decoupled Parallel Manipulators

*In this chapter, a new family of decoupled parallel manipulators is presented. These manipulators are called PAMINSA (**PA**rallel **M**anipulator of the **I.N.S.A.**). The characteristic of these manipulators is the decoupling of the displacements in the horizontal plane from the displacements along/about the other directions. Their conceptual design, in which the copying properties of pantograph linkage are used, makes it possible to obtain a large payload capability.*

Based on these considerations, parallel structures with 4 DOF are firstly synthesized and a systematic approach for motion generation of input point of each limb is presented. It is then shown that this approach can be extended to manipulators from 3 to 6 DOF.

A basic structure with 4 DOF is studied in order to analytically demonstrate the design concept.

A prototype of PAMINSA manipulator is presented and, then, the experimental validation of the design concept is carried out. It is shown experimentally that the static loads on the rotating actuators, which move the platform in the horizontal plane, are cancelled.

2.1. Design analysis of PAMINSA manipulators.

It has been shown in the previous chapter that the non-linearity in the kinematic and dynamic models of parallel manipulators is not attractive for industrial applications. In order to solve this problem, over the last few years, new structures had been developed. Our literature review of previous research on decoupling of the kinematic and dynamic input/output relationships of parallel manipulators has shown that, in most of the cases, two approaches are developed (see chapter 1):

- decoupling between position and orientation;
- full-decoupling, i.e. the decoupling of the displacements around all the degrees of freedom of the platform.

Despite rather encouraging results, as for example the increase in positioning accuracy due to the linear input/output relationships, we would like to remember that the fully-decoupled manipulators have drawbacks also, such as a lack of rigidity or an increase in the number of joints. It is obvious that it is not easy to solve the problem of the full decoupling of the movements and to conserve the principal advantages of the parallel structures. However, there is a need of structures which could be used in industrial applications for the manipulation of heavy equipment with great positioning accuracy.

This is the reason why we have tried to find a compromise between the decoupling of the movements and the architectural characteristics of the parallel structures. In other words, we have changed the statement of the problem: it is not essential that a parallel architecture be fully-decoupled, it can also be partially decoupled. But it is important to obtain a mechanical architecture with high payload capacities.

Let us consider a new conceptual design approach of decoupling in which the displacements of the platform in the horizontal plane (two translations about $\boldsymbol{x}$ and $\boldsymbol{y}$-axes and one rotation about the vertical axis) are independent on its translations along the vertical axis.

Why is this approach more effective? To answer this question, it is necessary to take into account the following considerations.

2.1.1. A new approach to the problem of the design of decoupled parallel manipulators.

An energetic analysis shows that the work of gravity applied on a body moving in the horizontal plane is equal to zero (the gravitational forces are always perpendicular to the displacements, Fig. 2.1). But the work of the same force when the body is moving along the vertical axis is other than zero (the gravitational forces are parallel to the displacements). This phenomenon is used in the design of the hand operated manipulators [Arakelian 1998] [Arakelian 2004], in which the horizontal displacements of the payload are carried out manually and the vertical displacements are actuated. This principle is applied in the design of the new parallel PAMINSA manipulators.

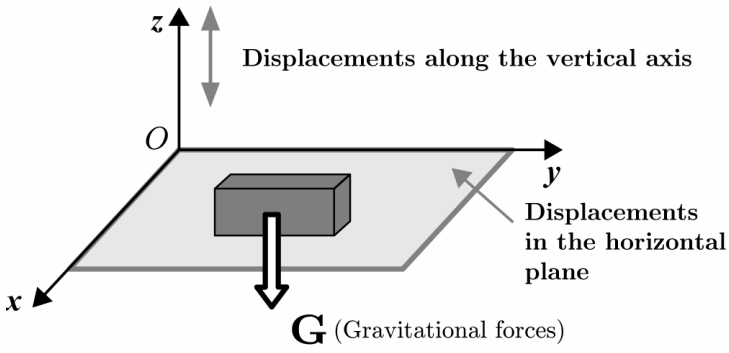

Figure 2.1. – Gravity work in space: motions in the horizontal plane and along the vertical axis.

Let us consider in the following part the mechanical architecture of the suggested manipulators.

2.1.2. Mechanical architecture of PAMINSA.

The first idea was to develop a parallel architecture of which displacements of the platform in the horizontal plane are independent on its vertical displacements. For this purpose, the pantograph linkage is used as a leg. The pantograph is a mechanical system with two input points A_i and B_i and one output point C_i (Fig. 2.2) [Lu 1996]. These input points linearly control the displacement of the output point C_i. Thus, one linear actuator connected to input point B_i can control the vertical displacement of the

output point C_i and the other linear actuator with horizontal axis can control its horizontal displacements (Fig. 2.3). Please note that these motions are completely decoupled, i.e. they can be carried out independently.

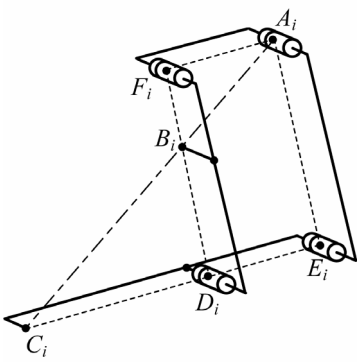

Figure 2.2. – Scheiner pantograph linkage.

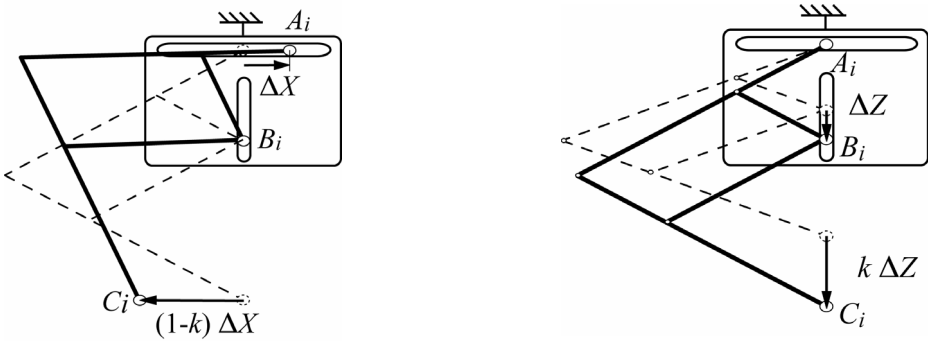

(a) along a horizontal axis. (b) along a vertical axis.

Figure 2.3. – Control of the displacement of the pantograph linkage.

Let us suppose that there is a concentrated mass in the point C_i. In this case, the load of the gravitational forces on the actuator of the horizontal displacements will be equal to zero (the gravitational forces are always perpendicular to the displacements). With regard to the actuator of vertical displacements, the load of the gravitational forces is not zero (the gravitational forces are parallel to the displacements). Moreover, the input/output relationship for vertical displacement is linear and it is determined by the magnification factor k of the pantograph ($k = A_iC_i/A_iB_i$). These properties of the pantograph mechanism are used in PAMINSA manipulators (this is demonstrated in section 2.2).

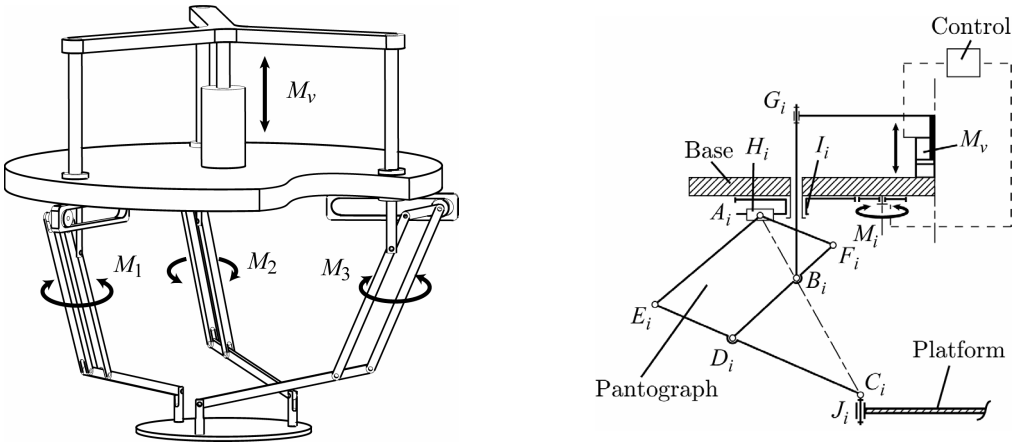

(a) (b)

Figure 2.4. – PAMINSA with 4 DOF (a); kinematic chain of each leg (b).

Now let us connect three identical Scheiner pantograph linkages with the base and the platform as is shown in Fig. 2.4. In the obtained structure, one vertical actuator M_v controls the vertical displacement of points B_i of the pantograph linkages, and as a result, the vertical displacement of pairs C_i of the moving platform. The generation of motion in the horizontal plane is achieved by the actuators M_1, M_2 and M_3 connected through two passive pairs (H_i and I_i) with input joints A_i. The movement of each chain $M_iI_iH_i$ is planar as well as the displacement of input joints A_i. As a result, the actuators M_i control the horizontal displacements of points C_i.

Thus, it is easy to see that, for the suggested architecture, the vertical translation of the platform along $\boldsymbol{z}$-axis is decoupled from its displacements in the horizontal plane (translations about $\boldsymbol{x}$ and $\boldsymbol{y}$-axes and rotation ϕ about $\boldsymbol{z}$-axis). This implies that the kinematic models controlling the displacement of the manipulator can be divided into two parts:

- one model for the displacements in the horizontal plane (Fig. 2.5.a); this model is equivalent to a 3-RPR manipulator of which first revolute joints are actuated;
- one model for the translations along the vertical axis (Fig. 2.5.b) equivalent to a pantograph linkage.

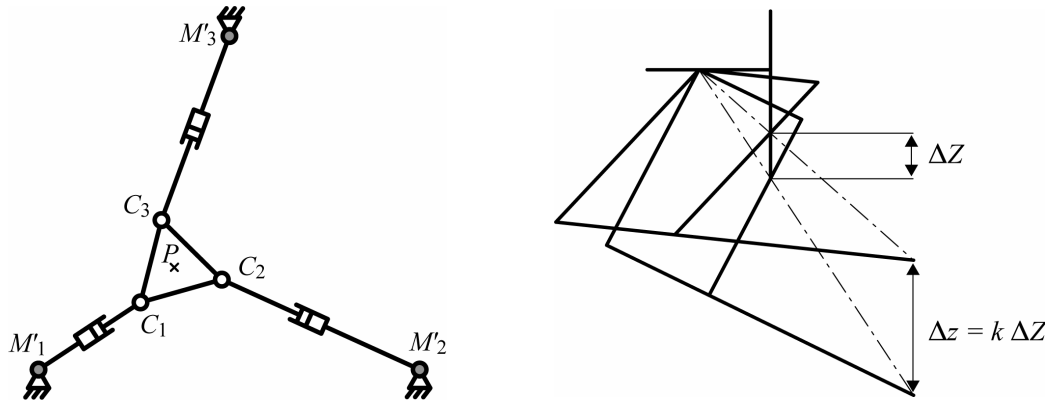

(a) Planar displacements. (b) Vertical translations.

Figure 2.5. – Kinematic models for the displacements of the manipulator under study.

Among the obvious advantages of the suggested manipulator architecture, we have noted following points:

(i) the decoupling of the control powers in two parts makes it possible to raise an important payload to a fixed altitude by powerful actuators and, then, to displace it on the horizontal plane by less powerful actuators;

(ii) a great accuracy in the horizontal positioning, because the payload can be locked in the horizontal plane by the mechanical architecture of the manipulator (in other words, if the position of the vertical actuator is fixed, the altitude of the platform cannot change);

(iii) the cancellation of loads of gravity on the rotating actuators which move the platform in the horizontal plane;

(iv) the simplification of the vertical control based on linear input/output relationships.

It should be noted that the motion generation of the input point A_i can be carried out in several ways. All architectures shown in table 2.1 have the same properties mentioned above. Their kinematic models can be divided as previously into one model for the vertical translations and one model for the planar displacements. As a result, the different schematics for input motion generation can be easily distinguished by the planar equivalent models of the structure (the pair M'_i – or H'_i – corresponds to the displacement of both pair M_i – or H_i – and pantograph linkage; the grey pairs stand for the actuated pairs). All the planar equivalent models presented in table 2.1 are well known and their kinematics have been widely studied [Bonev 2003b] [Merlet 1996] [Merlet 2006a].

Table 2.1. – Examples of motion generation of the input point A_i of pantograph linkages.

Kinematic chain	**Planar equivalent model**		**3D representation**
	Type	**Schematics**	
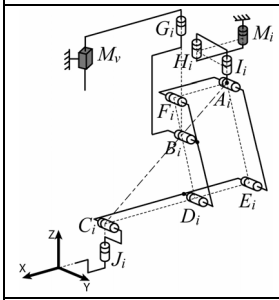	**3-RRR**	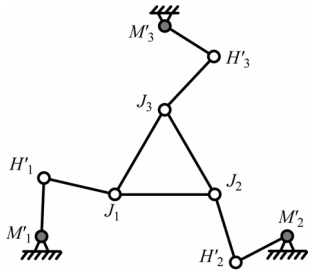	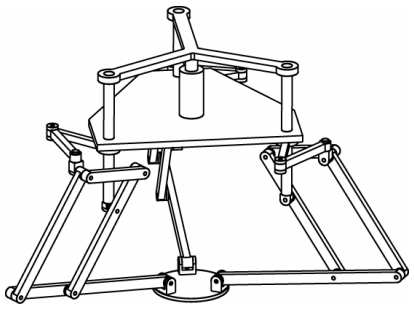
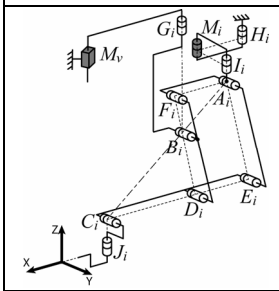	**3-RRR**	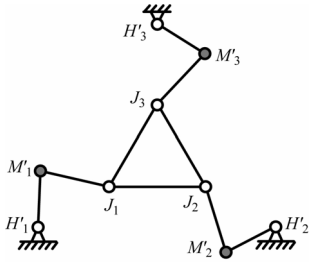	
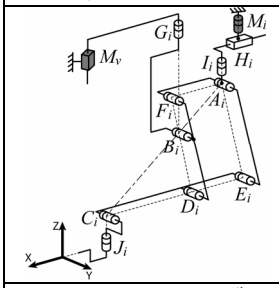	**3-RPR**	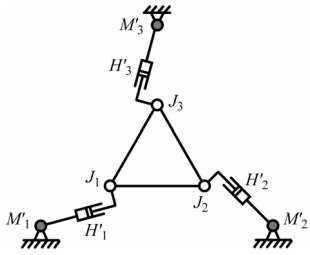	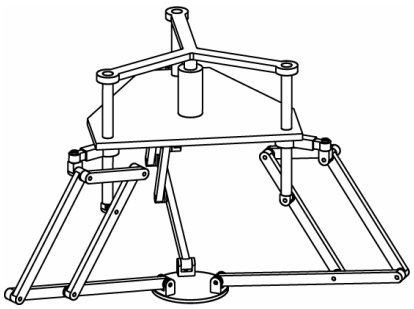
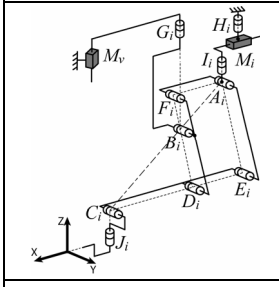	**3-RPR**	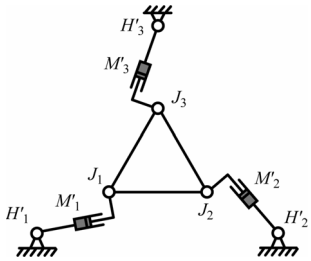	
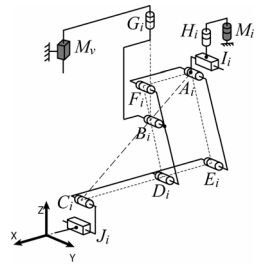	**3-RRP**	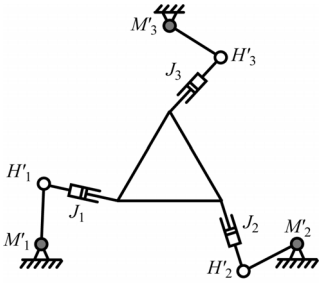	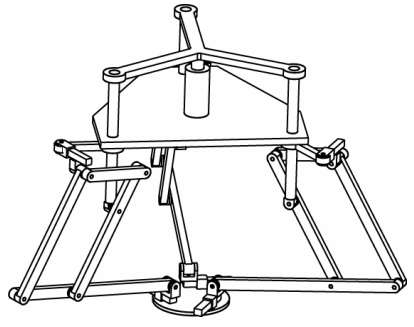

Table 2.1. – Examples of motion generation of the input point A_i of pantograph linkages (continued).

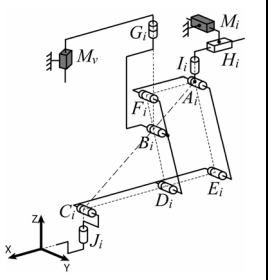	3-PPR	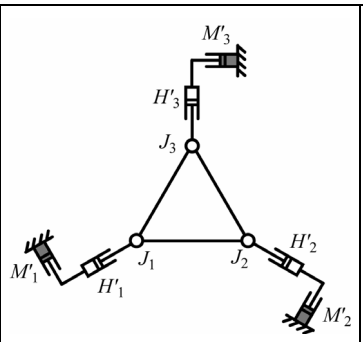	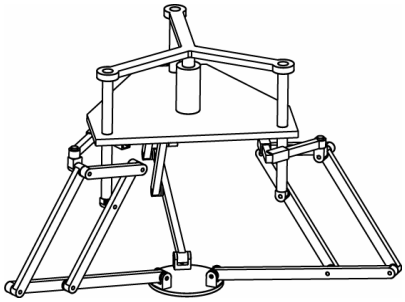
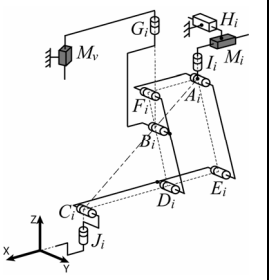	3-PPR	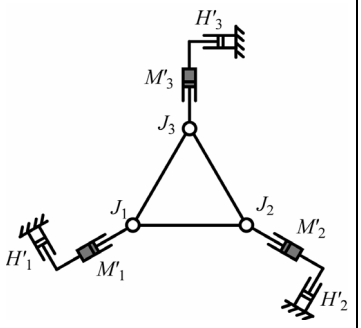	
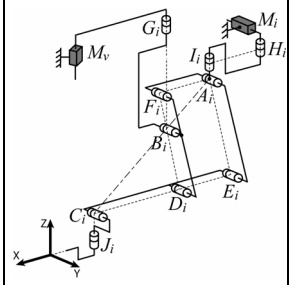	3-PRR	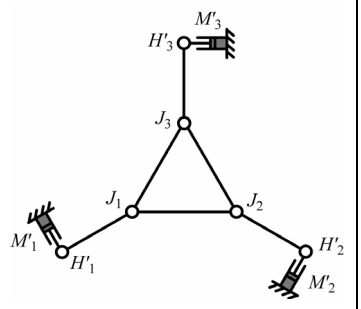	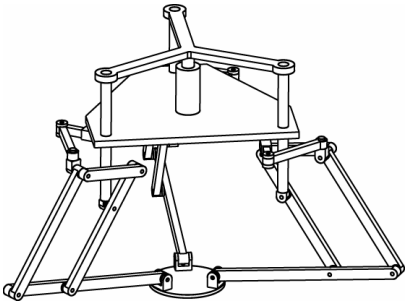
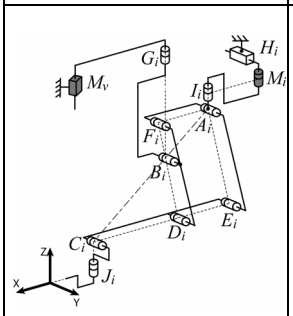	3-PRR	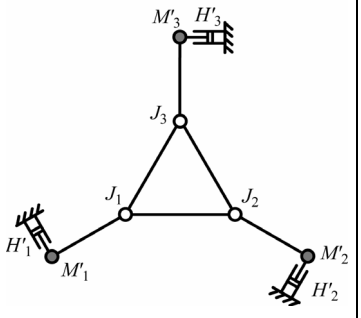	
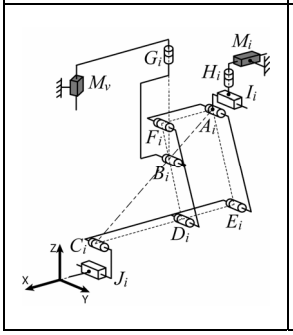	3-PRP	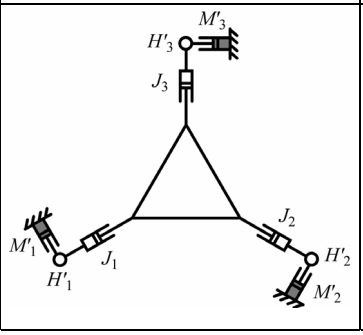	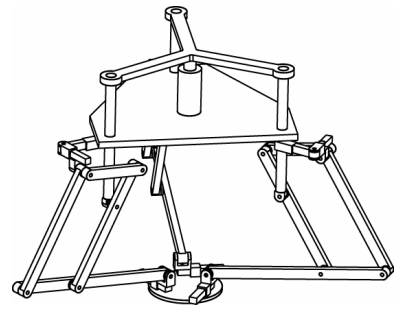

It appears to us that the proposed manipulators could be used in industrial applications for the manipulation of heavy equipment with great positioning accuracy. But this is not the only utility of such architectures. Various fields are possible depending on the type of the industrial application, as for example the use of PAMINSA manipulators in micro-manipulation (as long as the magnification factor of the pantograph linkages does not enlarge the displacements but, on the contrary, reduces the movement quantity).

2.1.3. The manipulators from 3 to 6 DOF.

Our observations have shown that the structures with 4 DOF of table 2.1 can be modified in order to increase/decrease the number of DOF of the manipulators, without changing the properties of the design approach. Table 2.2 presents PAMINSA manipulators from 3 to 6 degrees of freedom with a planar equivalent model which is a 3-RPR structure. Notation PAMINSA-*j*D*n*L means that the manipulator has j degrees of freedom and n legs (j = 3 to 6, n = 2, 3). In table 2.2, the output parameters, the actuated joints, as well as the type of connection between the platform and the legs are also represented. Such modifications can be easily extended to the other types of kinematic chains represented in table 2.1.

For each kind of manipulator, the rotations of the legs allow the horizontal displacements of the platform at a given altitude with given inclinations. Please note that the inclinations about $\boldsymbol{x}$ and $\boldsymbol{y}$-axes and the translation along $\boldsymbol{z}$-axis are obtained by the vertical translations of points B_i of each leg.

Each kind of PAMINSA has its own advantages and can be used differently. Let us consider the characteristics of each architecture:

- PAMINSA-4D3L, as was mentioned above, makes it possible to improve the positioning accuracy about the vertical axis because the structure is kinematically locked during the displacement on the horizontal plane. Such a design allows the fixation of an important load in a given altitude, and then its positioning on the horizontal plane.
- PAMINSA-4D2L is able to perform the same task as the PAMINSA-4D3L with only two legs. It should be noted that, in this case, the motorization is a bit different. The displacements in the horizontal plane are allowed by two rotary motors M'_i fixed on the base and one linear actuator H'_1 which is mounted in series with the actuator M'_1.

Table 2.2. – The family of PAMINSA manipulators from 3 to 6 DOF.

<table>
<tr><td colspan="3">PAMINSA-4D2L</td></tr>
<tr><td rowspan="3">DOF: 3 Translations and 1 Rotation

Type of connection between the platform and the legs: Universal (Cardan) joints

Actuated joints:
M_1, H_1, M_2 and M_v</td><td>3D view</td><td>Planar equivalent model</td></tr>
<tr><td> 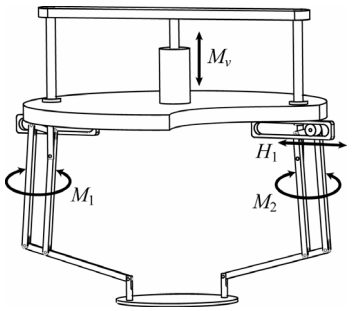
</td><td> 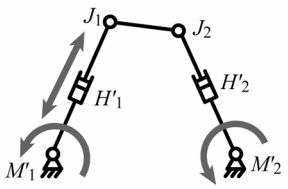
</td></tr>
<tr><td colspan="3">PAMINSA-3D3L*</td></tr>
<tr><td rowspan="3">DOF: 3 Translations

Type of connection between the platform and the legs: Universal (Cardan) joints

Actuated joints:
M_1, M_2 and M_v</td><td>3D view</td><td>Planar equivalent model</td></tr>
<tr><td> 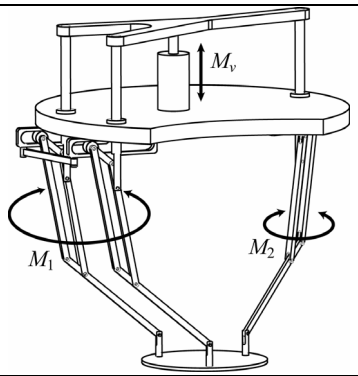
</td><td> 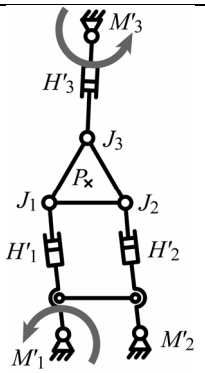
</td></tr>
<tr><td colspan="3">PAMINSA-4D3L*</td></tr>
<tr><td rowspan="3">DOF: 3 Translations and 1 Rotation

Type of connection between the platform and the legs: Spherical pairs

Actuated joints:
M_1, M_2 and M_{v1}, M_{v2}</td><td>3D view</td><td>Planar equivalent model [1]</td></tr>
<tr><td> 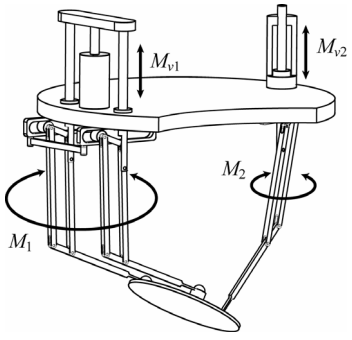
</td><td> 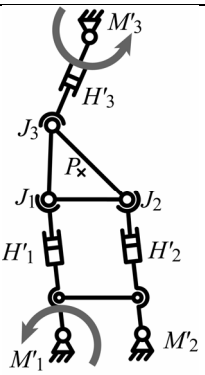
</td></tr>
</table>

* Two of the three legs of such a type of manipulator are actuated with the same motor and stay parallel to each other.

[1] The size of the platform of the planar equivalent model changes with the variation of the orientation of the platform of the spatial PAMINSA manipulator.

Table 2.2. – The family of PAMINSA manipulators from 3 to 6 DOF (continued).

<table>
<tr><td colspan="3">PAMINSA-4D3L</td></tr>
<tr><td rowspan="2">DOF: 3 Translations and 1 Rotation

Type of connection between the platform and the legs: Universal (Cardan) joints

Actuated joints:
M_1, M_2, M_3 and M_v</td><td>3D view</td><td>Planar equivalent model</td></tr>
<tr><td> 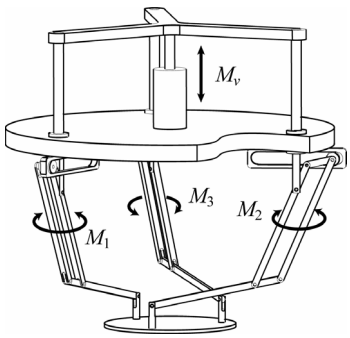
</td><td> 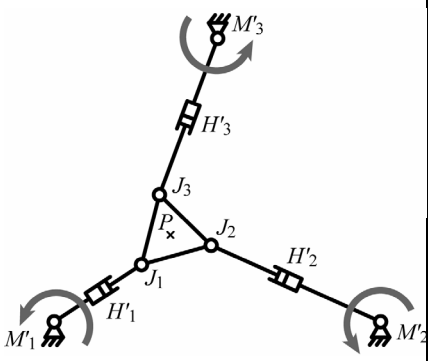
</td></tr>
<tr><td colspan="3">PAMINSA-5D3L</td></tr>
<tr><td rowspan="2">DOF: 3 Translations and 2 Rotations

Type of connection between the platform and the legs: Spherical pairs

Actuated joints:
M_1, M_2, M_3 and M_{v1}, M_{v2}</td><td>3D view</td><td>Planar equivalent model [1]</td></tr>
<tr><td> 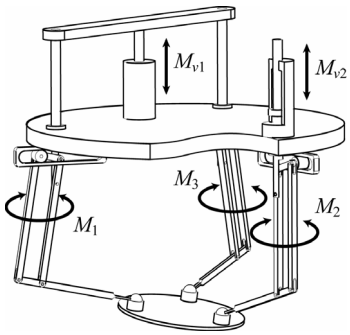
</td><td> 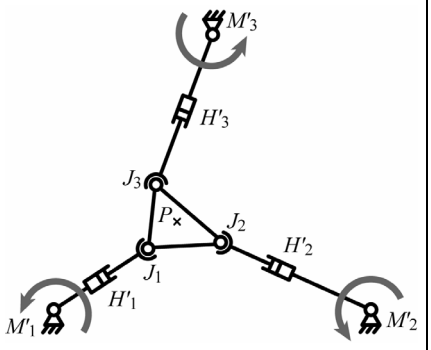
</td></tr>
<tr><td colspan="3">PAMINSA-6D3L</td></tr>
<tr><td rowspan="2">DOF: 3 Translations and 3 Rotations

Type of connection between the platform and the legs: Spherical pairs

Actuated joints:
M_1, M_2, M_3 and
M_{v1}, M_{v2}, M_{v3}</td><td>3D view</td><td>Planar equivalent model [1]</td></tr>
<tr><td> 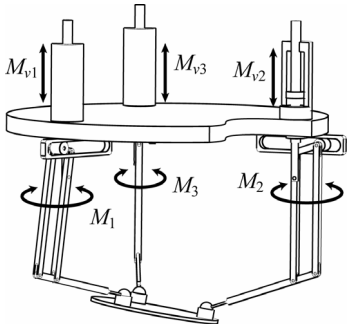
</td><td> 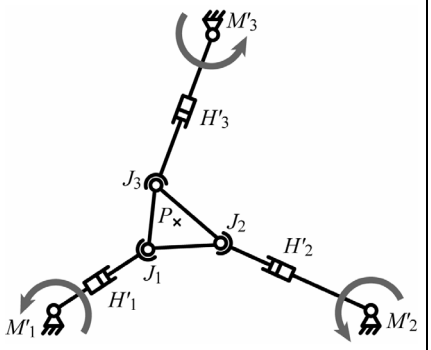
</td></tr>
</table>

- PAMINSA-3D3L* can be used in any application where only 3 translations along three axis are needed.
- PAMINSA-4D3L* is useful for any task with 3 translations and one orientation about the ***x*** or ***y***-axis.
- PAMINSA-5D3L allows the carrying out of all displacements in the horizontal plane with an inclination angle ψ of the platform (Fig. 2.6). The angle of the inclination ψ can be defined as an angle between the normal $\boldsymbol{N_{pl}}$ to the platform and the normal $\boldsymbol{N}$ of the plane ***xOy***. Thus, it is possible to move the platform on the horizontal plane with any inclination relative to the horizontal plane. In this case, the inclination is defined by the rotation of the point C_3 about the line C_1C_2.
- PAMINSA-6D3L allows any orientation ϕ of the platform about the ***z***-axis and its displacements on the horizontal plane. Two other inclinations of the platform and its vertical translation are allowed.

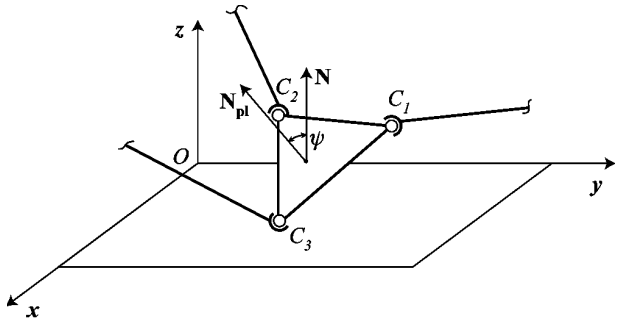

Figure 2.6. – The angle of the inclination ψ of the platform for the PAMINSA-5D3L.

We would like to mention that for all versions of presented PAMINSA manipulators, there is a decoupling between the displacements on the horizontal plane and the other displacements. The kinematics of each architecture from 3 to 6 DOF will be discussed in chapter 3.

Among several structures, the manipulators for the generation of Schoenflies motions (table 2.1) are more appealing for industrial applications because they allow the positioning of a device at a given point and then its orientation about one given

axis. However, the next evolution of PAMINSA manipulators showed that it is also possible to create fully-decoupled structures based on the pantograph linkages.

2.1.4. A particular structure with 3 fully-decoupled translatory motions.

Let us consider a fully-decoupled PAMINSA manipulator with translatory motions.

Fully-decoupling the three possible translations of a manipulator is an important challenge for many researchers [Carricato 2002] [Carricato 2004b] [Gosselin 2004] [Kong 2002a] [Kong 2002b] [Li 2004]. Such manipulators are able to replace the existing serial Cartesian robot (XYZ).

As for the basic versions of PAMINSA with 4 DOF (table 2.1), one vertical actuator M_v (Fig. 2.7) controls the vertical displacement of points B_i of the pantograph linkages and, as a result, the vertical displacement of pairs C_i of the moving platform.

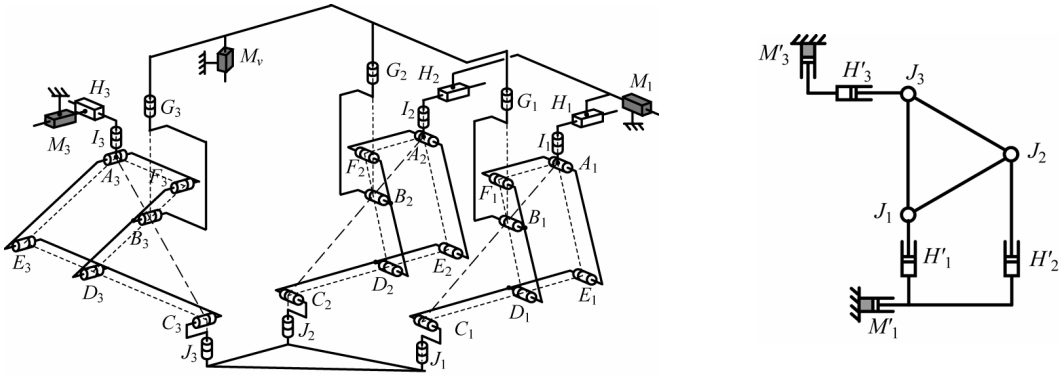

(a) Kinematic chain. (b) Planar equivalent model.

Figure 2.7. – Fully-decoupled PAMINSA with 3 DOF.

The horizontal displacements of the manipulator along ***x*** and ***y***-axes are allowed by the translations of actuators M_1 and M_3. Let us suppose legs 1 and 2 are disconnected from leg 3. Input points A_1 and A_2 are linked to actuator M_1 through the two kinematic chains H_1I_1 and H_2I_2. Thus, if actuators M_1 and M_v are fixed, the permitted passive motion of the platform is a pure translation along an axis parallel to joint H_1 and H_2. Analogically, the passive displacement of point J_3 of the third leg is a pure translation along an axis parallel to H_3. As a result, the planar equivalent model of the manipulator is the decoupled planar parallel manipulator presented in Fig. 2.7.b.

The kinematics of such a manipulator is very simple. Let q_1, q_3 and q_v respectively be the articular coordinates of actuators M_1, M_3 and M_v. The coordinates of the controlled point of the platform are x, y and z. Thus we have the following relationship:

$$\mathbf{x} = \mathbf{J}\mathbf{q}\,, \tag{2.1}$$

with

$$\mathbf{J} = \begin{bmatrix} 1-k & 0 & 0 \\ 0 & 1-k & 0 \\ 0 & 0 & k \end{bmatrix} \tag{2.2}$$

where $\mathbf{x} = [x,\ y,\ z]^T$, $\mathbf{q} = [q_1,\ q_2,\ q_v]^T$ and k is the magnification factor of the pantograph linkages. Thus, the velocity equation is:

$$\dot{\mathbf{x}} = \mathbf{J}\dot{\mathbf{q}} \tag{2.3}$$

So, **J** is the Jacobian matrix of the manipulator. Since **J** is a constant diagonal matrix with non zero elements, the manipulator does not have any singularities of Type 1, 2 and 3 [Gosselin 1990]. However, please note that only cases of singularities appear with the degeneracy of the parallelograms $A_iE_iD_iF_i$.

Our observations showed that, in the typical fully-decoupled manipulators, the payload is supported by only one limb. In the case of the suggested structure, the distribution of the payload is more efficient because each limb carries only a fraction of the load. As a result, the manipulator based on these properties should have a better rigidity.

2.2. Static analysis of the PAMINSA structures.

In section 2.1, we have stated that the load of the gravitational forces on the actuator for the horizontal displacements of PAMINSA manipulators will be equal to zero because the gravitational forces are always perpendicular to the displacements. This statement is demonstrated in this part.

Let us derive the potential energy of a basic PAMINSA manipulator with 4 DOF of which planar equivalent model is a 3-RPR manipulator with equilateral base and platform triangles. Its kinematic chain is represented in figure 2.8. We consider its

articular coordinates are represented by $\mathbf{q} = [q_1, q_2, q_3, q_v]^T$ (respectively corresponding to actuators M_1, M_2, M_3 and M_v) and the controlled coordinates are the position $[x, y, z]^T$ of the centre P of the platform and its orientation ϕ about z-axis. It is supposed the centre of masses of each link B_{ji} is located at their middle.

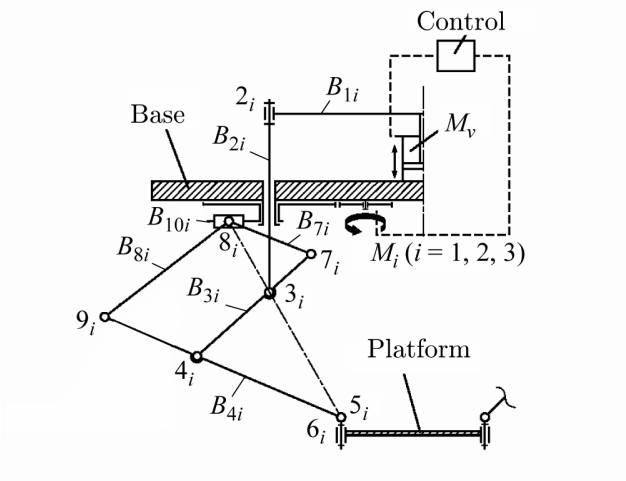

Figure 2.8. – Joints and links description for the static analysis of the studied manipulator.

The potential energy V of the manipulator can be expressed as follows:

$$V = V_{pl} + \sum_{i=1}^{3} V_{leg_i} \tag{2.4}$$

where V_{pl} is the potential energy of the platform and V_{leg_i} is the potential energy of the leg i (i = 1, 2, 3).

Developing equation (2.4) and considering that the coordinates of all of the points of the pantograph linkages can be found as a linear combination of the coordinates of points 3_i, 5_i and 9_i (appendix A), one can express the terms V_{pl} and V_{leg_i} as follows:

$$V_{pl} = m_{pl}\, g\, z \tag{2.5}$$

$$V_{leg_i} = C_{v1}\, z_{5i} + C_{v2}\, z_{9i} + C_{v3}\, q_v + C_{v4} \tag{2.6}$$

with,

$$C_{v1} = g\left(m_5 + \sum_{j=2,3,4,7}\left(\frac{m_j}{k}\right) + \frac{m_{B4}}{2} + \sum_{j=1,7}\left(\frac{m_{Bj}}{2\,k}\right) + \sum_{j=2}^{3}\left(\frac{m_{Bj}}{k}\right)\right), \tag{2.7}$$

$$C_{v2} = g\left(\frac{(k-1)\,m_4 - m_7 + k\,m_9}{k} + \frac{(k-2)\,m_{B3} - m_{B7}}{2\,k} + \frac{m_{B4} + m_{B8}}{2}\right), \tag{2.8}$$

$$C_{v3} = g\,\frac{m_{B1}}{2}, \tag{2.9}$$

$$C_{v4} = g\,L_{B2}\left(m_2 + \frac{m_{B1} + m_{B2}}{2}\right). \tag{2.10}$$

In these relations, C_{vj} (j = 1, 2, 3, 4) are constant terms of which dimension is equivalent to a mass multiplied by the gravitational acceleration g, m_{pl} is the mass of the platform with the payload, m_j is the mass of the j-th joint of the leg i (i = 1, 2, 3), m_{Bj} is the mass of the link B_{ji}, L_{Bj} is the length of link B_{ji} and z_{5i} and z_{9i} are the altitude of joints 5_i and 9_i. The expressions of the coordinates of joints 5_i and 9_i are given in appendix A.

The efforts $\boldsymbol{\tau}$ applied on the actuators by the gravitational effects (i.e. in a static mode of operation) are given by:

$$\boldsymbol{\tau} = \frac{\partial V}{\partial \mathbf{q}}. \tag{2.11}$$

Let τ_1, τ_2, τ_3 and τ_v be the efforts applied respectively on the actuators M_1, M_2, M_3 and M_v. Their expressions are given by:

$$\tau_p = \frac{\partial V}{\partial q_p} = \sum_{i=1}^{3} C_{v2}\,\frac{\partial z_{9i}}{\partial q_p},\ p = 1,\ 2,\ 3, \tag{2.12}$$

$$\tau_v = \frac{\partial V}{\partial q_v} = k\,m_{pl}\,g + \sum_{p=1}^{3}\left(k\,C_{v1} + C_{v2}\,\frac{\partial z_{9i}}{\partial q_v}\right) + C_{v3}. \tag{2.13}$$

It is possible to see that the term C_{v2} is only dependent on the masses of the legs of the mechanism and does not vary with the increase in the mass m_{pl} of the payload. This is the reason why a mass embedded on the platform does not produce any efforts on the actuators M_1, M_2 and M_3 which allow the horizontal displacements.

Thus, we have analytically proved on an example the veracity of the design concept of the manipulator. Please however note that this approach could be generalized in order to demonstrate it is valuable for any PAMINSA structures.

The next part will deal with the design of a prototype of the proposed basic architecture.

2.3. Design of a prototype and experimental validations.

We have developed at I.N.S.A. of Rennes a prototype of PAMINSA-4D3L of which kinematic chain is represented in the figure 2.4 (the CAD model of the prototype itself is represented in figure 2.9). The aim of this prototype is to validate the design concept of PAMINSA manipulators.

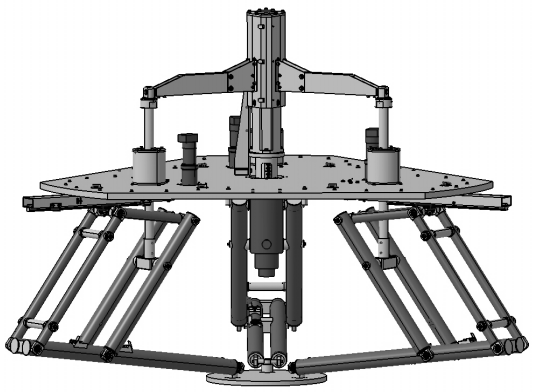

Figure 2.9. – CAD model of the PAMINSA manipulator.

This part aims to give some design considerations about this prototype. Its aim is not to present an exhaustive list of the chosen design solutions but to make the reader understand the key points in the design of our manipulator.

The first stage in the development of our prototype is to choose the dimensions of the elements of the robot.

2.3.1. Workspace analysis.

The lengths of the links of the robot have been numerically found to ensure the dextrous workspace[3] of the robot to be a cylinder with the following characteristics:

- the workspace must be reachable for all the orientation of the platform in the interval [–60 deg., +60 deg.];
- its radius is equal to 150 mm;
- its height is equal to 300 mm.

To choose the lengths of the desired links, we have to deal with these constraints:

- in order to avoid the negative effects of the degeneracy of the pantograph linkages inside the workspace, the angle between links A_iE_i and E_iC_i must be comprised between 30 and 150 degrees;
- the passive slider must not collide with the vertical limb G_iB_i. Therefore, its stroke must not be inferior to 50 mm;
- the lengths of the links have to be minimal in order to minimize the deformations of the structure;
- the radius of the circumscribed circle of the base triangle $M'_1M'_2M'_3$ cannot be superior to 350 mm because of machining constraints;
- for reasons of design simplicity and in order to limit the manufacturing time, the prototype is foreseen symmetrical.

Therefore, the lengths of the links can be found by experimental tests:

- the radii of the circumscribed circles of the base and platform triangles $M'_1M'_2M'_3$ and $J_1J_2J_3$ are respectively equal to 350 mm and 100 mm;
- the magnification factor of the pantograph k is equal to 3;
- the lengths of limbs A_iE_i and E_iC_i are respectively equal to 420 mm and 630 mm;
- the length of the vertical limb G_iB_i is equal to 442 mm;
- the maximal stroke of the passive slider is equal to 300 mm.

The workspace of a PAMINSA manipulator with such characteristics is represented in figure 2.10. As the system is symmetrical, we shall only represent the workspace for the orientation angles comprised between 0 and 60 degrees.

[3] The dextrous workspace is the region which can be reached by the reference point with any orientations [Merlet 1998].

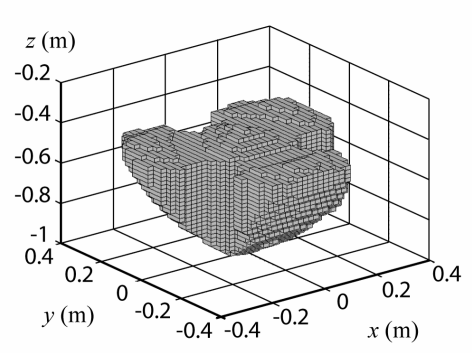

(a) $\phi = 0$ deg.

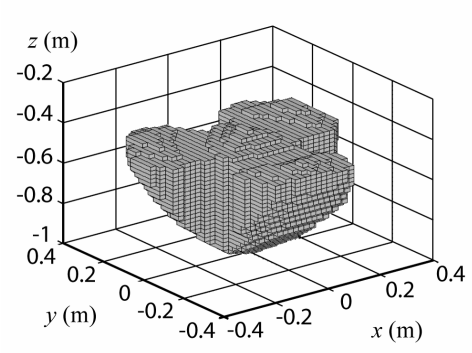

(b) $\phi = 10$ deg.

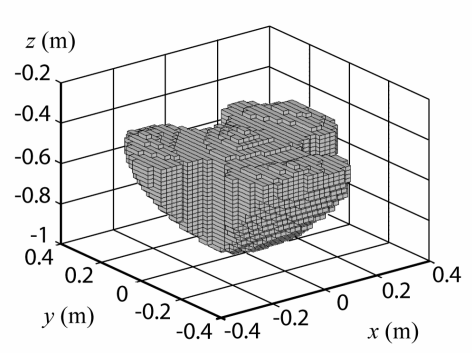

(c) $\phi = 20$ deg.

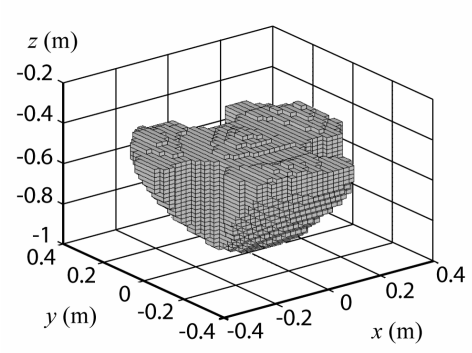

(d) $\phi = 30$ deg.

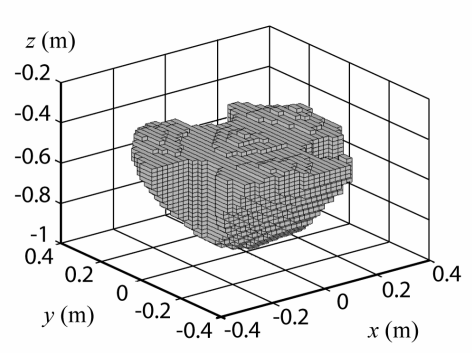

(e) $\phi = 40$ deg.

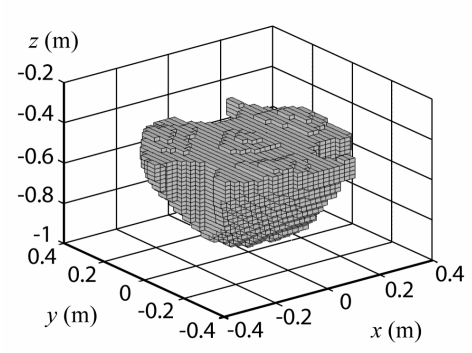

(f) $\phi = 50$ deg.

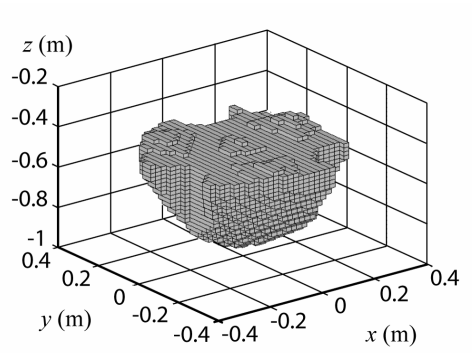

(g) $\phi = 60$ deg.

Figure 2.10. – Workspace of the prototype of PAMINSA.

Once we have chosen the lengths of the links, we must deal with the design of the different elements of the manipulator.

2.3.2. On the design of the prototype elements.

This section will give some information about the realization of our prototype.

The most important characteristic of the prototype is the following: the manipulator should be able to be displaced with at least 20 kg on the platform during quasistatic movements.

Please note that the aim of this prototype is to validate the design concept of PAMINSA manipulators. It is obvious that we would have designed an industrial version of the prototype differently, using more rigid links and other different manufactured components.

From our point of view, the key points in the realization of our prototype are the following elements:

- *the pantograph linkages* because they ensure the appropriate rigidity of the manipulator;
- *the passive slider* because the prismatic pairs are usually more complicated to design than the rotoid pairs and because, in our particular structure, even a small clearance in this joint would lead to the poor accuracy of the manipulator;
- *the vertical guides* of limbs B_iG_i because they must allow the actuation of the legs of the mechanism but must also ensure the passive movements of the vertical limbs;
- *the actuators* because the actuator for the vertical translations has to be powerful enough to carry the embedded payload and the actuators for the horizontal displacements must be accurate to ensure the correct behaviour of the manipulator during its movements.

The prototype designed using the above considerations is represented in figure 2.11. The key points of the design are detailed below.

So, let us begin with the design of the pantograph linkages.

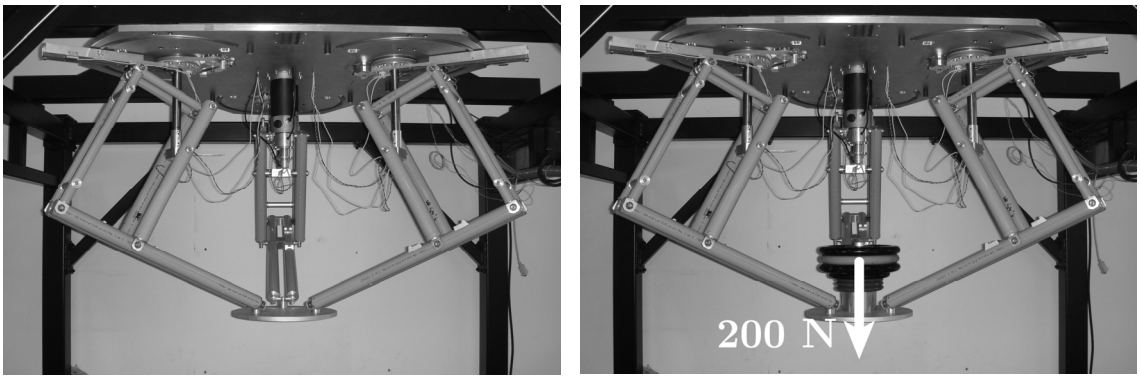

(a) with no payload. (b) with a payload of 200 N.

Figure 2.11. – Prototype of the PAMINSA manipulator.

2.3.2.1. Design of the pantograph linkages.

The optimal design of the pantograph linkages is an important challenge as they mainly ensure the correct rigidity of the robot.

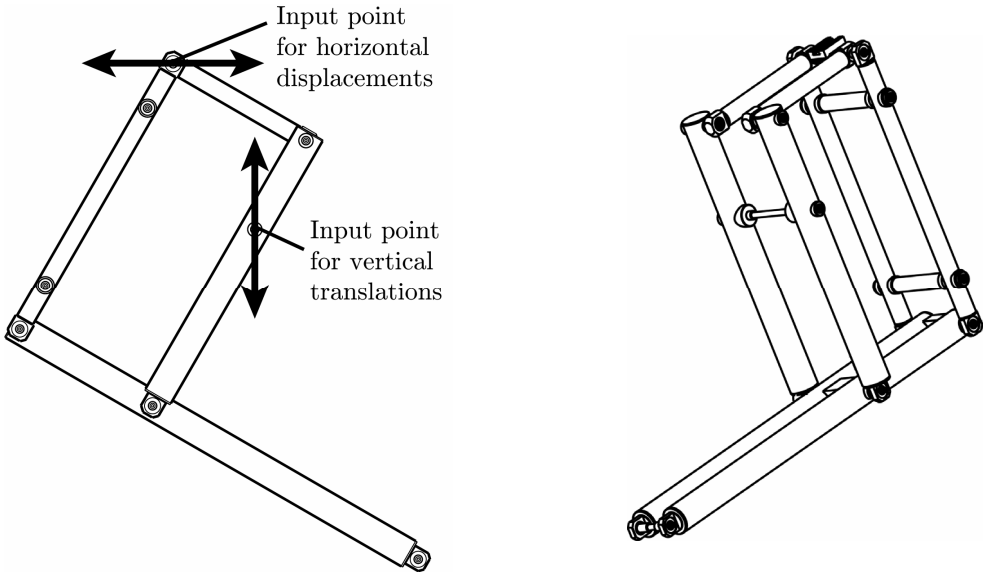

(a) planar view. (b) 3D view.

Figure 2.12. – CAD model of a pantograph linkage of the PAMINSA manipulator.

The pantograph linkages have been made with double hollow aluminium tubes of which thickness is equal to 1.5 mm (Fig. 2.12). Taking into account this consideration, the deformation of the structure under an embedded load of 20 kg is inferior to 1 mm.

While the rotational velocities of the axes of the pantograph linkages are quite slow (compared with cyclic mechanisms), they have been completed with bearings in order to avoid problems of clearance.

It is obvious that such a design is not optimal. To minimize the deformations of the structure, it would have been preferable to create pantograph linkages of which limbs are designed in order to resist flexure solicitations (Fig. 2.13). Moreover, from an industrial point of view, the numerous joints are not appealing and a less complicated design would have been more attractive. However, such a solution has been chosen with regards to cost and manufacturing time considerations.

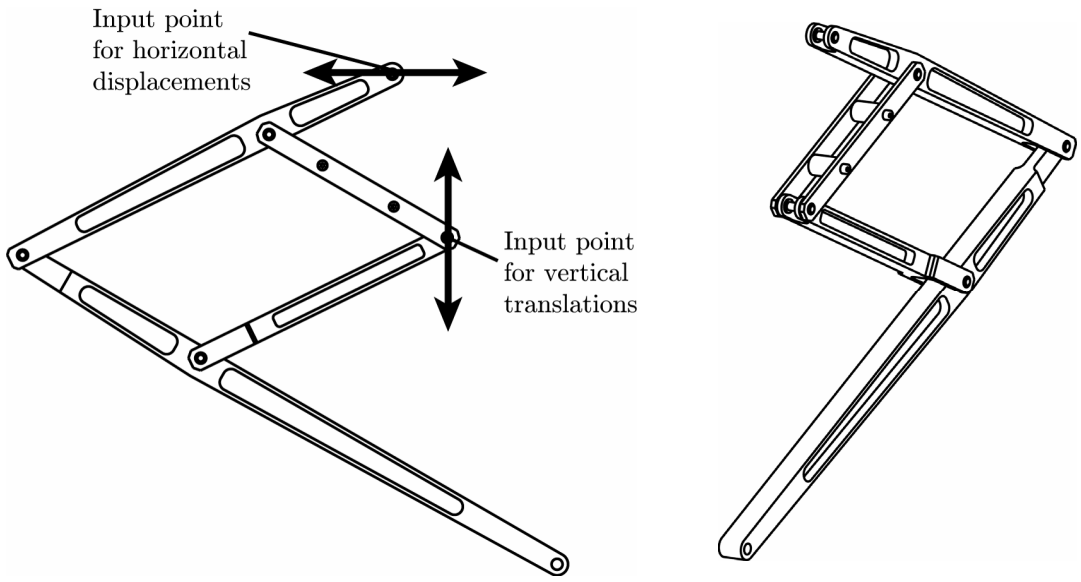

(a) planar view. (b) 3D view.

Figure 2.13. – CAD model of an optimized pantograph linkage.

2.3.2.2. Design of the passive prismatic pairs.

The passive sliders are perhaps the most important pairs of the mechanism because even a small clearance implies a positioning error of the pantograph linkage which leads to the poor accuracy of the controlled point of the platform. Moreover, each passive slider has to support a load equal to (1–k) times the load applied to the platform (due

to the pantograph properties). This is the reason why we have decided to use profile rail guides (Fig. 2.14).

Such profile rail guides are accuracy rolling bearings for linear movements. The contact with rails is made at two contact points. The use of circular balls allows absorbing deformations and leads to running modes without backlashes and clearances. Moreover, the small difference between the static and dynamic friction coefficients and the right response to a solicitation of the actuated system lead to a very high positioning accuracy. The references of the chosen guides are CSR SBM15.1.350L (running parallelism accuracy in operation: about 10 μm; friction coefficient: 0.005).

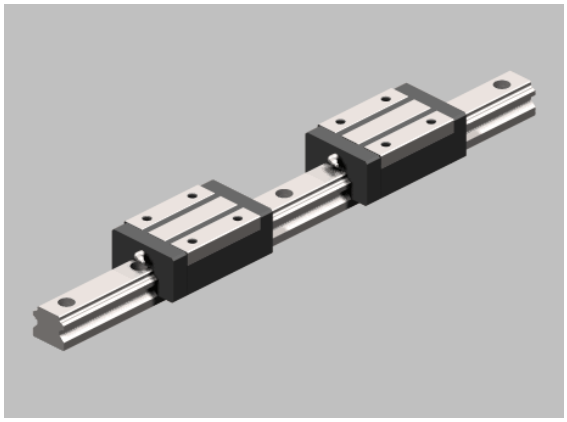

Figure 2.14. – CAD model of a profile rail guide.

2.3.2.3. Design of the guides of the vertical limbs B_iG_i.

The vertical guides must allow at the same time the actuation of the pantograph linkages by the rotary motors but also the passive translations and rotations of the vertical limbs B_iG_i.

The limbs B_iG_i will be manufactured with hollow steel tubes with a thickness of 4.7 mm, which will provide deformations superior to 0.1 mm under the small efforts applied on these elements.

In order to ensure the vertical translations of the limbs, we use plain bearings with high accuracy which will reduce the angular clearances. The plain bearings will be fixed to the actuation systems and will rotate at the same speed as the limbs B_iG_i which is preferable to avoid any lockage (Fig. 2.15).

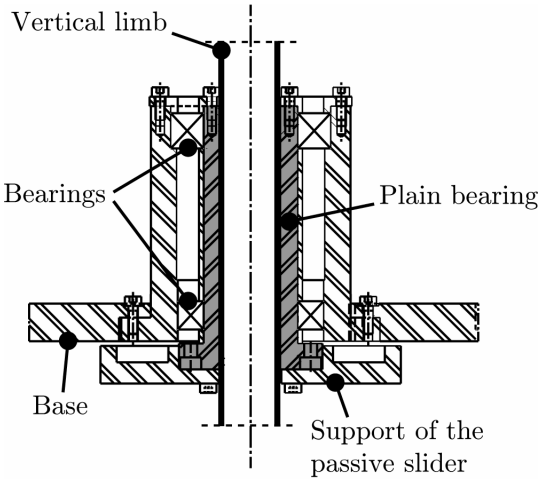

Figure 2.15. – Design of the guides of the vertical limbs.

2.3.2.4. Motorization for the horizontal displacements.

The displacements on the horizontal plane of the developed prototype are obtained by the use of three DC Harmonic Drive motors (ref. 3557 012 CR) connected at the legs by means of toothed-belt transmissions (Fig. 2.16).

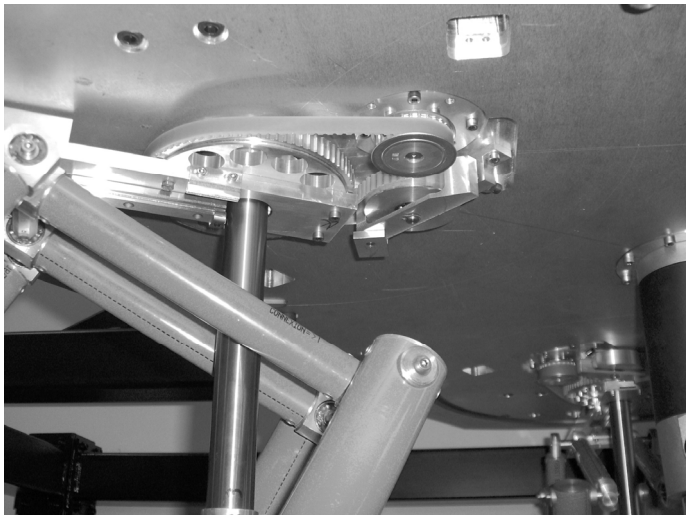

Figure 2.16. – Actuation system of each leg.

These motors have the following characteristics:

- gear ratio: 50;
- rated output torque: 3.5 N.m;
- rated input speed: 3500 $rad.min^{-1}$;
- transmission accuracy: < 1.5 arcmin;
- repeatability: $< \pm 0.1$ arcmin.

The choice of tooth-belt transmissions has been preferred to the use of gears because such a design solution is simple to use and it respects the desired characteristics for the velocities (quasistatic displacements) and effort transmission in the mechanism.

2.3.2.5. Motorization for the vertical translations.

The translations along the vertical axis are obtained by the use of one DC Parvex motor (ref. RX 320 D) connected to the legs by means of a ball-screw transmission. This actuated system has the following characteristics:

- ball-screw pitch: 10 mm;
- rated output torque: 1.1 N.m;
- rated input speed: 1300 $rad.min^{-1}$;
- encoder: 10000 steps.

The use of a DC motor with a ball-screw transmission for the vertical translations has been preferred to the use of hydraulic jacks or another actuation system because:

- a DC current generator is already necessary for the control of the 3 rotary actuators for the planar displacements;
- it is less constraining than an hydraulic system (an hydraulic pump should be added in order to pressurize the system and a DC motor needs less maintenance than an hydraulic device);
- a DC motor is strong enough to support the loads that we want to apply on the platform (20 kg).

In this section, we have presented the design considerations of the mechanical key points of our prototype. The next part will deal with the experimental validation of the design concept.

2.3.3. Experimental validation of the decoupling concept.

In order to validate the suggested design concept, we have measured the input torques/force of the actuators with a payload of 200 N applied on the platform (Fig. 2.11.b) and without this (Fig. 2.11.a) for the trajectory given in figure 2.17. The obtained results are presented in figure 2.18.

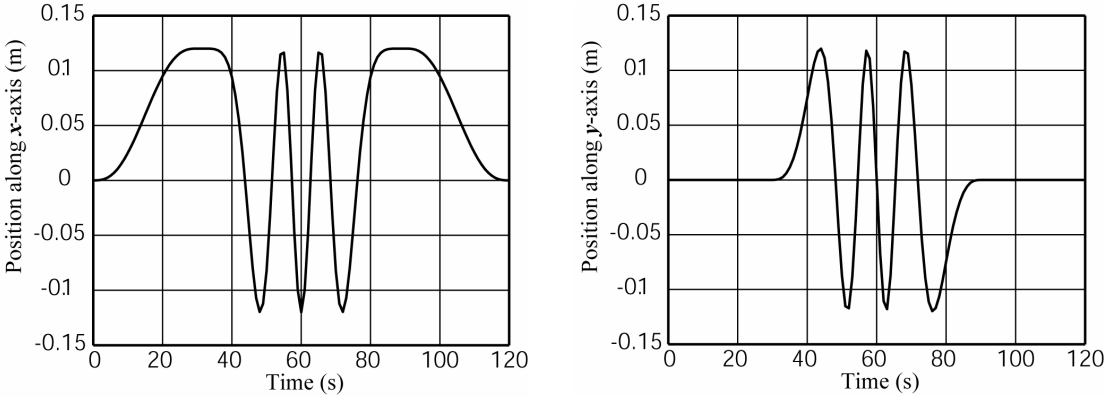

Figure 2.17. – Position of the platform for $z = -0.6$ m and $\phi = 0$ deg.

The analytical demonstrations (section 2.2) were validated by experimental tests. The curves with and without payload for the 3 rotating actuators (Fig. 2.18.a, b, c) are superposed. We can see that they are similar, i.e. the loads on these actuators are cancelled. The small differences might result from friction in the joints, manufacturing errors, elasticity of the links and tracking errors.

Regarding the vertical actuator (Fig. 2.18.d), it supports the payload and the increase in the input force is significant.

Thus, we can note that the obtained measures prove all theoretical results presented above.

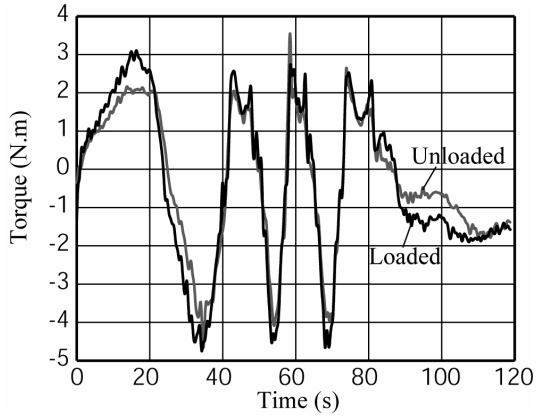

(a) Input torque of actuator M_1.

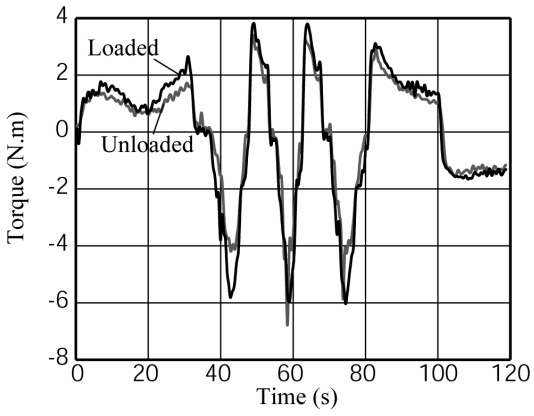

(b) Input torque of actuator M_2.

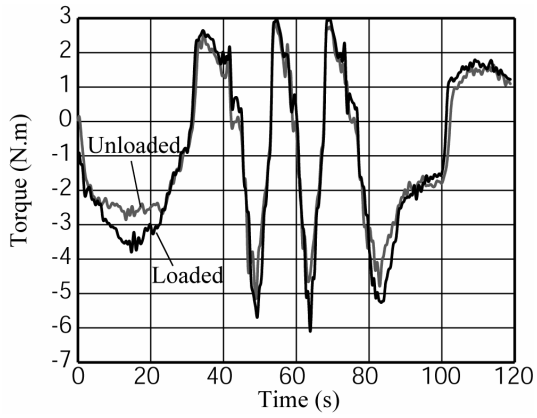

(c) Input torque of actuator M_3.

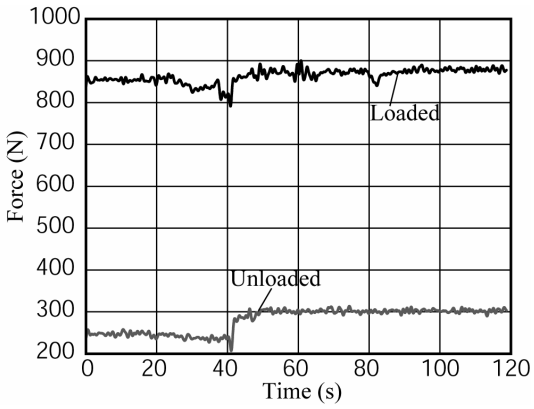

(d) Input force of actuator M_v.

Figure 2.18. – Input torques/effort on the actuators with and without an embedded load of 200 N.

2.4. Summary.

In this chapter, a new family of decoupled parallel manipulators is presented. This new family is based on the hand-operated systems approach. The structures are carried out with the use of pantograph linkages. Among the obvious advantages of such an approach, we may note:

- the decoupling of the control powers in two parts, making it possible to raise an important payload to a fixed altitude by powerful actuators and, then, to displace it on the horizontal plane by less powerful actuators;

- a great accuracy in the horizontal positioning because the payload can be locked in the horizontal plane by the mechanical architecture of the manipulator (in other words, if the position of the vertical actuator is fixed, the altitude of the platform cannot change);
- the cancellation of static loads on the rotating actuators which move the platform in the horizontal plane;
- the simplification of the vertical control based on linear input/output relationships.

First, different possible architectures with 4 DOF have been presented. It is shown that their control models can be divided between two parts: a model for the displacements in the horizontal plane and a model for the vertical translations. This approach can be systematized for manipulator from 3 to 6 DOF. Particularly, a new architecture with 3 fully-decoupled translatory motions is disclosed.

Then, the input efforts of a basic version of the PAMINSA with 4 DOF have been calculated using an energetic approach. It has been analytically shown that the load embedded on the platform does not produce any supplementary efforts on the actuators for the horizontal displacements.

Finally, a prototype of PAMINSA and experimental tests have been presented. It was shown that the experimental tests prove the validity of the suggested design concept.

The next step of the analysis of these new manipulators is the study of their kinematics, and particularly their singularities, because they may be the worst drawbacks of parallel manipulators.

Chapter 3

Singularity Analysis of PAMINSA Manipulators

This chapter presents the analysis of the singular configurations of PAMINSA manipulators of which planar equivalent models are the 3-RPR mechanisms.

In the first section, the singularity loci of PAMINSA manipulators from 3 to 6 DOF are determined by studying the degeneracy of the determinant of the Jacobian matrix of the manipulators. It is shown that the singular configurations of the manipulators are similar to those of the 3-RPR mechanisms.

In the second section, it is also shown that one particular case of singularity corresponds to an unusual type of self motion. Thus, the geometric conditions for such a type of self motion are derived by studying the degeneracy of the direct kinematic model and the global behaviour of the manipulators inside the gained degree of freedom is kinematically interpreted. A practical example is discussed and experimental validations, performed on the prototype of PAMINSA-4D3L, are presented.

The obtained results can be used to design manipulators without self motions, to optimize the singularity-free workspace of this type of robots and to choose the optimal architectures of PAMINSA manipulators.

3.1. Determination of the singularity loci.

From an industrial point of view, the complexity and the numerous occurrences of singular configurations seem to be the worst drawback of parallel robots because these configurations reduce the size of the workspace, which is already smaller than that of similarly-sized serial robots.

The singularity analysis has attracted the attention of several researchers and different studies have been published [Bandyopadhyay 2004] [Glazunov 1990] [Gosselin 1990] [Karouia 2005] [Ma 1992] [Merlet 1989] [Pernkopf 2002] [Saint-Onge 2000] [Wen 2003] [Wolf 2004] [Zhao 2005] [Zlatanov 1994]. [Zlatanov 1994] presented a method that can serve to identify the singularities of both passive and active chains via a study of the deficiency of the rank of an augmented non-square Jacobian matrix. However, this analysis is quite difficult and not useful for PAMINSA manipulators. The singularity analysis presented here is carried out in the Gosselin and Angeles approach [Gosselin 1990], based on the properties of the Jacobian kinematic matrices of the mechanical structure, i.e. when the Jacobian matrices relating the input velocities and the output velocities become rank deficient. Three types of singular configurations can be observed:

- Type 1 singularities are configurations where the platform loses a degree of freedom because the serial chain of one of the legs is singular;
- Type 2 singularities are configurations where an uncontrollable motion of the platform occurs;
- Type 3 singularities are configurations where both Type 1 and Type 2 singular configurations appear at the same time.

The singularity analysis presented here is devoted only to PAMINSA manipulators from 3 to 6 DOF of which planar equivalent models are 3-RPR mechanisms (table 2.2). Similar approaches could be used in order to find the singular configurations of the other types of PAMINSA architectures (table 2.1).

PAMINSA are parallel manipulators in which singular configurations can be separated into two cases: singularities of the pantograph linkage used as a leg and singularities of the simplified schematic representation of PAMINSA manipulators in which the pantograph mechanism is replaced by a PRPS chain (Fig. 3.1). The pair H'_i corresponds to the free translational displacement of both prismatic pair H_i and pantograph linkage (Fig. 3.2). The actuators M'_i and M'_{vi} correspond to actuators M_i and M_{vi} of which displacements are copied by the pantograph linkage. In PAMINSA manipulators, these singularities are not coupled and may be examined separately.

It may be noted that the singular configurations of pantograph linkage can be found via an analysis of the articulated parallelogram. They are well known and we shall not deal with them. The study below is devoted only to the singularities of the 3-PRPS parallel structure.

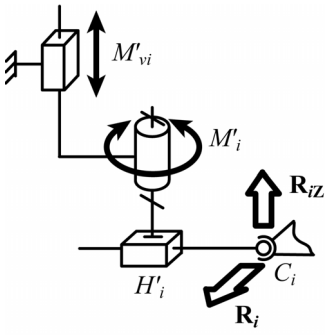

Figure 3.1. – Simplified schematic representation of the i-th actuated leg.

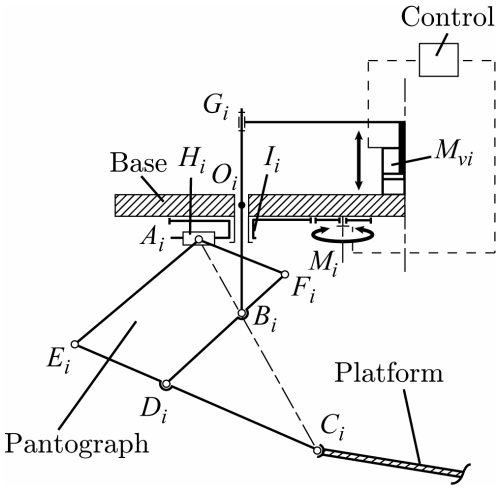

Figure 3.2. – Schematics of one leg of PAMINSA-6D3L.

3.1.1. Inverse kinematics of PAMINSA manipulators.

In the general case, the kinematics of the PAMINSA-6D3L describes the kinematics of the other manipulators (Fig. 3.2). The position of the centre of the platform P and the orientation of the moving frame $\{M\}$ (attached to the platform) in the base frame $\{B\}$ (the $\boldsymbol{x}$-axis of the base frame is collinear to $\mathbf{O_1O_2}$ and the $\boldsymbol{z}$-axis is vertical; its

origin is located at the centre of the circumscribed circle of $O_1O_2O_3$) are represented by $\mathbf{x} = [x,\ y,\ z,\ \phi,\ \psi,\ \theta]^T$ and the actuated variables by $\mathbf{q} = [q_1,\ q_2,\ q_3,\ q_{v1},\ q_{v2},\ q_{v3}]^T$. Parameters x, y, z, ϕ, ψ, θ represent the three components of the position of point P and the three rotation angles of the platform, respectively. The angles ϕ, ψ and θ can be obtained by expressing the directional cosines in terms of ***z-x-z*** Euler angles ϕ, ψ, θ. Parameters q_1, q_2, q_3, q_{v1}, q_{v2}, q_{v3} represent the rotations of the three legs of the manipulator about the ***z***-axis of frame $\{B\}$ and the vertical position of points B_i ($i = 1$, 2, 3), respectively. Note that for the analyses of PAMINSA-4, 5, 6D3L, $O_1O_2O_3$ and $C_1C_2C_3$ represent equilateral triangles.

The closed loop relations relative to $\mathbf{x}$ and $\mathbf{q}$ can be expressed as (for $i = 1$, 2, 3):

$$f_j = (x_{Ci} - x_{Oi})\sin q_i - (y_{Ci} - y_{Oi})\cos q_i = 0\,,\ \text{for } j = i \tag{3.1}$$

$$f_j = k\,q_{vi} - z_{Ci} = 0\,,\ \text{for } j = i + 3 \tag{3.2}$$

with

$$\begin{bmatrix} x_{Ci} \\ y_{Ci} \\ z_{Ci} \end{bmatrix} = \begin{bmatrix} x \\ y \\ z \end{bmatrix} + \mathbf{Rot}(\phi, \boldsymbol{z})\,\mathbf{Rot}(\psi, \boldsymbol{x})\,\mathbf{Rot}(\theta + \gamma_i, \boldsymbol{z}) \begin{bmatrix} R_{pl} \\ 0 \\ 0 \end{bmatrix} \tag{3.3}$$

where:

- k is the magnification factor of the pantograph;
- $x_{Oi} = R_b \cos\gamma_i$, $y_{Oi} = R_b \sin\gamma_i$ with $\gamma_i = (-5\pi/6, -\pi/6, \pi/2)$;
- R_{pl} and R_b are the platform and base radii respectively;
- $\mathbf{Rot}(\alpha, \boldsymbol{w})$ is the matrix representing the rotation of angle α ($\alpha = \phi, \psi, \theta + \gamma_i$) around the $\boldsymbol{w}$-axis of the intermediate frame ($\boldsymbol{w} = \boldsymbol{x}, \boldsymbol{y}$ and $\boldsymbol{z}$);
- x_{Ci}, y_{Ci} and z_{Ci} are the coordinates of point C_i.

3.1.2. Singularity analysis of the PAMINSA-6D3L.

Differentiating equations (3.1) and (3.2) with respect to time, we obtain a 6-dimensional system:

$$\mathbf{A}\,\mathbf{t} + \mathbf{B}\,\dot{\mathbf{q}} = \mathbf{0} \tag{3.4}$$

where:

- $\dot{\mathbf{q}} = [\dot{q}_1, \dot{q}_2, \dot{q}_3, \dot{q}_{v1}, \dot{q}_{v2}, \dot{q}_{v3}]^T$ is the vector of the derivatives of the articulated joints;
- $\mathbf{t}$ is the twist of the platform expressed in the base frame;

and:

$$\mathbf{B} = \begin{bmatrix} \rho_1 & 0 & 0 & 0 & 0 & 0 \\ & \rho_2 & 0 & 0 & 0 & 0 \\ & & \rho_3 & 0 & 0 & 0 \\ & & & k & 0 & 0 \\ & & & & k & 0 \\ sym & & & & & k \end{bmatrix} \tag{3.5}$$

$$\mathbf{A} = \begin{bmatrix} \sin q_1 & -\cos q_1 & 0 & -z_{PC1}\cos q_1 & -z_{PC1}\sin q_1 & -\mathbf{PC_1}^T\mathbf{d_1} \\ \sin q_2 & -\cos q_2 & 0 & -z_{PC2}\cos q_2 & -z_{PC2}\sin q_2 & -\mathbf{PC_2}^T\mathbf{d_2} \\ \sin q_3 & -\cos q_3 & 0 & -z_{PC3}\cos q_3 & -z_{PC3}\sin q_3 & -\mathbf{PC_3}^T\mathbf{d_3} \\ 0 & 0 & -1 & y_{PC1} & -x_{PC1} & 0 \\ 0 & 0 & -1 & y_{PC2} & -x_{PC2} & 0 \\ 0 & 0 & -1 & y_{PC3} & -x_{PC3} & 0 \end{bmatrix} \tag{3.6}$$

with $\rho_i = \sqrt{(x_{Ci} - x_{Oi})^2 + (y_{Ci} - y_{Oi})^2}$, $\mathbf{PC}_i = [x_{PCi}, y_{PCi}, z_{PCi}]^T = [x_{Ci} - x, y_{Ci} - y, z_{Ci} - z]^T$ and $\mathbf{d}_i = [\cos q_i \quad \sin q_i \quad 0]^T$ (for $i = 1, 2, 3$).

Singularities of parallel manipulators appear when matrices $\mathbf{A}$ and $\mathbf{B}$ are rank-deficient. We will deal only with the singularities of Type 1 and 2. Type 3 singularities are a mix of both Type 1 and 2 singular configurations.

Examining matrix $\mathbf{B}$ of the PAMINSA with 6 DOF, Type 1 singularities appears when:

$$\det(\mathbf{B}) = k^3 \, \rho_1 \, \rho_2 \, \rho_3 = 0 \, . \tag{3.7}$$

This expression is achieved when ρ_i is equal to 0 ($i = 1, 2, 3$), i.e. points O_i, B_i and C_i are aligned. In such a configuration, one rotation of the input link M_i cannot bring to the displacement of the platform (Fig. 3.3).

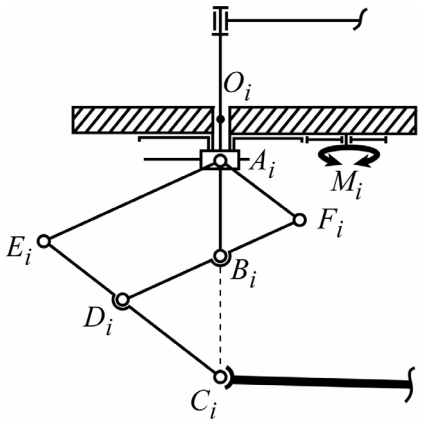

Figure 3.3. – Example of Type 1 singularity.

Type 2 singularities appear when $\det(\mathbf{A}) = 0$. Examining matrix $\mathbf{A}$ of the PAMINSA with 6 DOF, it appears that its determinant is a product of two factors:

$$\det(\mathbf{A}) = \det(\mathbf{A_1})\det(\mathbf{A_2}) \tag{3.8}$$

where

$$\mathbf{A_1} = \begin{bmatrix} -1 & y_{PC1} & -x_{PC1} \\ -1 & y_{PC2} & -x_{PC2} \\ -1 & y_{PC3} & -x_{PC3} \end{bmatrix},\ \mathbf{A_2} = \begin{bmatrix} \sin q_1 & -\cos q_1 & -\mathbf{PC_1}^T\mathbf{d_1} \\ \sin q_2 & -\cos q_2 & -\mathbf{PC_2}^T\mathbf{d_2} \\ \sin q_3 & -\cos q_3 & -\mathbf{PC_3}^T\mathbf{d_3} \end{bmatrix}. \tag{3.9}$$

Factorizing the determinant of matrix $\mathbf{A_1}$, it is possible to obtain:

$$\det(\mathbf{A_1}) = \cos\psi \tag{3.10}$$

This means that, if the inclination angle ψ is equal to $\pm\pi/2$, the rotation about the axis $\boldsymbol{x}$ of angle ψ is impossible and small rotations of the platform are allowed (Fig. 3.4.a).

The study of $\det(\mathbf{A_2})$ is much more interesting. One can see that the matrix $\mathbf{A_2}$ is composed of the planar components of the wrenches $\mathbf{R}_i$ [Dimentberg 1965] of which directions are located in the horizontal plane and which are perpendicular to the directions of the passive prismatic pairs (Fig. 3.1). Therefore, the PAMINSA-6D3L will have the same Type 2 singularities as the 3-RPR manipulator [Bonev 2003b].

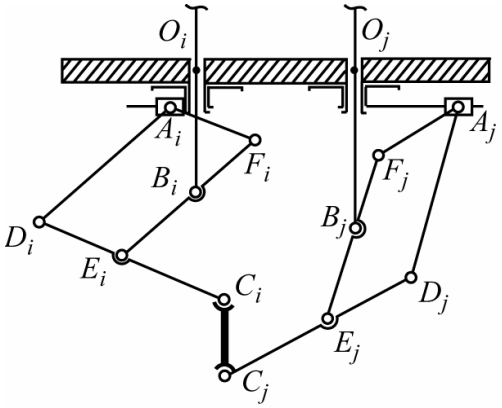

(a) singular configuration when $\psi = \pm\pi/2$, planar front view of the manipulator.

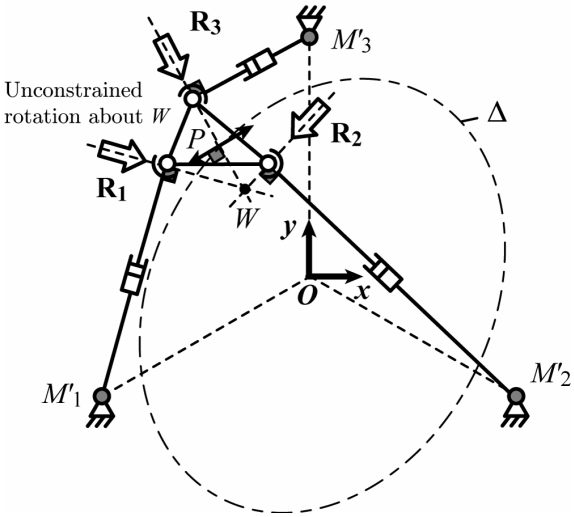

(b) singular configuration when $\Delta = 0$, top view of the 3-PRPS manipulator.

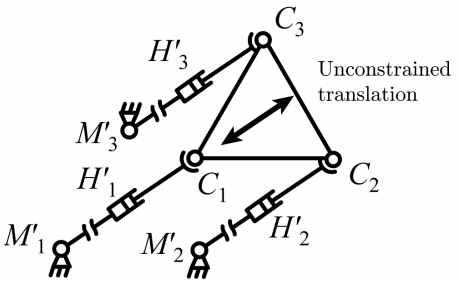

(c) singular configuration when $\rho_i = +\infty$, top view of the 3-PRPS manipulator.

Figure 3.4. – Example of Type 2 singularity for PAMINSA-4, 5, 6D3L.

Factorizing the determinant of matrix $\mathbf{A_2}$, one can obtain:

$$\det(\mathbf{A_2}) = 27\, R_{pl}^3\, \Delta / (8\rho_1\rho_2\rho_3) \tag{3.11}$$

Thus, $\det(\mathbf{A_2}) = 0$ if:

- for any fixed altitude, the platform is on a conic $\Delta = 0$ located in the horizontal plane. The coefficients of Δ *only* depend on the orientation angles of the

platform and are given in appendix B. Such a configuration appears when the three wrenches $\mathbf{R}_i$ intersect a unique line perpendicular to the horizontal plane and passing through the point W (Fig. 3.4.b) [Bonev 2003b]. In such a case, this line is the instantaneous axis of rotation of the moving plate;

- the length ρ_1, ρ_2 or ρ_3 tends to $+\infty$, what means that the legs of the manipulator are parallel. Thus, the platform is able to translate along the direction of the passive prismatic pairs H'_i (Fig. 3.4.c).

Please note that the expressions of det($\mathbf{A}$) and det($\mathbf{B}$) do not depend on the altitude z of the platform.

3.1.3. Singularity analysis of the PAMINSA-5D3L.

It can be shown that the PAMINSA with 5 DOF can be assimilated to a PAMINSA with 6 DOF of which first two linear actuators have the same displacements. Thus, angle θ is equal to 0. To find its singularity loci, these constraints have to be introduced in the expressions of the determinant of matrices $\mathbf{A}$ and $\mathbf{B}$.

As for the previous case, the manipulator is in Type 1 singularity when ρ_i is equal to 0 (i = 1, 2, 3), i.e. when points O_i, B_i and C_i are aligned. Furthermore, the manipulator is in Type 2 singularity when:

- the inclination angle ψ is equal to $\pm\pi/2$. This case corresponds to figure 3.4.a;
- for any fixed altitude, the platform is on a conic $\Lambda = 0$ located in the horizontal plane. The coefficients of Λ *only* depend on the orientation angles ϕ and ψ of the platform. Their expressions are given at appendix B. This case corresponds to figure 3.4.b;
- the length ρ_1, ρ_2 or ρ_3 tends to $+\infty$. This case corresponds to figure 3.4.c.

The kinematic interpretation of these singularities is the same as for the previous manipulator.

3.1.4. Singularity analysis of the PAMINSA-4D3L.

Similarly to the previous case, the PAMINSA with 4 DOF can be assimilated to a PAMINSA with 6 DOF of which linear actuators have the same displacements. Thus, angles ψ and θ are equal to 0. These new constraints have to be introduced in the expressions of the determinant of matrices **A** and **B**.

From this point, we shall not deal with the Type 1 singularities because, for the whole studied PAMINSA structures, they are not different from the previous manipulators. So, the Type 2 singularities appear when:

- the angle ϕ is equal to $\pm \cos^{-1}(R_{pl} / R_b)$ (Fig. 3.4.b);
- the length ρ_1, ρ_2 or ρ_3 tends to $+\infty$ (Fig. 3.4.c).
- for any fixed altitude, the platform is situated on a circle located in the horizontal plane, of which radius depends on angle ϕ (Fig. 3.4.b). The expression of this circle is:

$$x^2 + y^2 = R_b^2 + R_{pl}^2 - 2\,R_{pl}\,R_b \cos\phi \tag{3.12}$$

3.1.5. Singularity analysis of the PAMINSA-4D3L*.

The PAMINSA-4D3L* can be assimilated to a PAMINSA with 5 DOF of which two of the legs stay parallel. Thus, angles ϕ and θ are equal to 0. Moreover, the base triangle must not be equilateral.

Its Type 2 singularities appear when:

- the inclination angle ψ is equal to $\pm\pi/2$. This case corresponds to figure 3.4.a;
- the three legs are parallel, which corresponds to $q_1 = q_3 + n\,\pi$ $(n = 0, 1, 2, \ldots)$ (Fig. 3.5.a). In such a configuration, the manipulators gains one self motion of translation along the passive prismatic guides;
- the three wrenches $\mathbf{R}_i$ intersect in the same point, which will appear when $q_1 = \pm\,\pi/2$ (Fig. 3.5.b). In such a case, the vertical line passing through W is the instantaneous axis of rotation of the moving plate.

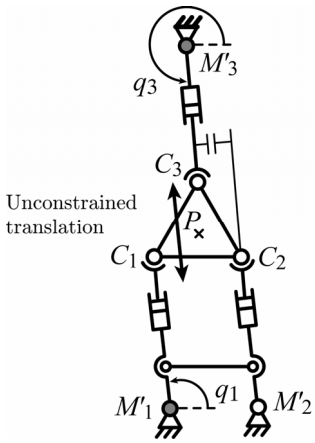

(a) singular configuration when $q_1 = q_3 + n\pi$ $(n = 0, 1, 2, \ldots)$, top view of the 3-PRPS manipulator.

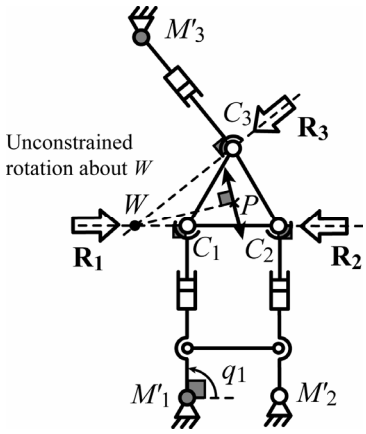

(b) singular configuration when $q_1 = \pm\pi/2$, top view of the 3-PRPS manipulator.

Figure 3.5. – Example of Type 2 singularity for PAMINSA-3, 4D3L*.

3.1.6. Singularity analysis of the PAMINSA-3D3L*.

The PAMINSA-3D3L* can be assimilated to a PAMINSA-4D3L* of which all linear actuators have the same displacements. Thus, angles ϕ, ψ and θ are equal to 0. Therefore its Type 2 singularities appear when:

- the three legs are parallel, which corresponds to $q_1 = q_3 + n\pi$ $(n = 0, 1, 2, \ldots)$ (Fig. 3.5.a);
- the three wrenches $\mathbf{R}_i$ intersect in the same point, which will appear when $q_1 = \pm\pi/2$ (Fig. 3.5.b).

3.1.7. Singularity analysis of the PAMINSA-4D2L.

This manipulator is a bit different from the others. However, the screw theory will help us to solve the problem of its singular configurations. Geometrically, it is easy to see that its Type 2 singularities appear when the 3 wrenches $\mathbf{R}_i$ intersect in one point (obligatorily J_1), i.e. when $q_3 = \phi \pm \pi/2$ (Fig. 3.6). The unconstrained motion corresponds to small rotations of the platform about point J_1.

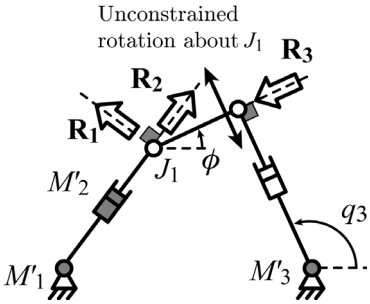

Figure 3.6. – Example of Type 2 singularity for PAMINSA-4D2L.

Thus, in this part, we have found the singular configurations of the family of PAMINSA manipulators of which planar equivalent models are the 3-RPR structures. However, with the presented approach, it is not possible to characterize the true nature of each kind of Type 2 singular configuration (infinitesimal or finite gained motion). It will be shown in the next part that we need to study the degeneracy of the direct geometric model in order to fill in this gap.

3.2. The self motions of PAMINSA manipulators.

We have just seen that Type 2 singular configurations can be divided into two classes, depending on the nature of the gained degree(s) of freedom, being either infinitesimal or finite, i.e. self motion. However, merely studying the Jacobian, one cannot identify the nature of Type 2 singularities.

Symmetry and, more precisely, design conditions that simplify the generally too complex direct kinematics of parallel robots are often privileged by robot designers. Unfortunately, such design conditions usually lead to self motions, which are certainly the worst type of singularity. Furthermore, as we shall show in this section, self motions also occur in unsymmetrical seemingly general designs without simplified direct kinematic models. Hence, it is essential that such self motions be well understood in order to be avoided.

Several papers discuss the existence of self motions in parallel robots. Not surprisingly, most of them deal with the Gough-Stewart platform, of which direct kinematic model leads to as much as 40 real solutions, for a relatively general design. Design conditions simplifying the direct kinematics of Gough-Stewart platforms, and

subsequently leading to self motions, are given in [Husty 1994] [Husty 2000] [Karger 1998a] [Karger 2001] [Karger 2003] [Wohlhart 2003]. A classification of all self motions of the Stewart-Gough platform is presented in [Karger 1998a]. It is shown that the self motions can be translations, pure rotations, generalized screw motions, motions equivalent to the displacements of spherical four-bar mechanisms, or more complex spatial motions.

The Stewart-Gough platform is not the only parallel robot with self motions. A few other parallel robots having self motions have also been studied. For example, in [Bonev 2006], it is shown that all singularities of the special 3-RRR spherical parallel robot, known as the Agile Eye, are self motions. The analysis of self mobility of spatial 5R closed-loop mechanisms with one degree of freedom are presented in [Karger 1998b]. Reference [Bandyopadhyay 2004] discusses the determination of generalized analytical expressions for the analysis of self motions and presents several examples for both planar and spatial mechanisms with legs composed of R joints.

Recently, the self motions of a particular design of a 3-RPR planar parallel robot with congruent equilateral base and platform were studied in [Chablat 2006], mainly from a theoretical point of view. This section basically generalizes this study and will analyse the self motions of general 3-RPR planar parallel robots, which have the same kinematics and singularities as the PAMINSA manipulators studied above.

3.2.1. Direct kinematics of the 3-RPR planar parallel manipulator.

We have already said we need more information for characterizing the complete kinematic behaviour of the robot inside Type 2 singular configuration. This can be found by studying the degeneracy of the direct kinematic model of the manipulator.

The following analysis is based on the schematics of the robot shown in Fig. 3.7. The revolute joints M'_i are fixed on the base and are actuated. Each leg is composed of one passive prismatic joint, placed between points M'_i and K_i, and of one passive revolute joint J_i, connected to the mobile platform.

We consider that we control the position $[x, y]^T$ of point P of the mobile platform and the orientation ϕ of the platform. The active joints variables are the angles q_i ($i = 1, 2, 3$). The origin of the base frame is chosen at point O. Points O and P are located at the centres of the circumscribed circles of triangles $M'_1M'_2M'_3$ and $J_1J_2J_3$, respectively (Fig. 3.8). Finally, let $\rho_i = M'_iK_i$ and $l_i = K_iJ_i$ (an offset).

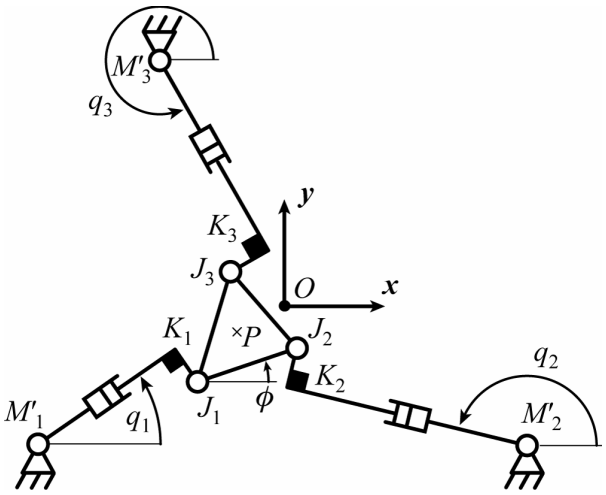

Figure 3.7. – Schematic representation of the studied 3-RPR planar parallel robot**.**

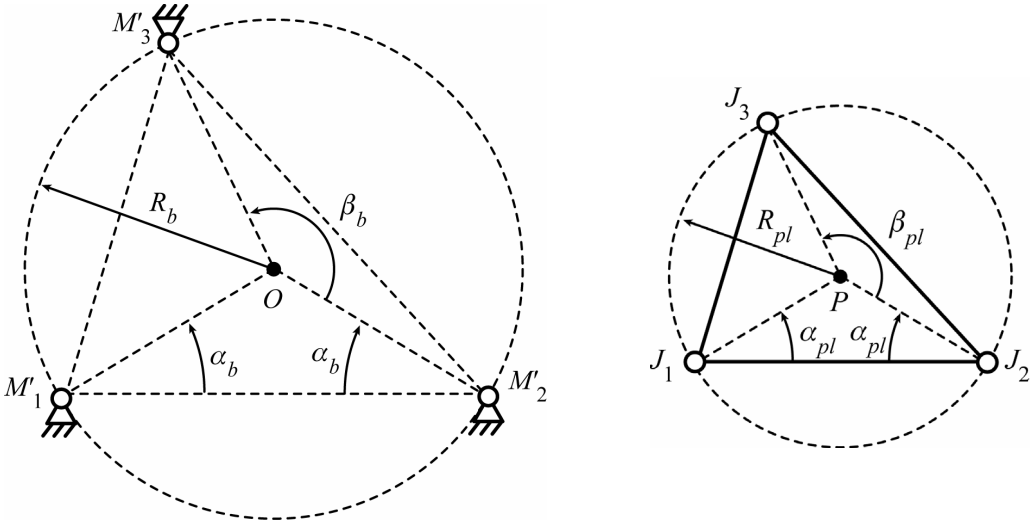

(a) fixed base (b) mobile platform

Figure 3.8. – Parameterisation of the base and platform triangles.

Thus, it is possible to express the position of points M'_i and J_i as:

$$\mathbf{OM'}_i = \begin{bmatrix} x_{M'i} \\ y_{M'i} \end{bmatrix} = R_b \begin{bmatrix} \cos\gamma_i \\ \sin\gamma_i \end{bmatrix}, \ \mathbf{OJ}_i = \begin{bmatrix} x_{Ji} \\ y_{Ji} \end{bmatrix} = \begin{bmatrix} x \\ y \end{bmatrix} + R_{pl} \begin{bmatrix} \cos(\phi + \delta_i) \\ \sin(\phi + \delta_i) \end{bmatrix}, \quad (3.13)$$

where $\gamma_i = (\alpha_b + \pi, -\alpha_b, -\alpha_b + \beta_b)$ and $\delta_i = (\alpha_{pl} + \pi, -\alpha_{pl}, -\alpha_{pl} + \beta_{pl})$.

From these expressions and referring to [Bonev 2003b], one can determine the closure equations of the system:

$$\mathbf{OJ}_i - \mathbf{OK}_i = \begin{bmatrix} x_{Ji} - x_{M'i} - \rho_i \cos q_i \\ y_{Ji} - y_{M'i} - \rho_i \sin q_i \end{bmatrix} = l_i \begin{bmatrix} -\sin q_i \\ \cos q_i \end{bmatrix}. \tag{3.14}$$

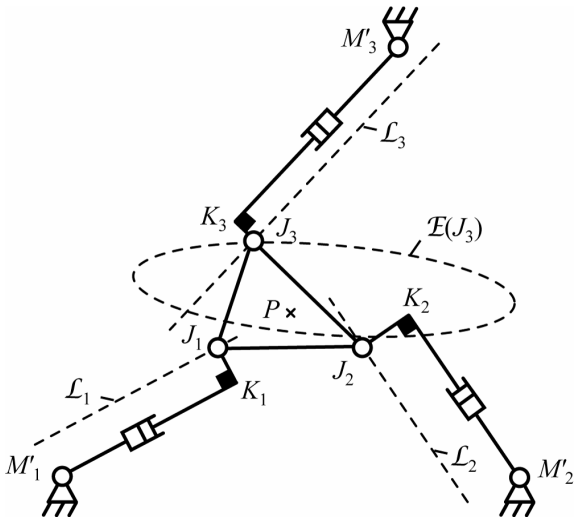

Figure 3.9. – Geometric interpretation of the direct kinematics.

It was shown in [Merlet 1996] that the solution of the direct kinematics of a 3-RPR planar parallel robot is equivalent to finding the intersection points between an ellipse and a line, but no analytical expressions are given. Let us dismount the revolute joint at J_3. For given active joint variables q_1 and q_2, points J_1 and J_2 are constrained to move along two lines, $\mathcal{L}_1$ and $\mathcal{L}_2$, respectively, and the mobile platform undergoes a Cardanic movement [Sekulie 1998] [Tischler 1998] (Fig. 3.9). As a result, any points Q from the mobile platform, including P and J_3, describes a curve $\mathcal{E}(Q)$, which can be an ellipse, two parallel lines or a doubly-traced line segment. Thus, the direct kinematics can be solved by finding the intersection points between the curve $\mathcal{E}(J_3)$ and the line $\mathcal{L}_3$.

Let us now derive the expression of the elliptic curve $\mathcal{E}(J_3)$. It is possible to write the following closure equation:

$$\mathbf{OJ_3} = \mathbf{OM'_1} + \mathbf{M'_1 K_1} + \mathbf{K_1 J_1} + \mathbf{J_1 J_3}\,. \tag{3.15}$$

This yields the following expression:

$$\mathbf{OJ_3} = \begin{bmatrix} x_{J3} \\ y_{J3} \end{bmatrix} = \begin{bmatrix} x_{M'1} \\ y_{M'1} \end{bmatrix} + \rho_1 \begin{bmatrix} \cos q_1 \\ \sin q_1 \end{bmatrix} + l_1 \begin{bmatrix} -\sin q_1 \\ \cos q_1 \end{bmatrix} + 2R_{pl} \cos\left(\frac{\beta_{pl}}{2} - \alpha_{pl}\right) \begin{bmatrix} \cos\left(\frac{\beta_{pl}}{2} + \phi\right) \\ \sin\left(\frac{\beta_{pl}}{2} + \phi\right) \end{bmatrix}. \tag{3.16}$$

In this expression, all parameters are known except ρ_1 and ϕ. However, they are dependent on each other. Without loss of generality, we chose the parameter ϕ as independent variable and express ρ_1 as a function of ϕ, using the following closure equation:

$$\mathbf{M'_1 M'_2} = \mathbf{M'_1 K_1} + \mathbf{K_1 J_1} + \mathbf{J_1 J_2} + \mathbf{J_2 K_2} + \mathbf{K_2 M'_2}\,. \tag{3.17}$$

Developing this relation, we obtain:

$$\begin{bmatrix} x_{M'2} - x_{M'1} \\ y_{M'2} - y_{M'1} \end{bmatrix} = \rho_1 \begin{bmatrix} \cos q_1 \\ \sin q_1 \end{bmatrix} + l_1 \begin{bmatrix} -\sin q_1 \\ \cos q_1 \end{bmatrix} + 2R_{pl} \cos\alpha_{pl} \begin{bmatrix} \cos\phi \\ \sin\phi \end{bmatrix} - l_2 \begin{bmatrix} -\sin q_2 \\ \cos q_2 \end{bmatrix} - \rho_2 \begin{bmatrix} \cos q_2 \\ \sin q_2 \end{bmatrix}. \tag{3.18}$$

Expressing ρ_1 and ρ_2 as a function of ϕ from (3.18), we obtain:

$$\rho_j = a_{j1} + a_{j2}\cos\phi + a_{j3}\sin\phi\,, \quad (j = 1,\ 2) \tag{3.19}$$

where the expressions for a_{ji} are given in appendix C. Reintroducing expression (3.19) in equation (3.16), we find the following relation:

$$\mathbf{OJ_3} = \begin{bmatrix} x_{J3} \\ y_{J3} \end{bmatrix} = \begin{bmatrix} b_{11} + b_{12}\cos\phi + b_{13}\sin\phi \\ b_{21} + b_{22}\cos\phi + b_{23}\sin\phi \end{bmatrix}, \tag{3.20}$$

where b_{ji} $(j = 1,\ 2)$ are given in appendix C.

Thus, for any fixed input parameters q_i, we have found in (3.20) the parametric expression of the elliptic curve $\mathcal{E}(J_3)$ depending on the orientation ϕ of the platform. Furthermore, we know that point J_3 belongs to line $\mathcal{L}_3$, of which expression is:

$$y = \tan q_3(x + l_3 \sin q_3 - x_{M'3}) + y_{M'3} + l_3 \cos q_3 . \tag{3.21}$$

Introducing (3.20) into (3.21), we find:

$$0 = \sin q_3(x_{J3} + l_3 \sin q_3 - x_{M'3}) + \cos q_3(y_{M'3} + l_3 \cos q_3 - y_{J3}) . \tag{3.22}$$

Developing (3.22),

$$c_1 + c_2 \cos\phi + c_3 \sin\phi = 0 , \tag{3.23}$$

where c_i are given in appendix C. Thus, from (3.23), it is possible to find the solution for ϕ:

$$\phi = 2\tan^{-1}\left(\frac{-c_3 \pm \sqrt{c_3^2 - c_1^2 + c_2^2}}{c_1 - c_2} \right). \tag{3.24}$$

Note that this solution is not unique and corresponds to the two assembly modes of the robot. Finally, it is possible to find the expression for the position using the following closure equation:

$$\mathbf{OP} = \mathbf{OM'_1} + \mathbf{M'_1 K_1} + \mathbf{K_1 J_1} + \mathbf{J_1 P} , \tag{3.25}$$

which yields:

$$\mathbf{OP} = \begin{bmatrix} x \\ y \end{bmatrix} = \begin{bmatrix} x_{M'1} \\ y_{M'1} \end{bmatrix} + \rho_1 \begin{bmatrix} \cos q_1 \\ \sin q_1 \end{bmatrix} + l_1 \begin{bmatrix} -\sin q_1 \\ \cos q_1 \end{bmatrix} + R_{pl} \begin{bmatrix} \cos(\phi + \alpha_{pl}) \\ \sin(\phi + \alpha_{pl}) \end{bmatrix}. \tag{3.26}$$

In a Type 2 singularity, the lines normal to the directions of the prismatic joints and passing through points J_i are concurrent or parallel (Fig. 3.10) [Bonev 2003b].

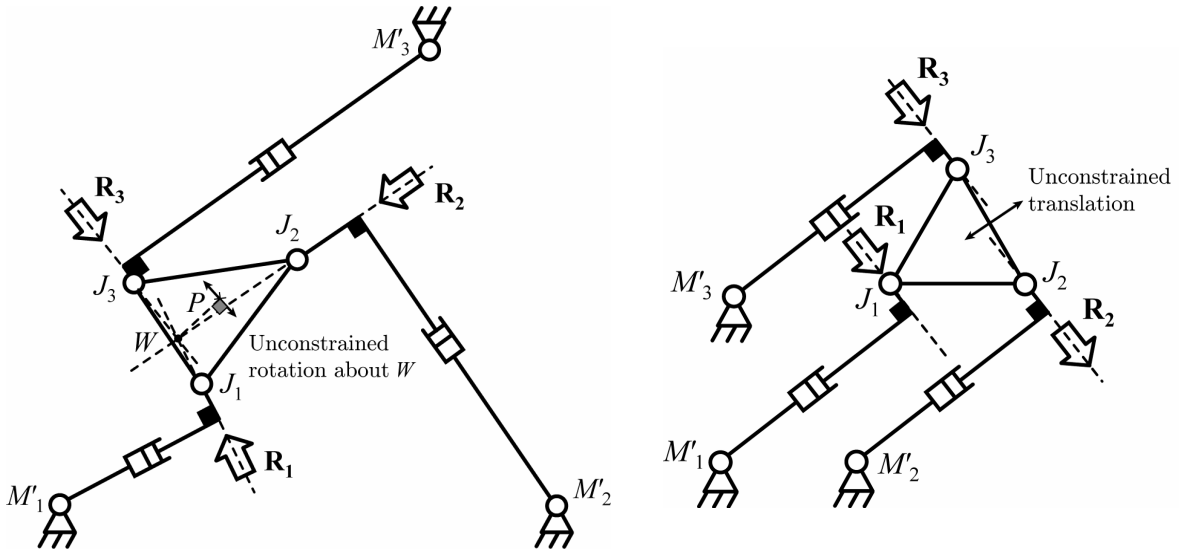

(a) Infinitesimal rotation about W

(b) Finite translation (self motion) along the direction of the prismatic joints

Figure 3.10. – Type 2 singularities of the 3-RPR manipulator.

These lines coincide with the direction of the forces $\mathbf{R}_i$ applied to the platform by the actuators.

However, we need more information for characterizing the complete kinematic behaviour of the robot inside such a singular configuration. This can be found by studying the degeneracy of the direct kinematic model. Thus, there are Type 2 singularities if:

- $\mathcal{E}(J_3)$ is an ellipse tangent to $\mathcal{L}_3$: in such a case, the directions of the three forces $\mathbf{R}_i$ intersect in one point W, and the robot gains one infinitesimal rotation about this point (Fig. 3.10.a);
- $\mathcal{L}_1$, $\mathcal{L}_2$ and $\mathcal{L}_3$ are parallel and $\mathcal{E}(J_3)$ degenerates to two lines parallel to $\mathcal{L}_1$ and $\mathcal{L}_2$ (and $\mathcal{L}_3$): in such a case, the directions of the three forces $\mathbf{R}_i$ are parallel and the manipulator gains one self motion of translation (Fig. 3.10.b);
- $\mathcal{E}(J_3)$ degenerates to a doubly-traced line segment parallel to $\mathcal{L}_3$ (this case will be discussed in the following section).

3.2.2. Analysis of self motions.

The self motions are certainly the worst type of singularity a parallel robot could cross. If the robot enters such a singularity, as there are infinitely many possible poses for the same active-joint variables, the information on the pose of the platform is lost. As a result, it may be impossible to exit such a singularity (even with external help such as inertia) and the robot may break. For the robot under study, one could think that such a singularity exists only when $\mathcal{L}_1$, $\mathcal{L}_2$ and $\mathcal{L}_3$ are parallel. In this case, we observe the apparition of a self motion of translation, corresponding to the case shown in Fig. 3.10.b.

It turns out that a second case of self motion will appear when $\mathcal{E}(J_3)$ degenerates into a doubly traced line segment parallel to $\mathcal{L}_3$. This case corresponds to a Cardanic self motion (Fig. 3.11).

Note that such a singularity is a particular case of the singular configurations where the three forces $\mathbf{R}_i$ intersect at one point W (Fig. 3.10.a).

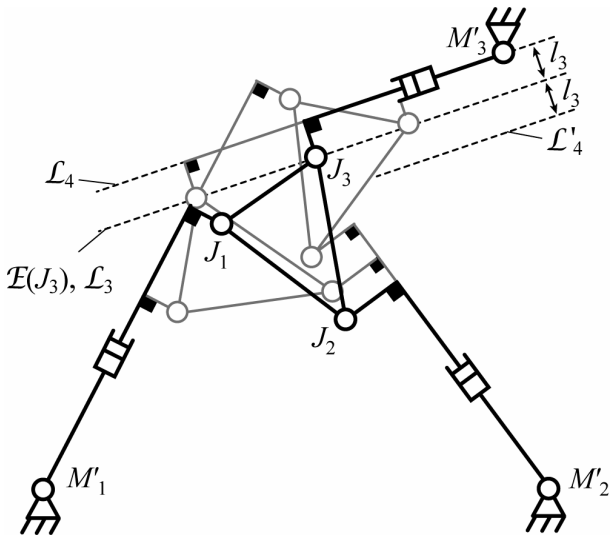

Figure 3.11. – Cardanic self motion.

3.2.2.1. Design conditions leading to Cardanic self motions.

We have to find the geometric conditions which lead to Cardanic self motions. Thus, $\mathcal{E}(J_3)$ degenerates into a doubly-traced line segment if y_{J3} is linearly dependant on x_{J3} for $\sin(q_1 - q_2) \neq 0$. Rewriting equation (3.20), one can obtain:

$$\mathbf{OJ_3} = \begin{bmatrix} x_{J3} \\ y_{J3} \end{bmatrix} = \begin{bmatrix} b_{11} \\ b_{21} \end{bmatrix} + \mathbf{b} \begin{bmatrix} \cos\phi \\ \sin\phi \end{bmatrix}, \text{ where } \mathbf{b} = \begin{bmatrix} b_{12} & b_{13} \\ b_{22} & b_{23} \end{bmatrix}. \tag{3.27}$$

$\mathcal{E}(J_3)$ will degenerate to a line if the determinant of matrix $\mathbf{b}$ vanishes. This would be the case if:

$$q_1 = q_2 + \varepsilon_{pl}, \text{ where } \varepsilon_{pl} = \alpha_{pl} \pm \pi/2. \tag{3.28}$$

Thus, for such a condition, it is possible to find that:

$$y_{J3} = m(x_{J3} - b_{11}) + b_{21}, \tag{3.29}$$

where $m = \tan(q_2 + \delta_{pl})$ and $\delta_{pl} = \beta_{pl}/2 + n\pi$ $(n = 0, 1, 2, \ldots)$.

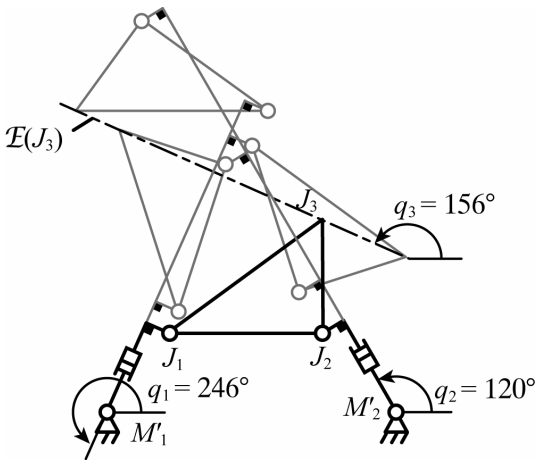

Figure 3.12. – Example of Cardanic motion for a 3-RPR planar parallel robot with $R_{pl} = 0.2$ m, $R_b = 0.35$ m, $l_1 = l_2 = 0.05$ m, $\alpha_{pl} = 36°$ and $\beta_{pl} = 72°$.

Therefore, when $\mathcal{L}_1$ and $\mathcal{L}_2$ make an angle of ε_{pl} and $\mathcal{L}_2$ and $\mathcal{L}_3$ make an angle of δ_{pl}, the manipulator gains a Cardanic self motion (Fig. 3.12). However, such a motion appears for several given particular configuration of the active joint space, while it is possible to see in [Chablat 2006], for a particular design of 3-RPR planar parallel robot with congruent equilateral base and platform triangles, that if condition (3.28) is satisfied, there exists an infinity of active joint configurations in which the robot gains a Cardanic self motion. Thus, it may be possible to find other conditions for the robot to have Cardanic self motion for any values of the angle q_2.

This particularity appears for configurations where $q_1 = q_2 + \varepsilon_{pl}$, if the line $\mathcal{E}(J_3)$ always coincides with $\mathcal{L}_3$ for any values of q_2. This means that one of two lines $\mathcal{L}_4$ or $\mathcal{L}'_4$ (which are parallel to $\mathcal{E}(J_3)$ and at the distance l_3 from $\mathcal{E}(J_3)$) passes through M'_3, for any given values of q_2 (Fig. 3.11). Their equations are given by:

$$y_{\mathcal{L}4/\mathcal{L}'4} = m(x - b_{11} + h_3 \sin q_3) + b_{21} + h_3 \cos q_3 \quad \text{where } h_3 = \pm l_3. \tag{3.30}$$

Line $\mathcal{L}_4$ or $\mathcal{L}'_4$ passes through one fixed point F from the base, for any q_2, if and only if:

$$\frac{\partial}{\partial q_2} y_{\mathcal{L}4/\mathcal{L}'4}(F) = 0 \tag{3.31}$$

Developing (3.31) and simplifying, one finds the coordinate x_F of the fixed point:

$$x_F = R_b \cos\alpha_b(\cos\beta_{pl} + \sin\beta_{pl} \tan\alpha_{pl}) - g(q_2) \tag{3.32}$$

where:

$$g(q_2) = \left(\frac{l_1 \sin\delta_{pl} - l_2 \sin(\delta_{pl} - \varepsilon_{pl}) + h_3 \sin\varepsilon_{pl}}{\sin\varepsilon_{pl}} \right) \sin(q_2 + \delta_{pl}) \tag{3.33}$$

Thus, one fixed point exists if and only if $g(q_2) = 0$ for any q_2, i.e. if:

$$l_1 \sin\delta_{pl} - l_2 \sin(\delta_{pl} - \varepsilon_{pl}) + h_3 \sin\varepsilon_{pl} = 0\,. \tag{3.34}$$

Therefore $g(q_2) = 0$ if:

$$l_3 = \pm \frac{l_1 \sin \delta_{pl} - l_2 \sin(\delta_{pl} - \varepsilon_{pl})}{\sin \varepsilon_{pl}}. \tag{3.35}$$

Introducing equation (3.35) into equations (3.30) and (3.32), one can determine the coordinates of the fixed point F of the line $\mathcal{L}_4$ or $\mathcal{L}'_4$:

$$\begin{cases} x_F = R_b \cos\alpha_b (\cos\beta_{pl} + \sin\beta_{pl} \tan\alpha_{pl}) \\ y_F = R_b (\cos\alpha_b (\sin\beta_{pl} + 2\tan\alpha_{pl} \sin^2(\beta_{pl}/2)) - \sin\alpha_b) \end{cases} \tag{3.36}$$

Since $F = M'_3$, the following conditions on the base and platform shapes must hold:

$$\alpha_b = \alpha_{pl} \text{ and } \beta_b = \beta_{pl}. \tag{3.37}$$

Thus, the base and the mobile platform should be similar triangles.

In summary, any 3-RPR planar parallel robot will have Cardanic self motions if and only if $q_1 = q_2 + \varepsilon_{pl}$ and $q_3 = q_2 + \delta_{pl}$. Moreover, if the base and the mobile platform are similar and if $l_3 = \pm(l_1 \sin\delta_{pl} - l_2 \sin(\delta_{pl} - \varepsilon_{pl}))/\sin\varepsilon_{pl}$, there are Cardanic self motions for any values of angle q_2. Of course, these conditions would have been different if we had examined the degeneracy of $\mathcal{E}(J_1)$ for given values of angles q_2 and q_3 (or $\mathcal{E}(J_2)$ for given values of angles q_1 and q_3). However, such conditions could be easily found by a circular permutation of the indices of the articulated legs.

3.2.2.2. Kinematic analysis of the Cardanic self motion.

Let us now analyse the allowable displacement of the centre P of the platform when the base and the mobile platform are similar triangles, $q_1 = q_2 + \varepsilon_{pl}$, and $l_3 = \pm(l_1 \sin\delta_{pl} - l_2 \sin(\delta_{pl} - \varepsilon_{pl}))/\sin\varepsilon_{pl}$. The expressions of the coordinates of point P, function of q_2, are found using the following closure equation:

$$\mathbf{OP} = \mathbf{OM'_2} + \mathbf{M'_2 K_2} + \mathbf{K_2 J_2} + \mathbf{J_2 P}. \tag{3.38}$$

Developing this expression, one can obtain:

$$\mathbf{OP} = \begin{bmatrix} x \\ y \end{bmatrix} = \begin{bmatrix} x_{M'2} \\ y_{M'2} \end{bmatrix} + \rho_2 \begin{bmatrix} \cos q_2 \\ \sin q_2 \end{bmatrix} + l_2 \begin{bmatrix} -\sin q_2 \\ \cos q_2 \end{bmatrix} - R_{pl} \begin{bmatrix} \cos(-\alpha_{pl} + \phi) \\ \sin(-\alpha_{pl} + \phi) \end{bmatrix}, \quad (3.39)$$

where the expression of ρ_2 is given at equation (3.19). Developing and introducing relations (3.28), (3.35) and (3.37) in (3.39), it can be found that:

$$\mathbf{OP} = \begin{bmatrix} R_{pl}\cos(\alpha_{pl} + 2q_2 - \phi) - R_b \cos(\alpha_{pl} + 2q_2) - l_2 \sin(q_2 + \alpha_{pl}) - l_1 \cos q_2 \\ R_{pl}\sin(\alpha_{pl} + 2q_2 - \phi) - R_b \sin(\alpha_{pl} + 2q_2) + l_2 \cos(q_2 + \alpha_{pl}) - l_1 \sin q_2 \end{bmatrix}. \quad (3.40)$$

From the previous expression, it is possible to conclude that, in such a particular configuration, varying the orientation ϕ of the mobile platform, point P moves on a circle S centred in O' of which radius is R_{pl} (Fig. 3.13). The coordinates of point O' are defined by:

$$\mathbf{OO'} = -R_b \begin{bmatrix} \cos(\alpha_{pl} + 2q_2) \\ \sin(\alpha_{pl} + 2q_2) \end{bmatrix} + l_2 \begin{bmatrix} -\sin(q_2 + \alpha_{pl}) \\ \cos(q_2 + \alpha_{pl}) \end{bmatrix} - l_1 \begin{bmatrix} \cos q_2 \\ \sin q_2 \end{bmatrix}. \quad (3.41)$$

Computing the expressions of the coordinates of point W, the intersection point of the three wrenches $\mathbf{R}_i$, one obtains:

$$\mathbf{OW} = \begin{bmatrix} 2R_{pl}\cos(\alpha_{pl} + 2q_2 - \phi) - R_b \cos(\alpha_{pl} + 2q_2) - l_2 \sin(q_2 + \alpha_{pl}) - l_1 \cos q_2 \\ 2R_{pl}\sin(\alpha_{pl} + 2q_2 - \phi) - R_b \sin(\alpha_{pl} + 2q_2) + l_2 \cos(q_2 + \alpha_{pl}) - l_1 \sin q_2 \end{bmatrix}. \quad (3.42)$$

Thus, W is located on a circle $\mathcal{K}$ centred in O' of which radius is $2R_{pl}$. It is also possible to observe that the platform and vector $\mathbf{O'P}$ rotate in opposite senses.

One can rewrite expression (3.40) as follows:

$$\mathbf{OP} = \begin{bmatrix} R\cos(\eta + 2q_2) - l_2 \sin(q_2 + \alpha_{pl}) - l_1 \cos q_2 \\ R\sin(\eta + 2q_2) + l_2 \cos(q_2 + \alpha_{pl}) - l_1 \sin q_2 \end{bmatrix} \quad (3.43)$$

with

$$R = \sqrt{R_b^2 + R_{pl}^2 - 2R_b R_{pl}\cos\phi} \quad \text{and} \quad \eta = \tan^{-1}\left(-\frac{R_{pl}\sin(\phi - \alpha_{pl}) - R_b \sin\alpha_{pl}}{R_{pl}\cos(\phi - \alpha_{pl}) - R_b\cos\alpha_{pl}}\right). \quad (3.44)$$

For a given angle ϕ and variable angle q_2, expression (3.43) represents the singularity loci (for the Cardanic self motions) of the manipulator with specified parameters. The obtained result corresponds to the parametric expression of an epicycloid $\mathcal{P}$. The epicycloids $\mathcal{P}_1$ and $\mathcal{P}_2$ represented in Fig. 3.13 are the curves corresponding to angles $\phi = 0$ and $\phi = \pi$ respectively.

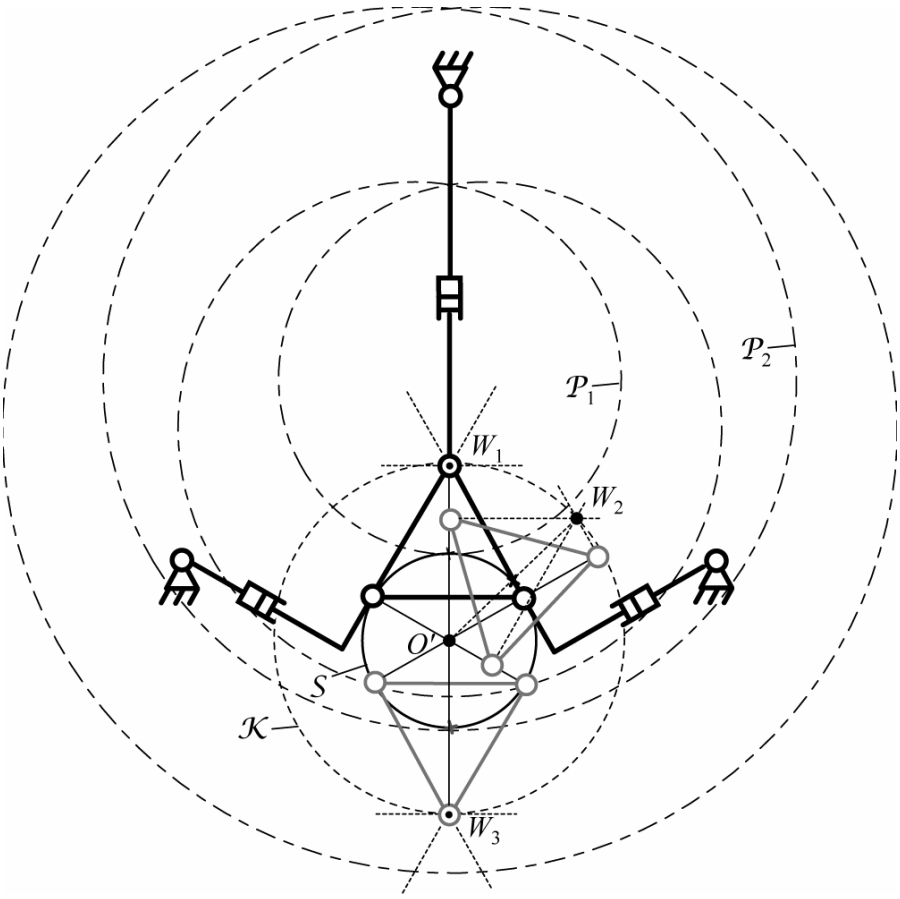

Figure 3.13. – Schematics of a Cardanic self motion of the studied manipulator with $R_{pl} = 0.1$ m, $R_b = 0.35$ m, $l_1 = l_2 = 0.07$ m, $l_3 = 0$ m, $\alpha_b = 30°$ and $\beta_b = 120°$.

3.2.3. Examples and experimental validations.

As was previously said, the prototype of the PAMINSA manipulator presents the same Type 2 singularities as a symmetric 3-RPR planar parallel robot, which will be studied in this section. Indeed, the planar equivalent model of the prototype of the PAMINSA manipulator corresponds to a 3-RPR planar parallel robot of which base and platform are non-identical equilateral triangles and of which offsets are zero, $l_i = 0$. These conditions correspond to a robot with Cardanic self motions within its workspace.

It has been shown in section 3.1.4 that the prototype, which corresponds to a PAMINSA-4D3L, is in a Type 2 singularity when:

$$\rho_i = +\infty \text{, for } i = 1, 2 \text{ or } 3 \tag{3.45}$$

or

$$\phi = \phi_s = \pm \cos^{-1}(R_{pl} / R_b) \tag{3.46}$$

or

$$x^2 + y^2 = R_b^2 + R_{pl}^2 - 2R_b R_{pl} \cos\phi \,. \tag{3.47}$$

Condition (3.45) implies that the platform is located at an infinite distance from the centre of the base frame. This is equivalent to the fact that the three legs of the manipulator are parallel (Fig. 3.10.b). Condition (3.46) implies that the robot gains one degree of freedom for any considered position of the workspace, for a fixed platform angle ϕ_s. Finally, condition (3.47) implies that the manipulator gains one degree of freedom when the point P is located on a circle centred in O of which radius is $R = \sqrt{R_b^2 + R_{pl}^2 - 2R_b R_{pl} \cos\phi}$. Thus, we have to find which of the last two conditions correspond to Cardanic self motions.

Introducing the constraints $l_i = 0$, $\alpha_b = \alpha_{pl}$ and $\beta_b = \beta_{pl}$ into equation (3.40), one can find:

$$\mathbf{OP} = \begin{bmatrix} x \\ y \end{bmatrix} = \begin{bmatrix} R_{pl}\cos(\alpha_{pl} + 2q_2 - \phi) - R_b \cos(\alpha_{pl} + 2q_2) \\ R_{pl}\sin(\alpha_{pl} + 2q_2 - \phi) - R_b \sin(\alpha_{pl} + 2q_2) \end{bmatrix}. \tag{3.48}$$

Raising the norm of vector **OP** to square, we obtain equation (3.47). Thus, this particular design of 3-RPR planar parallel robot gains one Cardanic self motion when the end effector is positioned on a circle $\mathcal{P}$ centred at O and with radius equal to $R = \sqrt{R_b^2 + R_{pl}^2 - 2R_bR_{pl}\cos\phi}$ (Fig. 3.14). The circles $\mathcal{P}_1$ and $\mathcal{P}_2$ represented on Fig. 3.14 are the circles $\mathcal{P}$ corresponding to angles $\phi = 0$ and $\phi = \pi$ respectively.

Note that, for the angle ϕ_s, the robot gains one infinitesimal degree of freedom at any position, except if point P is located on a circle centred in O of which radius is equal to $R_s = \sqrt{R_b^2 + R_{pl}^2 - 2R_bR_{pl}\cos\phi_s}$. Such a position still corresponds to a Cardanic self motion. Moreover, for $R_{pl} = R_b$, the angle ϕ_s corresponds to a self motion of translation [Chablat 2006]. This means that, when the platform centre is located on the circle $\mathcal{P}_1$, the platform gains two self motions at the same time.

Observing equation (3.48), it is possible to conclude that the gained degree of freedom is a motion along a circle S centred in O' of which radius is R_{pl}. The coordinates of point O' are:

$$\mathbf{OO'} = -R_b\begin{bmatrix}\cos(\alpha_{pl} + 2q_2)\\ \sin(\alpha_{pl} + 2q_2)\end{bmatrix}. \tag{3.49}$$

Note that the circle S is tangent to circles $\mathcal{P}_1$ and $\mathcal{P}_2$. This means that the maximal singularity-free workspace is delimited by the circle $\mathcal{P}_1$. The radius of the circle $\mathcal{P}_1$ is equal to:

$$R_1 = \left|R_b - R_{pl}\right|. \tag{3.50}$$

Dividing equation (3.50) by R_b yields:

$$\nu = R_1 / R_b = \left|1 - R_{pl} / R_b\right|. \tag{3.51}$$

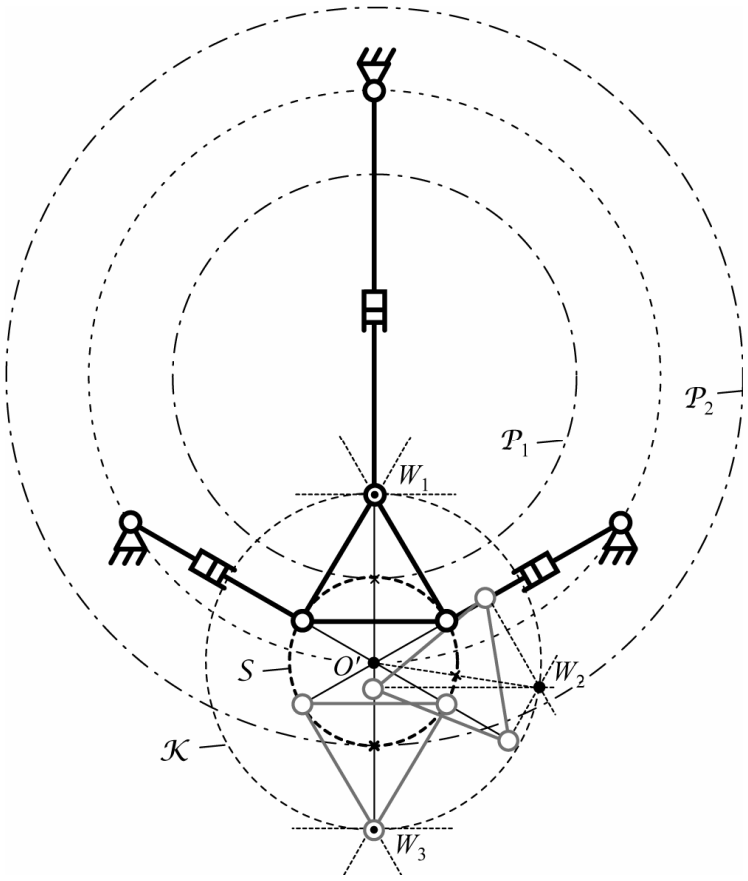

Figure 3.14. – Schematics of a Cardanic self motion of the studied manipulator with $R_{pl} = 0.1$ m, $R_b = 0.35$ m, $\alpha_b = 30°$ and $\beta_b = 120°$.

Thus, the smaller the ratio R_{pl}/R_b, the greater the value of ν. So it is possible to conclude that, for having a larger singularity-free workspace, the rate R_{pl}/R_b has to be smaller. However, the smaller the mobile platform with respect to the base, the less accurate is its orientation.

In order to demonstrate the previous results, we have positioned the PAMINSA prototype in a singular configuration with Cardanic self motion ($x = 0$ m, $y = -0.25$ m, $\phi = 0°$). This position is shown on Fig. 3.15.g. For such a configuration, the three actuators are blocked. However, it is possible to see on Figs. 3.15.a to 3.15.l that the platform is not constrained and undergoes a Cardanic self motion when external force is applied to the platform.

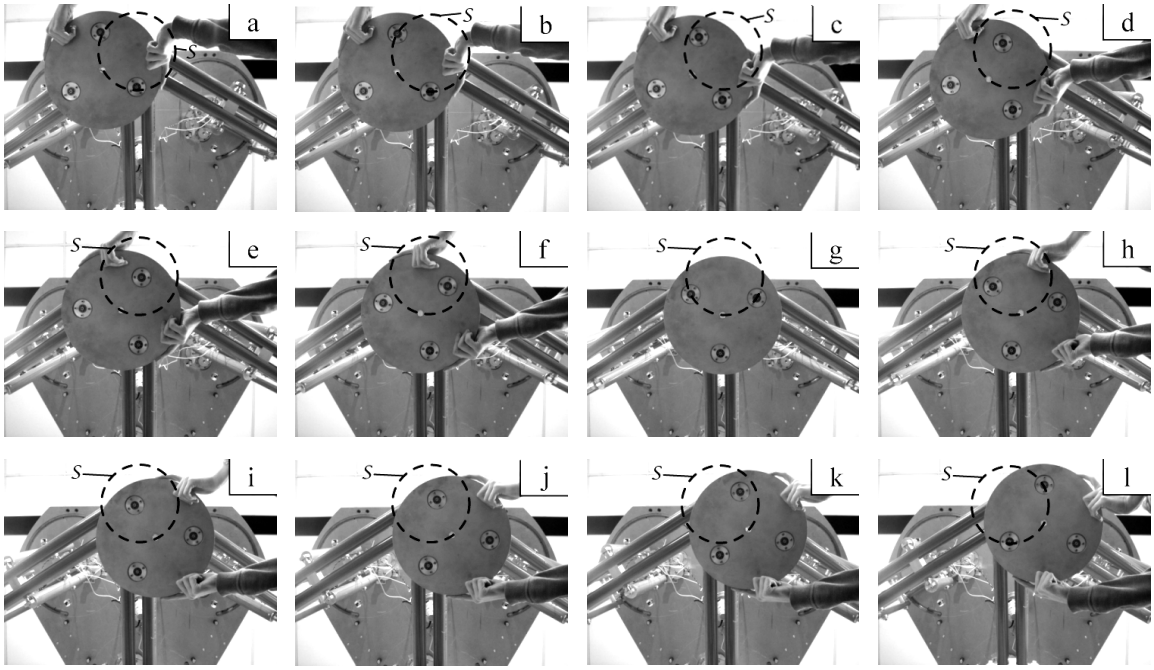

Figure 3.15. – Cardanic self motion of the mobile platform of the PAMINSA prototype starting from the configuration $x = 0$ m, $y = -0.25$ m, $\phi = 0°$ (view from below).

3.3. Summary.

In this chapter the singularity analysis of PAMINSA with three, four, five and six degrees of freedom is presented. The singularities have been determined in analytic form by an algebraic approach based on the analysis of the properties of the Jacobian matrices. The nature of each kind of singularity is discussed and kinematically analysed.

We also analyse the self motions of the PAMINSA manipulators under study. Two kinds of Cardanic self motions have been identified: for only several active-joint configurations in the case of a relatively general design and for infinitely many active-joint configurations in the case of designs with similar base and platform triangles and special conditions on the offsets.

For many different values of the design parameters, the robot will have Cardanic self motions and it is important to have exact knowledge of them. The results, in terms of singularity loci and of associated finite displacements, have been validated on an

actual robot prototype. These results can be used to optimize the singularity-free workspace of this type of robots and to choose the optimal architectures of PAMINSA.

Finally, we would like to mention that, in this work, the singularity analysis was carried out by taking into account only the kinematic relationships. In practice, this problem is much more complicated and it may be studied with kinetostatic and dynamic aspects.

Moreover, the singular configurations limit the workspace of parallel manipulators, which is less than that of serial manipulators. In the following chapter, a means of enlarging the workspace of parallel manipulators by passing through singular configurations will be proposed.

Chapter 4

Increase of Singularity-Free Zones in the Workspace of PAMINSA Manipulators Using Mechanisms of Variable Structure

This chapter deals with the solution that consists of increasing the singularity-free zones in the workspace of PAMINSA manipulators.

The singularity zones are defined no longer only via a kinematic analysis of the degeneracy of the Jacobian matrix of the theoretical perfect model of the manipulator, but also by the quality of force transmission.

For this purpose, the pressure angle is used as an indicator of force transmission. The optimal control of the pressure angle for a given trajectory of the manipulator is obtained by means of legs with variable structure. The suggested procedure used in the determination of the optimal structure of parallel manipulators is performed on a 3-RPR mechanism, of which kinematic parameters are equivalent to the prototype of the PAMINSA-4D3L.

It is illustrated by means of two numerical simulations, which show that the singularity-free workspace is increased to 100% of the real workspace of the manipulator.

4.1. The quality of motion transmission and the pressure angle.

It has already been said that the closed-loop of parallel manipulators limits the motion of the platform and creates special singular zones inside the workspace [Merlet 2006a]. The workspace of parallel manipulators, which is less than that of serial manipulators, is reduced and limits their functional performance.

One of the most evident solutions to this problem is the introduction of complementary actuators in the initial system, which make it possible to eliminate the singular configurations of parallel manipulators by means of optimal control of the motion [Alvan 2003] [Glazunov 2004]. However, it is an expensive solution to the problem because of the use of additional actuators. Moreover, the control of the manipulator caused by actuation redundancy is much more complicated.

In this chapter we propose a new solution, which is carried out by using mechanisms of variable structure, i.e. mechanisms of which structure parameters can be altered. With regard to the determination of singularity-free zones inside the workspace, we propose a kinetostatic approach taking into account the force transmission.

4.1.1. The pressure angle.

As seen in the previous chapter, the physical interpretation of a singularity in kinematics refers to those configurations in which the number of degrees of freedom of the mechanical structure changes instantaneously, either the manipulator gains some additional, uncontrollable movements or loses some degrees of freedom. Algebraically, a singularity analysis is based on the properties of the Jacobian matrices of the mechanical structure, i.e. when the Jacobian matrices relating the input speeds and the output speeds, become rank deficient (see chapter 3). However, it is also well known that, when a parallel manipulator is close to a singular configuration, it loses its rigidity. Moreover, the quality of motion transmission is deteriorated and, as a result, the manipulator loses its payload capability. Thus, the singularity zones must be avoided, and an indicator of the quality of motion transmission close to the singular configurations of parallel manipulators must be defined. In the present work, we use a kinetostatic approach for the evaluation of the quality of motion transmission by using the pressure angle, well known in the mechanism design but not so often applied to

parallel mechanisms. One defines the pressure angle as an angle between vectors of force and velocity of a point at which force is applied. Thus, for the best force transmission, it is desirable to have the pressure angle close to zero. One also knows the transmission angle, which is equal to 90° minus pressure angle and, accordingly, the transmission angle is desirable if it will be close to 90°.

S. Balli and S. Chand [Balli 2002] considered several examples to determine the transmission angle of planar and spatial mechanisms, particularly, for mechanisms with two degrees of freedom. G. Sutherland and B. Roth [Sutherland 1973] showed that the input link of a spatial mechanism tends to move the output link when the transmission wrench is not reciprocal to the output link velocity screw. On the base of this consideration, a general index of motion transmission for spatial mechanisms is proposed. The quality of motion and force transmission was successfully summarized in the work of G. Sutherland [Sutherland 1981] and C.-C. Lin and W.-T. Chang [Lin 2002]. The study of G. Sutherland and B. Roth [Sutherland 1973] was generalized for any spatial single-loop mechanism in the recent study C. Chen and J. Angeles [Chen 2005]. O. Alba-Gomez, P. Wenger and A. Pamanes [Alba-Gomez 2005] have evaluated the quality of motion in the three-degrees-of-freedom manipulators by means of a kinetostatic indicator, which is similar to the pressure angle.

In the present study, we use the pressure angle as an indicator of the quality of motion transmission and, in our opinion, this shows the nature of the inaccessibility of parallel manipulators' singular zones better than the kinematic approach.

4.1.2. Application on the PAMINSA-4D3L.

Let us consider the basic version of PAMINSA-4D3L. The Type 2 singularities of such a mechanism do not depend on the altitude of the platform, i.e. the force transmission on the platform does not change with the altitude. This is the reason why it is possible to analyse solely the force transmission of its simplified planar equivalent model: the 3-RPR manipulator (Fig. 4.1).

The workspace of the manipulator can be defined as the totality of positions that a moving platform can reach. However, these accessible positions are limited not only by geometrical parameters and the type of actuation of the parallel mechanism, but also by force transmission. Especially in the configurations close to the singular positions, the force transmission becomes unfavorable and the transmission of motion can be disrupted, and as a result, leads to the breakdown of the parallel mechanism or

undesirable motion. The pressure angle is an important criterion for the analysis of the inaccessible zone of parallel manipulators.

However, when the number of links or the degree of freedom increases, the determination of the pressure angles becomes more complicated. Let us exanimate the pressure angles of the considered manipulator. We consider that the revolute pairs M'_i are actuated and passive joints are located at H'_i and J_i.

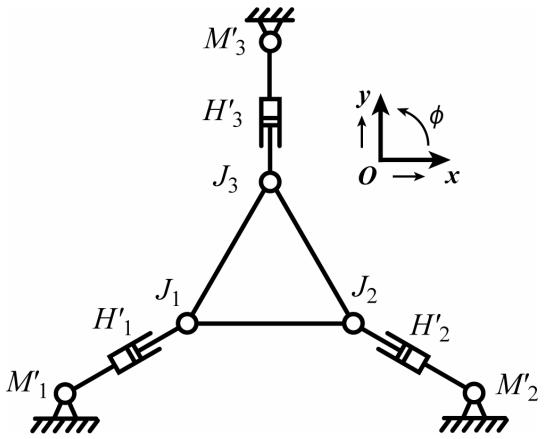

Figure 4.1. – Planar parallel manipulator 3-RPR.

Thus, each kinematic chain includes one actuated and two passive pairs. The wrench acting to the output link is reciprocal to the unit vectors situated along the axes of non-actuated pairs. Let $\mathbf{E}_{i\mathbf{1}}$, $\mathbf{E}_{i\mathbf{2}}$, $\mathbf{E}_{i\mathbf{3}}$ (Fig. 4.2) be the unit vectors of the axes of kinematic pairs.

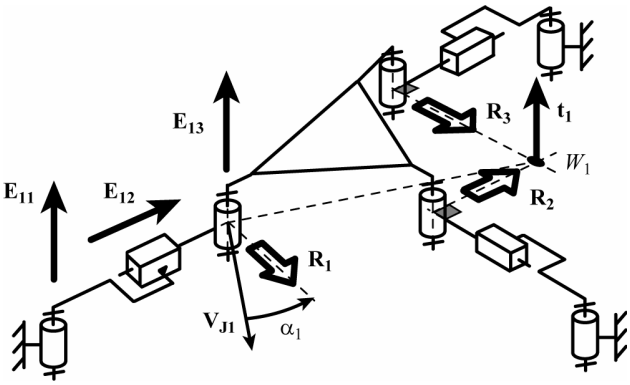

Figure 4.2. – Representation of the planar parallel manipulator 3-RPR in 3D.

Here, $\mathbf{E}_{i1}$ corresponds to the rotating actuated pair, $\mathbf{E}_{i2}$ and $\mathbf{E}_{i3}$ correspond to sliding and rotating passive pairs accordingly ($\mathbf{E}_{i1}$ and $\mathbf{E}_{i2}$ directed perpendicular to the plane of the mechanism). These unit screws in any position of the mechanism have the following Plucker coordinates:

$$\mathbf{E}_{i1} = \begin{bmatrix} 0 & 0 & 1 & e^0_{i1x} & e^0_{i1y} & 0 \end{bmatrix}, \tag{4.1}$$

$$\mathbf{E}_{i2} = \begin{bmatrix} 0 & 0 & 0 & e^0_{i2x} & e^0_{i2y} & 0 \end{bmatrix}, \tag{4.2}$$

$$\mathbf{E}_{i3} = \begin{bmatrix} 0 & 0 & 1 & e^0_{i3x} & e^0_{i3y} & 0 \end{bmatrix}, \tag{4.3}$$

where:

$$e^0_{i1x} = y_{M'i}\,,\ e^0_{i1y} = -x_{M'i}\,, \tag{4.4}$$

$$e^0_{i2x} = (x_{Ji} - x_{M'i})/\rho_i\,,\ e^0_{i2y} = (y_{Ji} - y_{M'i})/\rho_i\,, \tag{4.5}$$

$$e^0_{i3x} = y_{Ji}\,,\ e^0_{i3y} = -x_{Ji}\,. \tag{4.6}$$

$x_{M'i}$, x_{Ji}, $y_{M'i}$, y_{Ji} are the coordinates of the point M'_i and J_i, ρ_i is the distance between the points M'_i and J_i.

The Plucker coordinates of the unit screws can be described in the matrix $\mathbf{E}$:

$$\mathbf{E} = \begin{bmatrix} 1 & e^\circ_{i1z} & e^\circ_{i1y} \\ 0 & e^\circ_{i2z} & e^\circ_{i2y} \\ 1 & e^\circ_{i3z} & e^\circ_{i3y} \end{bmatrix}. \tag{4.7}$$

The determinant of the matrix $\mathbf{E}$ vanishes if the axes $\mathbf{E}_{i1}$ and $\mathbf{E}_{i3}$ coincide. This corresponds to the Type 1 singular configuration of the manipulator [Bonev 2003b].

We can obtain the wrenches $\mathbf{R}_i$, which are reciprocal to the unit vectors of the axes of the passive kinematic pairs [Dimentberg 1965]. They can be written as:

$$\mathbf{R}_i = \begin{bmatrix} r_{ix} & r_{iy} & 0 & 0 & 0 & r^0_{iz} \end{bmatrix}. \tag{4.8}$$

The conditions of reciprocity are:

$$e^0_{i2x} r_{ix} + e^0_{i2y} r_{iy} = 0\,;\; e^0_{i3x} r_{ix} + e^0_{i3y} r_{iy} + r^0_{iz} = 0\,. \tag{4.9}$$

The equation (4.9) means that each connecting kinematic chain determines one wrench of zero pitch (vector). It is perpendicular to the axis $\mathbf{E_{i2}}$ and intersects the point J_i. The coordinates of wrenches in the form of the matrix $\mathbf{R}$ are given by:

$$\mathbf{R} = \begin{bmatrix} r_{1x} & r_{1y} & r^{\circ}_{1z} \\ r_{2x} & r_{2y} & r^{\circ}_{2z} \\ r_{3x} & r_{3y} & r^{\circ}_{3z} \end{bmatrix}. \tag{4.10}$$

In Type 2 singular configurations, it has been shown that the system of the wrenches $\mathbf{R}_i$ degenerates and that they intersect in the same point or are parallel (see chapter 3). This can be shown by the representation of the components of this matrix. If all the wrenches are parallel, then the first two columns are proportional. If all the wrenches intersect in the same point $W = [x_W,\ y_W]^T$, then the coordinate r^0_{iz} can be written as:

$$r^0_{iz} = r_{1x} y_W - r_{1y} x_W\,. \tag{4.11}$$

In the matrix $\mathbf{R}$, the third column is a linear combination of the first and seconds columns:

$$\mathbf{R} = \begin{bmatrix} r_{1x} & r_{1y} & r_{1x} y_W - r_{1y} x_W \\ r_{2x} & r_{2y} & r_{2x} y_W - r_{2y} x_W \\ r_{3x} & r_{3y} & r_{3x} y_W - r_{3y} x_W \end{bmatrix}. \tag{4.12}$$

To find the pressure angle, we consider the wrenches $\mathbf{R}_i$ and the directions of the velocities of the points J_i determined by the twists reciprocal to these wrenches. The velocity of the point J_i is determined by the two wrenches $\mathbf{R_2}$ and $\mathbf{R_3}$. One can find the twist $\mathbf{t}_1 = [0,\ 0,\ w_{1z},\ v_{1x},\ v_{1y},\ 0]$ reciprocal to the wrenches $\mathbf{R_2}$ and $\mathbf{R_3}$ using the equations:

$$v_{1x}r_{1x} + v_{1y}r_{1y} + w_{1z}r_{1z}^0 = 0 \;;\; v_{1x}r_{2x} + v_{1y}r_{2y} + w_{1z}r_{2z}^0 = 0\,. \tag{4.13}$$

It is obvious that the axis of the twist $\mathbf{t_1}$ is situated perpendicular to the plane of the mechanism and intersects the centre W_1 of velocities of the platform according to the wrenches $\mathbf{R_2}$ and $\mathbf{R_3}$ (Fig. 4.2). Without loss of generality, the twist $\mathbf{t_1}$ can be expressed as:

$$\mathbf{t_1} = \begin{bmatrix} 0 & 0 & 1 & y_{W1} & -x_{W1} & 0 \end{bmatrix}. \tag{4.14}$$

The velocity $\mathbf{V_{J1}}$ of point $\mathbf{J_1}$, when the leg 1 is disconnected of the platform, has the coordinates (Fig. 4.2):

$$v_{xJ1} = v_{1x} - w_{1z}y_{J1} = y_{W1} - y_{J1}\,,\; v_{yJ1} = v_{1y} + w_{1z}x_{J1} = -x_{W1} + x_{J1}\,. \tag{4.15}$$

Finally, the pressure angle can be written as (Fig. 4.2):

$$\alpha_1 = \left|\cos^{-1}\left(\mathbf{V_{J1}}\mathbf{R_1} / \|\mathbf{V_{J1}}\|\,\|\mathbf{R_1}\|\right)\right|. \tag{4.16}$$

It was noted that, in the singular configurations, all the pressure angles are equal to 90°. Indeed, in this case, the axis of the wrench $\mathbf{R_1}$ intersects the axes of the wrenches $\mathbf{R_2}$ and $\mathbf{R_3}$ and the velocity $\mathbf{V_{J1}}$ is perpendicular to the axis of the wrench $\mathbf{R_1}$.

Thus, the pressure angles can be determined at the joints of each kinematic chain by similar ways. Then, the maximum values of the three pressure angles can be compared with their limit values. In this way, we have mapped the whole workspace of the parallel manipulator to detect the inaccessible zones with unfavourable values of the pressure angles (see section 4.3).

If the prescribed path of the parallel manipulator intersects any unacceptable zone in which the pressure angle has an inadmissible value, the transmission of the motion can be disrupted. In this case, it is necessary to change the structural parameters of the mechanism, i.e. the input motions. This will be shown in the following section.

4.2. The legs with variable structure.

Figure 4.3 shows a schematic of the modified leg with the added articulated dyad. The rotating actuators are mounted on the base and connected by electromagnetic clutches with the links M'_iK_i and $M'_iH'_i$. These two input links cannot be actuated simultaneously, and the input motion can be transmitted either by link M'_iK_i or $M'_iH'_i$. In this way, we can obtain the legs of the mechanism with different structural parameters, which allows an increase in the singularity-free zones in the workspace of the considered parallel manipulator.

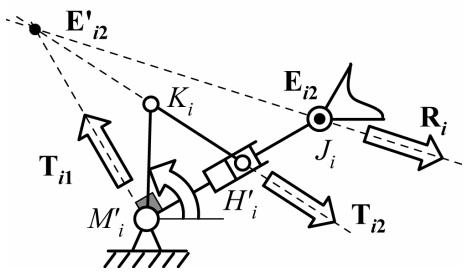

Figure 4.3. – Leg with variable structure.

By example, one or all of the pairs M'_i (Fig. 4.1) can be passive and the prismatic pairs can be actuated by the chain $M'_iK_iH'_i$. In this case, the actuator torque is transmitted to link M'_iK_i, which becomes an input link and moves the prismatic pair.

Let us consider the system of wrenches existing in this case. The link H'_iJ_i is constrained by two wrenches of zero pitch $\mathbf{T}_{i1}$ and $\mathbf{T}_{i2}$. The axis of wrench $\mathbf{T}_{i1}$ is perpendicular to the line M'_iJ_i and the axis of wrench $\mathbf{T}_{i2}$ coincides with the axis of the link H'_iK_i. The unit screw $\mathbf{E'}_{i2} = \begin{bmatrix} 0 & 0 & 1 & e^{0'}_{i2x} & e^{0'}_{i2y} & 0 \end{bmatrix}$ of the twist of link H'_iJ_i is reciprocal to wrenches $\mathbf{T}_{i1}$ and $\mathbf{T}_{i2}$. This twist is of zero pitch and is perpendicular to the plane of the mechanism. $\mathbf{T}_{i1}$ and $\mathbf{T}_{i2}$ coincides with the point of intersection of the axis $\mathbf{E'}_{i2}$ and the plane of the mechanism. If link H'_iK_i is perpendicular to the link H'_iJ_i, then the wrenches $\mathbf{T}_{i1}$ and $\mathbf{T}_{i2}$ are parallel and the instantaneous motion of the link H'_iJ_i is translational. The wrench $\mathbf{R}_i$ can be determined using the equation analogous to (4.9). The pressure angle can be found using the equation (4.16).

Thus, in each position we determine m pressure angles corresponding to all m degrees of freedom. Then we consider the maximum value of these angles. Then, by

such a way, we can determine the pressure angles corresponding to the different structures distinguished by different input links and obtain all possible workspace with singularity-free zones. It is examined in the next section.

4.3. Plotting of singularity-free zones taking into account the pressure angles.

In this section, we would like to show the singularity-free zones in the workspace of a 3-RPR parallel manipulator with modified legs. These zones have been determined by analysing the maximum values of the pressure angles.

For numerical simulations, we consider a 3-RPR parallel manipulator, in which the base triangle $M'_1M'_2M'_3$ is equilateral with a radius equal to 0.35 m (Fig. 4.1) and the platform also represents an equilateral triangle with a radius equal to 0.1 m. The rotation of the revolute joints M'_i is limited to ±90°. For the added dyads, $M'_iK_i = K_iH'_i = 0.25$ m. The articulated dyads are always located on the left of the prismatic pairs as is shown in Fig. 4.3 and the translation of the prismatic pairs are limited relative to the joints M'_i and H'_i by values $(M'_iH'_i)_{\min} = (H'_iJ_i)_{\min} = 0.05$ m.

Taking into account that the manipulator can be actuated either by links M'_iK_i or by links $M'_iH'_i$, for given output parameters $\mathbf{x} = [x,\ y,\ \phi]^T$ of the platform, we have 8 different combinations of actuation, i.e. we have 8 different combinations of input parameters presented below (underlined letters show the input pairs, R for input links $M'_iH'_i$ with input angles q_i and P for input links M'_iK_i with input displacements ρ_i):

$$\mathbf{x} = [x, y, \phi]^T \Rightarrow \begin{array}{l} \underline{\mathrm{RRR}}\text{: }\underline{\mathrm{R}}\text{PR- }\underline{\mathrm{R}}\text{PR- }\underline{\mathrm{R}}\text{PR} : \mathbf{q}_{(1)} = [q_1,\ q_2,\ q_3]^T \\ \underline{\mathrm{RRP}}\text{: }\underline{\mathrm{R}}\text{PR- }\underline{\mathrm{R}}\text{PR- R}\underline{\mathrm{P}}\text{R} : \mathbf{q}_{(2)} = [q_1,\ q_2,\ \rho_3]^T \\ \underline{\mathrm{RPR}}\text{: }\underline{\mathrm{R}}\text{PR- R}\underline{\mathrm{P}}\text{R- }\underline{\mathrm{R}}\text{PR} : \mathbf{q}_{(3)} = [q_1,\ \rho_2,\ q_3]^T \\ \underline{\mathrm{RPP}}\text{: }\underline{\mathrm{R}}\text{PR- R}\underline{\mathrm{P}}\text{R- R}\underline{\mathrm{P}}\text{R} : \mathbf{q}_{(4)} = [q_1,\ \rho_2,\ \rho_3]^T \\ \underline{\mathrm{PRR}}\text{: R}\underline{\mathrm{P}}\text{R- }\underline{\mathrm{R}}\text{PR- }\underline{\mathrm{R}}\text{PR} : \mathbf{q}_{(5)} = [\rho_1,\ q_2,\ q_3]^T \\ \underline{\mathrm{PRP}}\text{: R}\underline{\mathrm{P}}\text{R- }\underline{\mathrm{R}}\text{PR- R}\underline{\mathrm{P}}\text{R} : \mathbf{q}_{(6)} = [\rho_1,\ q_2,\ \rho_3]^T \\ \underline{\mathrm{PPR}}\text{: R}\underline{\mathrm{P}}\text{R- R}\underline{\mathrm{P}}\text{R- }\underline{\mathrm{R}}\text{PR} : \mathbf{q}_{(7)} = [\rho_1,\ \rho_2,\ q_3]^T \\ \underline{\mathrm{PPP}}\text{: R}\underline{\mathrm{P}}\text{R- R}\underline{\mathrm{P}}\text{R- R}\underline{\mathrm{P}}\text{R} : \mathbf{q}_{(8)} = [\rho_1,\ \rho_2,\ \rho_3]^T \end{array}$$

Tables 4.1 and 4.2 show the workspaces of each case of actuation with 0° and 45° orientation angles (the origin of the fixed base frame is located at the centre of the equilateral triangle $M'_1M'_2M'_3$). In these figures, several zones can be seen, which correspond to the variations of the maximum values of the pressure angle for given positions of the platform. The contrast intensity shows the variations of the pressure angle (see Fig. 4.4).

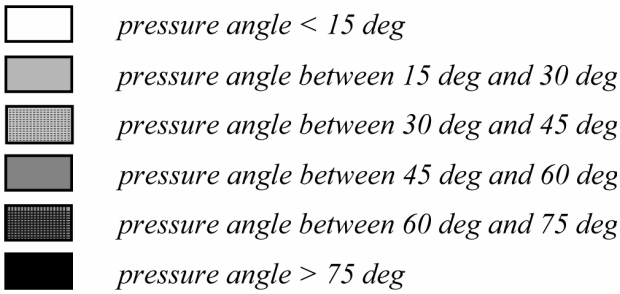

Figure 4.4. – The contrast intensity corresponding to the pressure angle.

Thus, the black zones are the surfaces where the pressure angle has inadmissible values, and as a result, these are the zones which cannot be reached by the parallel mechanism.

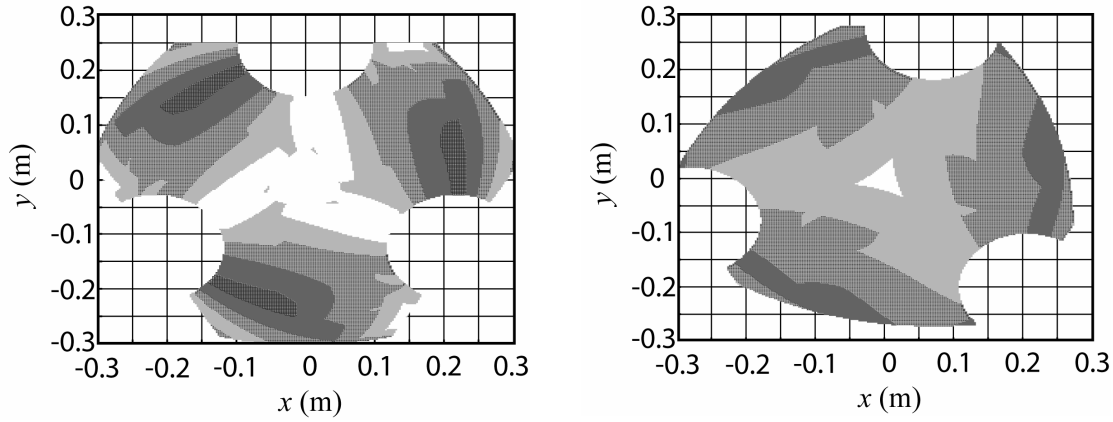

(a) $\phi = 0$ deg. (b) $\phi = 45$ deg.

Figure 4.5. – The reachable workspace of the parallel manipulator with modified legs.

Table 4.1. – Maximum values of the pressure angles ($\phi = 0°$).

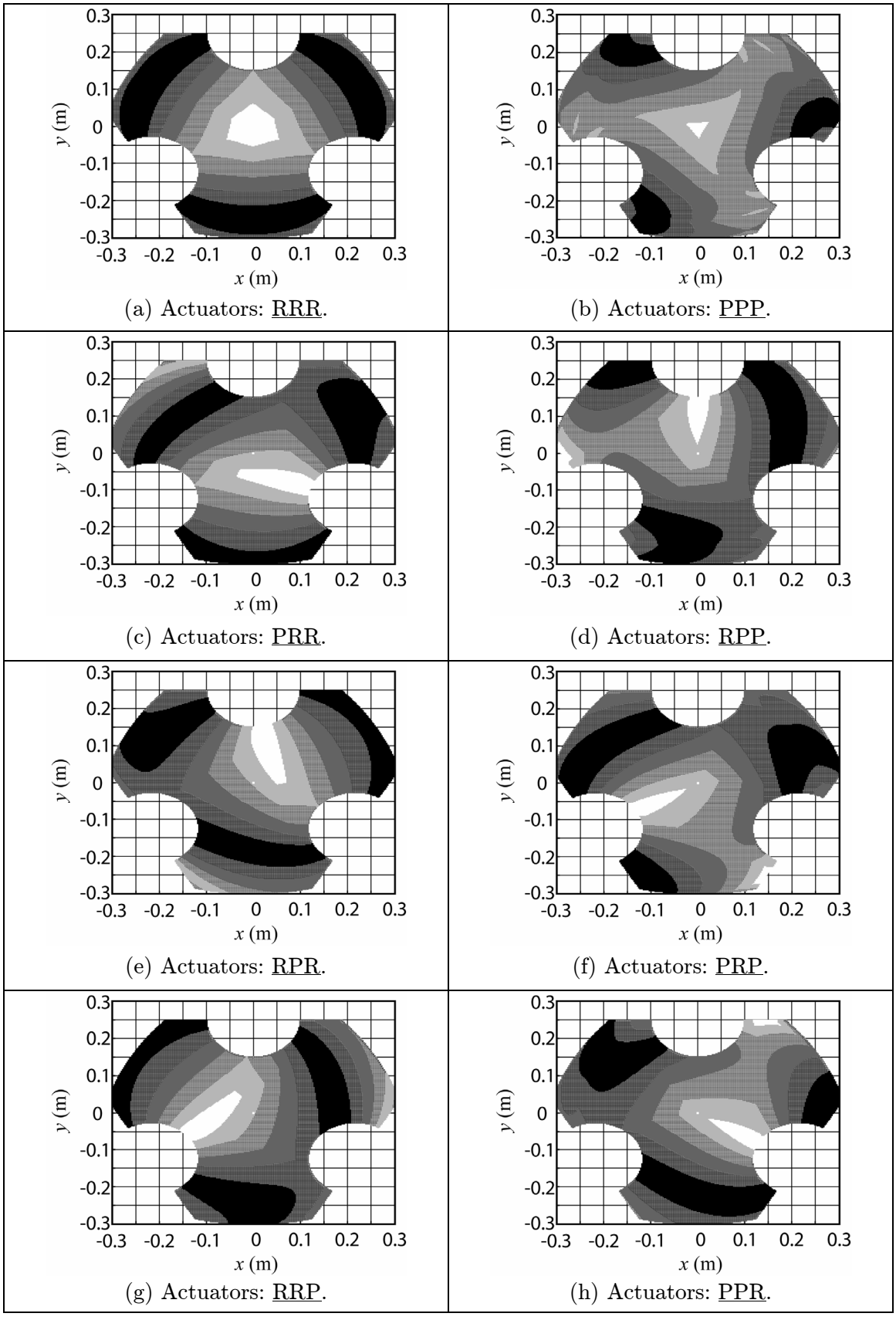

(a) Actuators: RRR.

(b) Actuators: PPP.

(c) Actuators: PRR.

(d) Actuators: RPP.

(e) Actuators: RPR.

(f) Actuators: PRP.

(g) Actuators: RRP.

(h) Actuators: PPR.

Table 4.2. – Maximum values of the pressure angles ($\phi = 45°$).

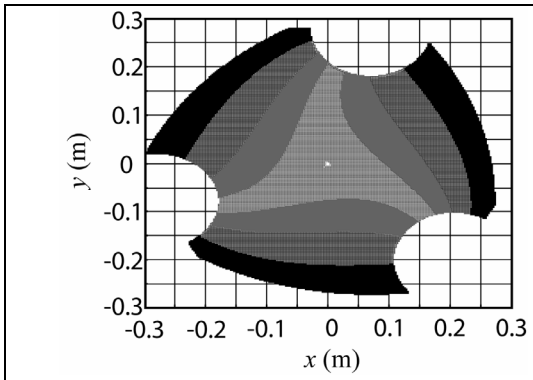

(a) Actuators: RRR

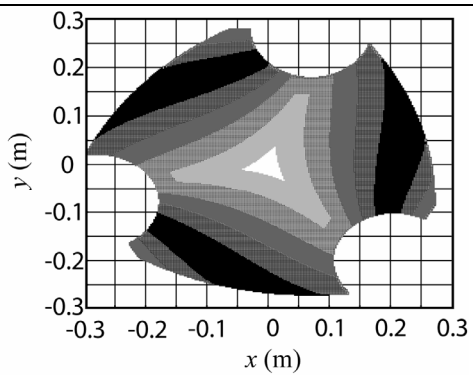

(b) Actuators: PPP

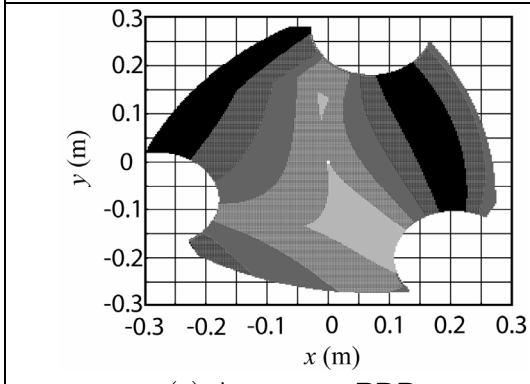

(c) Actuators: PRR

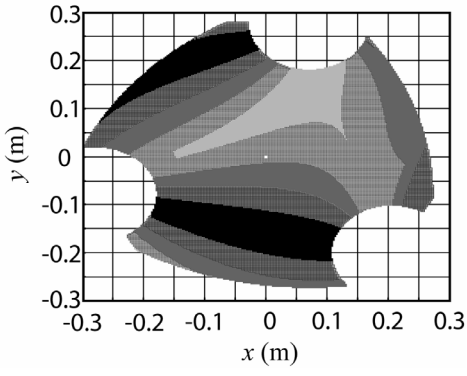

(d) Actuators: RPP

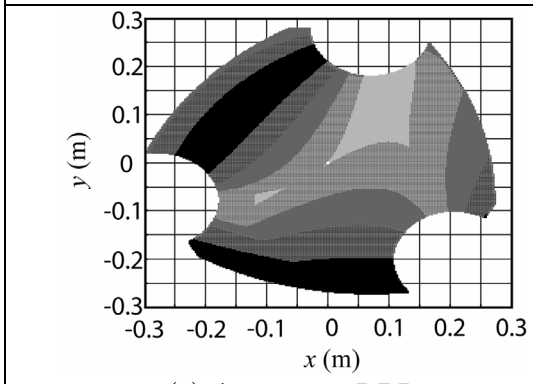

(e) Actuators: RPR

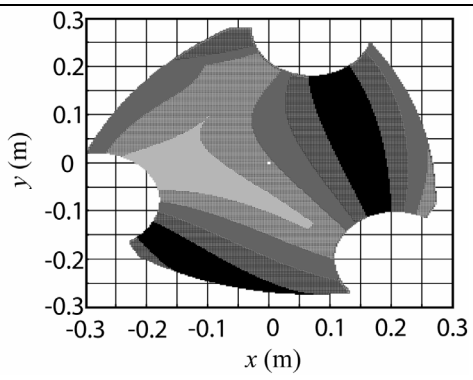

(f) Actuators: PRP

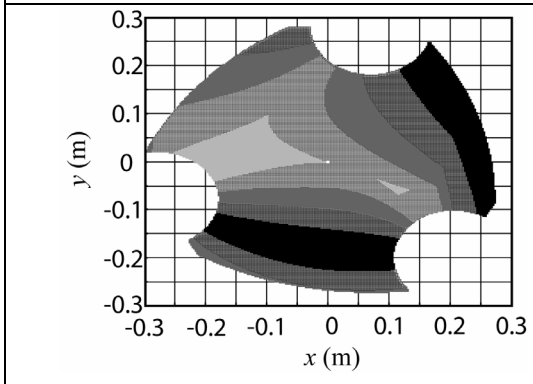

(g) Actuators: RRP

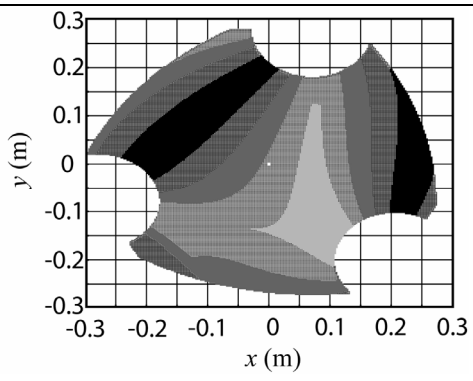

(h) Actuators: PPR

Table 4.3. – Total value of singularity-free volumes for each case of actuation.

Type of actuation	$\phi = 0°$ (workspace surface: 0.21 m²)		$\phi = 45°$ (workspace surface: 0.2 m²)	
	Singularity-free zones, $\alpha \leq 75°$ (m²)	Singularity-free zones relative to the whole workspace	Singularity-free zones, $\alpha \leq 75°$ (m²)	Singularity-free zones relative to the whole workspace
RRR	0.137	65%	0.147	74%
PPP	0.181	86%	0.152	76%
PRR	0.152	72%	0.158	79%
RPR	0.152	72%	0.158	79%
RRP	0.152	72%	0.158	79%
RPP	0.155	74%	0.165	83%
PRP	0.155	74%	0.165	83%
PPR	0.155	74%	0.165	83%

The table 4.3 shows the ratio between the total value of singularity-free volumes and the total workspace for each case of actuation (for two examined cases: $\phi = 0°$ and $\phi = 45°$).

Figure 4.5 shows the reachable workspace of the modified parallel mechanism with legs of variable structure. We can see that the workspace of the modified manipulator is only composed of singularity-free zones and the whole workspace of the manipulator is reachable (increase to 100%).

4.4. Trajectory planning.

In order to obtain the best structural architecture of the manipulator for a given trajectory, we propose in this section a procedure that allows the determination of the optimal system of actuation. This algorithm is based on the control of the pressure angles in the joints of the manipulator along the given trajectory (Fig. 4.6).

Two numerical examples are considered below in order to illustrate the application of the suggested design procedure.

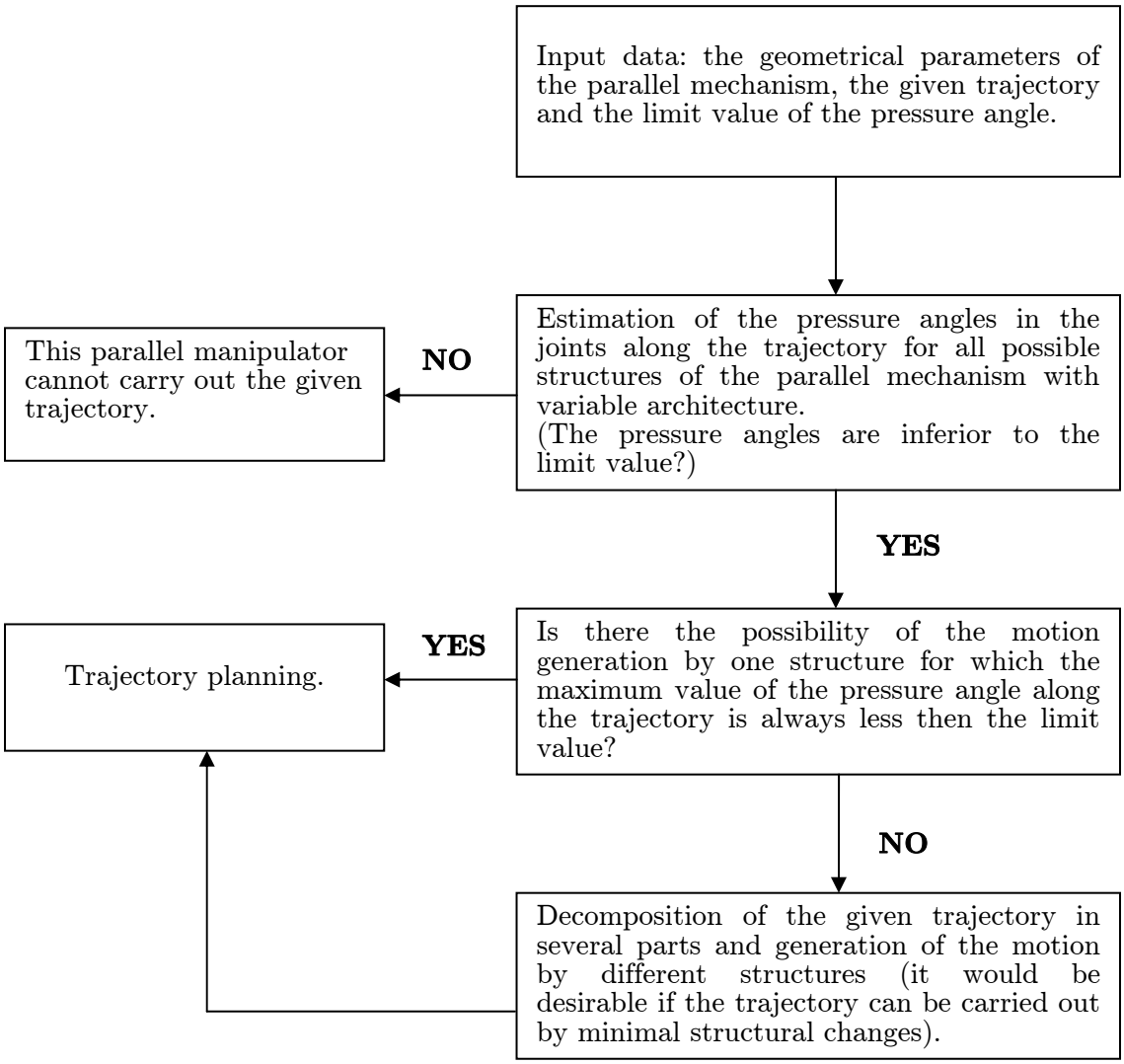

Figure 4.6. – Procedure for the determination of the optimal structure of the parallel manipulator taking into account the pressure angles.

4.4.1. Example 1.

For the given parallel manipulator (Fig. 4.1) with legs of variable structure (Fig. 4.3), we want to generate the trajectory by a straight line from the initial position $P_1 = (x_1 = 0,\ y_1 = 0,\ \phi_1 = 0)$ to the final position $P_2 = (x_2 = -0.25\ \text{m},\ y_2 = 0,\ \phi_2 = 0)$.

The estimation of the pressure angle along the given trajectory shows that the best structural solution to generate motion is the RPR-RPR-RPR mechanism, i.e. when the first actuator is connected to the link $M'_1H'_1$ and the two others with the links M'_2K_2 and M'_3K_3. In this case, the maximum values of the pressure angles in the joints are always less than the limit value.

In order to illustrate the variations of torques for the examined case, we developed a model of the manipulator with the given trajectory using the ADAMS software. The gravity field was disabled and a force parallel to the $\boldsymbol{x}$-axis and equal to 100 N was applied to the platform and the friction coefficients in the prismatic pairs were equal to 0.01. The obtained torques are shown in figure 4.7. It is easy to observe that the torques have admissible values along the trajectory.

Please note that, in absence of gravity, these torques are completely equivalent to those of the rotary actuators of a PAMINSA mechanism.

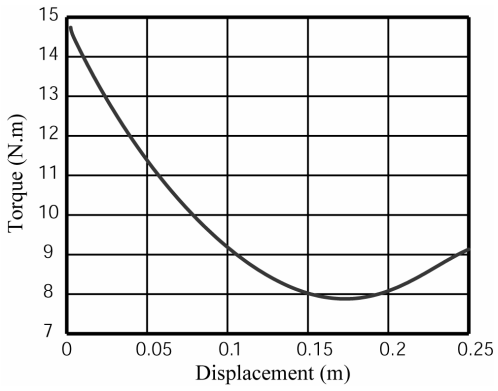

(a) Actuator 1

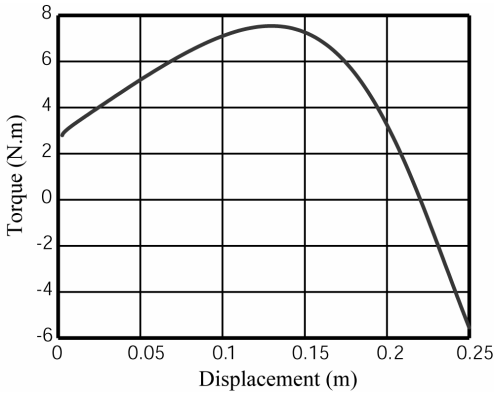

(b) Actuator 2

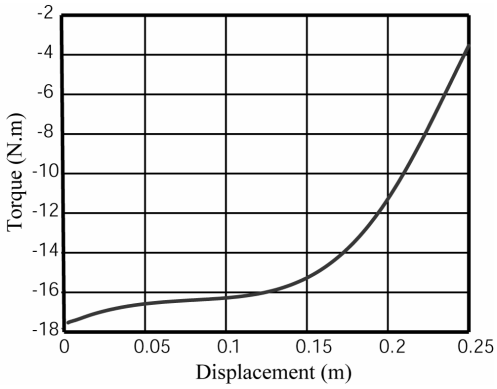

(c) Actuator 3

Figure 4.7. – Torques of the actuators.

4.4.2. Example 2.

For the given parallel manipulator (Fig. 4.1) with legs of variable structure (Fig. 4.3), we want to generate the trajectory by straight lines from the initial position $P_1 = (x_1 = 0,\ y_1 = 0,\ \phi_1 = 0)$ to the second position $P_2 = (x_2 = 0.1$ m, $y_2 = -0.25$ m, $\phi_2 = 0)$ and, then, to the final position $P_3 = (x_3 = -0.1$ m, $y_3 = -0.25$ m, $\phi_3 = 0)$.

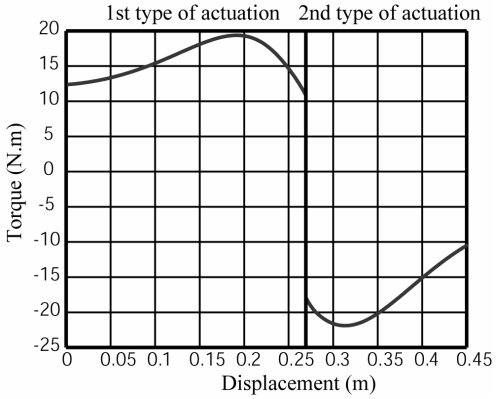

(a) Actuator 1

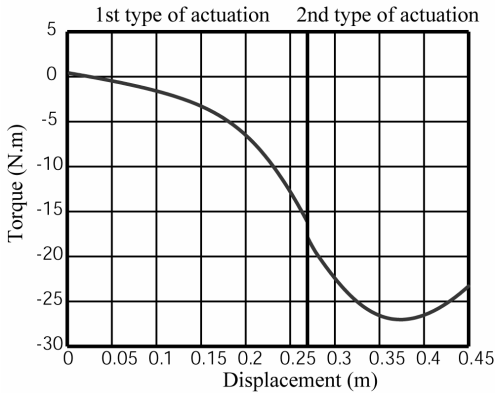

(b) Actuator 2

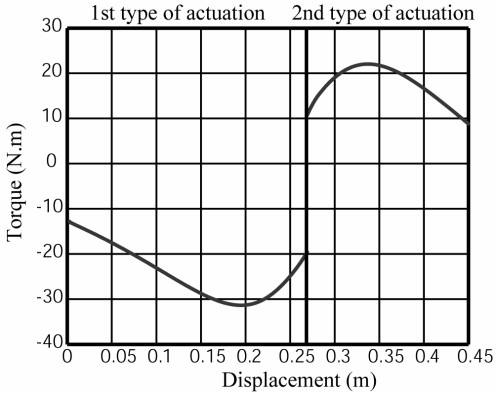

(c) Actuator 3

Figure 4.8. – Torques of the actuators.

In this case, the estimation of pressure angle shows that it is impossible to carry out the given trajectory by one structural system. First, the trajectory from initial position $P_1 = (x_1 = 0,\ y_1 = 0,\ \phi_1 = 0)$ to the second position $P_2 = (x_2 = 0.1$ m, $y_2 = -0.25$ m, $\phi_2 = 0)$ must be carried out by the R<u>P</u>R-<u>R</u>PR-R<u>P</u>R mechanism. Then,

from the second position $P_2 = (x_2 = 0.1$ m, $y_2 = -0.25$ m, $\phi_2 = 0)$ to the final position $P_3 = (x_3 = -0.1$ m, $y_3 = -0.25$ m, $\phi_3 = 0)$, the trajectory must be carried out by the RPR-RPR-RPR mechanism. Thus, the suggested solution based on these structural architectures makes it possible to obtain the optimal actuation system of the manipulator considering the pressure angle.

The obtained torques are shown in figure 4.8. We can note that the torques have admissible values along the trajectory but there is a discontinuity in the point P_2 caused by the structural change of the parallel mechanism.

It should be noted that the mechanism of variable structure shown above was developed by means of the added articulated dyads, but, it is obvious that such a mechanism can be designed on the base of the screw or cam systems, rhombic pantographs, etc.

In a similar way, one obtains the increase of singularity-free zones in the workspace of planar parallel manipulators only with revolute pairs (and, as a result, in the workspace of PAMINSA manipulators with corresponding structural parameters). In figure 4.9 is illustrated a 3-RRR parallel manipulator with the legs of variable structure.

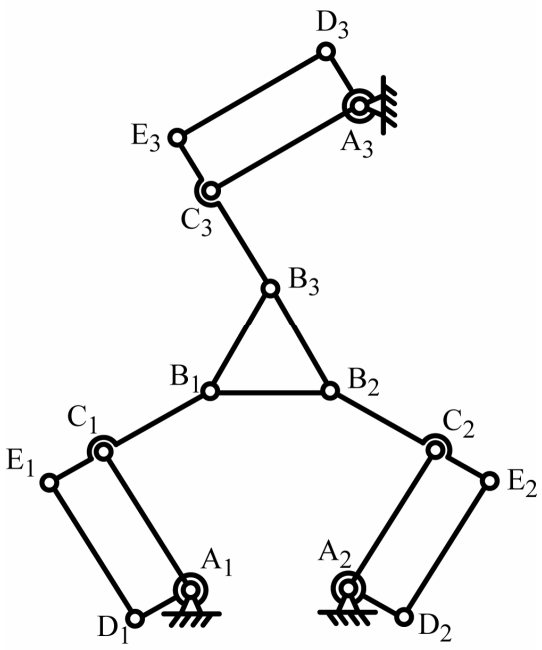

Figure 4.9. – Planar parallel manipulator 3-RRR with legs of variable structure.

The rotating actuators are mounted on the base and connected by electromagnetic clutches with the links A_iC_i and A_iD_i. These two input links cannot be actuated simultaneously and the input motion can be transmitted either by the link A_iC_i or A_iD_i. In this way, we can obtain the leg's mechanism with different structural parameters and carry out the given trajectory taking into account the limit value of the pressure angle. We shall not treat the procedure of resolution because it differs from the previous case only by the determination of the pressure angle.

The legs of variable structure can also be applied on general spatial mechanisms, as for example the 3-RPS mechanism (Fig. 4.10). A schematic of the modified leg with the added articulated dyad which makes it possible to change the input motion is shown on figure 4.11. The rotating actuators are mounted on the base and connected by electromagnetic clutches with the links A_iD_i and A_iC_i.

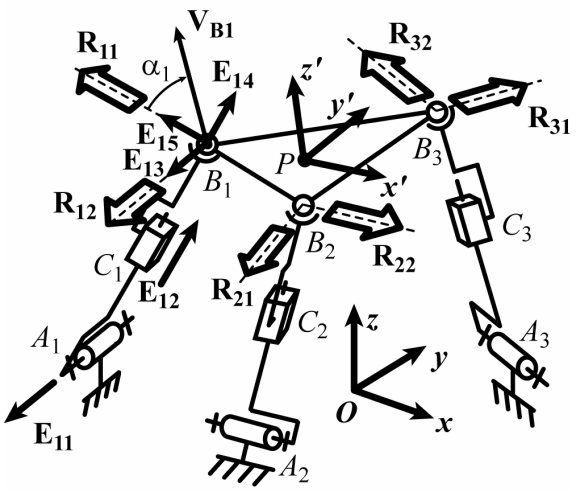

Figure 4.10. – Spatial parallel manipulator 3-RPS.

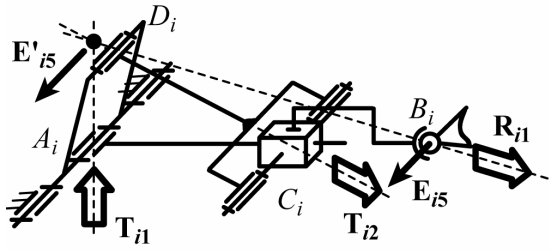

Figure 4.11. – Planar representation of the leg with variable structure.

The input motion can be transmitted either by the link A_iD_i or A_iC_i. In this way, we can obtain the leg of the mechanisms with different structural parameters, which changes the direction of the wrench $\mathbf{R}_{i1}$ and makes it possible to increase the singularity-free zones.

This approach can be applied for mechanisms with different degrees of freedom and different structures of legs. Particularly at the point A_i of the 3-RPS mechanism can be situated a universal joint. Then, each kinematic chain determines only one wrench $\mathbf{R}_i$ of which direction can be changed by choosing different input links. Thus, by such a way, we can determine the pressure angles corresponding to the different structures and obtain all possible workspace with singularity-free zones.

4.5. Summary.

A procedure for the increase of singularity-free zones in the workspace of planar parallel manipulators is presented in this chapter. The procedure is based on the known kinematic singularity equations and the control of the pressure angles in the joints of the manipulator along the given trajectory of the platform. The zones that could not be reached by the manipulator were detected. To increase of the reachable workspace of the manipulator, the legs of variable structure are proposed. Such a solution makes it possible to obtain the best structural architecture of the manipulator for any trajectory. The design of the optimal structure of the planar parallel manipulator 3-RPR (which is the planar equivalent model of the PAMINSA-4D3L) is illustrated by two numerical simulations.

Please note that this approach can be generalized to several planar or spatial manipulators. We believe that the suggested method is a useful tool for the improvement of the functional performances of parallel manipulators with singular zones.

In the following chapter, another method for enlarging the workspace of parallel mechanisms is also presented. This method is based on the optimization of the dynamic parameters of the manipulators.

Chapter 5

Determination of Optimum Dynamic Parameters of Parallel Manipulators for Passing through the Singular Positions

In this chapter, for the first time, the optimal dynamic conditions are determined, which allow the stable generation of motion inside the singular zones.

The obtained results show that the general condition for passing through a singularity can be defined as the following: the end-effector of the parallel manipulator can pass through the singular positions without perturbation of motion if the wrench applied on the end-effector by the legs of the manipulator and the external loads is orthogonal to the twist along the direction of the uncontrollable motion (in other terms, if the work of applied forces and moments on the platform along the uncontrollable motion is equal to zero).

This condition is obtained from the inverse dynamics and analytically demonstrated by the study of the Lagrangian of a general parallel manipulator. The obtained results are illustrated by two numerical simulations on a planar 5R mechanism and a PAMINSA manipulator with 4 DOF and validated by experimental tests.

5.1. Path planning of parallel manipulators in the presence of singular positions.

The singularity analysis of parallel manipulators has attracted the attention of several researchers and different studies have been published. Previous works on this problem may be arranged in three principal groups:

- kinematic study of the singular positions of parallel manipulators (chapter 3);
- kinetostatic study of the singular configurations taking into account the force transmission (chapter 4);
- path planning of parallel manipulators in the presence of singular positions; this point is developed in the remainder of this section.

The further study of singularity in parallel manipulators has revealed an interesting problem that concerns the path planning of parallel manipulators under the presence of singular positions, i.e. the motion feasibility in the neighborhood of singularities. In this case the dynamic conditions can be considered in the design process. One of the most evident solutions for the stable motion generation in the neighbourhood of singularities is to use redundant sensors and actuators (see chapter 4). However, it is an expensive solution to the problem because of the additional actuators and the complicated control of the manipulator caused by actuation redundancy. Another approach concerns with motion planning to pass through singularity [Bhattacharya 1998] [Dasgupta 1998] [Jui 2005] [Kemal Ider 2005] [Maas 2006] [Nenchev 1997] [Perng 1999], i.e. a parallel manipulator may track a path through singular poses if its velocity and acceleration are properly constrained. This is a promising path for the solution of this problem. However only a few research papers on this approach have addressed the path planning for obtaining a good tracking performance but they have not adequately addressed the physical interpretation of dynamic aspects.

In this chapter, for the first time, the dynamic condition for passing through the singular positions is defined in general. It allows the stable motion generation inside in the presence of singularity by means of the optimum force control. The disclosed condition can be formulated as follows: “In the presence of a Type 2 singularity, the platform of the parallel manipulator can pass through the singular positions without perturbation of motion if the wrench applied on the platform by the legs and external forces is orthogonal to the direction of uncontrollable motion”. In other terms, the condition is that the work of applied forces and moments on the platform along the uncontrollable motion is equal to zero. This condition is obtained from the inverse

dynamics and analytically demonstrated by the study of the Lagrangian of a general parallel manipulator. The obtained results are illustrated by numerical simulations and validated by experimental tests.

The chapter is organized as follows. Starting from the Lagrange equations, part 5.2 derives the analytical conditions on the effort distribution of a general parallel mechanism for passing through a Type 2 singularity. The section 5.3 applies these general conditions on two examples of parallel mechanisms (a 5R planar parallel robot and a PAMINSA manipulator with 4 DOF). Finally in part 5.4, experimental tests are carried out on the prototype of PAMINSA manipulator.

5.2. Optimal dynamic conditions for passing through Type 2 singularities.

Let us consider a parallel manipulator composed of m links, which has n degrees of freedom and driven by n actuators.

As it is well known, the Lagrangian dynamic formulation for a parallel manipulator can be expressed as:

$$\boldsymbol{\tau} = \frac{\mathrm{d}}{\mathrm{dt}}\left(\frac{\partial L}{\partial \dot{\mathbf{q}}}\right) - \frac{\partial L}{\partial \mathbf{q}} + \mathbf{B}^T\boldsymbol{\lambda}\,, \tag{5.1}$$

where,

- $\boldsymbol{\tau}$ is the vector of the input efforts;
- L is the Lagrangian of the examined manipulator;
- $\mathbf{q} = [q_1, q_2, ..., q_n]^T$ and $\dot{\mathbf{q}} = [\dot{q}_1, \dot{q}_2, ..., \dot{q}_n]^T$ represent the vector of active joints variables and the active joints velocities respectively;
- $\mathbf{x} = [x, y, z, \phi, \psi, \theta]^T$ and $\mathbf{v} = [\dot{x}, \dot{y}, \dot{z}, \dot{\phi}, \dot{\psi}, \dot{\theta}]^T$ represent the trajectory parameters and their derivatives respectively (x, y, z represent the position of the controlled point and ϕ, ψ and θ the rotation of the platform about three axes $\boldsymbol{a}_\phi$, $\boldsymbol{a}_\psi$ and $\boldsymbol{a}_\theta$);
- $\boldsymbol{\lambda}$ is the Lagrange multipliers vector, which is related to the wrench applied on the platform by:

$$\boldsymbol{\lambda} = \mathbf{A}^{-T}\mathbf{W_p} \tag{5.2}$$

where,

- $\mathbf{A}$ and $\mathbf{B}$ are two matrices relating the vectors $\mathbf{v}$ and $\dot{\mathbf{q}}$ according to $\mathbf{Av} = \mathbf{B}\dot{\mathbf{q}}$ which can be found by the derivation of the closure equations with respect to time [Gosselin 1990].
- $\mathbf{W_p}$ is the wrench applied on the platform by the legs and the external forces [Khalil 2002], which is defined as:

$$\mathbf{W_p} = \left(\frac{\mathrm{d}}{\mathrm{dt}}\left(\frac{\partial L}{\partial \mathbf{v}}\right) - \frac{\partial L}{\partial \mathbf{x}}\right) = \begin{bmatrix}\mathbf{f_p}\\ \mathbf{n_p}\end{bmatrix}. \tag{5.3}$$

where $\mathbf{f_p}$ is the force expressed along the directions of the global frame and $\mathbf{n_p}$ is the torque expressed about the axes $\boldsymbol{a}_\phi$, $\boldsymbol{a}_\psi$ and $\boldsymbol{a}_\theta$.

The term $\mathbf{W_p}$ can be rewritten in the base frame using a transformation matrix $\mathbf{D}$ [Merlet 2006a]:

$$\mathbf{W_p} = \mathbf{D}({}^{\mathbf{R}_0}\mathbf{W_p}) \tag{5.4}$$

where ${}^{\mathbf{R}_0}\mathbf{W_p}$ is the expression of the wrench $\mathbf{W_p}$ in the base frame, and

$$\mathbf{D} = \begin{bmatrix}\mathbf{I_{3\times3}} & \mathbf{0_{3\times3}}\\ \mathbf{0_{3\times3}} & \mathbf{R_{3\times3}}\end{bmatrix} \tag{5.5}$$

where $\mathbf{I_{3\times3}}$, $\mathbf{0_{3\times3}}$ and $\mathbf{R_{3\times3}}$ are respectively the identity matrix, the zero matrix and the transformation matrix between axes $\boldsymbol{a}_\phi$, $\boldsymbol{a}_\psi$ and $\boldsymbol{a}_\theta$ and the base frame, of which dimensions are 3×3.

Introducing equation (5.4) into equation (5.1), one can obtain:

$$\boldsymbol{\tau} = \mathbf{W_b} + \mathbf{J}^{T\,\mathbf{R}_0}\mathbf{W_p}, \quad \mathbf{W_b} = \frac{\mathrm{d}}{\mathrm{dt}}\left(\frac{\partial L}{\partial \dot{\mathbf{q}}}\right) - \frac{\partial L}{\partial \mathbf{q}} \tag{5.6}$$

where $\mathbf{J} = \left({}^{\mathbf{R}_0}\mathbf{A}\right)^{-1}\mathbf{B}$ is the Jacobian matrix between the twist $\mathbf{t}$ of the platform (expressed in the base frame) and $\dot{\mathbf{q}}$, ${}^{\mathbf{R}_0}\mathbf{A} = \mathbf{A}\,\mathbf{D}$ is the expression of matrix $\mathbf{A}$ in the base frame.

For any prescribed trajectory $\mathbf{x}(t)$, the values of vectors $\ddot{\mathbf{q}}$, $\dot{\mathbf{q}}$ and $\mathbf{q}$ can be found using the inverse kinematics. Thus, taking into account that the manipulator is not in a Type 1 singularity [Gosselin 1990], the terms $\mathbf{W_b}$ and ${}^{\mathbf{R}_0}\mathbf{W_p}$ can be computed. However, for a trajectory passing through a Type 2 singularity, the determinant of matrix $\mathbf{J}$ tends to infinite. Numerically, the values of the efforts applied by the actuators become infinite. In practice, the manipulator either is locked in such a position of the end-effector or it generates an uncontrolled motion. That is the end-effector of the manipulator produces a motion, different to the prescribed trajectory.

It is known that a Type 2 singularity appears when the determinant of matrix ${}^{\mathbf{R}_0}\mathbf{A}$ vanishes, in other words, when at least two of its columns are linearly dependant [Merlet 2006a].

Let us rewrite the matrix ${}^{\mathbf{R}_0}\mathbf{A}$ as:

$$ {}^{\mathbf{R}_0}\mathbf{A} = \begin{bmatrix} a_{11} & a_{12} & \dots & a_{16} \\ a_{21} & a_{22} & \dots & a_{26} \\ \vdots & \vdots & \ddots & \vdots \\ a_{61} & a_{62} & \dots & a_{66} \end{bmatrix}. \tag{5.7} $$

In the presence of Type 2 singularity the columns of matrix ${}^{\mathbf{R}_0}\mathbf{A}$ are linearly dependant, i.e.

$$ \sum_{u=1}^{6} \alpha_u \, a_{ju} = 0 \,,\; j = 1,\, \dots,\, 6 \tag{5.8} $$

where α_j are coefficients, which in general can be functions of q_p (p = 1, …, n). It should be noted that the vector $\mathbf{t_s} = [\alpha_1, \alpha_2, \dots, \alpha_n]^T$ represents the direction of the uncontrollable motion of the platform in a Type 2 singularity.

Rewriting equation (5.8) in a vector form, we obtain:

$$\sum_{u=1}^{6} \alpha_u \mathbf{N}_u = \mathbf{0}\,,\ \mathbf{N}_u = [a_{1u},\ a_{2u},\ \ldots,\ a_{nu}]^T,\ u = 1,\ \ldots,\ 6 \tag{5.9}$$

where $\mathbf{N}_u$ represents the u-th column of matrix ${}^{\mathbf{R}_0}\mathbf{A}$.

By substituting (5.9) into (5.2), we obtain:

$$\mathbf{N}_u^T \boldsymbol{\lambda} = W_u\,,\ u = 1,\ \ldots,\ 6 \tag{5.10}$$

where W_u is the u-th line of vector ${}^{\mathbf{R}_0}\mathbf{W}_\mathbf{p}$.

Then, from equations (5.9) and (5.10), the following conditions are derived:

$$\sum_{u=1}^{6} \left(\alpha_u \mathbf{N}_u^T \boldsymbol{\lambda}\right) = \sum_{u=1}^{6} \left(\alpha_u W_u\right) = 0\,. \tag{5.11}$$

The right term corresponds to the scalar product of vectors $\mathbf{t}_\mathbf{s}$ and ${}^{\mathbf{R}_0}\mathbf{W}_\mathbf{p}$.

Thus, in the presence of a Type 2 singularity, it is possible to satisfy conditions (5.11) if *the wrench applied on the platform by the legs and the external loads is orthogonal to the direction of the uncontrollable motion* (singular motion). Otherwise, the dynamic model is not consistent. Obviously, in the presence of a Type 2 singularity, the displacement of the end-effector of the manipulator has to be planned to satisfy (5.11).

Let us illustrate the considered problem by examples.

5.3. Illustrative examples.

In this section, two examples are chosen to illustrate the obtained theoretical results discussed above. The first example presents a planar 5R parallel manipulator, which allows obtaining relatively simple mathematical models for demonstrating the expected results by numerical simulations. The second example concerns with PAMINSA manipulator developed in the I.N.S.A. of Rennes. The fulfilled numerical simulations carried out on ADAMS software are validated on the built prototype.

5.3.1. Planar 5R parallel manipulator.

The planar 5R parallel manipulator, as shown in Fig. 5.1, is a structure of which output point is connected to the base by two legs, each of which consists of three revolute joints and two links. In each of the two legs, the revolute joint connected to the base is actuated. Thus, such a manipulator is able to position its output point in a plane.

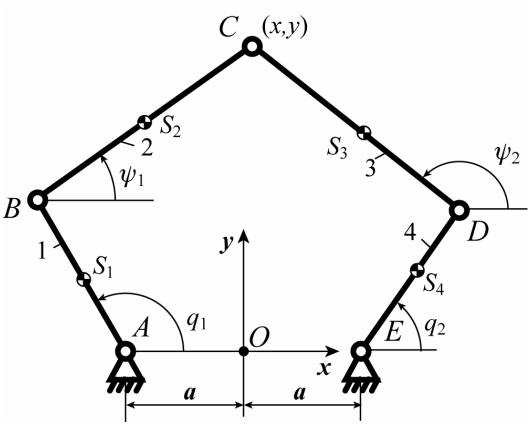

Figure 5.1. – Kinematic chain of the planar 5R parallel manipulator.

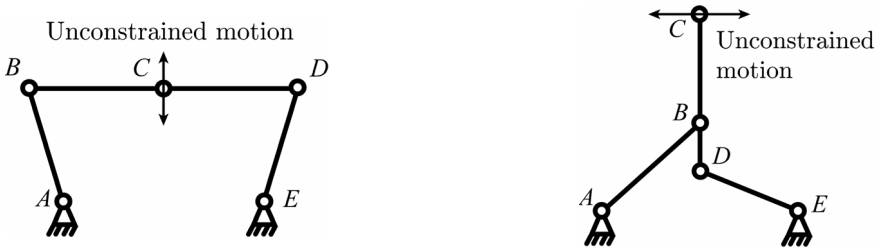

(a) $\psi_1 = \psi_2 \pm \pi$ (b) $\psi_1 = \psi_2 + 2n\pi$ $(n = 0, 1, 2...)$.

Figure 5.2. – Type 2 singularities of the planar 5R parallel manipulator.

As shown in Fig. 5.1, the actuated joints are denoted as A and E with input parameters q_1 and q_2. The common joint of the two legs is denoted as C, which is also the output point with controlled parameters x and y. A fixed global reference system ***xOy*** is located at the centre of AE with the ***y***-axis normal to **AE** and the ***x***-axis directed along **AE**. The lengths of the links AB, BC, BD, DE are respectively denoted

as L_1, L_2, L_3 and L_4. The positions of the centers of masses S_i of links from joint centers A, B, D and E are respectively denoted by dimensionless lengths r_1, r_2, r_3 and r_4, i.e. $AS_1 = r_1L_1$, $BS_2 = r_2L_2$, $DS_3 = r_3L_3$ and $ES_4 = r_4L_4$.

The singularity analysis of this manipulator [Liu 2006] shows that the Type 2 singularities appear when links 2 and 3 are parallel (Fig. 5.2). In both cases, the gained degree of freedom is an infinitesimal translation perpendicular to the links 2 and 3. However, if $L_2 = L_3$, the gained degree of freedom in case (b) becomes a finite rotary motion about point B.

5.3.1.1. Inverse dynamics.

In order to simplify the analytic expressions, we consider that the gravity effects are along the z-axis and consequently the input torques are only due to inertia effects. It is also preferable to replace the masses of moving links by concentrated masses [Seyferth 1974] [Wu 2007]. For a link j with mass m_j and its axial moment of inertia I_j, we have:

$$\begin{bmatrix} 1 & 1 & 1 \\ r_j & 0 & 1-r_j \\ r_j^2 L_j^2 & 0 & (1-r_j)^2 L_j^2 \end{bmatrix} \begin{bmatrix} m_{j1} \\ m_{j2} \\ m_{j3} \end{bmatrix} = \begin{bmatrix} m_j \\ 0 \\ I_j \end{bmatrix}, \ (j = 1, 2, 3, 4) \tag{5.12}$$

where m_{ji} ($i = 1, 2, 3$) are the values of the three point masses placed at the centers of the revolute joints and at the center of masses of the link j.

In this case, the kinetic energy T can be written as:

$$T = \frac{1}{2}\left(m_{S1}\mathbf{V}_{S1}^2 + m_{S2}\mathbf{V}_{S2}^2 + m_{S3}\mathbf{V}_{S3}^2 + m_{S4}\mathbf{V}_{S4}^2 + m_B\mathbf{V}_B^2 + m_C\mathbf{V}_C^2 + m_D\mathbf{V}_D^2\right) \tag{5.13}$$

where, $m_{S1} = m_{12}$, $m_{S2} = m_{22}$, $m_{S3} = m_{32}$, $m_{S4} = m_{42}$, $m_B = m_{13} + m_{21}$, $m_C = m_{23} + m_{21}$, $m_D = m_{33} + m_{41}$. The terms m_{ji} are deduced from the relation (5.12), $\mathbf{V}_{Sj}$ is the vector of the linear velocities of the centre of masses S_j and $\mathbf{V}_B$, $\mathbf{V}_C$ and $\mathbf{V}_D$ are the vectors of the linear velocities of the corresponding axes.

The input torques can be obtained from equation (5.6):

$$\boldsymbol{\tau} = \mathbf{W_b} + \mathbf{J}_{5R}^T\mathbf{W_p} \tag{5.14}$$

taking into account that for examined manipulator:

$$\mathbf{W_b} = \mathbf{J_B^T}\,\mathbf{F_B} + \mathbf{J_D^T}\,\mathbf{F_D}\,, \tag{5.15}$$

where,

$$\mathbf{J_B} = \begin{bmatrix} -L_1 \sin q_1 & 0 \\ L_1 \cos q_1 & 0 \end{bmatrix},\ \mathbf{J_D} = \begin{bmatrix} 0 & -L_4 \sin q_2 \\ 0 & L_4 \cos q_2 \end{bmatrix}, \tag{5.16}$$

$$\mathbf{F_B} = m_{B1}\,\mathbf{\Gamma_B} + m_{C1}\,\mathbf{\Gamma_C}\,,\ \mathbf{F_D} = m_{D2}\,\mathbf{\Gamma_D} + m_{C3}\,\mathbf{\Gamma_C}\,, \tag{5.17}$$

$$\mathbf{\Gamma_B} = L_1\left(\ddot{q}_1\begin{bmatrix} -\sin q_1 \\ \cos q_1 \end{bmatrix} - \dot{q}_1^2\begin{bmatrix} \cos q_1 \\ \sin q_1 \end{bmatrix}\right), \mathbf{\Gamma_D} = L_4\left(\ddot{q}_2\begin{bmatrix} -\sin q_2 \\ \cos q_2 \end{bmatrix} - \dot{q}_2^2\begin{bmatrix} \cos q_2 \\ \sin q_2 \end{bmatrix}\right), \mathbf{\Gamma_C} = \begin{bmatrix} \ddot{x} \\ \ddot{y} \end{bmatrix}, \tag{5.18}$$

$$m_{B1} = m_{S1}r_1^2 + m_B + m_{S2}(1-r_2)^2\,,\ m_{C1} = m_{S2}r_2(1-r_2)\,, \tag{5.19}$$

$$m_{C3} = m_{S3}r_3(1-r_3)\,,\ m_{D2} = m_{S4}r_4^2 + m_D + m_{S3}(1-r_3)^2\,. \tag{5.20}$$

The term $\mathbf{W_p}$ is given by:

$$\mathbf{W_p} = m_{C1}\mathbf{\Gamma_B} + m_{C2}\mathbf{\Gamma_C} + m_{C3}\mathbf{\Gamma_D}\,, \tag{5.21}$$

$$m_{C2} = m_{S2}r_2^2 + m_C + m_{S3}r_3^2\,, \tag{5.22}$$

and the Jacobian matrix $\mathbf{J}_{5R}$ by:

$$\mathbf{J}_{5R} = \mathbf{A}_{5R}^{-1}\mathbf{B}_{5R}\,, \tag{5.23}$$

where

$$\mathbf{A}_{5R} = \begin{bmatrix} a_{11} & a_{12} \\ a_{21} & a_{22} \end{bmatrix} = 2\begin{bmatrix} x - L_1\cos q_1 + a & y - L_1 \sin q_1 \\ x - L_4\cos q_2 - a & y - L_4 \sin q_2 \end{bmatrix}, \tag{5.24}$$

$$\mathbf{B}_{5R} = -\begin{bmatrix} L_1(a_{11}\sin q_1 - a_{12}\cos q_1) & 0 \\ 0 & L_4(a_{21}\sin q_2 - a_{22}\cos q_2) \end{bmatrix}. \tag{5.25}$$

We determine $\mathbf{t_s}$ in according with (5.8):

$$\mathbf{t_s} = [-\sin\psi_1, \cos\psi_1]^T . \tag{5.26}$$

Thus, the examined manipulator can pass through the given singular positions if the force $\mathbf{W_p}$ determined by (5.21) is orthogonal to the direction of the uncontrollable motion $\mathbf{t_s}$ described by (5.26).

5.3.1.2. Motion Planning.

Let us now consider the motion planning, which makes it possible to satisfy this condition. For this purpose the following parameters of manipulator's links are specified: $L_1 = L_2 = L_3 = L_4 = 0.25$ m; $r_1 = r_2 = r_3 = r_4 = 0.5$; $a = 0.2$ m; $m_1 = m_4 = 2.81$ kg; $I_1 = I_4 = 0.02$ kg/m^2; $m_2 = m_3 = 1.41$ kg; $I_2 = I_3 = 0.01$ kg/m^2.

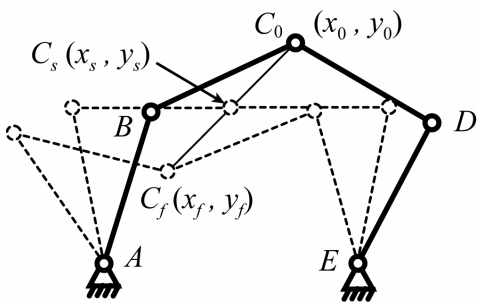

Figure 5.3. – Initial, singular and final positions of the planar 5R parallel manipulator.

The point C should reproduce a motion along a straight line between the initial position C_0 $(x_0, y_0) = C_0$ (0.1, 0.345) and the final point C_f $(x_f, y_f) = C_f$ (–0.1, 0.145) in $t_f = 2$ s. However, the manipulator will pass by a Type 2 singular position at point C_s $(x_s, y_s) = C_s$ (0, 0.245) (Fig. 5.3).

Thus, the given trajectory can be expressed as follows:

$$\mathbf{x} = \begin{bmatrix} x(t) \\ y(t) \end{bmatrix} = \begin{bmatrix} x_0 + s(t)(x_f - x_0) \\ y_0 + s(t)(y_f - y_0) \end{bmatrix}. \tag{5.27}$$

Developing the condition (5.11) for passing through the singular position for the planar 5R parallel manipulator at point C_s, we obtain:

$$m_{C1}\, L_1\, (248\, \dot{x}^2 - 48\, \dot{y}^2) - 3\sqrt{6} m_{C2}\, \ddot{y} = 0 \tag{5.28}$$

Then, taking into account that the velocity and the acceleration of the end-effector in initial and final positions are equal to zero, the following nine boundary conditions are found:

$$s(t_0) = 0, \tag{5.29}$$

$$s(t_f) = 1, \tag{5.30}$$

$$s(t_s = 1\ \mathrm{s}) = 0.5, \tag{5.31}$$

$$\dot{s}(t_0) = 0\,, \tag{5.32}$$

$$\dot{s}(t_f) = 0\,, \tag{5.33}$$

$$\dot{s}(t_s) = \dot{y}_s\,/(y_f - y_0) = \dot{x}_s\,/(x_f - x_0) = 1\,, \tag{5.34}$$

$$\ddot{s}(t_0) = \ddot{s}_0 = 0\,, \tag{5.35}$$

$$\ddot{s}(t_f) = \ddot{s}_f = 0\,, \tag{5.36}$$

$$\ddot{s}(t_s) = \ddot{s}_s = m_{C1} L_1 (248\, \ddot{x}_s^2 - 48\, \dot{y}_s^2)/(3\,(x_f - x_0)\sqrt{6} m_{C2})\,. \tag{5.37}$$

From (5.29) – (5.37), the following eighth order polynomial trajectory planning is found:

$$s(t) = -\,0.25851 t^3 + 3.84228 t^4 - 5.72792 t^5 + 3.58909 t^6 - 1.07101 t^7 + 0.12606 t^8\,. \tag{5.38}$$

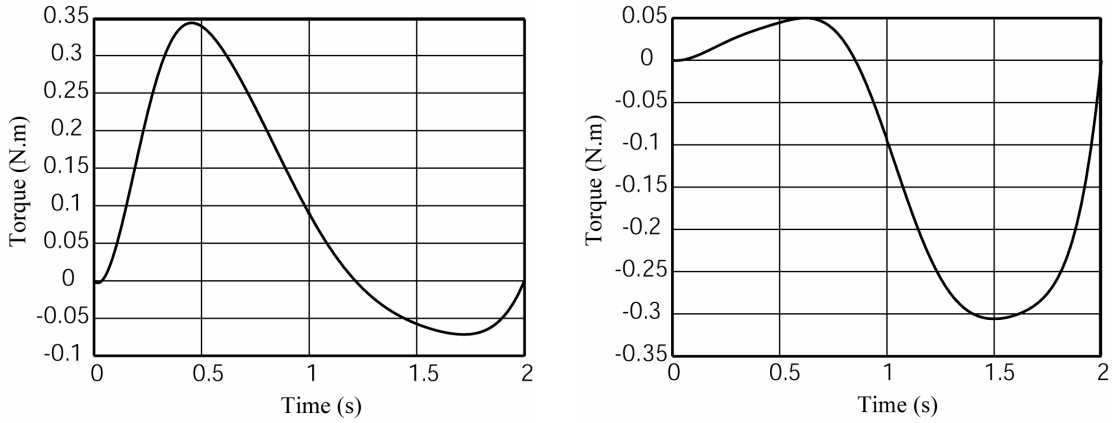

(a) actuator 1. (b) actuator 2.

Figure 5.4. – Input torques of the planar 5R parallel manipulator in the case of the sixth order polynomial trajectory planning, obtained by the ADAMS software.

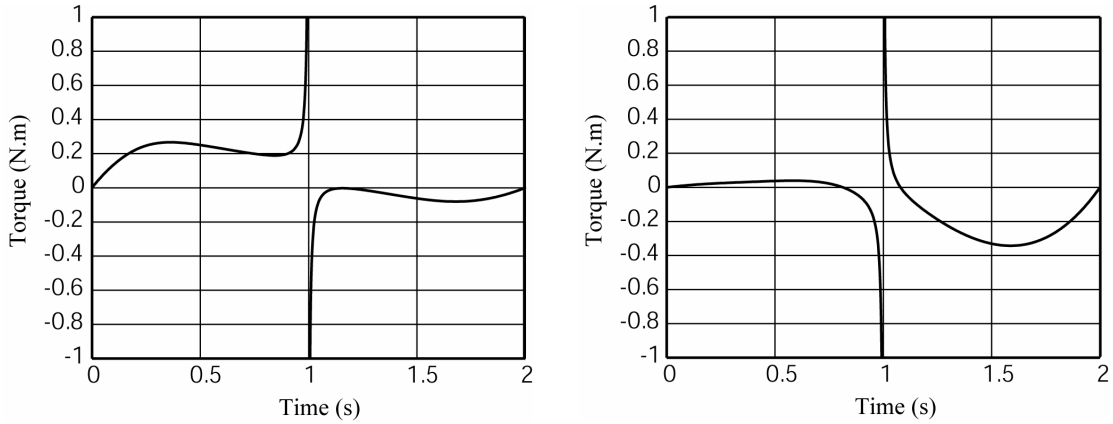

(a) actuator 1. (b) actuator 2.

Figure 5.5. – Input torques of the planar 5R parallel manipulator in the case of the fifth order polynomial trajectory planning, obtained by the ADAMS software.

Thus the generation of the motion by the obtained eighth order polynomial makes it possible to pass through the singularity without perturbation and the input torques remain in the limits of finite values, which are validated by numerical simulations carried out by the ADAMS software (Fig. 5.4).

Thus, we can assert that the obtained optimal dynamic conditions assume the passing of the manipulator's end-effector through the singular position.

Now, we would like to show that, in the case of the generation of the motion by any trajectory planning without meeting the adopted boundary conditions, the end-effector is not able to pass through the singular position. For the generation of motion between initial and final positions, let us generate by a fifth order polynomial trajectory planning:

$$s(t) = 1.25\,t^3 - 0.9375\,t^4 + 0.1875\,t^5 . \tag{5.39}$$

The obtained numerical simulations carried out by the software ADAMS are given in Fig. 5.5. We can see that, when the manipulator is close to the singular configuration (for $t_s = 1$ s), the values of the input torques tend to infinity.

5.3.2. PAMINSA-4D3L.

Chapter 3 disclosed that there are Type 2 singularities in the workspace of PAMINSA manipulators. In this section, we will study the possibility of passing through the singular positions of these manipulators. The obtained results will be illustrated by numerical simulations and validated by experimental tests in the following section.

Let us now study the inverse dynamics of the PAMINSA-4D3L described in figure 2.8.

5.3.2.1. Inverse dynamics.

We consider that the gravity effects are directed along the z-axis and, consequently, the input torques are due to both gravity and inertia effects.

In the case of the studied PAMINSA manipulator, the Lagrangian can be written as:

$$L = T - V \tag{5.40}$$

where V is the potential energy and T the kinetic energy. The expression of V is presented in chapter 2.

We consider that the links are perfect tubes. Therefore the inertia matrix $\mathbf{I}_j$ of the link B_{ji} at the center of masses will be written as:

$$\mathbf{I}_j = \begin{bmatrix} I_{XX}^{(j)} & 0 & 0 \\ 0 & I_{YY}^{(j)} & 0 \\ 0 & 0 & I_{ZZ}^{(j)} \end{bmatrix}, \text{ with } I_{YY}^{(j)} = I_{ZZ}^{(j)}. \tag{5.41}$$

Thus, the kinetic energy T of the manipulator can be represented as:

$$T = T_{pl} + \sum_{i=1}^{3} T_{leg_i}, \tag{5.42}$$

where T_{pl} is the kinetic energy of the platform, T_{legi} is the kinetic energy of the leg i, with:

$$T_{pl} = \frac{1}{2}\left(m_{pl}\,(\dot{x}^2 + \dot{y}^2 + \dot{z}^2) + I_{pl}\,\dot{\phi}^2\right) \tag{5.43}$$

where m_{pl} and I_{pl} are respectively the mass and the axial moment of inertia of the platform about the vertical axis, and

$$T_{leg_i} = T_{trans_i} + T_{rot_i} \tag{5.44}$$

where

$$\begin{aligned} T_{trans_i} = {} & C_{c1}\,(\dot{x}_{5i}^2 + \dot{y}_{5i}^2) + C_{c2}\,\dot{z}_{5i}^2 + C_{c3}\,(\dot{x}_{9i}^2 + \dot{y}_{9i}^2 + \dot{z}_{9i}^2) + C_{c4}\,(\dot{x}_{5i}\,\dot{x}_{9i} + \dot{y}_{5i}\,\dot{y}_{9i}) \\ & + C_{c5}\,\dot{z}_{5i}\,\dot{z}_{9i} + C_{c6}\,\dot{q}_v + C_{c7}\,\dot{z}_{5i}\,\dot{q}_v + C_{c8}\,\dot{q}_i^2 \end{aligned} \tag{5.45}$$

and T_{rot_i} is the kinetic energy of the rotating links.

Note that there are two types of rotations (Fig. 2.8):

- rotation due to the actuators M_i ($i = 1, 2, 3$) (angle q_i), which is about the vertical axis,

- rotations due to the displacement of the pantograph in the linkage plane (angles ζ_i and ε_i denoted as the angles between the direction of the passive slider and links B_{4i} and B_{3i} respectively).

Thus, the kinetic energy of the rotating links can be written as:

$$T_{rot_i} = C_{c9}\,\dot{\zeta}_i^2 + C_{c10}\,\dot{\varepsilon}_i^2 + \dot{q}_i^2\,(C_{c13} + C_{c10}\sin^2\varsigma_i + C_{c9}\cos^2\varsigma_i + C_{c12}\sin^2\varepsilon_i + C_{c11}\cos^2\varepsilon_i) \tag{5.46}$$

The expressions for C_{cj} ($j = 1, \ldots, 13$) are given in appendix D.

The input torques can be obtained from equation (5.6):

$$\boldsymbol{\tau} = \mathbf{W_b} + \mathbf{J}^T\mathbf{W_p} \tag{5.47}$$

where the expressions of $\mathbf{J}$, $\mathbf{W_b}$ and $\mathbf{W_p}$ are presented in appendix D.

5.3.2.2. Motion planning.

The following parameters of manipulator's links are specified at appendix E for the trajectory generation.

The point P is desired to make a motion $x(t)$ along a straight line between point P_0 $(x_0, y_0) = P_0\ (0,\ 0)$ and point $P_f\ (x_f, y_f) = P_f\ (0.3,\ 0)$ in $t_f = 2.4$ s at an altitude $z = -0.45$ m and with a constant orientation of the platform equal to $\phi = 0$ deg. However, the manipulator will pass through a Type 2 singular position at point $P_s\ (x_s, y_s) = (0.25,\ 0)$ (Fig. 5.6).

In order to carry out a comparative analysis for the optimized and not optimized dynamic conditions for passing through Type 2 singularity, it has been considered two cases. The first is such a movement on the given trajectory, which is calculated from condition (5.11), and the second is an arbitrary motion.

At first let us consider an optimized trajectory which allows satisfying the condition (5.11), i.e. the force $\mathbf{W_p}$ should be perpendicular to the to the twist $\mathbf{t_s} = [0,\ 0,\ 1,\ 0,\ 0.1,\ 0]^T$ (equation (4.4)) defining the direction of the unconstrained motion.

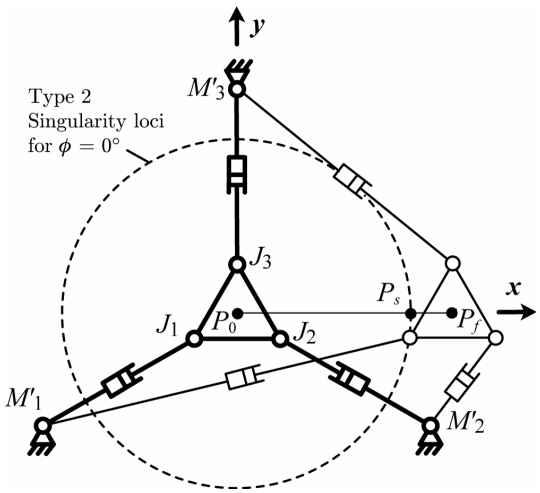

Figure 5.6. – Displacement of the PAMINSA along the prescribed straight line (planar equivalent model).

Developing expression (5.11) for the PAMINSA at point P_s, we obtain:

$$\begin{aligned} 0 = {} & 0.06441\,\ddot{x} + 1.2115\,\ddot{y} - 0.14649\,\ddot{z} + 0.04425\,\ddot{\phi} + 0.06827 + 6.85084\,\dot{x}^2 \\ & + 0.11720\,\dot{y}^2 - 0.18482\,\dot{z}^2 + 0.02947\,\dot{\phi}^2 - 0.85175\,\dot{\phi}\,\dot{x} + 0.05643\,\dot{\phi}\,\dot{y} + \\ & 0.19423\,\dot{\phi}\,\dot{z} - 5.17625\,\dot{x}\,\dot{y} + 0.46477\,\dot{x}\,\dot{z} + 2.94694\,\dot{y}\,\dot{z} \end{aligned} \quad (5.48)$$

Now considering that the end-effector of the manipulator moves along a straight line directed along the ***x***-axis, we can note that $\dot{y}(t_s) = \dot{z}(t_s) = \ddot{y}(t_s) = \ddot{z}(t_s) = \dot{\phi}(t_s) = \ddot{\phi}(t_s) = 0$. Thus, the relationships, which satisfy the passing through of the singular positions, taking into account that the velocity and the acceleration of the platform in the initial and final positions are equal to zero, can be expressed by the following boundary conditions:

$$x(t_0) = x_0, \quad (5.49)$$

$$x(t_f) = x_f, \quad (5.50)$$

$$x(t_s = 2\text{ s}) = x_s, \quad (5.51)$$

$$\dot{x}(t_0) = 0\,, \tag{5.52}$$

$$\dot{x}(t_f) = 0\,, \tag{5.53}$$

$$\ddot{x}(t_0) = 0\,, \tag{5.54}$$

$$\ddot{x}(t_f) = 0\,, \tag{5.55}$$

$$\dot{x}(t_s) = \dot{x}_s = 0.05\,\text{m/s}, \tag{5.56}$$

$$\ddot{x}(t_s) = \ddot{x}_s = -1.32583\ \text{m/s}^2. \tag{5.57}$$

In this case, a motion for passing of the platform through the singular position can be found from the following eighth order polynomial form:

$$x(t) = 3.41\,t^8 - 37.65\,t^7 + 166.05\,t^6 - 365.23\,t^5 + 400.63\,t^4 - 175.27\,t^3 \tag{5.58}$$

However, a trajectory obtained by (5.58) cannot be reproduced by the prototype because of the limited capability of drivers' deceleration. Therefore, the trajectory was divided into two parts, i.e. the first sixth order polynomial trajectory assumes the motion from an initial to the singular position (P_0P_s) and the second sixth order polynomial trajectory from singular to the final position (P_sP_f). The core of the problem is the same but it allows for generating motions for the prototype.

Thus, the trajectory planning equations can be written as:

$$x(t) = x_0 + (x_s - x_0)\left(b_3t^3 + b_4t^4 + b_5t^5 + b_6t^6\right) \text{ for } t \le t_s; \tag{5.59}$$

$$x(t) = x_s + (x_f - x_s)\left(c_1(t_f - t_s) + c_2(t_f - t_s)^2 + c_4(t_f - t_s)^4 + c_5(t_f - t_s)^5 + c_6(t_f - t_s)^6\right)$$
$$\text{for } t > t_s. \tag{5.60}$$

with $b_3 = -3.3033$, $b_4 = 5.10456$, $b_5 = -2.45207$, $b_6 = 0.37844$, $c_1 = 1$, $c_2 = -13.25829$, $c_4 = 2365.3672$, $c_5 = -11953.07236$ and $c_6 = 16158.76157$.

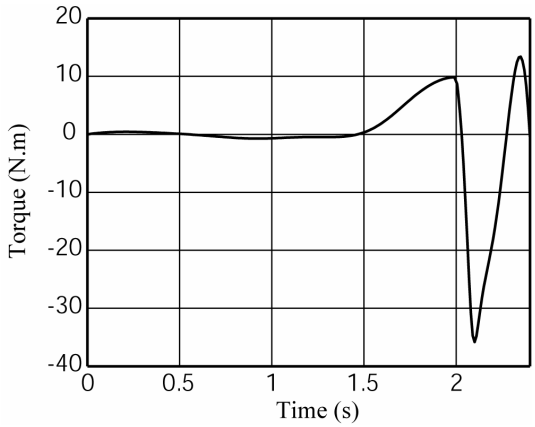

(a) actuator M_1.

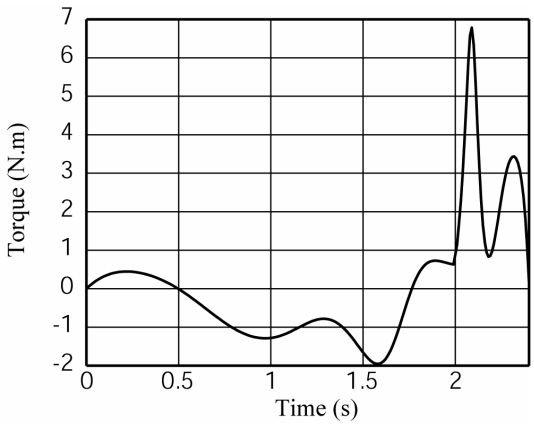

(b) actuator M_2.

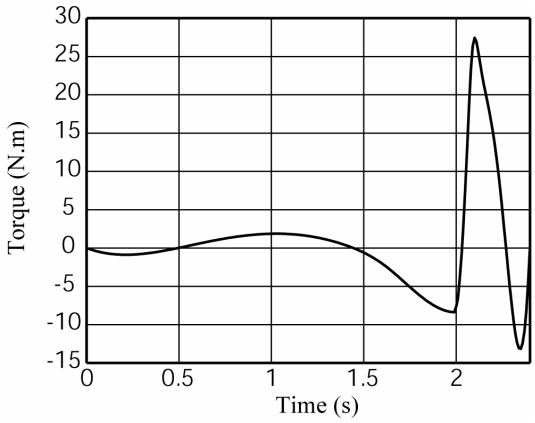

(c) actuator M_3.

Figure 5.7. – Input efforts of the PAMINSA in the case of the sixth order polynomial trajectory planning, computed with ADAMS software.

Thus, the motion obtained from the following sixth order polynomial equations

$$x(t) = -0.826\,t^3 + 1.276\,t^4 - 0.613\,t^5 + 0.095\,t^6 \quad \text{for t} \le 2\text{s}; \tag{5.61}$$

$$x(t) = 72722.7 - 206718.3\,t + 244555.2\,t^2 - 154122.4\,t^3 + 54571.1\,t^4 - 10292.9\,t^5 + 807.9\,t^6$$
$$\text{for t} > 2\text{s}; \tag{5.62}$$

allows for passing through the singularity without perturbation, and the input efforts take on finite values (Fig. 5.7).

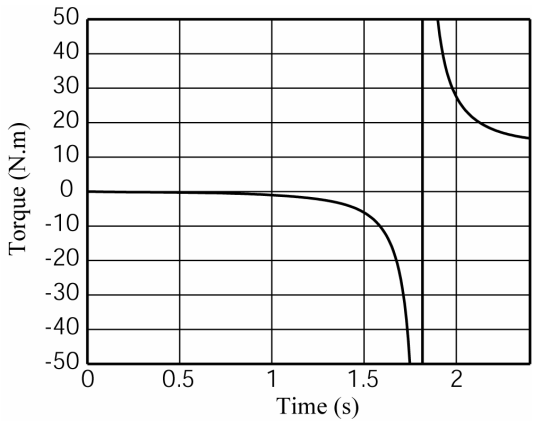

(a) actuator M_1.

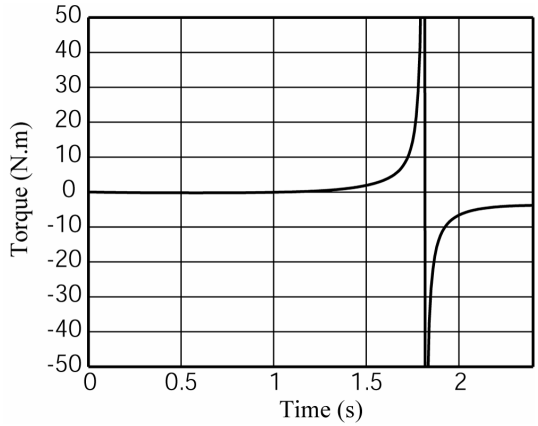

(b) actuator M_2.

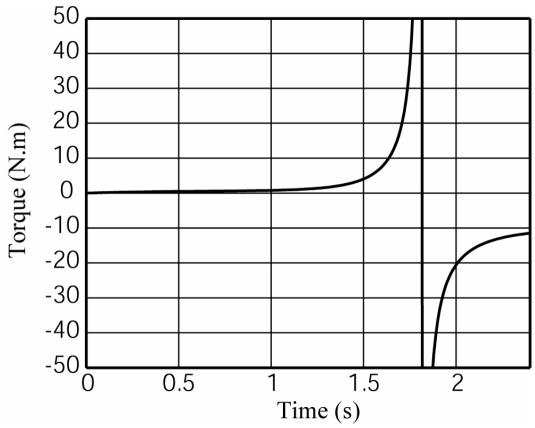

(c) actuator M_3.

Figure 5.8. – Input efforts of the PAMINSA in the case of the fifth order polynomial trajectory planning, computed with ADAMS software.

It can be seen that the input torques remain in the limits of finite values, but, by the end of the motion there is an increase in the input efforts, caused by a quick deceleration to stop the manipulator before it reaches the workspace boundary. It will be shown further that in the case of the motion generated by any trajectory planning without meeting the adopted boundary conditions (5.49) – (5.57), the manipulator platform is not able to pass through the singular position. For this purpose, the generation of motion between initial and final positions is carried out by a fifth order polynomial trajectory planning.

In this case, for $y(t) = 0\,\text{m}$, $z(t) = -0.45\,\text{m}$ and $\phi(t) = 0$, the fifth order polynomial trajectory planning is the following:

$$x(t) = 0.217\,t^3 - 0.137\,t^4 + 0.023\,t^5 \tag{5.63}$$

The obtained input efforts computed by the software ADAMS are represented in Fig. 5.8.

It can be noted that, while the manipulator passes through the singular configuration (for $t_s \approx 1.8$ s), the value of the input torques tend to infinity.

Let us now validate the obtained results by experimental tests.

5.4. Experimental validation of obtained results.

First of all, we have implemented the fifth order control law described in the previous section. We observed the reproduction of the desired motion during the displacement of the platform. The obtained trajectory is shown in Fig. 5.9 (dotted line). The different positions are classified by time. For positions from (a) to (d), the platform moves towards the singular zone but yet it is outside of it. In this case, the reproduction of the real trajectory is similar to the desirable. At position (e), the manipulator enters the singular zone, which is close to the circle of the theoretical singular loci, and starts an uncontrollable motion. Thus, since the motion generation is carried out by non optimized dynamic parameters, the platform moves along an unplanned trajectory (see positions (f), (g) and (h) in Fig. 5.9).

Next, we have implemented the sixth order control laws as it was shown in the previous section and observed the behavior of the platform during the displacement (Fig. 5.10). The different positions are classified by time. During all these displacements, the manipulator retains its orientation and passes through the singular configuration without any perturbation.

Thus, we can note that the obtained optimum dynamic conditions allow the passing of the manipulator through the singular position

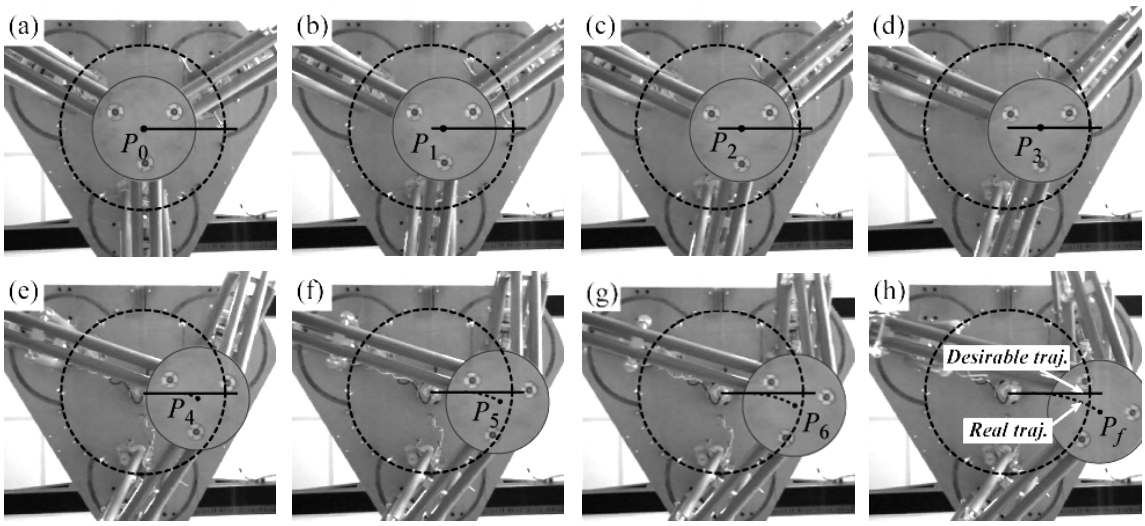

Figure 5.9. – Trajectory reproduction on the PAMINSA during the displacement of the platform with the fifth order polynomial law (view from below).

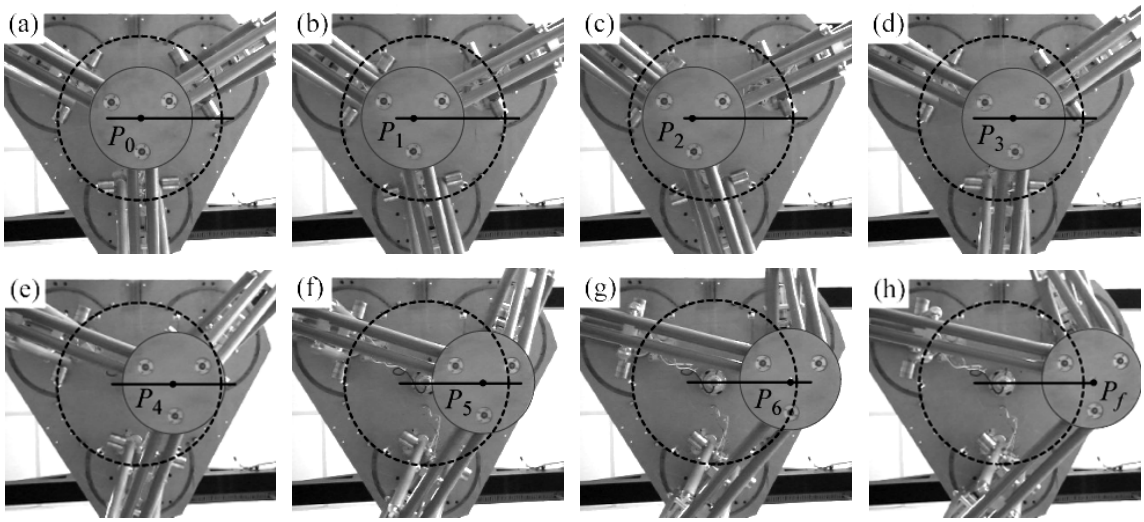

Figure 5.10. – Trajectory reproduction on the PAMINSA during the displacement of the platform with the sixth order polynomial law (view from below).

5.5. Summary.

In a singular configuration, a manipulator can gain one or more degrees of freedom, and at such a configuration it may becomes uncontrollable, i.e. it may not reproduce stable motion with prescribed trajectory. Nevertheless there are several proven motion

planning techniques which make it possible to pass through these singular zones. These approaches are simulated by numerical examples and illustrated on several parallel structures. It is a promising option for the solution of this problem. However, attention is focused only on control aspects of this problem and very little attention has been paid to dynamic interpretation, which is a crucial factor for governing the behavior of parallel manipulators at the singular zones.

In this chapter we have found the optimal dynamic conditions, for making the pass through the Type 2 singular configurations possible. The general definition of the condition for passing through the singular position is formulated as follows: in the presence of Type 2 singular configuration, the platform of a parallel manipulator can pass through the singular positions without perturbation of motion if the wrench applied on the platform by the legs and external efforts are orthogonal to the direction of the uncontrollable motion, or in other words, if the work of applied forces and moments on the platform along the uncontrollable motion is equal to zero. This condition has been verified by numerical simulations carried out with the software ADAMS and validated by experimental tests on the prototype of PAMINSA.

The passing of any parallel manipulator through the singular positions by the proposed technique is carried out by optimal generation of inertia forces. Hence, it is impossible to stop the manipulator in the singular locus and to start again from fixed position.

Finally, it should be noted that for the case of non controllable external forces applied on the platform the proposed technique cannot be used. Therefore, the most prominent field of the industrial application is a “fast pick and place” manipulation, when the generation of motion is determined by input, gravitational and inertia forces.

The next chapter deals with optimization methods which can be used in design procedures of PAMINSA manipulators.

Chapter 6

Optimization of PAMINSA Manipulators

In this chapter, methods for the optimization of PAMINSA manipulators are shown. In the first part, a new, fast and efficient method of accuracy analysis of planar parallel manipulators (which may be easily applied to the PAMINSA manipulators) is presented. This method is achieved by following a detailed mathematical proof that gives important insight into the accuracy of planar parallel robots. The method is illustrated on two practical designs. This method can be used in design optimization procedures that seek maximum accuracy.

In the second part, we propose new compensation schemes, which consist of the introduction into the initial system of complementary units making it possible to cancel the positioning errors due to the elasticity of the links. Two different approaches are proposed and the performances of such designs are shown.

Finally, the reduction of the input torques is also studied. It is shown in simulation and by experimental tests that, for a dynamic mode of operation, the complete static balancing may be ineffective in terms of input torques. In the case of accelerated motions, it is proposed to carry out an optimal redistribution of the movable masses and to achieve a partial mass balancing.

6.1. Accuracy analysis.

Parallel robots are increasingly being used for precision positioning, and a number of them are used as 3-DOF planar alignment stages. Clearly, in such industrial applications, accuracy is of utmost importance. Therefore, simple and fast methods for computing the accuracy of a given robot design are needed in order to use them in design optimization procedures which seek maximum accuracy.

Errors in the position and orientation of a parallel robot are due to several factors:

- manufacturing errors, which can however be taken into account through calibration;
- backlash, which can be eliminated through proper choice of mechanical components;
- compliance, which can also be eliminated through the use of more rigid structures (though this would increase inertia and decrease operating speed);
- active-joint errors, coming from the finite resolution of the encoders, sensor errors, and control errors.

Therefore, as pointed out by Merlet [Merlet 2006c], active-joint errors (input errors) are the most significant source of errors in a properly designed, manufactured, and calibrated parallel robot. In this section, we address the problem of computing the accuracy of a parallel robot in the presence of active-joint errors only. In the balance of section 6.1, the term "accuracy" will therefore refer to the position and orientation errors of a parallel robot that is subjected to active-joint errors only.

The classical approach consists of considering the first order approximation that maps the input error to the output error:

$$\boldsymbol{\delta x} = \mathbf{J}\boldsymbol{\delta q} \tag{6.1}$$

where $\boldsymbol{\delta q}$ represents the vector of the active-joint (input) errors, $\boldsymbol{\delta x}$ the vector of output errors and $\mathbf{J}$ is the Jacobian matrix of the robot. However, this method will give only an approximation of the output maximum error. Indeed, as we will prove in this section, given a nominal configuration and some uncertainty ranges for the active-joint variables, a local maximum position error and a local maximum orientation error not only occur at different sets of active-joint variables in general, but these active-joint variables are not necessarily all at the limits of their uncertainty ranges.

Several performance indices have been developed and used to roughly evaluate the accuracy of serial and parallel robots. A recent study [Merlet 2006b] reviewed most of these performance indices and discussed their inconsistencies when applied to parallel robots with translational and rotational degrees of freedom. The most common performance indices used to indirectly optimize the accuracy of parallel robots are the dexterity index [Gosselin 1992], the condition number and the global conditioning index [Gosselin 1991]. However, in a recent study of the accuracy of a class of 3-DOF planar parallel robots [Yu 2007], it was demonstrated that dexterity has little to do with robot accuracy, as we define it.

Obviously, the best accuracy measure for an industrial parallel robot would be the maximum position and maximum orientation errors over a given portion of the workspace [Merlet 2006c] [Yu 2007] or at a given nominal configuration, given actuator inaccuracies. A general method based on interval analysis for calculating close approximations of the maximum output error over a workspace was proposed recently in [Merlet 2006c]. Obviously, the maximum output error over a workspace is the most important information for a designer. However, this method is relatively difficult to implement, gives no information on the evolution of the accuracy of the manipulator within its workspace and gives no kinematic insight into the problem of optimal design. In contrast, a very simple geometric method for computing the exact value of the accuracy of 3-DOF 3-PRP planar parallel robots was described in [Yu 2007]. This method proposes to replace the existing dexterity maps by maximum position error maps and maximum orientation error maps. While this method covers three of the most promising designs for precision parallel robots (one of which is commercialized and the other two built into laboratory prototypes), it does not always work for other 3-DOF planar parallel robots.

This section generalizes the method proposed in [Yu 2007] by following a detailed mathematical proof that gives us important insight into the accuracy of planar parallel robots. The present study considers only 3-DOF three-legged planar parallel robots with prismatic and/or revolute joints, one actuated joint per leg, and at most one passive prismatic joint in a leg. Although this method is developed for planar parallel manipulators, it is well adapted for the study of the accuracy of PAMINSA manipulators with 4 DOF because of the decoupling between the kinematic model for the vertical displacements and the planar simplified representation for the movements in the horizontal plane (the maximum accuracy along the vertical axis $\boldsymbol{z}$ is constant and equal to $k\ \varepsilon_Z$, where k is the magnification factor of the pantograph and ε_Z the maximal accuracy of the linear actuator).

The method is illustrated on two practical designs, which are the planar equivalent models of different types of PAMINSA manipulators:

- a 3-RPR planar parallel robot;
- a planar 3-PRR robot [Gosselin 1996].

This section is organized as follows. The next part briefly outlines the mathematical theorems used in this section. Then, we will present the method used for the analysis of the orientation and position errors. Finally, several numerical examples are presented and conclusions are given.

6.1.1. Mathematical background.

Analysing the (local) maximum position error and the (local) maximum orientation error of a parallel robot, induced by bounded errors in the active-joint variables, is basically studying, on a set of closed intervals, the maxima of functions ΔX and $\Delta\phi$ defined as:

$$\Delta X = \sqrt{(x - x_0)^2 + (y - y_0)^2}\ , \tag{6.2}$$

$$\Delta\phi = \sqrt{(\phi - \phi_0)^2}\ , \tag{6.3}$$

where x_0, y_0 and ϕ_0 are the Cartesian coordinates corresponding to the nominal (desired) platform pose (position and orientation) of the studied parallel robot, and x, y and ϕ are the actual platform coordinates.

In the case of a 3-DOF planar fully-parallel robot, ΔX and $\Delta\phi$ are functions of three variables: the active-joint variables of the robot (the inputs), which will be denoted by q_i ($i = 1, 2, 3$). Thus, we have to find the maxima of ΔX and $\Delta\phi$ on the set of intervals $q_i \in [q_{i0}-\varepsilon,\ q_{i0}+\varepsilon]$, where q_{i0} are the active-joint variables corresponding to the nominal pose (x_0, y_0, ϕ_0) of the platform (in the selected working mode, i.e. the selected solution to the inverse kinematics) and ε is the error bound on the active-joint variables (Fig. 6.1).

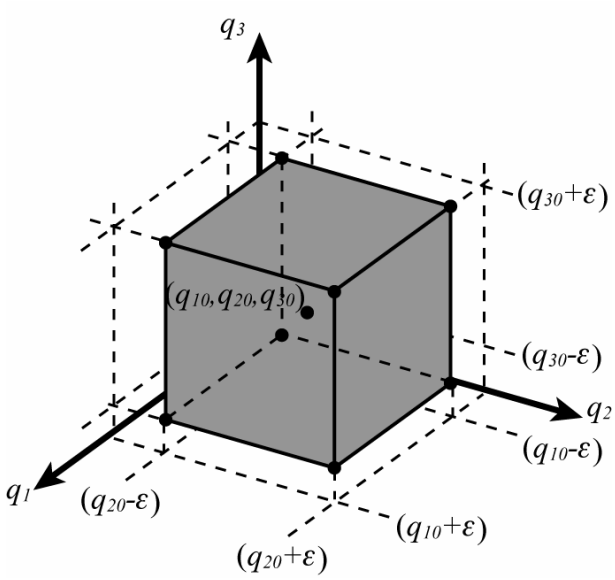

Figure 6.1. – Input error bounding box.

To simplify our error analysis, we will make the practical assumption that the nominal configuration is sufficiently far from (Type 1 and Type 2) singularities. Type 1 singularities [Gosselin 1990] are configurations where a parallel robot loses its desired functionality – it loses one or more degrees of freedom. These are the internal and the external boundaries of workspace. For this reason, the usable workspace of an industrial parallel robot will be away from these singularities. Similarly, Type 2 singularities [Gosselin 1990] are another kind of configurations where a parallel robot loses its desired functionality – this time it loses control of the mobile platform. Furthermore, near these configurations, the output error increases exponentially. For these reasons, industrial parallel robots are designed to exclude such singularities. Therefore, we will obviously perform our error analysis only for configurations that are sufficiently far from singularities, i.e. for nominal configurations from which the robot cannot enter into singularity while the active-joint variables stay within their error-bounded intervals.

Once we made this practical assumption, we address the problem of finding the global maxima of ΔX and $\Delta\phi$. It is well known that the maximum of a continuous multivariable function, f, over a given set of intervals can be found by analysing the Hessian matrix, $\mathbf{H}$:

$$\mathbf{H} = \begin{bmatrix} \dfrac{\partial^2 f}{\partial q_1^2} & \dfrac{\partial^2 f}{\partial q_1 \partial q_2} & \dfrac{\partial^2 f}{\partial q_1 \partial q_3} \\ & \dfrac{\partial^2 f}{\partial q_2^2} & \dfrac{\partial^2 f}{\partial q_2 \partial q_3} \\ sym & & \dfrac{\partial^2 f}{\partial q_3^2} \end{bmatrix}. \tag{6.4}$$

Using this Hessian matrix, the set of variables (q_{1m}, q_{2m}, q_{3m}), where $q_{im} \in [q_{i0} - \varepsilon, q_{i0} + \varepsilon]$, leads to a maximum of f if $\partial f / \partial q_i(q_{1m}, q_{2m}, q_{3m}) = 0$ and $\mathbf{H}$ is negative definite. If such a point exists (q_{1m}, q_{2m}, q_{3m}), we will call it *a maximum of the first kind*.

The global maximum of f could also be on the faces of the input error bounding box shown in figure 6.1. This time, we have to study the maxima of six functions of two variables each, defined as:

$$g_1\colon (q_2, q_3) \to f(q_{10} + \varepsilon, q_2, q_3), \qquad g_4\colon (q_1, q_3) \to f(q_1, q_{20} - \varepsilon, q_3),$$
$$g_2\colon (q_2, q_3) \to f(q_{10} - \varepsilon, q_2, q_3), \qquad g_5\colon (q_1, q_2) \to f(q_1, q_2, q_{30} + \varepsilon),$$
$$g_3\colon (q_1, q_3) \to f(q_1, q_{20} + \varepsilon, q_3), \qquad g_6\colon (q_1, q_2) \to f(q_1, q_2, q_{30} - \varepsilon).$$

If such points exist, we will call them *maxima of the second kind*.

The global maximum of f could also be on the edges of the input error bounding box. This time, we have to study the maxima of twelve univariate functions:

$$h_1\colon q_1 \to f(q_1, q_{20} + \varepsilon, q_{30} + \varepsilon), \qquad h_7\colon q_2 \to f(q_{10} + \varepsilon, q_2, q_{30} - \varepsilon),$$
$$h_2\colon q_1 \to f(q_1, q_{20} + \varepsilon, q_{30} - \varepsilon), \qquad h_8\colon q_2 \to f(q_{10} - \varepsilon, q_2, q_{30} - \varepsilon),$$
$$h_3\colon q_1 \to f(q_1, q_{20} - \varepsilon, q_{30} + \varepsilon), \qquad h_9\colon q_3 \to f(q_{10} + \varepsilon, q_{20} + \varepsilon, q_3),$$
$$h_4\colon q_1 \to f(q_1, q_{20} - \varepsilon, q_{30} - \varepsilon), \qquad h_{10}\colon q_3 \to f(q_{10} + \varepsilon, q_{20} - \varepsilon, q_3),$$
$$h_5\colon q_2 \to f(q_{10} + \varepsilon, q_2, q_{30} + \varepsilon), \qquad h_{11}\colon q_3 \to f(q_{10} - \varepsilon, q_{20} + \varepsilon, q_3),$$
$$h_6\colon q_2 \to f(q_{10} - \varepsilon, q_2, q_{30} + \varepsilon), \qquad h_{12}\colon q_3 \to f(q_{10} - \varepsilon, q_{20} - \varepsilon, q_3).$$

If such points exist, we will call them *maxima of the third kind*.

Finally, the global maximum of f could also be on one of the eight corners of the input error bounding box. These eight points will be referred to as *extrema of the fourth kind*.

Finding the global maxima of functions ΔX and $\Delta\phi$ is equivalent to finding the maxima of functions ΔX^2 and $\Delta\phi^2$. In the next section, we will study the extrema of the functions ΔX^2 and $\Delta\phi^2$.

6.1.2. Analysis of the orientation and position errors.

6.1.2.1. Maximum orientation error.

The partial derivatives of $\Delta\phi^2$ are given as:

$$\frac{\partial\left(\Delta\phi^2\right)}{\partial q_i} = 2\frac{\partial\phi}{\partial q_i}\left(\phi - \phi_0\right) \quad (i = 1, 2, 3). \tag{6.5}$$

These derivatives are equal to zero if $\partial\phi / \partial q_i = 0$ or if $\phi - \phi_0 = 0$. Obviously, however, a maximum can exist only if $\partial\phi / \partial q_i = 0$.

For a 3-DOF planar parallel robot, two different situations correspond to the condition $\partial\phi / \partial q_i = 0$:

- the robot is at a Type 1 singularity. However, we already assumed that the robot cannot enter a Type 1 singularity within the studied interval;
- the twist of the mobile platform, when legs j and p ($j, p = 1, 2, 3,\ i \neq j \neq p$) are fixed, is a pure translation. Figure 6.2 represents the mobile platform of a robot linked to three actuated legs, through revolute joints (these could be prismatic joints as well). Each leg applies a wrench $\mathbf{R}_i$ on the mobile platform, of which centre is denoted by P. The intersection point W_3 of the wrenches $\mathbf{R_1}$ and $\mathbf{R_2}$ represents the instantaneous rotation centre of the mobile platform when actuators 1 and 2 are fixed and the third actuator is moving. Thus, if $\mathbf{x} = [x,\ y]^T$, vector $\partial\mathbf{x} / \partial q_3$, defined as $\partial\mathbf{x} / \partial q_3 = \left[\partial x / \partial q_3 \quad \partial y / \partial q_3\right]^T$, represents the instantaneous displacement of the platform under the action of the third actuator only. For the twist of the platform to be a pure translation, wrenches $\mathbf{R_1}$ and $\mathbf{R_2}$ need to be parallel (Fig. 6.3). When such a configuration is

inside the studied interval, the corresponding orientation error is a local extemum.

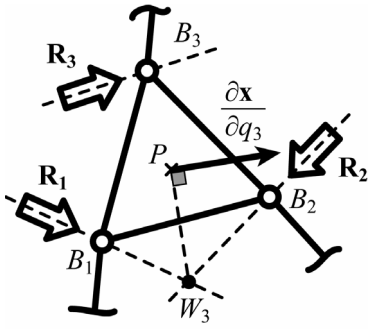

Figure 6.2. – The leg wrenches applied to the mobile platform.

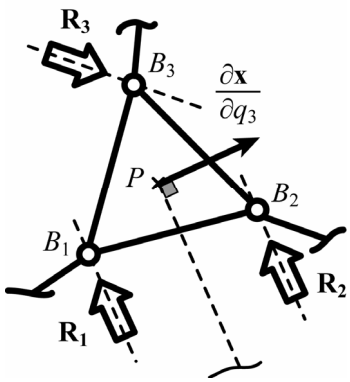

Figure 6.3. – Pure translational motion following a variation in q_3 only.

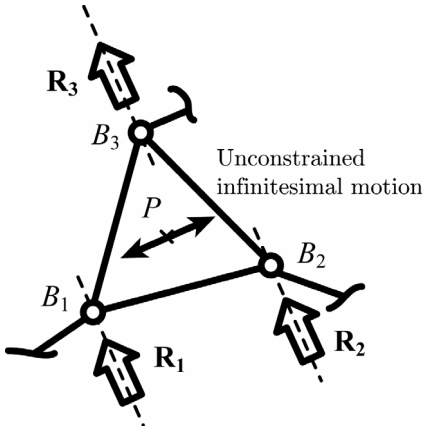

Figure 6.4. – Extrema of the first and second type for the function $\Delta\phi^2$.

Therefore, a maximum of the first kind exists if and only if $\mathbf{R_1}//\mathbf{R_2}$ and $\mathbf{R_2}//\mathbf{R_3}$ and $\mathbf{R_1}//\mathbf{R_3}$ (Fig. 6.4). However, such a configuration corresponds to a Type 2 singularity, and we already assumed that there are no Type 2 singularities for the set of studied intervals.

A maximum of the second kind exists if $\mathbf{R}_i//\mathbf{R}_j$ and $\mathbf{R}_i//\mathbf{R}_p$ (i, j, p = 1, 2, 3), $i \neq j \neq p$. This, however, is equivalent to the previous case and is therefore impossible.

A maximum of the third kind exists if $\mathbf{R}_i//\mathbf{R}_j$ (i, j = 1, 2, 3). If such a configuration is possible, it has to be tested to determine its nature.

Finally, extrema of the fourth kind will always exist and should always be tested.

Thus, in the analysis of the orientation error, only maxima of the third and fourth kind might appear. Maxima of the third kind are very difficult to compute analytically even for simple 3-DOF planar parallel robots. Therefore, we are confident that the best way to proceed, in areas of the workspace where one feels that the robot might be in configurations in which two wrenches are parallel and this could be a local maximum (rather than a minimum) for the orientation angle, is to discretize the edges of the input error bounding box (Fig. 6.1), compute $\Delta\phi$ at each discrete point, and retain the maximum value. Obviously, such a discretization will be somewhat time-consuming and less accurate, but this approach will still produce much more meaningful results than a simple dexterity plot. Note, however, that in most of the cases, it will be obvious that such configurations cannot occur. For these cases, one must only compute $\Delta\phi$ at each corner of the input error bounding box and retains the maximal value. This will be the exact local orientation error.

6.1.2.2. Maximum position error.

The partial derivatives of ΔX^2 are given as:

$$\frac{\partial\left(\Delta X^2\right)}{\partial q_i} = 2\left(\frac{\partial \mathbf{x}}{\partial q_i}\right)^{\mathrm{T}}\left(\mathbf{x}-\mathbf{x}_0\right),\ (i = 1,\ 2,\ 3). \tag{6.6}$$

These derivatives are equal to zero if $\partial\mathbf{x}/\partial q_i = 0$, if $\partial\mathbf{x}/\partial q_i$ is orthogonal to $\mathbf{x} - \mathbf{x_0}$, or if $\mathbf{x} - \mathbf{x_0} = \mathbf{0}$. Obviously, however, the condition $\mathbf{x} - \mathbf{x_0} = \mathbf{0}$ corresponds to an absolute minimum, and will therefore be ignored.

For a 3-DOF planar parallel robot, two different situations correspond to the condition $\partial \mathbf{x} / \partial q_i = 0$:

- the robot is at a Type 1 singularity. However, we already assumed that the robot cannot enter in a Type 1 singularity within the interval of interest;
- the twist of the mobile platform, when legs j and p ($j, p = 1, 2, 3, \ i \neq j \neq p$) are fixed, is a pure rotation. When the twist of the platform is a pure rotation, this means that the intersection point W_3 of wrenches $\mathbf{R_1}$ and $\mathbf{R_2}$ coincides with point P (Fig. 6.5). When such a configuration is inside the studied interval, the corresponding position error is a local extemum.

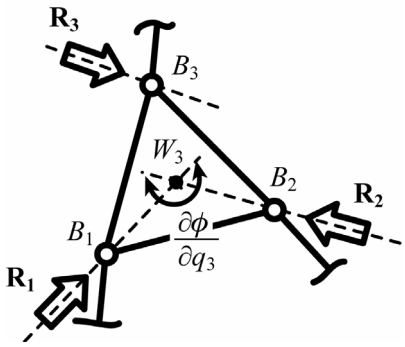

Figure 6.5. – Pure rotational motion following a variation in q_3 only.

Next, we will show geometrically that an absolute maximum of ΔX^2 can exist only on the edges (including the corners) of the input error bounding box. Indeed, finding this maximum is equivalent to finding the point from the uncertainly zone of the platform centre that is farthest from the nominal position of the mobile platform. This uncertainty zone is basically the maximal workspace of the robot (i.e. the set of all attainable positions of the platform centre) obtained by sweeping the active-joint variables in their corresponding intervals, $q_i \in [q_{i0}-\varepsilon, \ q_{i0}+\varepsilon]$. Obviously, the point that we are looking for will be on the boundary of this maximal workspace.

A geometric algorithm for computing this boundary is presented in [Merlet 1998], but we will not discuss it here in detail. We only need to mention that this boundary is composed of segments of curves that correspond to configurations in which at least one leg is at a Type 1 singularity (which we exclude from our study) or at an active-joint limit (we also consider that there are no limits on the passive joints). A segment for which only one active-joint is at a limit is a line segment (in the case of a passive

prismatic joint) or a circular arc of which radius depends on the leg lengths and platform size (in the case of two passive revolute joints).

In error analysis, the studied intervals are extremely small compared to the overall dimensions of the robot, and so is the uncertainty zone for a given nominal configuration. This means that, in practice, the radius of a circular arc that belongs to the boundary of the uncertainty zone will be much greater than the maximum position error. Therefore, for such a tiny arc of large radius, the point that is farthest from the nominal position will be at one of the two extremities of the arc. This point will therefore correspond to at least two active-joint variables at a limit.

Thus, thanks to this geometric analysis, we were able to demonstrate that the maximum position error cannot be elsewhere but on the edges of the input error bounding box. Next, a deeper analysis will guarantee, to a certain precision, that in some cases, the maximum position error occurs only at one of the eight corners of the input error bounding box.

For legs j and p ($j, p = 1, 2, 3,\ i \neq j \neq p$), the condition for having a maximum of the third kind on the interval $\left[q_{i0} - \varepsilon, q_{i0} + \varepsilon\right]$ is that:

- case (a): $\partial\mathbf{x} / \partial q_i = 0$;
- case (b): $\partial\mathbf{x} / \partial q_i$ is orthogonal to $\mathbf{x} - \mathbf{x_0}$.

Condition (a) has already been discussed. Such a configuration has to be examined in order to determine whether it corresponds to an absolute maximum or not. However, it is very difficult to analytically identify such configurations. Therefore, once again, we are confident that the best way to proceed, in areas of the workspace where one feels that the robot might be in configurations in which two leg wrenches intersect at the centre of the mobile platform, is to discretize the edges of the input error bounding box, compute ΔX at each discrete point, and retain the maximum value. Note, however, that in most of the cases it will be obvious that such configurations cannot occur. For these cases, one must only consider condition (b).

Condition (b) is even more complicated to analyse analytically. The partial derivative $\partial\mathbf{x} / \partial q_i$ represents the first two elements of column i ($i = 1, 2, 3$) of the Jacobian matrix of the robot. If the direction of vectors $\partial\mathbf{x} / \partial q_i$ is close to a constant in the studied interval (which is far from Type 2 singularities), then it is possible to say that, on this interval, the displacement of the robot, when legs j and p are fixed, is close to a straight line. This can be verified approximately by computing vector $\partial\mathbf{x} / \partial q_i$ at each corner of the input-error bounding box. If the variation of the

direction of the vector $\partial\mathbf{x}/\partial q_i$ is inferior to a given value (for example 1 degree), then one can consider that the direction of $\partial\mathbf{x}/\partial q_i$ does not change in the studied interval.

Let B be a point for which $\partial\mathbf{x}/\partial q_i$ is orthogonal to $\mathbf{x}-\mathbf{x_0}$ (Fig. 6.6). Vector $\mathbf{u}$ defines the direction of the allowed displacement at point B. If we represent a line passing through point B, of which direction is defined by vector $\mathbf{u}$, this line defines the locus for the displacement of the platform around point B when only actuator i is moving. If we represent two points A and C located on this line around B, the direction of vector $\mathbf{u}$ defines the direction of the displacement when leg i is actuated in the positive sense of q_i. Thus, point A represents the point before passing point B and point C the point after when actuator i is moving.

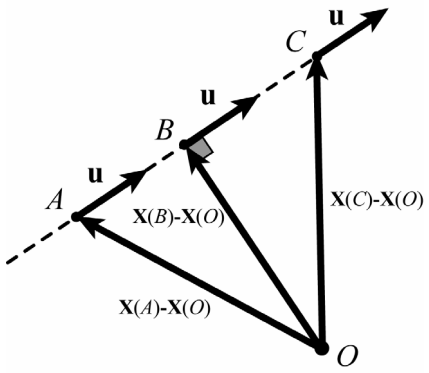

Figure 6.6. – Analysis of a local extremum for which $\partial\mathbf{x}/\partial q_i$ is orthogonal to $(\mathbf{x}-\mathbf{x_0})$.

It is so possible to determine the signs of the product $(\partial\mathbf{x}/\partial q_i)^T(\mathbf{x}-\mathbf{x_0})$ at points A and C. At point A it is negative and at point C it is positive. This shows that point B is a local minimum of ΔX^2. Thus, such a configuration does not represent a maximum of the third kind.

Of course, there are exceptions to our rule of thumb, but they are extremely rare and occur only for some particular mechanism designs. For example, consider a 3-RPR planar parallel robot. The curve described by the platform centre, when two of the actuators are blocked, is an ellipse. Therefore, if one takes a segment at which endpoints the slope is nearly the same, this segment is clearly close to a line. However, if a 3-RRR planar parallel robot is considered, the curve is a sextic. Theoretically, it is possible to have a segment at which endpoints the slope is nearly the same, yet the

segment is far from linear (e.g., there is a cusp point, or a tiny loop). However, we consider that such situations are extremely unlikely to happen, and even if they do, they will occur for only certain configurations and not throughout the workspace. Therefore, for simplicity, we will exclude this small possibility from our study.

6.1.2.3. Conclusions.

To sum up, the proposed method is very simple to implement and, for most practical 3-DOF planar robot designs, fast and accurate. For most designs, at each nominal configuration, we have to compute the direct kinematics for eight sets of active-joint variables, which can either be done analytically, or using a very accurate numerical method (since we are far from singularities). Thus, for computing the local maximum orientation error and local maximum position error of a 3-DOF planar parallel robot for a given nominal configuration, one should, at worst, compute the direct kinematics at only $12n$ points, where n is the number of discretization points on each of the edges of the input error bounding box. As already mentioned, such a discretization is unfortunately somewhat time-consuming and might lead to a certain computational inaccuracy. However, relatively simple analysis can show that, for a given robot design, only the eight vertices of the input error bounding box should be verified. Namely, for the computation of the maximum orientation error, this is the case if no two wrenches can be parallel and lead to a local maximum, and for the computation of the maximum position error, this is the case if no two wrenches can intersect at the platform centre and the variation of the direction of each vector $\partial \mathbf{x} / \partial q_i$ is very small.

6.1.3. Examples.

6.1.3.1. 3-DOF 3-RPR planar parallel robot.

In this part, we will study the accuracy of a 3-DOF 3-RPR planar parallel robot (Fig. 4.1), which is the planar equivalent model of a type of a PAMINSA manipulator (table 2.1). This robot is designed as follows:

- the actuators are mounted on the base and are located at revolute joints M_i;

- triangles $M'_1M'_2M'_3$ and $J_1J_2J_3$ are equilateral;
- the centre O of frame $\boldsymbol{xOy}$ is located at the geometric centre of triangle $M'_1M'_2M'_3$;
- $R_b = OM'_i = 0.35$ m and $R_{pl} = PJ_i = 0.1$ m;
- the error bound on the active-joint variables is $\varepsilon = 2 \cdot 10^{-4}$ rad.

The Type 2 singularities of this robot are well known (chapter 3). They appear when the robot is in such a configuration that:

- the rotation angle is $\phi = \cos^{-1}(R_{pl} / R_b) \approx \pm 73.4°$;
- the platform centre P is located on a circle of which centre is O and of which radius is equal to $\sqrt{R_b^2 + R_{pl}^2 - 2\,R_b\,R_{pl}\cos\phi}$.

These characteristics are those of the planar equivalent model of the prototype of PAMINSA-4D3L.

The Type 1 singularities for this robot occur when point M'_i coincides with point J_i. These three Type 1 singularity points lie on the Type 2 singularity circle.

Thus we propose to analyse a usable workspace defined by a circle of which centre is O and of which radius is equal to 0.245 m for two different orientation angles ϕ, 0 and 10 degrees. This workspace is free of singularities (the radius for the Type 2 singularity circle at $\phi = 0°$ and at 10° is 0.25 m and 0.2521 m, respectively).

The direct kinematic model of the robot is quite simple to obtain and has two distinct solutions (see chapter 3), for active-joint variables that do not lead to singularities. We have to study here three different cases:

- Case (a): Configurations where two wrenches are parallel. These configurations can be either a local maximum or a local minimum for the orientation error. In our example, the wrenches are perpendicular to the directions of the prismatic joints and pass through points J_i. Thus, this case appears when the directions of two of the prismatic joints are parallel (Fig. 6.7.a). For such configurations, the orientation of the platform remains constant if only the actuated joint of the third leg moves. Therefore, this configuration is a local minimum for the orientation error;
- Case (b): Configurations where two wrenches intersect at the platform centre. These configurations can be either a local maximum or a local minimum for the position error. In our example, it is easy to verify that such configurations appear only outside the studied workspaces (Fig. 6.7.b);

- Case (c): Configurations in which the direction of vectors $\partial\mathbf{x}/\partial q_i$ is not nearly constant. Figures 6.8.a and 6.8.b represent the variation in the direction of vectors $\partial\mathbf{x}/\partial q_1$ in the studied interval (the figures for $\partial\mathbf{x}/\partial q_2$ and $\partial\mathbf{x}/\partial q_3$ are obtained by 120° rotations). It is possible to note that this variation is extremely small in the studied workspace (less than 0.6°).

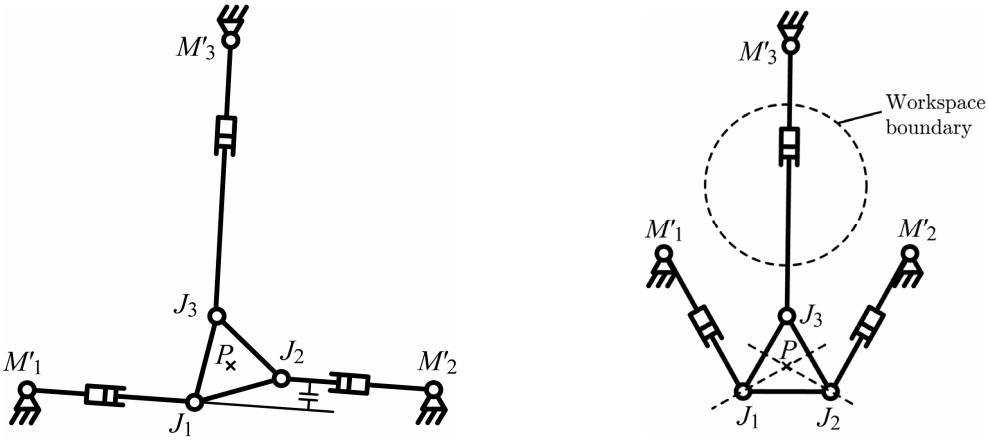

(a) $\partial\phi/\partial q_3 = 0$ (b) $\partial\mathbf{x}/\partial q_3 = 0$

Figure 6.7. – Configurations of the 3-RPR parallel manipulator corresponding to local extrema in (a) the orientation error and (b) the position error.

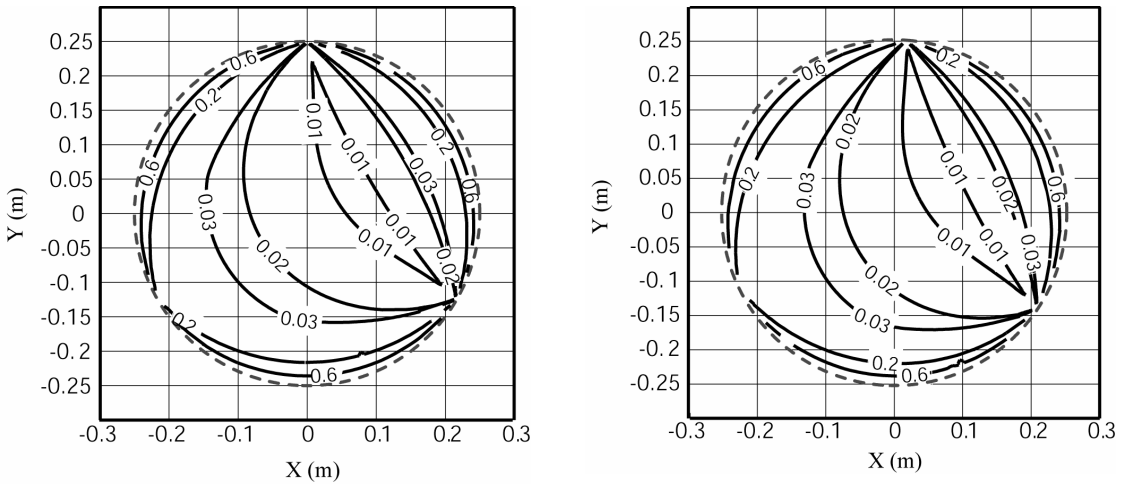

(a) $\phi = 0°$. (b) $\phi = 10°$.

Figure 6.8. – Variation in the direction of vector $\partial\mathbf{x}/\partial q_1$ (degrees).

Thus, there are only eight active-joint variable sets to test for computing the maximum orientation and maximum position error of the robot for a given nominal pose. For each set, the two possible platform poses are obtained analytically, and the corresponding orientation error and position error are computed for the solution that is closest to the nominal pose. The resulting contour plots for two orientations are presented in Figs. 6.9 and 6.10.

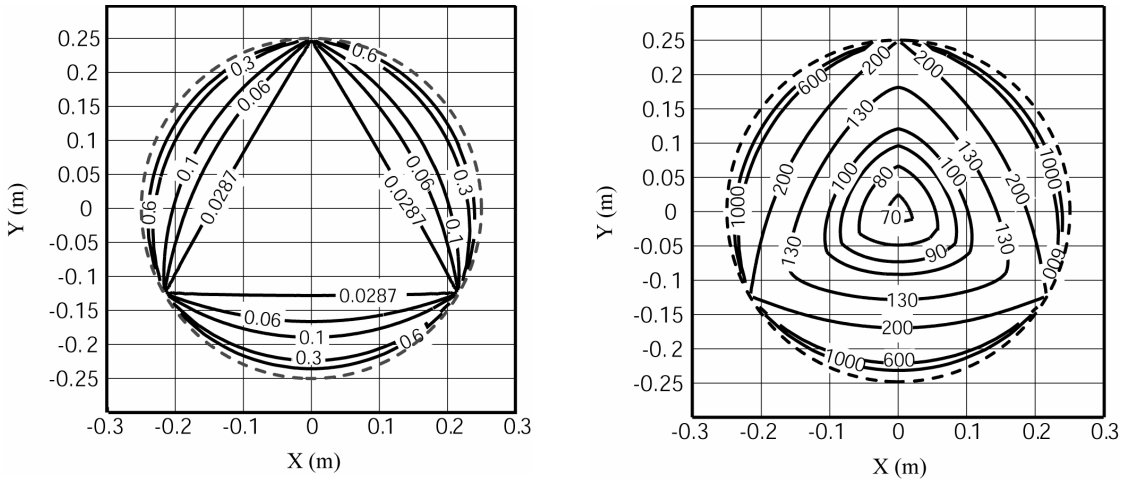

(a) maximum orientation error (degrees) (b) maximum position error (μm)

Figure 6.9. – Maximum orientation and position errors for the 3-RPR manipulator at $\phi = 0°$.

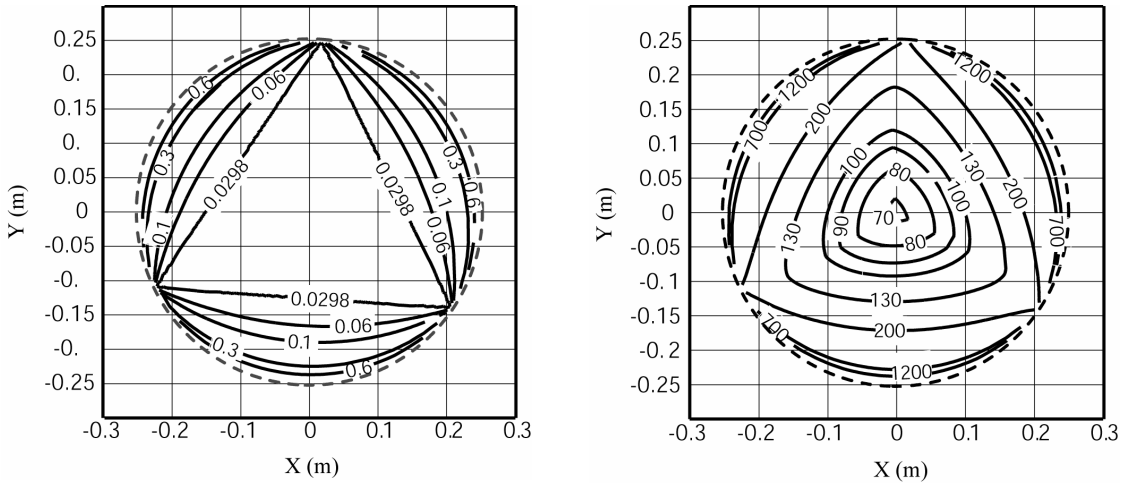

(a) maximum orientation error (degrees) (b) maximum position error (μm)

Figure 6.10. – Maximum orientation and position errors for the 3-RPR manipulator at $\phi = 10°$.

As expected, it can be seen that the robot is more accurate in the centre of its workspace, far from singularities. The closer the robot to the singularity circle, the poorer is its accuracy. It is interesting to note that, while there is always a substantial position error, the orientation error is virtually zero in the central part of the workspace.

6.1.3.2. 3-DOF 3-PRR planar parallel robot.

In this part, we will study the accuracy of a 3-PRR planar parallel robot (Fig. 6.11).

This robot is designed as follows:

- the actuators are mounted on the base and are located at prismatic joints $P_iM'_i$;
- the centre O of frame ***xOy*** is located at the geometric centre of the triangle $P_1P_2P_3$;
- triangles $P_1P_2P_3$ and $J_1J_2J_3$ are equilateral and the guides of the prismatic joints are tangent to the circle of which centre is O and of which radius is OP_1;
- $OM'_i = 0.35$ m, $M'_iJ_i = 0.4$ m and $PJ_i = 0.1$ m;
- the stroke of the actuators is 76 cm;
- the error bound on the active-joint variables is $\varepsilon = 10$ μm.

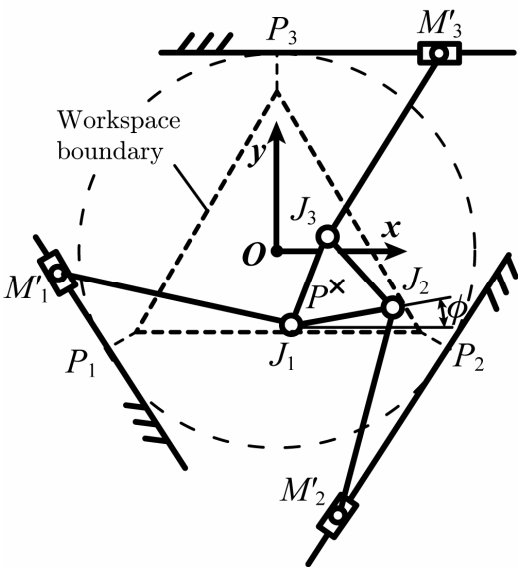

Figure 6.11. – Schematic of the studied 3-PRR manipulator.

The direct kinematics of this robot allows up to six real solutions and cannot be solved analytically [Merlet 1996]. Since we only need the solution that can be reached from the nominal pose, while the active-joint variables remain in their intervals, the best solution is to use an iterative numerical method such as the Newton-Raphson method. This method requires only the computation of the Jacobian matrix of the robot, which is very simple to obtain. In our error analysis, we will always start the algorithm at the nominal configuration and vary the active-joint variables in a very small interval of length up to ε. Furthermore, we will use this algorithm for configurations that are sufficiently far from singularities. Therefore, as verified in this example, the algorithm converges very quickly (usually, in only two iterations for a precision of 10^{-20} m and 10^{-20} degrees).

The singularities of this robot have been studied in [Bonev 2003b], but correspond to quite complex curves. Fortunately, however, it is easy to find a design for which there are no singularities inside the workspace for the given working mode (given set of inverse kinematic solutions). The studied workspace of our robot corresponds to an equilateral triangle inscribed in a circle centred in O and of which radius is equal to 0.3 m. One edge of the triangle is parallel to $\boldsymbol{x}$. This workspace will be studied for orientation angles equal to 0° and 10°. There are no Type 2 singularities in it.

We have to study here three different cases:

- Case (a): Configurations where two wrenches are parallel. These configurations can be either a local maximum or a local minimum for the orientation error. In our example, the instantaneous wrenches are along the lines M_iJ_i. Thus, this case appears when two of the legs are parallel (Fig. 6.12). Two types of such configurations exist. Figure 6.12.a represents a configuration which corresponds to a local minimum for the orientation error. For this configuration, the two legs form a parallelogram and the orientation of the platform remains constant while the third actuator moves alone. Figure 6.12.b represents a configuration which corresponds to a local maximum for the orientation error. In this configuration, if the mobile platform is pushed away in any direction by the third leg, it will rotate in the same sense. However, in our example, it is easy to verify that such configurations cannot appear inside the studied workspace;
- Case (b): Configurations where two wrenches intersect at the platform centre. These configurations can be either a local maximum or a local minimum for the position error. In our example, it is easy to verify that such configurations cannot appear inside the studied workspace;

- Case (c): Configurations in which the direction of vectors $\partial\mathbf{x}/\partial q_i$ $(i = 1, 2, 3)$ is not nearly constant. Figures 6.13.a and 6.13.b represent the variation in the direction of vectors $\partial\mathbf{x}/\partial q_1$ in the studied interval (the figures for $\partial\mathbf{x}/\partial q_2$ and $\partial\mathbf{x}/\partial q_3$ are obtained by rotations of 120°). It is possible to note that this variation is very small in the studied workspaces (less than 0.01°). As already mentioned, this is not a 100% guarantee that the maximum position error occurs at one of the eight corners of the input error bounding box. Therefore, for the purposes of this demonstration, we have also verified on the edges of the bounding box (using 20 discretization intervals on each edge). Not even one nominal configuration was found for which the maximum position error is not at one of the eight corners. Therefore, the assumption that we make is valid in this example.

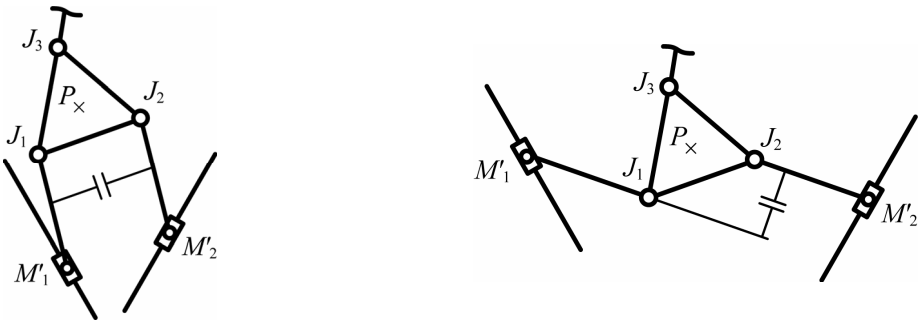

(a) local minimum (b) local maximum

Figure 6.12. – Configurations of the 3-PRR parallel manipulator corresponding to local (a) minimum and (b) maximum of the orientation error.

Thus, for this robot too, there only are eight sets of active-joint variable to test for computing the local maximum orientation error and local maximum position error of the robot. The resulting contour plots for two different orientations are presented in figures 6.14 and 6.15.

It can be noted that the position error of this parallel robot is nearly constant for both orientations, from about 11 μm to 17 μm, and only slightly larger than the input errors $\varepsilon = 10$ μm. This may be explained by the fact that the robot stays far from Type 2 singularities in the studied workspace. Furthermore, it appears the orientation error is nearly constant and virtually zero, throughout the workspace. Therefore, this parallel robot is an excellent candidate for precision positioning, as demonstrated by the authors of [Hesselbach 2004].

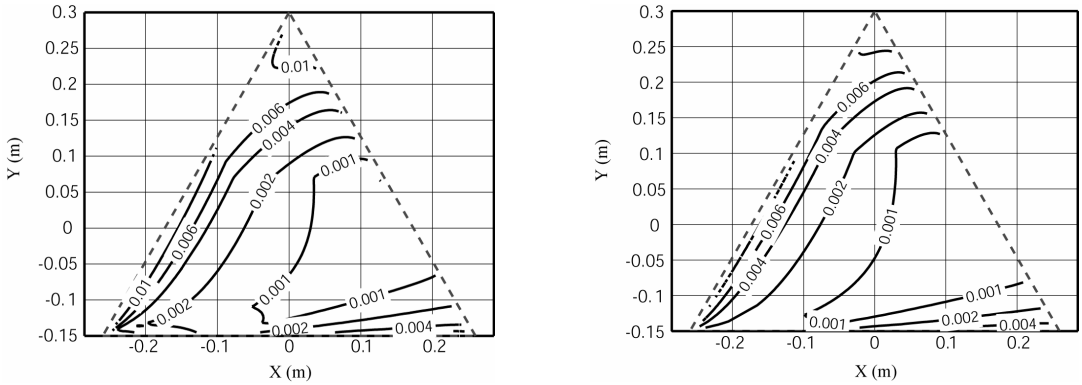

(a) $\phi = 0°$. (b) $\phi = 10°$.

Figure 6.13. – Variation in the direction of vector $\partial \mathbf{x} / \partial q_1$ (degrees).

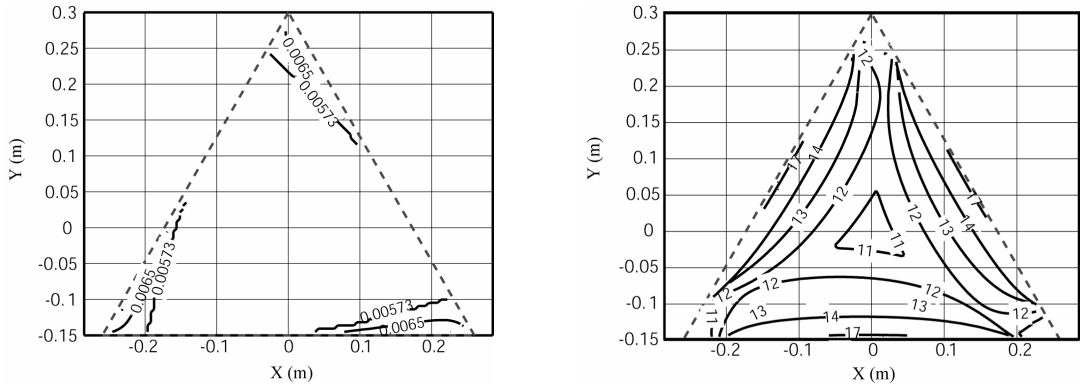

(a) maximum orientation error (degrees) (b) maximum position error (μm)

Figure 6.14. – Max. orientation and position errors for the 3-PRR manipulator (ϕ=0°).

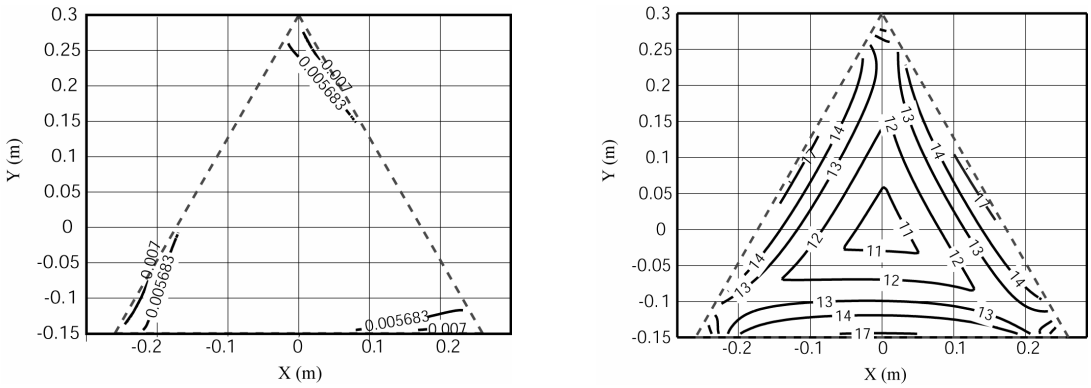

(a) maximum orientation error (degrees) (b) maximum position error (μm)

Figure 6.15. – Max. orientation and position errors for the 3-PRR manipulator ($\phi = 10°$).

6.1.4. Conclusion.

This section presented an analytic study of the local maximum orientation and position errors occurring in 3-DOF planar parallel robots subjected to errors in the inputs. It was proven that, when sufficiently far from singularities, the local maximum orientation and position errors occur only when at least two inputs suffer a maximum error. However, a simple procedure was proposed to evaluate, for a given design, whether these output errors might occur when only two inputs are at a maximum error. Thanks to this analytic study, a simple method was proposed to calculate the local maximum orientation and position errors for a given nominal configuration and given error bound on the inputs. The method involves solving the direct kinematics for eight, or a maximum of $12n$ (n being the number of discretization steps), sets of inputs. This method is relatively fast and accurate, but above all, very simple to implement and gives valuable insight into the kinematic accuracy of parallel robot. We believe that the proposed method should be used for all 3-DOF planar fully-parallel robots instead of the much less meaningful dexterity maps.

This method can be used in design optimization procedures which seek maximum accuracy and in the choice of the appropriate actuators for PAMINSA manipulators.

The next step of the optimization of PAMINSA manipulators is the minimization of the deformations due to the elasticity of the links.

6.2. Minimization of the deformations.

Among the obvious advantages of PAMINSA manipulators, we may note the improvement of positioning accuracy along the vertical axis because the kinematical locking of the structure does not allow the altitude variations during the displacements in the horizontal plane. However, the positioning accuracy also depends on the elasticity of the elements of the manipulator.

Many industrial applications of parallel manipulators, such as the assembly of electronic, optical units, or several medical applications require high accuracy. It should be noted that most of parallel manipulators used today are much better at repeatability than at accuracy. For improvement of position accuracy of parallel manipulators, it is possible to use calibration methods, to increase the rigidity of links or the lack of backlashes in drive systems. A new approach called Geometric and Elastic Error Compensation (GEC) was proposed in the study [Meggiolaro 2001]. It was shown that

the two techniques can be effectively combined to achieve high absolute positioning accuracy.

In this section, for improvement of positioning accuracy of PAMINSA, we propose new compensation schemes, which consist of the introduction into the initial system of complementary units making it possible to cancel the positioning errors. Two different approaches are proposed and the performances of such designs are shown.

6.2.1. Accuracy analysis.

The rigidity of the developed prototype of PAMINSA is studied taking into account the elasticity of the links of the pantograph linkages with the Castem software (the geometry and mass distribution parameters of the links are listed in Table 6.1). Two cases were examined: the errors due to the deformations of the manipulator without any payload (Fig. 6.16) and with a load of 20 kg (Fig. 6.17).

Static rigidity is defined as the 6×6 symmetrical matrix $\mathbf{K}$ that maps generalized infinitesimal displacements $\boldsymbol{\delta}\mathbf{x} = [\delta x,\ \delta y,\ \delta z,\ \delta\phi_x,\ \delta\phi_y,\ \delta\phi_z]^T$ of the platform to generalized external loads $\mathbf{W} = [F_x,\ F_y,\ F_z,\ M_x,\ M_y,\ M_z]^T$.

Thus, we have

$$\mathbf{W} = \mathbf{K}\,\boldsymbol{\delta}\mathbf{x}\,. \tag{6.7}$$

The analysis of the obtained results shows that the position in which the structure is less deformed is the central position. When the platform moves away from this position, the manipulator becomes less rigid and loses its accuracy. However, it is important to note that the absolute errors along the vertical axis are rather small (δz_{max}= 0.02 mm). Thus, we can note that the suggested manipulator allows the displacements of the platform on the horizontal plane with great accuracy. It should be also noted that the positioning errors do not depend on the elasticity of actuator systems. The gravitational forces are also vertical and do not have any action on the rotating actuators.

Table 6.1. – Dimensions and characteristics of the prototype's links.

Location	Section	Dimensions
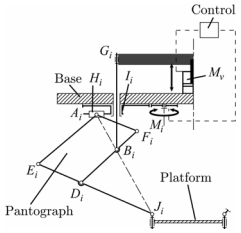	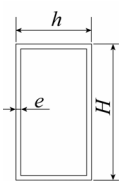	Beam [1] $H = 50$ mm $h = 25$ mm $e = 3$ mm $L = 308$ mm
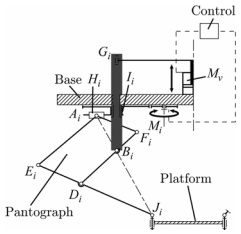	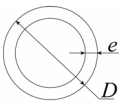	Beam [1] $D = 25$ mm $e = 4.7$ mm $L = 442$ mm
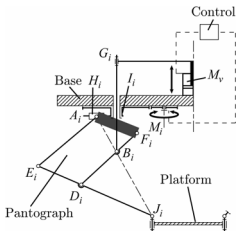	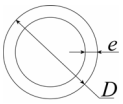	Beam [1] $D = 25$ mm $e =1.5$ mm $L = 210$ mm
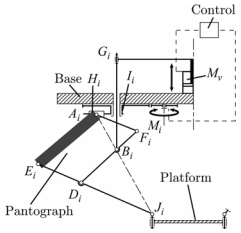	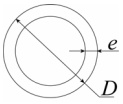	Beam [1] $D = 25$ mm $e = 1.5$ mm $L = 420$ mm
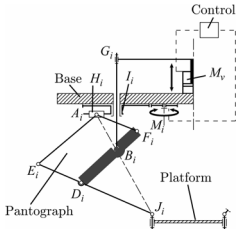	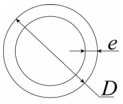	Beam [1] $D = 40$ mm $e = 1.5$ mm $L = 420$ mm

Location	Section	Dimensions
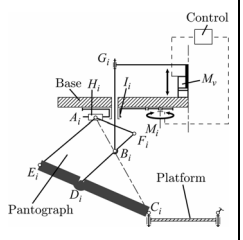	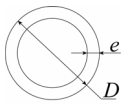	Beam [1] $D = 40$ mm $e = 1.5$ mm $L = 630$ mm
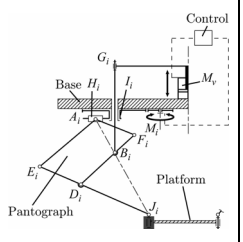		Solid [2] $D = 25$ mm $L = 15$ mm
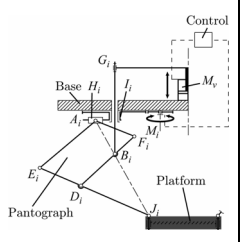	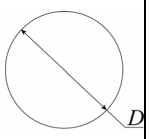	Solid [2] D =310 mm $L = 12$ mm
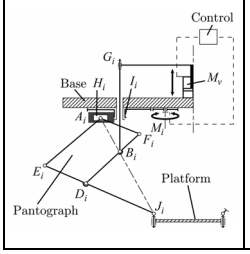	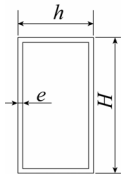	Beam [1] $H = 25$ mm $h = 50$ mm $e = 2$ mm $L = 363.5$ mm

[1] **Material:** AU4G,
Characteristics: $E = 74000$ MPa, $\nu = 0.33$, $\rho = 2800$ kg/m^3.

[2] **Material:** Steel,
Characteristics: $E = 210000$ MPa, $\nu = 0.28$, $\rho = 7850$ kg/m^3.

Masses of joints:

$m_{Ai} = 0.305$ kg, $m_{Bi} = 0.338$ kg, $m_{Ci} = 0.233$ kg, $m_{Di} = 0.259$ kg, $m_{Ei} = 0.262$ kg, $m_{Fi} = 0.28$ kg, $m_{Gi} = 0.214$ kg

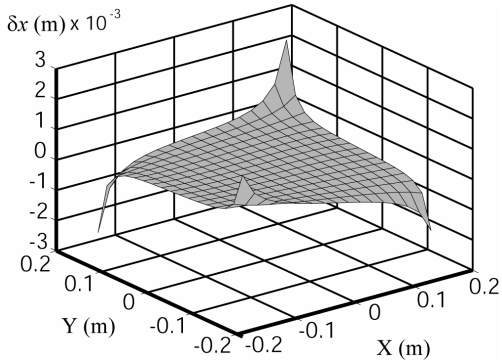

(a) Positioning error along ***x***-axis.

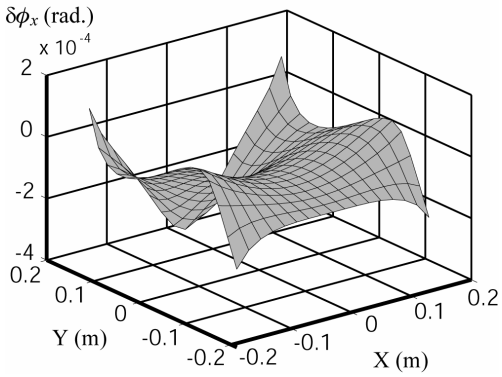

(b) Orientation error about ***x***-axis.

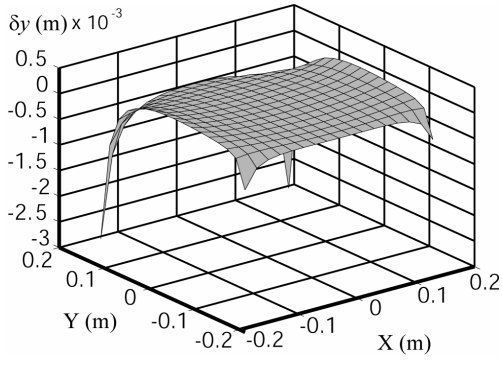

(c) Positioning error along ***y***-axis.

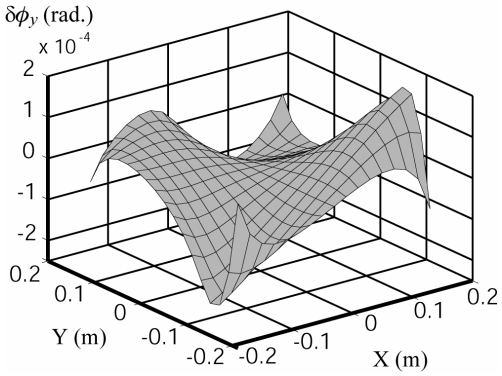

(d) Orientation error about ***y***-axis.

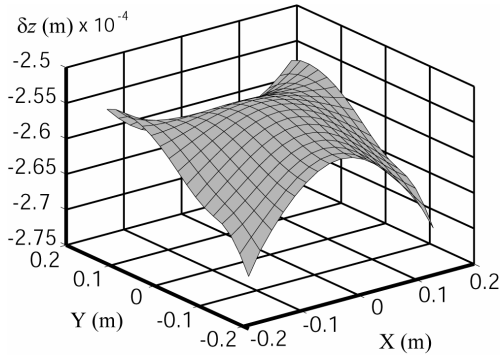

(e) Positioning error along ***z***-axis.

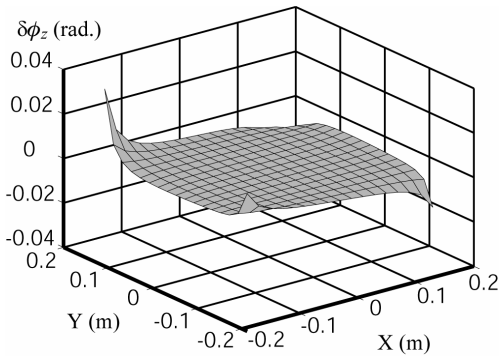

(f) Orientation error about ***z***-axis.

Figure 6.16. – Absolute positioning errors of the platform with orientation $\phi = 0°$ at the altitude $z = -0.6$ m.

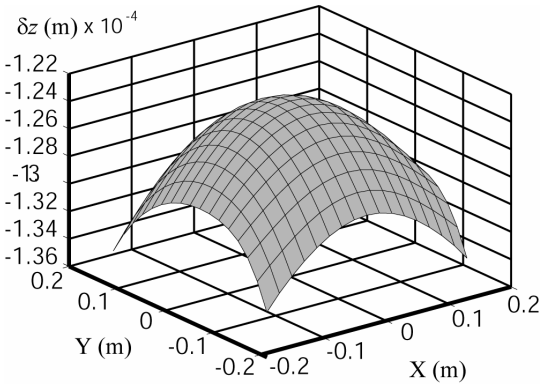

Figure 6.17. – Absolute positioning errors of the platform along the ***z***-axis with a load of 20 kg (at altitude $z = -0.6$ m and with platform orientation $\phi = 0°$).

With a payload of 20 kg applied on the platform, the variations of the positions along the vertical axis are represented in Fig. 6.17. The maximal error is less than 140 μm, which is small, taking into account that the pantograph links are hollow tubes with a thickness of 1.5 mm. It is obvious that positioning errors for the manipulator can be reduced using high stiffness links.

In the remainder of this section, we will present two new approaches for the improvement of positioning accuracy of PAMINSA manipulators.

6.2.2. Improvement of positioning accuracy of PAMINSA by means of correcting systems mounted on the drive system.

Most of the research papers devoted to the study of parallel manipulators deal with the mechanical structures with rigid links and without clearances in the joints. So in this case, the position of the platform is considered perfectly parallel to the base. But in reality, the errors due to the elastic deformations of the mechanical structure of the manipulator change the position of the platform (attitude and inclination).

The positioning errors are less important if the output point P (Fig. 6.18), i.e. the end of a surgical device or a sensor, is located on the horizontal plane of the platform. But the error becomes more important if this output point is moved from the horizontal plan of the platform. For example, if the output point is located on the plane ***xOz*** and is moved away 200 mm from the horizontal plane of the platform (with 100

mm radius), the error 0.14 mm of the platform along the *z*-axis increases at the end of the output point to 0.57 mm (see Fig. 6.18).

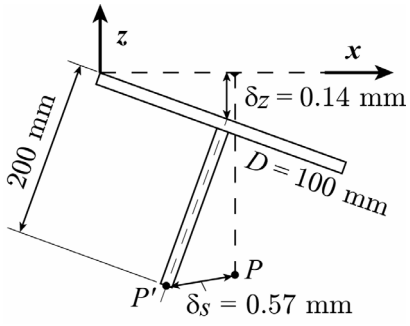

Figure 6.18. – Absolute positioning errors of the output point, which is moved away 200 mm from the horizontal plane of the platform.

It is obvious that the improvement of positioning accuracy can be achieved by the increase in the rigidity of links. However, it is also promising to develop design methods for the improvement of positioning accuracy by the use of additional correcting systems.

Figure 6.19 shows PAMINSA with two compensation systems, which are presented in figure 6.20. It should be noted that, in the modified design of the manipulator, the joints on the platform are also changed: the universal joints used in the initial version are replaced by spherical pairs. The compensation systems, which cancel the errors due to the elasticity of links, are provided with two complementary actuators M_{cj}. These actuators allow the displacements of the pantograph's points B_i making it possible to eliminate the inclination error of the platform. These modifications allow the correction of the vertical positions of two spherical pairs of the platform, which is absolutely enough for cancellation of the positioning error of the inclination of the platform.

The vertical positions of such a spherical pair located on the platform can be determined analytically for the whole workspace (or given altitude) of the manipulator on the base of equation (6.7) or by using three sensors mounted on the platform. Measuring the spherical joint motion errors for the manipulators with three and six prismatic joints (for Tripod and Hexapod types), as well as several installation examples of the sensors, was discussed in the study [Oiwa 2002].

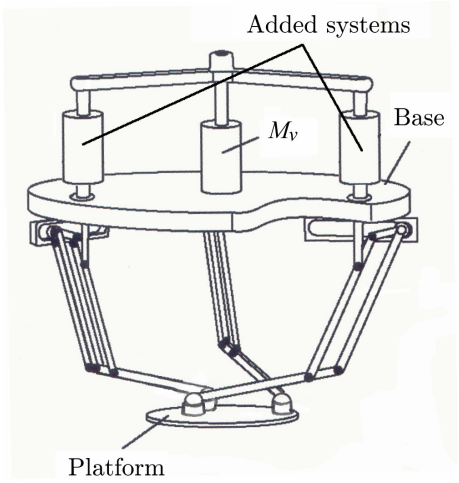

Figure 6.19. – PAMINSA with added compensation systems.

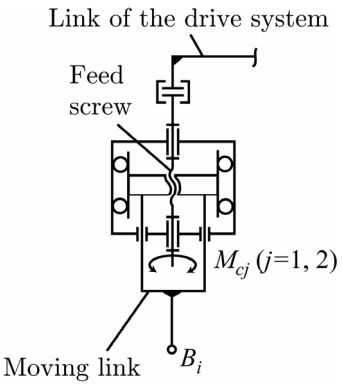

Figure 6.20. – Kinematic schema of the added compensation systems for the correction of the positioning errors of the platform along the vertical axis.

Note that the compensation scheme developed for PAMINSA is constructively more efficient because it is mounted on the drive system of the vertical displacements. As a result, the variable length of the compensation device is always vertical. It should be also noted that it is simpler for computation because the translational displacement in the added system can be found directly from positioning errors of the platform's joint taking into account the magnification factor of the pantograph linkage. In this manner, the significant reduction of errors can be achieved and the obtained results are shown in figure 6.21. It is seen that, after compensation of the errors due to the elasticity of

links, the vertical positions of the platform's joints have constant values and the inclination error is eliminated.

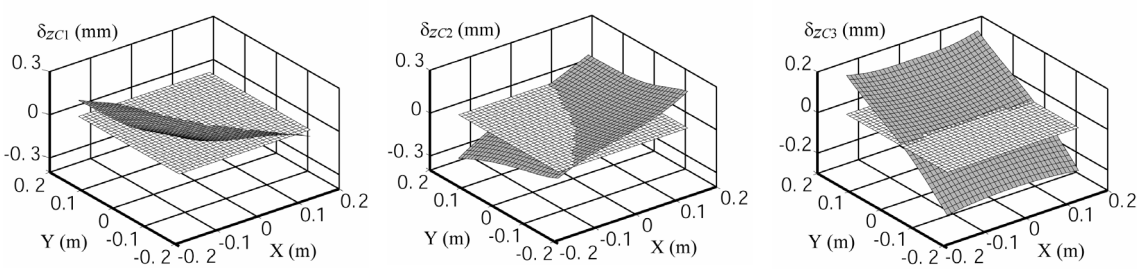

Figure 6.21. – The vertical positioning errors of the platform's joints C_1, C_2 and C_3 of the initial and modified manipulators (the examined case correspond to the platform with orientation $\phi = 0°$ at the altitude $z = -0.6$ m).

6.2.3. Improvement of positioning accuracy of PAMINSA by means of correcting systems mounted on the platform.

Let us consider another correcting system mounted on the platform of PAMINSA. Such a system can be added on any parallel structure for the correction of positioning error of the inclination of the platform. The suggested system consists of a correcting mass, which has the possibility to turn about the vertical axis of the platform and to carry out translational displacements on the horizontal plane (Fig. 6.22).

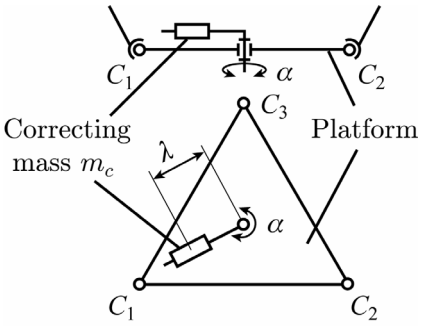

Figure 6.22. – Representation of the correcting system mounted on the platform.

Introducing the correcting conditions into equation (6.7), we obtain:

$$\boldsymbol{\delta x} = \mathbf{K}^{-1}\,\mathbf{W} + \mathbf{K}^{-1}\begin{bmatrix}0 & 0 & -m_c g & M_{st(x)} & M_{st(y)} & 0\end{bmatrix}^T, \tag{6.8}$$

from which, taking into account that after correction

$$\boldsymbol{\delta x} = \begin{bmatrix}\delta x & \delta y & \delta z & 0 & 0 & \delta\phi_z\end{bmatrix}^T, \tag{6.9}$$

we determine the static moments $M_{st(x)}$ and $M_{st(y)}$ and then the position λ and orientation α of the correcting mass m_c.

In other words, the correcting mass m_c should be located on the platform in such a manner that its gravity effects eliminate the inclination error of the platform.

For a PAMINSA-4D3L with parameters of the prototype (see table 6.1), the values of the position λ and orientation α for the correcting mass m_c = 3 kg are shown in figure 6.23.

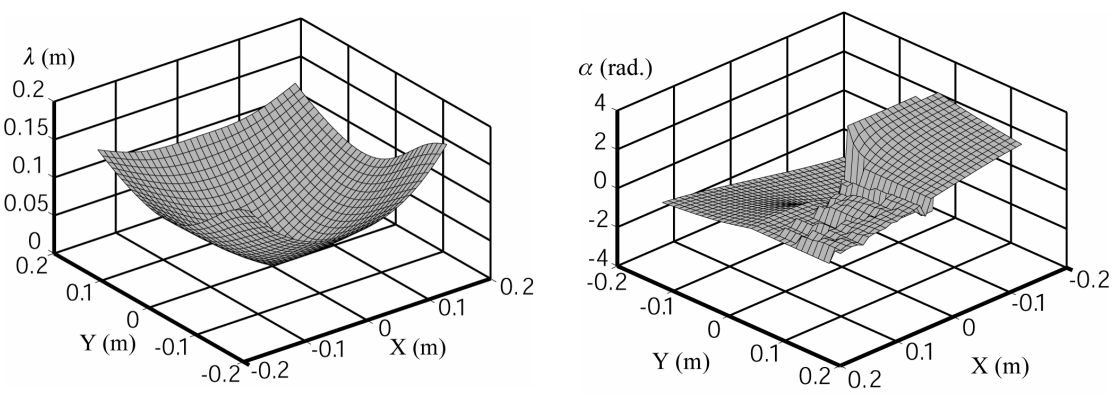

Figure 6.23. – Position λ and orientation α of the correcting mass m_c.

These values are obtained for the platform having a constant orientation $\phi = 0°$ at the altitude $z = -0.6$ m. The obtained results are the same as the previous case (Fig. 6.21), i.e. after compensation of the errors due to the elasticity of links, the vertical positions of the platform's joints have constant values and the platform becomes perfectly parallel to the base.

6.2.4. Conclusions.

In this section, new design approaches for the improvement of positioning accuracy of a 4-DOF PAMINSA manipulator are discussed. Usually the studies devoted to parallel manipulators deal with the mechanical structures on the base of rigid body mechanics and consider that the platform is perfectly parallel to the base. It has been shown that the elasticity of links has an influence on the positioning accuracy of the developed parallel manipulator. For the cancellation of these positioning errors due to the elasticity of links, two approaches are presented. The first solution is carried out by means of two correcting systems mounted on the drive system of the vertical displacements. The second solution is carried out by use of a correcting mass mounted on the platform. The obtained results show that, after compensation of the errors due to the elasticity of links, the vertical positions of the platform's joints have constant values and the inclination of the platform in relation to the base is cancelled.

The next step of our optimization procedure is the reduction of the input torques of the manipulator.

6.3. Input torques minimization.

An important challenge in industrializing a new manipulator is the reduction of its manufacturing cost. This cost can be reduced by different manners, as for example:

- by using common pieces which can easily be found in industry, as ball bearings;
- by designing the manipulator with the simplest structure which can be easily reproduced and of which links have simple shapes;
- by having actuators with relatively small power, which can be obtained by minimizing the efforts that the motors have to apply.

In this section, the minimization of input torques of the PAMINSA manipulator with 4 DOF is discussed. The optimal results obtained are based of the static and dynamic models of the manipulator developed in chapter 2 and chapter 5.

6.3.1. Reduction of input torques in static mode of operation.

In [Arakelian 1998], it is shown that the input torques due to the effect of gravitational forces on the pantograph linkage can be cancelled by the optimal redistribution of its movable masses. Thus, by complete static balancing of legs, it should be possible to cancel the loads due to the movable masses of the legs on the rotating actuators of PAMINSA manipulators.

In our case, the static balancing can be achieved by canceling the term C_{v2} of equation (2.6). We propose to add masses on point F_i (Fig. 2.4) of each leg in order to statically balance the mechanism.

Figure 6.24 shows the variations of the torque of actuator M_1 before and after mass balancing. After complete static balancing, the potential energy of the manipulator is constant for any configuration and zero actuator torques are required.

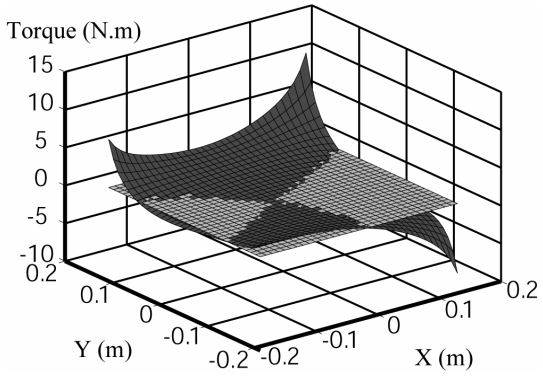

Figure 6.24. – Variations of the actuator torques for $z = -0.6$ m and $\phi = 0°$ before (dark grey) and after (bright grey) static balancing of legs (motor 1).

The presented example was calculated using the link parameters of the developed prototype (see appendix E). The value of the added masses are 2.8 kg (to observe the increase in masses after balancing, it should be noted that the mass of each pantograph linkage before balancing was 3.1 kg).

It is obvious that such a balancing is very useful for a static mode of operation of the manipulator. However, with the increase in the accelerations of moving links, the complete static balancing becomes ineffective because the increase in inertia forces leads to complementary loads. That is why an optimal balancing of limbs is considered below.

6.3.2. Reduction of input torques in dynamic mode of operation.

In chapter 5, we presented an analytic dynamic model of PAMINSA based on the Lagrange equations.

For a comparative analysis of the unbalanced and statically balanced manipulators in dynamic mode of operation, a prescribed trajectory in horizontal plane is defined (Fig. 6.25) and, for the manipulator parameters given in appendix E, the input torques are determined (Fig. 6.26).

Thus, the obtained results showed that, in the case of accelerated motions for input torques minimization, it is better to achieve a partial mass balancing.

The minimization problem can be expressed as the following:

$$\max\left|\tau_p^{dyn}\right| \rightarrow \min_{m_{ji}, r_{ji}} \tag{6.10}$$

i.e. it is necessary to find such a distribution r_{ji} of moving masses m_{ji} which allows the minimization of the maximum values of the input torques.

The calculated values of added masses located at the axis F_i of each leg are 1.3 kg. The values of the input torques after complete static balancing and optimal balancing are presented in figure 6.27.

Thus, the analysis of obtained results shows that such an optimization allows the reduction of the maximal values of the input torques in dynamic mode of operation up to 45%.

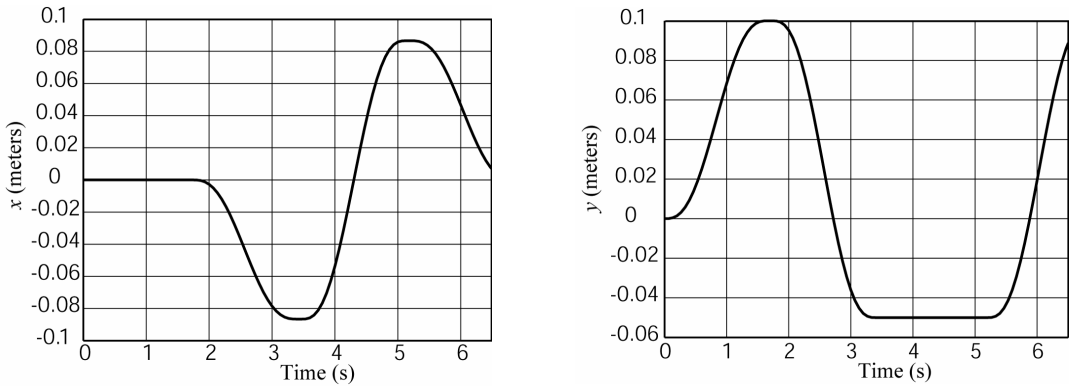

(a) Displacement along ***x***-axis. (b) Displacement along ***y***-axis.

Figure 6.25. – The prescribed trajectory for $z = -0.7$ m and $\phi = 0°$.

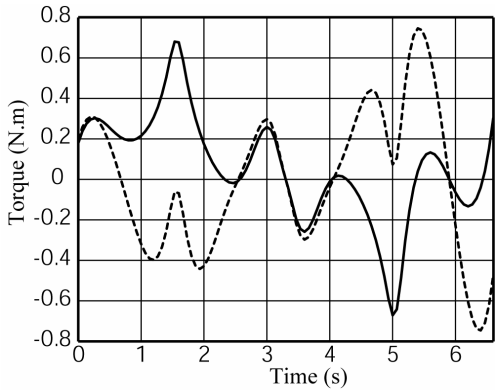

(a) Torque of the actuator M_1

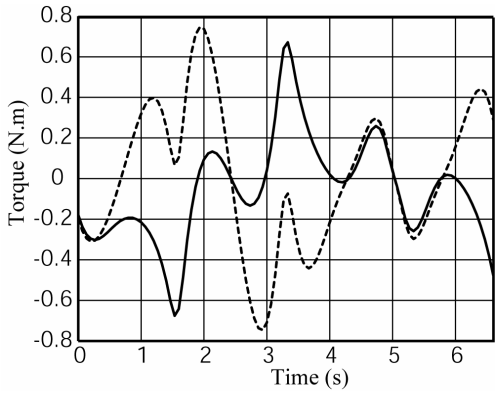

(b) Torque of the actuator M_2

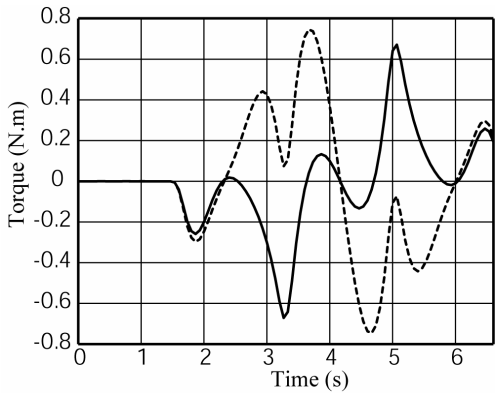

(c) Torque of the actuator M_3

Figure 6.26. – Actuators' torques for unbalanced (full line) and statically balanced manipulators (dotted line).

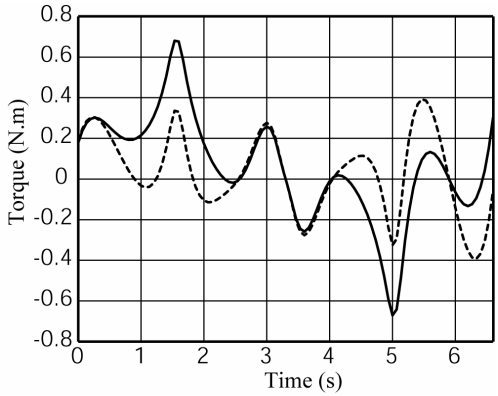

(a) Torque of the actuator M_1

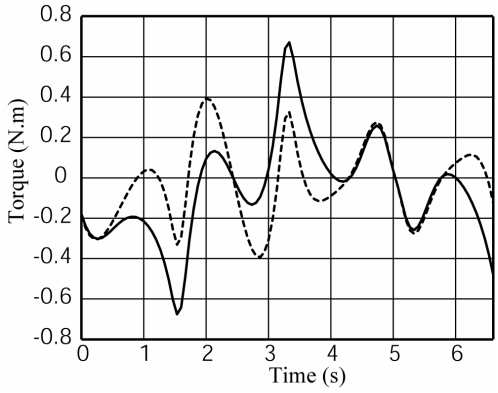

(b) Torque of the actuator M_2

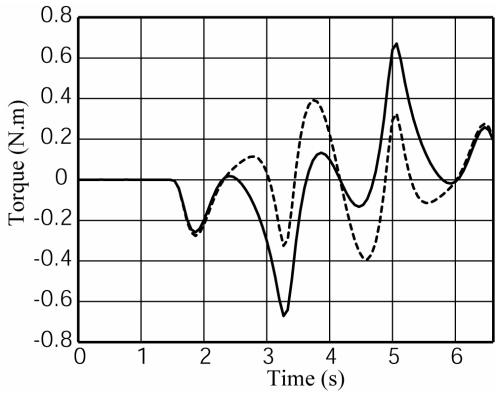

(c) Torque of the actuator M_3

Figure 6.27. – Actuators' torques for unbalanced (full line) and partially balanced manipulators (dotted line).

We would like to mention that the minimization was carried out for a prescribed trajectory. This trajectory may be either the generalized trajectory with maximum acceleration, which is generated by the robot (for example, pick-and-place motion) or a trajectory, which is variable with unknown parameters. In the first case, the masses of the balancing counterweights can be constant and the influence of the trajectory variations on the torque minimization will be small. In the second case, the balancing counterweights should be designed with adjustable parameters and they can be adapted to the given trajectory [Arakelian 1989] [Arakelian 1990].

6.3.3. Experimental validations.

6.3.3.1. Reduction of input torques in static mode of operation.

The static balancing of the manipulator is experimentally accomplished by adding counterweights of 2.8 kg at the axis F_i of the pantograph linkages (Fig. 6.28).

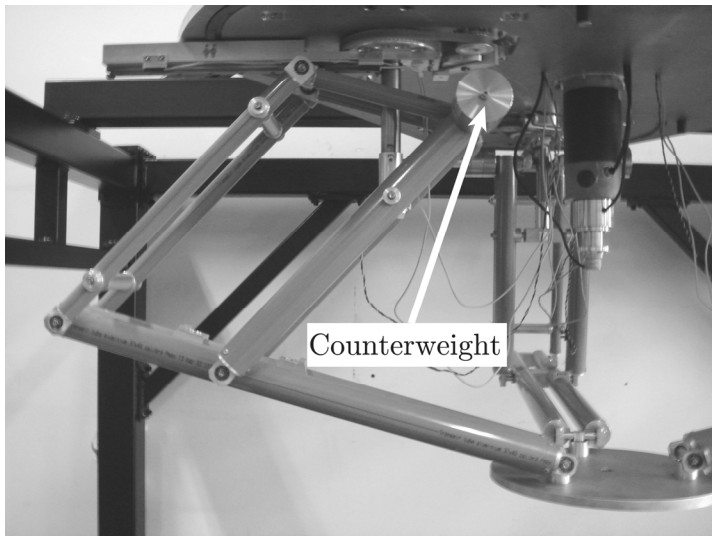

Figure 6.28. – Counterweights added on pantograph linkages.

In order to prove the minimization of input torques before and after balancing, some arbitrary configurations of the manipulator were examined. The tested poses are given in table 6.2.

Table 6.2. – The poses for the experimental validation of the static balancing.

Pose	**1**	**2**	**3**	**4**	**5**	**6**	**7**
x **(m)**	0.124	0.015	-0.149	0.072	-0.053	-0.134	-0.173
y **(m)**	0.096	0.047	0.009	0.129	0.09	-0.075	-0.042
z **(m)**	-0.6	-0.615	-0.733	-0.497	-0.540	-0.389	-0.687
ϕ **(deg.)**	34.72	-20.23	4.53	9.23	33.92	-3.5	15.64

Table 6.3. – The absolute values of the maximal input torques before (case 1) and after (case 2) static balancing.

Pose	**1**	**2**	**3**	**4**	**5**	**6**	**7**
Case 1 (N.m)	1.78	1.81	1.38	3.31	3.23	1.93	2.4
Case 2 (N.m)	0.46	0.26	0.34	0.47	0.59	0.35	0.55
Reduction	74 %	86 %	76 %	86 %	82 %	82 %	77 %

For these seven positions of the platform, the maximal absolute values of the input torques of the 3 rotating actuators before and after complete static balancing are measured (table 6.3). The reduction of the maximal input torques varies from 74% to 86%.

6.3.3.2. Reduction of input torques in dynamic mode of operation.

As proposed above, for the trajectory given in figure 6.25, we measure the input torques of the three rotary actuators for the three different cases:

- without added masses for torques reduction;
- with added masses for static balancing;
- with added masses for dynamic optimization.

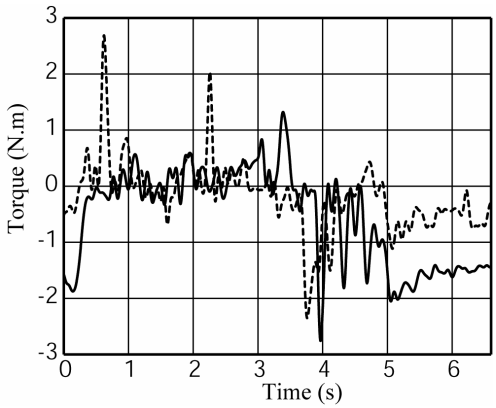

(a) Torque of the actuator M_1.

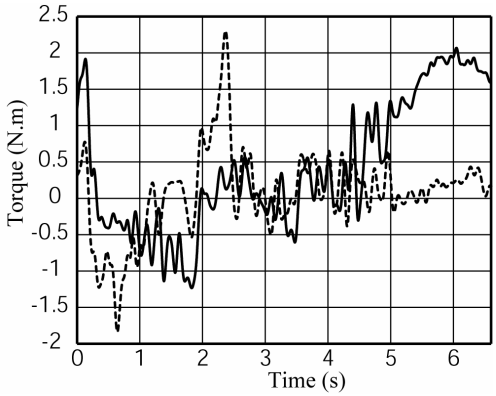

(b) Torque of the actuator M_2.

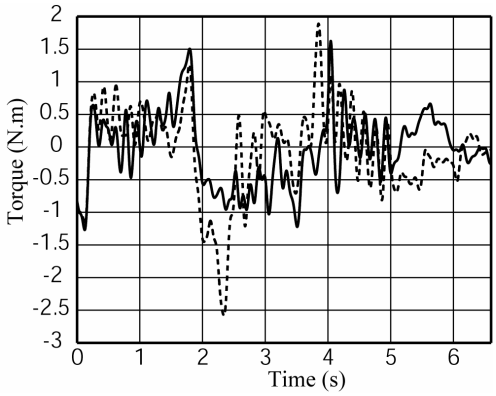

(c) Torque of the actuator M_3.

Figure 6.29. – Actuators' torques without (full line) and with (dotted line) added masses for static balancing.

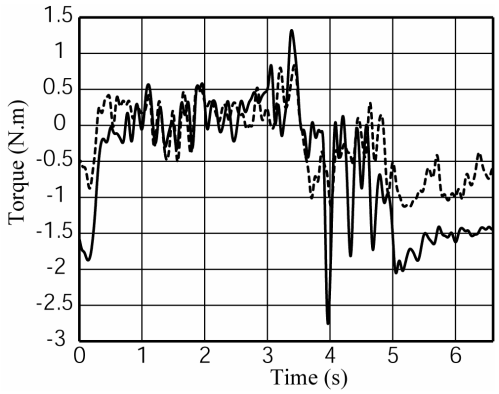

(a) Torque of the actuator M_1.

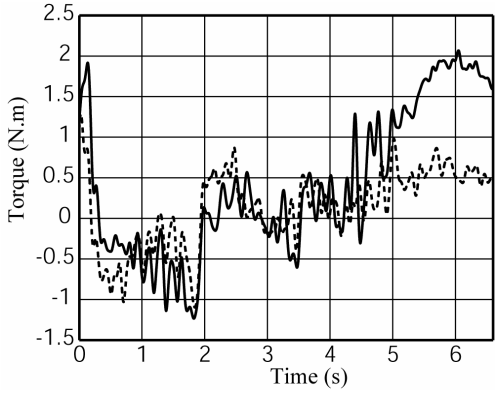

(b) Torque of the actuator M_2.

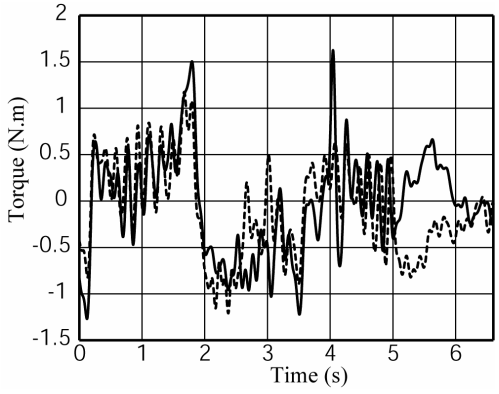

(c) Torque of the actuator M_3.

Figure 6.30. – Actuators' torques without (full line) and with (dotted line) added masses for dynamic optimization.

The results are presented in figures 6.29 and 6.30.

As seen previously, the masses of 2.8 kg for the static balancing becomes inefficient. Thus, an optimal redistribution of the movable masses becomes useful. The reduction of the input torques with the added masses of 1.3 kg varies from 41% to 55%.

Thus, we can note that the obtained measures prove all numerical simulations presented above.

6.4. Summary.

This section presents an analytic study of the maximum orientation and position errors occurring in PAMINSA manipulators subjected to errors in the inputs. It was proven for the planar equivalent models of PAMINSA manipulators that, when sufficiently far from singularities, the local maximum orientation and position errors occur only when at least two inputs suffer a maximum error. However, a simple procedure is proposed to evaluate, for a given design, whether these output errors might occur when only two inputs are at a maximum error. Thanks to this analytic study, a simple method is proposed to calculate the local maximum orientation and position errors for a given nominal configuration and given error bound on the inputs. The method involves solving the direct kinematics for eight, or a maximum of $12n$ (n being the number of discretization steps) sets of inputs. This method is relatively fast and accurate, but above all, very simple to implement and gives a valuable insight into the kinematic accuracy of parallel robot.

Also, new design approaches for the improvement of positioning accuracy of a 4-DOF PAMINSA manipulator are discussed. It is shown that the elasticity of links has an influence on the positioning accuracy of the developed parallel manipulator. For the cancellation of these positioning errors due to the elasticity of links, two approaches are presented. The first solution is obtained by means of two correcting systems mounted on the drive system of the vertical displacements. The second solution is carried out using a correcting mass mounted on the platform. The obtained results show that, after compensation of the errors due to the elasticity of links, the vertical positions of the platform's joints have constant values and the inclination of the platform in relation to the base is cancelled.

The reduction of the input torques is also studied. It is shown that, for a dynamic mode of operation, the complete static balancing may be ineffective in terms of input

torques. In the case of accelerated motions, it is proposed to carry out an optimal redistribution of the movable masses and to achieve a partial mass balancing.

Finally, tests on the prototype of PAMINSA are presented. It is shown experimentally that it is possible to reduce the torques of the actuators by the optimal redistribution of the movable masses (from 74% to 86% in static mode of operation and from 41% to 55% in dynamic mode of operation).

Conclusion

Summary and contribution of the thesis.

The subject of this thesis was the analysis and the optimization of a new family of parallel manipulators called PAMINSA (**PA**rallel **M**anipulator of the **I.N.S.A.**).

The first chapter of our manuscript dealt with the history of parallel kinematic machines and briefly reviewed the historical evolution of parallel mechanisms developed for the industry, patented or prototyped. While it was promised they would have greater rigidity, better velocities and dynamic characteristics, and high accuracy compared with their serial counterparts, such mechanisms have achieved little success in the industrial word. This may be explained by several factors:

- the presence of singularities in the workspace, some of them leading to huge positioning errors; however, solutions have already been proposed and validated;
- the use of links with weaker masses which leads to a loss of rigidity of the structure; such a problem may be easily avoided by the use of more rigid links;
- manufacturing errors and joint clearances, which can be rectified by calibration and an appropriate design;
- the non-linearity of the static and dynamic models of parallel manipulators which leads to positioning errors.

In order to solve the problem in the non-linearity in the relationships of parallel robots, several researchers have thought of decoupling/simplifying the control laws of such structures. Our literature review has shown that, in most of the cases, two approaches are developed: (i) the decoupling between position and orientation; (ii) the full-decoupling of the movements. Despite these rather encouraging results, the fully-decoupled manipulators have drawbacks also, such as a lack of rigidity or the increase in the number of joints.

This is the reason why we proposed, in chapter 2, a compromise between the decoupling of the movements and the architectural characteristics of parallel structures.

In other words, we changed the statement of the problem: it is not essential that a parallel architecture be fully-decoupled, it can also be partially decoupled. But it is important to obtain a mechanical architecture with high payload capacities.

Thus, we proposed a new design approach of decoupling in which the displacements of the platform in the horizontal plane are independent on its displacements along the vertical axis. Based on this concept, a new family of decoupled parallel manipulators from 3 to 6 DOF was created. The structures are obtained with the use of pantograph linkages. Among the obvious advantages of such an approach, we may note:

- the decoupling of the control powers in two parts, making it possible to raise an important payload to a fixed altitude by powerful actuators and, then, to displace it on the horizontal plane by less powerful actuators;
- a great accuracy in the horizontal positioning because the payload can be locked in the horizontal plane by the mechanical architecture of the manipulator (in other words, if the position of the vertical actuator is fixed, the altitude of the platform cannot change);
- the cancellation of static loads on the rotating actuators which move the platform in the horizontal plane;
- the simplification of the vertical control based on linear input/output relationships.

The proposed manipulators could be used in many industrial applications such as the manipulation of heavy equipment with great positioning accuracy or in micro-manipulation (as long as the magnification factor of the pantograph linkages does not enlarge the displacements but, on the contrary, reduces the movement quantity).

At the end of chapter 2, a prototype of PAMINSA and experimental tests were presented. It was shown that the experimental tests prove the validity of the suggested design concept.

The following step of the analysis of these new manipulators was the study of their kinematics, and particularly their singularities, because they may be the worst drawbacks of parallel manipulators. This is the reason why we analysed in chapter 3 the singular configurations of PAMINSA with three, four, five and six degrees of freedom, of which planar equivalent models are the 3-<u>R</u>PR manipulators. The singularities have been determined in analytic form by an algebraic approach based on the analysis of the properties of the Jacobian matrices. The nature of each kind of singularity has been discussed and kinematically analysed.

We have also shown that this kind of PAMINSA manipulators may have Cardanic self motions within their workspace. As the self motions may be the worst type of

singular configurations a parallel manipulator could have, the geometric conditions leading to Cardanic self motions have been derived. The results, in terms of singularity loci and of associated finite displacements, have been validated on an actual robot prototype. These results can be used to optimize the singularity-free workspace of this type of robots and in choosing the optimal architectures of PAMINSA.

As the singular configurations also limit the workspace of parallel manipulators, which is less than that of serial manipulators, the following point of our analysis was to find a means of enlarging the workspace of parallel manipulators by passing through singular configurations. Therefore, chapter 4 presented a new procedure for the increase of singularity-free zones in the workspace of planar parallel manipulators. The procedure is based on the known kinematic singularity equations and the control of the pressure angles in the joints of the manipulator along the given trajectory of the platform. The zones that could not be reached by the manipulator were detected. In order to increase of the reachable workspace of the manipulator, legs of variable structure were proposed. Such a solution makes it possible to obtain the best structural architecture of the manipulator for any trajectory. The design of the optimal structure of the PAMINSA, of which planar equivalent model is a 3-RPR manipulator, was illustrated by two numerical simulations.

Chapter 5 presented another method, based on the optimization of the dynamic parameters of parallel manipulators, which makes it possible to pass through the Type 2 singular configurations, and as a result, to enlarge the workspace of parallel mechanisms. The principal contribution of this chapter is the presentation, for the first time, of the general definition of the condition for passing through the Type 2 singular positions, which can be formulated by the following: in the presence of Type 2 singular configurations, the platform of a parallel manipulator can pass through the singular positions without perturbation of motion if the wrench applied on the platform by the legs and the external loads is orthogonal to the direction of the uncontrollable motion (in other terms, if the work of applied forces and moments on the platform along the uncontrollable motion is equal to zero). This condition has been verified by simulations on two examples (a planar 5R parallel robot and a PAMINSA-4D3L) and validated by experimental tests on the prototype of PAMINSA.

Finally, chapter 6 introduced new methods which can be used in the design optimization of PAMINSA manipulators. These methods may be defined as follows:

- *method for accuracy analysis*: it was proven for the planar equivalent model of PAMINSA that, when sufficiently far from singularities, the local maximum orientation and position errors occur only when at least two inputs suffer a

maximum error. However, a simple procedure was proposed to evaluate, for a given design, whether these output errors might occur when only two inputs are at a maximum error. Thanks to this analytic study, a simple method was proposed to calculate the local maximum orientation and position errors for a given nominal configuration and given error bound on the inputs. The method involves solving the direct kinematics for eight, or a maximum of $12n$ (n being the number of discretization steps) sets of inputs. This method is relatively fast and accurate, but above all, very simple to implement and gives a valuable insight into the kinematic accuracy of parallel robot;

- *method to minimize the deformations*: new design approaches for the improvement of positioning accuracy of a 4-DOF PAMINSA manipulator have been discussed. It has been shown that the elasticity of links has an influence on the positioning accuracy of the developed parallel manipulator. For the cancellation of these positioning errors due to the elasticity of links, two approaches have been presented. The first solution is obtained by means of two correcting systems mounted on the drive system of the vertical displacements. The second solution is carried out by use of a correcting mass mounted on the platform. The obtained results show that, after compensation of the errors due to the elasticity of links, the vertical positions of the platform's joints have constant values and the inclination of the platform in relation to the base is cancelled;
- *method for reducing input efforts*: the reduction of the input torques was studied. It was shown that, for a dynamic mode of operation, the complete static balancing may be ineffective in terms of input torques. In the case of accelerated motions, it was proposed to carry out an optimal redistribution of the movable masses and to achieve a partial mass balancing. Finally, tests on the prototype of PAMINSA are presented. It is shown experimentally that it is possible to reduce the torques of the actuators by the optimal redistribution of the movable masses (from 74% to 86% in static mode of operation and from 41% to 55% in dynamic mode of operation).

We would like to mention that these works have been presented in several articles (of which list is given in appendix F). Moreover, the family of PAMINSA manipulators is patented (the text of the international patent is given in appendix G).

Direction for future works.

Concerning the future research and developments on the subject of PAMINSA manipulators, it could be interesting to make a comparative analysis between the different architectures in order to find the manipulator which is the most appropriate for a desired task. Effectively, although we have, for the time being, proposed a family of new manipulators, but we do not yet know which manipulator is the most accurate, provides the largest workspace, the best effort transmission (and as a result the best efficiency), has the highest velocity, is the least sensitive to manufacturing errors or is the easiest to design. Such an analysis is of great interest for the future industrial applications.

A second axis of research could be the cancellation of the shaking forces and shaking moments of PAMINSA manipulators via the optimal redistribution of the movable masses. Mass balancing of the moving links brings about a reduction of vibration that considerably improves the performances of mechanisms. However, complete shaking force and shaking moment balancing of parallel manipulators is a complicated problem and few research papers have been presented on this subject [Fattah 2006] [Ricard 2000] [Wu 2003] [Wu 2005]. In [Arakelian 1999], the author demonstrates it is possible to completely eliminate the shaking forces and moments of four-bar mechanism by the use of pantograph linkages. This result may be generalized in order to obtain the cancellation of the shaking forces and shaking moments of PAMINSA manipulators.

Another axis of research could be the linearization of the relationships of the dynamic model of PAMINSA manipulators. The present industrial robots limit their working speed and payload due the difficulty of maintaining tracking and positioning accuracy. This difficulty arises since, inherently, the robot dynamics are highly coupled, which result in complexity in the controller design. Some methodologies for decoupling the dynamic equations have been applied on 1-DOF mechanisms [Arakelian 2003] [Nishioka 1995] [Wu 2001] or serial structures [Abdel-Rahman 1991] [Coelho 2004] [Minotti 1991] [Yang 1986] [Youcef-Toumi 1987], but, due to the high-coupling of parallel manipulators, the dynamic decoupling is very difficult to obtain on such structures and some important research has to be achieved on this subject.

All the propositions detailed above apply to PAMINSA manipulators. However, my future research interests are not limited to these types of manipulators. Many research fields are attractive, such as finding new solutions for increasing the singularity-free

zones in the workspace of parallel manipulators, or better understanding the effort transmission at Type 2 singular configurations.

I am also interested in creating new structures for different purposes, such as medical applications. In the past few years, more and more medical robots have been created, mainly for surgery operations [Bidaud 2002]. However, there are many other potential medical applications where parallel structures can be used, such as in the creation of mechanisms for 3D ultrasound imaging or for in vitro testing of cadaveric spine specimens. For example, at this moment in time, existing spine test devices are only capable of applying loads or displacements at one end of a spine segment, thus failing to reproduce realistic testing conditions involving muscles actions. In contrast, new parallel systems based on the use of steel wires, instead of rigid links, could replace completely the action of muscles and hence reproduce realistic testing conditions. Thus, my works would naturally be orientated to find new solutions for these problems.

Bibliography

[Abdel-Rahman 1991] T.M. Abdel-Rahman and M.A. Elbestawi, 1991, "Synthesis and dynamics of statically balanced direct-drive manipulators with decoupled inertia tensors," Mechanism and Machine Theory, Vol. 26, No. 4, pp. 389-402.

[Alba-Gomez 2005] O. Alba-Gomez, P. Wenger and A. Pamanes, 2005, "Consistent kinetostatic indices for planar 3-DOF parallel manipulators, application to the optimal kinematic inversion," Proceedings of the ASME 2005 Design Engineering Technical Conferences & Computers and Information in Engineering Conference (IDETC/CIE), Long Beach, California, USA, September 24-28.

[Alvan 2003] K. Alvan and A. Slousch, 2003, "On the control of the spatial parallel manipulators with several degrees of freedom," Mechanism and Machine Theory, Saint-Petersburg, No. 1, pp. 63-69.

[Angeles 2003] J. Angeles, 2003, "Fundamentals of robotic mechanical systems," 2nd ed., Springer.

[Angeles 2006] J. Angeles, S. Caro, W. Khan and A. Morozov, 2006, "Kinetostatic design of an innovative Schoenflies motion generator," Proceedings of IMechE, Journal of Mechanical Engineering Science, Vol. 220, Part C, pp. 935-943.

[Arakelian 1989] V. Arakelian, 1989, "Manipulator," Patent SU 1,465,298, March 15.

[Arakelian 1990] V. Arakelian and V. Melikian, 1990, "Manipulator," Patent SU 1,537,518, January 23.

[Arakelian 1998] V. Arakelian, 1998, "Equilibrage des manipulateurs manuels," Mechanism and Machine Theory, Vol. 33, No. 4, pp. 437-442.

[Arakelian 1999] V. Arakelian and M.R. Smith, 1999, "Complete shaking force and shaking moment balancing of linkages," Mechanism and Machine Theory, Vol. 34, pp. 1141-1153.

[Arakelian 2003] V. Arakelian, 2003, "Minimisation des variations periodiques du couple d'un manipulateur a frequence fixe par l'optimisation de la trajectoire de la pince," Mecanique et Industrie, Vol. 4, pp. 565-568.

[Arakelian 2004] V. Arakelian, 2004, "The history of the creation and development of hand-operated balanced manipulators," Proceedings of the HMM2004, Kluwer Academic Publishers.

[Balli 2002] S. Balli and S. Chand, 2002, "Transmission angle in mechanisms," Mechanism and Machine Theory, Vol. 37, pp. 175-195.

[Bandyopadhyay 2004] S. Bandyopadhyay and A. Ghosal, 2004, "Analysis of configuration space singularities of closed-loop mechanisms and parallel manipulators," Mechanism and Machine Theory, Vol. 39, No. 5, pp. 519-544.

[Bernier 1995] D. Bernier, J.-M. Castelain and X. Li, 1995, "A new parallel structure with six degrees of freedom," Proceedings of the 9th World Congress on the Theory of Machines and Mechanisms (WCToMM), Milan, Italy, August, pp. 8-12.

[Bhattacharya 1998] S. Bhattacharya, H. Hatwal and A. Ghosh, 1998, "Comparison of an exact and approximate method of singularity avoidance in platform type parallel manipulators,"

Mechanism and Machine Theory, Vol. 33, No. 7, pp.965-974.

[Bidaud 2002] P. Bidaud and J.-C. Guinot, 2002, "Design and Control of micro robotics systems for micro-manipulation and minimally invasive surgery," Journal of Physics IV, EDP Sciences.

[Bonev 2003a] I.A. Bonev, 2003, "The true origins of parallel robots," www.parallemic.org.

[Bonev 2003b] I.A. Bonev, D. Zlatanov and C.M. Gosselin, 2003, "Singularity analysis of 3-DOF planar parallel mechanisms via screw theory," Transaction of the ASME Journal of Mechanical Design, Vol. 125, pp. 573-581.

[Bonev 2006] I.A. Bonev, D. Chablat and P. Wenger, 2006, "Working and assembly modes of the agile eye," Proceedings of the 2006 IEEE International Conference on Robotics and Automation (ICRA), Orlando, Florida, USA, May 15-19, pp. 2317-2322.

[Bouzgarrou 2004] B.C. Bouzgarrou, J.-C. Fauroux, G. Gogu and Y. Heerah, 2004, "Rigidity analysis of T3R1 parallel robot with uncoupled kinematics," Proceedings of the 35th International Symposium on Robotics (ISR), Paris, France, March 23-26.

[Carricato 2002] M. Carricato and V. Parenti-Castelli, 2004, "Singularity-free fully-isotropic translational parallel manipulators," Proceedings of the ASME 2002 Design Engineering Technical Conferences & Computers and Information in Engineering Conference (DETC), Montreal, Quebec, Canada, September 29 – October 2.

[Carricato 2004a] M. Carricato and V. Parenti-Castelli, 2004, "A novel fully decoupled two degrees of freedom parallel wrist," The International Journal of Robotic Research, Vol. 23, No. 6, pp. 661-667.

[Carricato 2004b] M. Carricato and V. Parenti-Castelli, 2004, "On the topological and geometrical synthesis and classification of translational parallel mechanisms," Proceedings of the 11th World Congress in Mechanism and Machine Science, Tianjin, China, April 1-4.

[Chablat 2000] D. Chablat and P. Wenger, 2000, "A new three-DOF parallel mechanism: milling machine applications," Proceedings of the 2nd Chemnitz Parallel Kinematics Seminar, Chemnitz, Germany, April.

[Chablat 2003] D. Chablat and P. Wenger, 2003, "A new concept of modular parallel mechanism for machining applications," Proceedings of the 2003 IEEE International Conference on Robotics and Automation (ICRA), Taipei, Taiwan, September 14-19.

[Chablat 2006] D. Chablat, P. Wenger and I.A. Bonev, 2006, "Self motions of a special 3-RPR planar parallel robot," Advances in Robot Kinematics, J. Lenarcic and B. Roth (eds.), Springer, pp. 221-228.

[Chen 2005] C. Chen and J. Angeles, 2005, "A generalized transmission index for spatial linkages," Proceedings of the ASME 2005 Design Engineering Technical Conferences & Computers and Information in Engineering Conference (IDETC/CIE), Long Beach, California, USA, September 24-28.

[Clavel 1990] R. Clavel, 1990, "Device for movement and displacing of an element in space," US Patent No. 4,976,582, December 11.

[Coelho 2004] T.A.H Coelho, L. Yong and V.F.A. Alves, 2004, "Decoupling of dynamic equations by means of adaptative balancing of 2-DOF open-loop mechanisms," Mechanism and Machine Theory, Vol. 39, pp. 871-881.

[Dasgupta 1998] B. Dasgupta and T. Mruthyunjaya, "Singularity-free path planning for the Steward platform manipulator," Mechanism and Machine Theory, Vol. 33, No. 6, pp. 715-725.

[Di Gregorio 2001] R. Di Gregorio, 2001, "A new decoupled parallel manipulator," Proceedings of the 10th International Workshop on Robotics of the Alpe – Adria – Danube Region (AAD), Vienna, Austria, May 16-18.

[Dimentberg 1965] F.M. Dimentberg, 1965, "The screw calculus and its applications in mechanics," Technical report, Foreign Technology Division, Wright-Paterson Air Force Base.

[Fattah 2002] A. Fattah and A.M. Hasan Ghasemi, 2002, "Isotropic design of spatial parallel manipulators," The International Journal of Robotic Research, Vol. 21, No. 9, pp. 811-824.

[Fattah 2006] A. Fattah and S.K. Agrawal, 2006, "On the design of reactionless 3-DOF planar parallel mechanisms," Mechanism and Machine Theory, Vol. 41, pp. 70-82.

[Glazunov 1990] V. Glazunov, A. Koliskor, A. Krainev and B. Model, 1990, "Classification principles and analysis methods for parallel-structure spatial mechanisms," Journal of Machinery Manufacture and Reliability, Allerton Press Inc., Vol. 1, pp. 30-37.

[Glazunov 2004] V. Glazunov, A. Kraynev, R. Bykov, G. Rashoyan and N. Novikova, 2004, "Parallel manipulator control while intersecting singular zones," Proceedings of the 15th Symposium on Theory and Practice of Robots and Manipulators (ROMANSY) CISM-IFToMM, Montreal, Quebec, Canada.

[Gogu 2004] G. Gogu, 2004, "Fully-isotropic over-constrained planar parallel manipulators," Proceedings of the 2004 IEEE/RSJ

International Conference on Intelligent Robots and Systems (IRoS), Sendai, Japan, September 28 – October 2, pp. 3519-3524.

[Gogu 2005a] G. Gogu, 2005, "Fully-isotropic over-constrained parallel wrists with two degrees of freedom," Proceedings of the 2005 IEEE International Conference on Robotics and Automation (ICRA), Barcelona, Spain, April, pp. 4025-4030.

[Gogu 2005b] G. Gogu, 2005, "Fully-isotropic T1R2-type parallel robots with three degrees of freedom," Proceedings of the ASME 2005 International Design Engineering Technical Conferences & Computers and Information in Engineering Conference (IDETC/CIE), Long Beach, California, USA, September 24-28.

[Gogu 2005c] G. Gogu, 2005, "Fully-isotropic parallel robots with four degrees of freedom T2R2-type," Proceedings of the 2005 IEEE/RSJ International Conference on Intelligent Robots and Systems (IRoS), Center Edmont, Alberta, Canada, August 2-6, pp. 1190-1195.

[Gogu 2005d] G. Gogu, 2005, "Singularity-free fully-isotropic parallel manipulators with Schoenflies motions," Proceedings of the 2005 IEEE 12-th IEEE International Conference on Advanced Robotics (ICAR 2005), Seattle, WA, USA, July 18-20, pp. 194-201.

[Gogu 2006a] G. Gogu, 2006, "Fully-isotropic parallel manipulators with five degrees of freedom," Proceedings of the 2006 IEEE International Conference on Robotics and Automation (ICRA), Orlando, Florida, USA, May, pp. 1141-1146.

[Gogu 2006b] G. Gogu, 2006, "Fully-isotropic parallel manipulators with Schoenflies motions and complex legs with rhombus loops," Proceedings of the 2006 IEEE International Conference on

Robotics and Automation (ICRA), Orlando, Florida, USA, May, pp. 1147-1152.

[Gogu 2006c] G. Gogu, 2006, "Fully-isotropic redundantly actuated parallel manipulators with five degrees of freedom," Proceedings of the 1st European Conference on Mechanism Science (EuCoMeS), Obergurgl, Austria, February 21-26.

[Gogu 2007] G. Gogu, "Structural synthesis of fully-isotropic parallel robots with Schoenflies motions via theory of linear transformations and evolutionary morphology," European Journal of Mechanics / A –Solids, in press.

[Gosselin 1990] C.M. Gosselin and J. Angeles, 1990, "Singularity analysis of closed-loop kinematic chains," IEEE Transactions on Robotics and Automation, Vol. 6, No. 3, pp. 281-290.

[Gosselin 1991] C.M. Gosselin and J. Angeles, 1991, "A global performance index for the kinematic optimization of robotic manipulators," Transaction of the ASME Journal of Mechanical Design, Vol. 113, No. 3, pp. 220-226.

[Gosselin 1992] C.M. Gosselin, 1992, "The optimum design of robotic manipulators using dexterity indices," Robotics and Autonomous Systems, Vol. 9, No. 4, pp. 213-226.

[Gosselin 1996] C.M. Gosselin, S. Lemieux and J.-P. Merlet, 1996, "A new architecture of planar three-degree-of-freedom parallel manipulator," Proceedings of the 1996 IEEE International Conference on Robotics and Automation (ICRA), Minneapolis, Minnesota, USA, pp. 3738–3743.

[Gosselin 2004] C.M. Gosselin, X. Kong, S. Foucault and I.A. Bonev, 2004, "A fully decoupled 3-DOF translational parallel mechanism", Proceedings of the Parallel Kinematic Machines International

Conference, Chemnitz, Germany, April 20-21, pp. 595-610.

[Gosselin 2007] C.M. Gosselin, M. Tale Masouleh, V. Duchaine, P.-L. Richard, S. Foucault and X. Kong, "Parallel mechanisms of the Multipteron family: kinematic architectures and benchmarking," Proceedings of the 2007 IEEE International Conference on Robotics and Automation (ICRA), April 10-14, Rome, Italy.

[Gough 1962] V.E. Gough and S.G. Whitehall, 1962, "Universal tyre test machine," Proceedings of the FISITA 9th International Technical Congress, May, pp. 117-317.

[Gwinnett 1931] J.E. Gwinnett, 1931, "Amusement devices," US Patent No. 1,789,680, January 20.

[Hesselbach 2004] J. Hesselbach, J. Wrege, A. Raatz and O. Becker, 2004, "Aspects on the design of high precision parallel robots," Assembly Automation, Vol. 24, No. 1, pp. 49-57.

[Husty 1994] M.L. Husty and P. Zsombor-Murray, 1994, "A special type of singular Stewart-Gough platform," A. J. Lenarcic and B. B. Ravani (eds.), Advances in Robot Kinematics and Computational Geometry, Kluwer Academic Publishers, pp. 449-458.

[Husty 2000] M.L. Husty and A. Karger, 2000, "Self-motions of Griffis-Duffy type parallel manipulators," Proceedings of the 2000 IEEE International Conference on Robotic and Automation (ICRA), San Francisco, California, April 24-28, pp. 7-12

[IFToMM 2003] 2003, "Terminology for the mechanism and machine science," Mechanism and Machine Theory, Vol. 38, pp. 597-605.

[Jin 2004] Q. Jin and T.-L. Yang, 2004, "Synthesis and analysis of a group of a 3 degree of freedom partially decoupled parallel

manipulators," Transaction of the ASME Journal of Mechanical Design, Vol. 126, pp. 301-306.

[Jui 2005] C.K.K. Jui and Q. Sun, 2005, "Path tracking of parallel manipulators in the presence of force singularity," Transaction of the ASME Journal of Dynamic Systems, Measurement and Control, Vol. 127, December, pp. 550-563.

[Karger 1998a] A. Karger and M.L. Husty, 1998, "Classification of all self motions of the original Stewart-Gough platform," Computer-Aided Design, Vol. 30, No. 3, pp. 205-215.

[Karger 1998b] A. Karger, 1998, "Classification of 5R closed kinematic chain with self mobility," Mechanism and Machine Theory, Vol. 33, No. 1, pp. 213-222.

[Karger 2001] A. Karger, 2001, "Singularities and self-motions of equiform platforms," Mechanism and Machine Theory, Vol. 36, pp. 801-815.

[Karger 2003] A. Karger, 2003, "Architecture singular planar parallel manipulators," Mechanism and Machine Theory, Vol. 38, pp. 1149-1164.

[Karouia 2005] M. Karouia, J.-M. Herve and P. Bidaud, 2005, "Analyse des singularites du manipulateur parallele spherique isostatique 3-RCC," Actes du 17eme Congres Francais de Mecanique, Universite de Technologie, Troyes, France, September.

[Kemal Ider 2005] S. Kemal Ider, 2005, "Inverse dynamics of parallel manipulators in the presence of drive singularities," Mechanism and Machine Theory, Vol. 40, pp. 33-44.

[Khalil 2002] W. Khalil and S. Guegan, 2002, "A Novel Solution for the Dynamic Modeling of Gough-Stewart Manipulators," Proceedings of the IEEE 2002 International Conference on

Robotics and Automation (ICRA), Washington DC., USA, May 11-15.

[Kong 2002a] X. Kong and C.M. Gosselin, 2002, "A class of 3-DOF translational parallel manipulators with linear input-output equations," Proceedings of the Workshop on Fundamental Issues and Future Research Directions for Parallel Mechanisms and Manipulators, Quebec City, Quebec, Canada, October 3-4.

[Kong 2002b] X. Kong, C.M. Gosselin, 2002, "Type synthesis of linear translational parallel manipulators," J. Lenarcic, F. Thomas (eds.), Advances in Robot Kinematics – Theory and Applications, Kluwer Academic Publishers, pp. 411-420.

[Lallemand 1997] J.-P. Lallemand, A. Goudali and S. Zeghloul, 1997, "The 6-DOF 2-Delta parallel robot," Robotica, Vol. 15, pp. 407-416.

[Lazarevic 1997] Z. Lazarevic, 1997, "Feasibility of a Stewart platform with fixed actuators as a platform for CABG surgery device," Master's Thesis, Columbia University, Department of Bioengineering.

[Lee 1995] M. K. Lee, 1995, "Design of a high stiffness machining robot arm using double parallel mechanism," Proceedings of the 1995 IEEE International Conference on Robotics and Automation (ICRA), Nagoya, Japan, pp. 234-240.

[Legnani 2005] G. Legnani, D. Tosi and I. Fassi, 2005, "A 6-DOF isotropic PKM with decoupled movements," Proceedings of the 36th International Symposium on Robotics (ISR), Tokyo, Japan, November 29 – December 1.

[Li 2004] W. Li, F. Gao and J. Zhang, 2004, "R-CUBE, a decoupled parallel manipulator only with revolute joints," Mechanism

and Machine Theory, Vol. 40, No. 4, pp. 467-473.

[Lin 2002] C.-C. Lin and W.-T. Chang, 2002, "The force transmissivity index of planar linkage mechanisms," Mechanism and Machine Theory, Vol. 37, p. 1465-1485.

[Liu 2006] X.-J. Liu, J. Wang and G. Pritschow, 2006, "Kinematics, singularity and workspace of planar 5R symmetrical parallel mechanism," Mechanism and Machine Theory, Vol. 41, No. 2, pp. 119-144.

[Lu 1996] D.-M. Lu and W.-M. Hwang, 1996, "Synthesis of planar five-bar pantograph configurations by a geometric method," Mechanism and Machine Theory, Vol. 31, No. 1, pp. 11-21.

[Ma 1992] O. Ma and J. Angeles, 1992, "Architecture singularities of parallel manipulators," The International Journal of Robotics and Automation, Vol. 7, No. 1, pp. 23-29.

[Maass 2006] J. Maass, M. Kolbus, C. Budde, J. Hesselbach and W. Schumacher, 2006, "Control Strategies for Elarging a Spatial Robot's Workspace by Change of Configuration", Proceedings of the 5-th Chemnitz Parallel Kinematics Seminar, Chemnitz, Germany, pp. 515-530.

[Meggiolaro 2001] M. Meggiolaro and S. Dubowsky, 2001, "Improving the positioning accuracy of powerful manipulators with application in nuclear maintenance," Anais do 16 Congresso Brasileiro de Engenharia Mecanica (COBEM), Robotics and Control, Vol. 15, ABCM, Uberlandia, pp. 210-219.

[Merlet 1989] J.-P. Merlet, 1989, "Singular configurations of parallel manipulators and Grassmann geometry," The International Journal of Robotics Research, Vol. 8, No. 5, pp. 45-56.

[Merlet 1996] J.-P. Merlet, "Direct kinematics of planar parallel

manipulators," Proceedings of the 1996 IEEE International Conference on Robotics and Automation (ICRA), Minneapolis, Minnesota, USA, pp. 3744-3749.

[Merlet 1998] J.-P. Merlet, C.M. Gosselin and N. Mouly, "Workspaces of planar parallel manipulators," Mechanism and Machine Theory, Vol. 33, No. 1, pp. 7-20.

[Merlet 2006a] J.-P. Merlet, 2006, "Parallel robots," 2nd ed., Springer.

[Merlet 2006b] J.-P. Merlet, 2006, "Jacobian, manipulability, condition number, and accuracy of parallel robots," Transaction of the Transaction of the ASME Journal of Mechanical Design, Vol. 128, No. 1, pp. 199-206.

[Merlet 2006c] J.-P. Merlet, 2006, "Computing the worst case accuracy of a PKM over a workspace or a trajectory," Proceedings of the 5th Chemnitz Parallel Kinematics Seminar, Chemnitz, Germany, pp. 83-96.

[Mianowski 1998] K. Mianowski, 1998, "Dextrous fully parallel manipulator with six degrees of freedom," Proceedings of the 12th Symposium ROMANSY, Paris, France, July, pp. 253-260.

[Minotti 1991] P. Minotti, 1991, "Decouplage dynamique des manipulateurs : propositions de solutions mecaniques," Mechanism and Machine Theory, Vol. 26, No. 1, pp. 107-122.

[Nabat 2005] V. Nabat, M. de la O Rodriguez, O. Company, S. Krut and F. Pierrot, 2005, "Par4: very high speed parallel robot for pick-and-place," Proceedings of the 2005 IEEE/RSJ International Conference on Intelligent Robots and Systems (IRoS), Center Edmont, Alberta, Canada, August 2-6.

[Nenchev 1997] D.N. Nenchev, S. Bhattacharya and M. Uchiyama, 1997,

"Dynamic analysis of parallel manipulators under the singularity-consistent parameterization," Robotica, Vol. 15, No. 4, pp. 375-384.

[Nishioka 1995] M. Nishioka, 1995, "State of the art of torque compensation cam mechanisms," Proceedings of the 9th World Congress on Theory of Machines and Mechanisms, Milan, Italy, August 29 – September 2.

[Oiwa 2002] T. Oiwa, 2002, "Accuracy improvement of parallel kinematic machine," Proceedings of the 6th International Conference on Mechatronics Technology, Kitakyushu, Japan, September 29 - October 3.

[Ottaviano 2001] E. Ottaviano, C.M. Gosselin and M. Ceccarelli, 2001, "Singularity analysis of CaPaMan: a three-degree of freedom spatial parallel manipulator," Proceedings of the 2001 IEEE International Conference on Robotics and Automation (ICRA), Seoul, Korea, May 21-26, pp. 1295-1300.

[Patarinski 1993] S.P. Patarinski and M. Uchiyama, 1993, "Position/ Orientation Decoupled Parallel Manipulators," Proceedings of the International Conference on Advanced Robotics (ICAR), Tokyo, Japan, November 1-2, pp. 153-158.

[Perng 1999] M.H. Perng and L. Hsiao, "Inverse kinematic solutions for a fully parallel robot with singularity robustness," The International Journal of Robotics Research, Vol. 18, No. 6.

[Pernkopf 2002] F. Pernkopf and M. Husty, 2002, "Singularity analysis of spatial Stewart-Gough platforms with planar base and platform," Proceedings of the ASME 2002 Design Engineering Technical Conferences & Computers and Information in Engineering Conference (DETC), Montreal, Quebec, Canada, September 29 – October 2.

[Ricard 2000] R. Ricard and C.M. Gosselin, 2000, "On the development of reactionless parallel manipulators," Proceedings of the ASME 2000 Design Engineering Technical Conferences & Computers and Information in Engineering Conference (DETC), Baltimore, Maryland, USA, September 10-13.

[Richard 2007] P.-L. Richard, C.M. Gosselin and X. Kong, 2007, "Kinematic analysis and prototyping of a partially decoupled 4-DOF 3T1R parallel manipulator," Transaction of the ASME Journal of Mechanical Design, Vol. 129, pp. 611-616

[Saint-Onge 2000] B.M. Saint-Onge and C.M. Gosselin, 2000, "Singularity analysis and representation of the general Gough-Stewart platform," The International Journal of Robotics Research, Vol. 19, No. 3, pp. 271-288.

[Sekulie 1998] A. Sekulie, 1998, "Method of synthesis of Cardanic motion," Facta Universitatis, Mechanical Engineering, University of NIS, Vol. 1, No. 5, pp. 565-572.

[Seyferth 1974] W. Seyferth, 1974, "Massenersatz duch punktmassen in raumlichen getrieben," Mechanism and Machine Theory, Vol. 9, pp. 49-59.

[Stewart 1965] D. Stewart, 1965, "A platform with six degrees of freedom," Proceedings of the IMechE, Vol. 180, Pt. 1, No. 15, pp. 371-385.

[Sutherland 1973] G. Sutherland and B. Roth, 1973, "A transmission index for spatial mechanisms," Transaction of the ASME Journal of Engineering for Industry, pp. 589-597.

[Sutherland 1981] G. Sutherland, 1981, "Quality of motion and force transmission," Mechanism and Machine Theory, Vol. 16, No. 3, pp. 221-225.

[Tischler 1998] C.R. Tischler, K.H. Hunt and A.E. Samuel, 1998, "A spatial extension of Cardanic movement: its geometry and some derived mechanisms," Mechanism and Machine Theory, Vol. 33, pp. 1249-1276.

[Wen 2003] J.T. Wen and J.F. Oapos Brien, 2003, "Singularities in three-legged platform-type parallel mechanisms," IEEE Transactions on Robotics and Automation, Vol. 19, No. 4.

[Wohlhart 2003] K. Wohlhart, 2003, "Mobile 6-SPS parallel manipulators," Journal of Robotic Systems, Vol. 20, No. 8, pp. 509-516.

[Wolf 2004] A. Wolf, E. Ottaviano, M. Shoham and M. Ceccarelli, 2004, "Application of line geometry and linear complex approximation to singularity analysis of the 3-DOF CaPaMan parallel manipulator," Mechanism and Machine Theory, Vol. 39, No. 1, pp. 75-95.

[Wu 2001] C.-J. Wu and J. Angeles, 2001, "The optimum synthesis of an elastic torque-compensating cam mechanism," Mechanism and Machine Theory, Vol. 36, pp. 245-259.

[Wu 2003] Y. Wu and C.M. Gosselin, 2003, "Singularity analysis of a reactionless 6-DOF parallel mechanism," Proceedings of the 11th World Congress in Mechanism and Machine Science, Tianjin, China, August 18-21.

[Wu 2005] Y. Wu and C.M. Gosselin, 2005, "Design of reactionless 3-DOF and 6-DOF parallel manipulators using parallelepiped mechanisms," IEEE Transactions on Robotics, No. 5, October, pp. 821-833.

[Wu 2007] Y. Wu and C.M. Gosselin, 2007, "On the dynamic balancing of multi-DOF parallel mechanisms with multiple legs," Transaction of the ASME Journal of Mechanical Design, Vol.

129, No. 4, pp. 234-238.

[Yang 1986] D.C.H. Yang and S.W. Tzeng, 1986, "Simplification and linearization of manipulators dynamics by the design of inertia distribution," The International Journal of Robotic Research, Vol. 5, No. 3, pp. 120-128.

[Youcef-Toumi 1987] K. Youcef-Toumi and H. Asada, 1987, "The design of open-loop manipulator arms with decoupled and configuration-invariant inertia matrix," Transaction of the ASME Journal of Dynamic Systems, Measurement, and Control, Vol. 109, September, pp. 268-275.

[Yu 2006] A. Yu, I.A. Bonev and P. Zsombor-Murray, 2006, "New XY-Theta positioning table with partially decoupled parallel kinematics," Proceedings of the 2006 IEEE International Symposium on Industrial Electronics (ISIE), Montreal, Quebec, Canada, July 9-12, pp. 3108-3112.

[Yu 2007] A. Yu, I.A. Bonev and P.J. Zsombor-Murray, 2007, "Geometric method for the accuracy analysis of a class of 3-DOF planar parallel robots," Mechanism and Machine Theory, in press.

[Zhao 2005] J.-S. Zhao, Z.-J. Feng, K. Zhou and J.-X. Dong, 2005, "Analysis of the singularity of spatial parallel manipulator with terminal constraints," Mechanism and Machine Theory, Vol. 40, No. 3, pp. 275-284.

[Zlatanov 1994] D. Zlatanov, R.G. Fenton and B. Benhabib, 1994, "Singularity analysis of mechanisms and robots via a velocity-equation model of the instantaneous kinematics," Proceedings of the 1994 IEEE International Conference on Robotics and Automation (ICRA), Vol. 2, pp. 980-991.

Appendix A

Computation of the Coordinates of the Pantograph Linkages Centre of Masses

Based on the description of the pantograph linkage of the figure 2.8, the coordinates of its centre of masses can be expressed as the barycentric coordinates of the centre of masses of each joint and link. Therefore, we need to calculate the coordinates of each point of the described linkage.

The coordinates of point 5_i ($i = 1, 2, 3$) are equal to:

$$\begin{bmatrix} x_{5i} \\ y_{5i} \\ z_{5i} \end{bmatrix} = \begin{bmatrix} x \\ y \\ z \end{bmatrix} + \begin{bmatrix} R_{pl}\cos(\phi + \gamma_i) \\ R_{pl}\sin(\phi + \gamma_i) \\ L_c \end{bmatrix} \tag{A.1}$$

where $[x,\ y,\ z]^T$ represents the position of the centre of the platform and ϕ its orientation about the vertical axis. L_c is the constant distance between points 6_i and 5_i and R_{pl} represents the radius of the circumscribed circle of the platform triangle $6_1 6_2 6_3$. Moreover, as the platform triangle is equilateral, $\gamma_1 = -5\pi/6$, $\gamma_2 = -\pi/6$ and $\gamma_3 = \pi/2$.

The coordinates of points 3_i, 2_i and 8_i can be expressed as:

$$\begin{bmatrix} x_{3i} \\ y_{3i} \\ z_{3i} \end{bmatrix} = \begin{bmatrix} R_b\cos\gamma_i \\ R_b\sin\gamma_i \\ z_{5i}/k \end{bmatrix}, \tag{A.2}$$

$$\begin{bmatrix} x_{2i} \\ y_{2i} \\ z_{2i} \end{bmatrix} = \begin{bmatrix} R_b \cos\gamma_i \\ R_b \sin\gamma_i \\ z_{5i} / k + L_{B2} \end{bmatrix}, \tag{A.3}$$

$$\begin{bmatrix} x_{8i} \\ y_{8i} \\ z_{8i} \end{bmatrix} = \frac{1}{1-k} \begin{bmatrix} x_{5i} - k\, x_{3i} \\ y_{5i} - k\, y_{3i} \\ 0 \end{bmatrix}, \tag{A.4}$$

where R_b represents the radius of the circumscribed circle of the base triangle, k is the magnification factor of the pantograph linkages and L_{Bj} is the length of the link B_{ji} ($j =$ 1 to 10).

The position of point 9_i can be found by solving a system of quadratic equations representing the intersection of two circles situated in the plane of the pantograph linkage:

- one circle centered in 8_i of which radius is L_{B8};
- one circle centered in 5_i of which radius is L_{B4}.

This system can be written under the form:

$$\begin{cases} L_{B4}^2 = (X_{5i} - X_{9i})^2 + (z_{5i} - z_{9i})^2 \\ L_{B8}^2 = (X_{8i} - X_{9i})^2 + z_{9i}^2 \end{cases} \tag{A.5}$$

where $X_{5i} = \sqrt{(x_{5i} - x_{3i})^2 + (y_{5i} - y_{3i})^2}$, $X_{8i} = -X_{5i} / (k-1)$ and X_{9i} represent the projection, in the plane of the pantograph linkage, of the coordinates of points 5_i, 8_i and 9_i, respectively.

Thus the coordinates of point 9_i can be deduced:

$$\begin{bmatrix} x_{9i} \\ y_{9i} \\ z_{9i} \end{bmatrix} = \begin{bmatrix} x_{3i} + X_{9i} \cos q_i \\ y_{3i} + X_{9i} \sin q_i \\ F \end{bmatrix} \tag{A.6}$$

with:

$$X_{9i} = A + B\,F, \qquad F = -(D - K)/(2E), \qquad K = \sqrt{D^2 - 4EC},$$

$$E = -(B^2 + 1), \qquad D = 2\,B\,(X_{8i} - A), \qquad C = L_{B3}^2 - X_{8i}^2 + 2\,A\,X_{8i} - A^2,$$
$$B = z_{5i}\,/(k\,X_{8i}) \qquad A = (L_{B4}^2 - L_{B3}^2 - X_{5i}^2 + X_{8i}^2 - z_{5i}^2)/(2\,k\,X_{8i}).$$

The coordinates of points 2_i and 4_i can be calculated as a linear combination of the coordinates of points 3_i, 5_i and 9_i:

$$\begin{bmatrix} x_{2i} \\ y_{2i} \\ z_{2i} \end{bmatrix} = \frac{1}{k(k-1)} \begin{bmatrix} x_{5i} \\ y_{5i} \\ (1-k)\,z_{5i} \end{bmatrix} - \frac{1}{k} \begin{bmatrix} x_{9i} \\ y_{9i} \\ z_{9i} \end{bmatrix} + \frac{k}{k-1} \begin{bmatrix} x_{3i} \\ y_{3i} \\ 0 \end{bmatrix}, \tag{A.7}$$

$$\begin{bmatrix} x_{4i} \\ y_{4i} \\ z_{4i} \end{bmatrix} = \frac{1}{k} \begin{bmatrix} x_{5i} + (k-1)\,x_{9i} \\ y_{5i} + (k-1)\,y_{9i} \\ z_{5i} + (k-1)\,z_{9i} \end{bmatrix}. \tag{A.8}$$

Supposing the centre of masses S_{ji} of each link B_{ji} (j = 1 to 10) is located at their middle, their coordinates can be expressed as:

$$\begin{bmatrix} x_{S1i} \\ y_{S1i} \\ z_{S1i} \end{bmatrix} = \begin{bmatrix} x_{3i}/2 \\ y_{3i}/2 \\ q_v \end{bmatrix}, \tag{A.9}$$

$$\begin{bmatrix} x_{S2i} \\ y_{S2i} \\ z_{S2i} \end{bmatrix} = \begin{bmatrix} x_{3i} \\ y_{3i} \\ (q_v + z_{5i})/2 \end{bmatrix}, \tag{A.10}$$

$$\begin{bmatrix} x_{S3i} \\ y_{S3i} \\ z_{S3i} \end{bmatrix} = \frac{1}{2} \begin{bmatrix} x_{7i} + x_{4i} \\ y_{7i} + y_{4i} \\ z_{7i} + z_{4i} \end{bmatrix}, \tag{A.11}$$

$$\begin{bmatrix} x_{S4i} \\ y_{S4i} \\ z_{S4i} \end{bmatrix} = \frac{1}{2} \begin{bmatrix} x_{5i} + x_{9i} \\ y_{5i} + y_{9i} \\ z_{5i} + z_{9i} \end{bmatrix}, \tag{A.12}$$

$$\begin{bmatrix} x_{S7i} \\ y_{S7i} \\ z_{S7i} \end{bmatrix} = \frac{1}{2}\begin{bmatrix} x_{7i}+x_{8i} \\ y_{7i}+y_{8i} \\ z_{7i}+z_{8i} \end{bmatrix}, \tag{A.13}$$

$$\begin{bmatrix} x_{S8i} \\ y_{S8i} \\ z_{S8i} \end{bmatrix} = \frac{1}{2}\begin{bmatrix} x_{9i}+x_{8i} \\ y_{9i}+y_{8i} \\ z_{9i}+z_{8i} \end{bmatrix}, \tag{A.14}$$

$$\begin{bmatrix} x_{S10i} \\ y_{S10i} \\ z_{S10i} \end{bmatrix} = \frac{1}{2}\begin{bmatrix} L_{B10}\cos q_i \\ L_{B10}\sin q_i \\ 0 \end{bmatrix} + \begin{bmatrix} x_{3i} \\ y_{3i} \\ 0 \end{bmatrix}. \tag{A.15}$$

Thus, the coordinates $[x_{Si},\ y_{Si},\ z_{Si}]^T$ of the centre of masses of the i-th pantograph linkage can be found by the following relation:

$$\begin{bmatrix} x_{Si} \\ y_{Si} \\ z_{Si} \end{bmatrix} = \frac{1}{m_{tot}}\left(\sum_{j=2}^{9} m_j \begin{bmatrix} x_{ji} \\ y_{ji} \\ z_{ji} \end{bmatrix} + \sum_{j=1,2,3,4,7,8,10} m_{Bj} \begin{bmatrix} x_{Bji} \\ y_{Bji} \\ z_{Bji} \end{bmatrix} \right) \tag{A.16}$$

with m_{tot} the total mass of the pantograph linkage.

$$m_{tot} = \sum_{j=2}^{9} m_j + \sum_{j=1,2,3,4,7,8,10} m_{Bj}\ . \tag{A.17}$$

Developing the term z_{Si}, one can note that:

$$z_{Si} = C_{z1}\, z_{5i} + C_{z2}\, z_{9i} + C_{z3}\, q_v + C_{z4} \tag{A.18}$$

with,

$$C_{z1} = \frac{1}{m_{tot}}\left(m_5 + \sum_{j=2,3,4,7} \left(\frac{m_j}{k} \right) + \frac{m_{B4}}{2} + \sum_{j=1,7} \left(\frac{m_{Bj}}{2\,k} \right) + \sum_{j=2}^{3} \left(\frac{m_{Bj}}{k} \right) \right), \tag{A.19}$$

$$C_{z2} = \frac{1}{m_{tot}}\left(\frac{(k-1)\,m_4 - m_7 + k\,m_9}{k} + \frac{(k-2)\,m_{B3} - m_{B7}}{2\,k} + \frac{m_{B4} + m_{B8}}{2}\right), \quad \text{(A.20)}$$

$$C_{z3} = \frac{m_{B1}}{2\,m_{tot}}, \quad \text{(A.21)}$$

$$C_{z4} = \frac{L_{B2}}{m_{tot}}\left(m_2 + \frac{m_{B1} + m_{B2}}{2}\right). \quad \text{(A.22)}$$

From these expressions, it is possible to see that the terms C_{vj} of equation (2.6) ($j = 1, 2, 3, 4$) are equal to $g\,m_{tot}\,C_{zj}$, where g is the gravitational acceleration.

Appendix B

Expressions of the Terms of the Conics Representing the Singularity Loci

In the following expressions, c_α and s_α will denote the cosines and the sinus of angle α respectively ($\alpha = \phi,\ \psi,\ \theta$).

The expression of the conic Δ of chapter 3 is equal to:

$$\Delta = A_6 x^2 + B_6 y^2 + C_6 xy + D_6 x + E_6 y + F_6 \tag{B.1}$$

with

$$A_6 = 2R_b(s_\phi c_\psi s_\theta + c_\theta c_\phi) - 2R_{pl} c_\psi\,, \tag{B.2}$$

$$B_6 = 2R_b(c_\phi c_\psi c_\theta + s_\theta s_\phi) - 2R_{pl} c_\psi\,, \tag{B.3}$$

$$C_6 = 2R_b(c_\psi - 1)s_{(\theta+\phi)}\,, \tag{B.4}$$

$$\begin{aligned} D_6 = (c_\psi - 1)(&-R_{pl}^2(c_\psi(c_\phi s_\theta(1 + c_\psi)(1 - 4c_\theta^2) + (4c_\theta^2 - 3)s_\phi c_\theta) + s_\phi c_\theta(4c_\theta^2 - 3)) \\ &- R_{pl}R_b(c_\psi(2s_\theta c_\theta(1 + c_\phi^2) + c_\phi s_\phi(2s_\phi c_\theta^2 - 1)) + c_\phi s_\phi(1 - 2c_\phi^2) + 2s_\theta c_\theta(2 - c_\phi^2)) \\ &- R_b^2 s_{(\phi+\theta)}) \end{aligned} \tag{B.5}$$

$$\begin{aligned} E_6 = (c_\psi - 1)(&-R_{pl}^2(c_\psi(s_\phi s_\theta(1 + c_\psi)(-1 + 4c_\theta^2) + c_\phi c_\theta(-3 + 4c_\theta^2)) + c_\phi c_\theta(-3 + 4c_\theta^2)) \\ &- R_{pl}R_b(c_\psi(c_\theta(-2s_\theta c_\phi s_\phi + 2c_\theta c_\phi^2 - 4c_\theta) - c_\phi^2 + 2) - 2c_\theta^2(c_\phi^2 + 1) + c_\phi^2 \\ &+ 2c_\theta s_\theta c_\phi s_\phi + 1) + R_b^2 c_{(\phi+\theta)}) \end{aligned} \tag{B.6}$$

$$\begin{aligned} F_6 = {} & R_{pl}^3(c_{3\psi} + 7c_\psi)/4 - R_b^3(c_{(\phi+\psi-\theta)} + c_{(\phi-\psi-\theta)} + 2c_{(\phi-\theta)})/2 + R_{pl}R_b^2(8c_\psi + 4c_{(-\psi-2\theta+2\phi)} \\ & + 6c_{2\psi} + 6c_{2(\phi-\theta)} + 18 + 4c_{(2\phi+\psi-2\theta)}c_{(2\phi-2\psi-2\theta)} + c_{(2\phi+2\psi-2\theta)})/8 - R_{pl}^2R_b(4c_{(\phi+2\psi-2\theta)} \\ & + 11c_{(-\psi-\theta+\phi)} + 11c_{(\psi-\theta+\phi)} + c_{(-3\psi-\theta+\phi)} + 16c_{(-\theta+\phi)} + 4c_{(\phi-2\psi-\theta)} + c_{(3\psi-\theta+\phi)})/8 \end{aligned} \tag{B.7}$$

The expression of the conic Λ of chapter 3 is equal to:

$$\Lambda = \Delta(\theta = 0) = A_5x^2 + B_5y^2 + C_5xy + D_5x + E_5y + F_5 \tag{B.8}$$

with

$$A_5 = 2R_bc_\phi - 2R_{pl}c_\psi\,, \tag{B.9}$$

$$B_5 = 2c_\psi(R_bc_\phi - R_{pl})\,, \tag{B.10}$$

$$C_5 = 2R_b(c_\psi - 1)s_\phi\,, \tag{B.11}$$

$$D_5 = (c_\psi - 1)(-R_{pl}^2s_\phi(c_\psi + 1) - R_{pl}R_bc_\phi(c_\psi - 1) + R_b^2s_\phi) \tag{B.12}$$

$$E_5 = -(c_\psi - 1)(R_{pl}^2(c_\phi(c_\psi + 1)) + R_{pl}R_b(c_\phi^2(c_\psi - 1) - 1 - 2c_\psi) + R_b^2c_\phi)\,, \tag{B.13}$$

$$\begin{aligned} F_5 = {} & (1 + c_\psi^2)R_{pl}^3c_\psi - R_b^3c_\phi(1 + c_\psi) + R_{pl}R_b^2(c_\phi(1 + c_\psi)(1 + c_\psi^2) + c_\phi^2(1 + c_\psi)^2) \\ & - R_{pl}^2R_bc_\phi(1 + c_\psi)(-c_\psi - 1 - c_\psi^2)) \end{aligned} \tag{B.14}$$

Appendix C

Expressions of the Intermediary Terms for the Analysis of the Self Motions

Expressions of a_{ji} ($j = 1, 2$, $i = 1, 2, 3$):

$$a_{11} = \frac{(x_{M'2} - x_{M'1})\sin q_2 + l_1 \cos(q_2 - q_1) - l_2}{\sin(q_2 - q_1)}, \tag{C.1}$$

$$a_{12} = -\frac{2R_{pl} \sin q_2 \cos \alpha_{pl}}{\sin(q_2 - q_1)}, \tag{C.2}$$

$$a_{13} = \frac{2R_{pl} \cos q_2 \cos \alpha_{pl}}{\sin(q_2 - q_1)}, \tag{C.3}$$

$$a_{21} = \frac{(x_{M'2} - x_{M'1})\sin q_1 - l_2 \cos(q_2 - q_1) + l_1}{\sin(q_2 - q_1)}, \tag{C.4}$$

$$a_{22} = -\frac{2R_{pl} \sin q_1 \cos \alpha_{pl}}{\sin(q_2 - q_1)}, \tag{C.5}$$

$$a_{23} = \frac{2R_{pl} \cos q_1 \cos \alpha_{pl}}{\sin(q_2 - q_1)}. \tag{C.6}$$

Expressions of b_{ji} ($j = 1, 2,$ $i = 1, 2, 3$):

$$b_{11} = x_{M'1} + a_{11}\cos q_1 - l_1 \sin q_1 , \tag{C.7}$$

$$b_{21} = y_{M'1} + a_{11}\sin q_1 + l_1 \cos q_1 , \tag{C.8}$$

$$b_{12} = a_{12}\cos q_1 + 2R_{pl}\cos\left(\alpha_{pl} - \frac{\beta_{pl}}{2}\right)\cos\frac{\beta_{pl}}{2} , \tag{C.9}$$

$$b_{22} = a_{12}\sin q_1 + 2R_{pl}\cos\left(\alpha_{pl} - \frac{\beta_{pl}}{2}\right)\sin\frac{\beta_{pl}}{2} , \tag{C.10}$$

$$b_{13} = a_{13}\cos q_1 - 2R_{pl}\cos\left(\alpha_{pl} - \frac{\beta_{pl}}{2}\right)\sin\frac{\beta_{pl}}{2} , \tag{C.11}$$

$$b_{23} = a_{13}\sin q_1 + 2R_{pl}\cos\left(\alpha_{pl} - \frac{\beta_{pl}}{2}\right)\cos\frac{\beta_{pl}}{2} . \tag{C.12}$$

Expressions of c_i ($i = 1, 2, 3$):

$$c_1 = (b_{21} - y_{M'3})\cos q_3 + (x_{M'3} - b_{11})\sin q_3 - l_3 , \tag{C.13}$$

$$c_2 = b_{22}\cos q_3 - b_{12}\sin q_3 , \tag{C.14}$$

$$c_3 = b_{23}\cos q_3 - b_{13}\sin q_3 . \tag{C.15}$$

Appendix D

Expressions of the Terms for the Inverse Dynamics of the PAMINSA-4D3L

From the time derivation of coordinates of each point of pantograph linkages expressed in appendix A, it is possible to deduce the terms C_{cj} (j = 1, …, 13) of equations (5.45) and (5.46). Thus:

$$C_{c1} = \frac{1}{2}\left(\frac{m_4}{k^2} + m_5 + \frac{m_7}{(k(k-1))^2} + \frac{m_8}{(k-1)^2} + \frac{m_{B3}(k-2)^2}{(2k(k-1))^2} + \frac{m_{B4}}{4} + \frac{m_{B7}(k+1)^2}{(2k(k-1))^2} + \frac{m_{B8}}{(2(k-1))^2}\right) \tag{D.1}$$

$$C_{c2} = \frac{1}{2}\left(\sum_{j=2,3,4,7}\left(\frac{m_j}{k^2}\right) + m_5 + \sum_{j=1,7}\left(\frac{m_{Bj}}{4k^2}\right) + \sum_{j=2}^{3}\left(\frac{m_{Bj}}{k^2}\right) + \frac{m_{B4}}{4}\right), \tag{D.2}$$

$$C_{c3} = \frac{1}{2}\left(\frac{(k-1)^2 m_4}{k^2} + \frac{m_7}{k^2} + m_9 + \frac{m_{B3}(k-2)^2}{4k^2} + \frac{m_{B4}}{4} + \frac{m_{B7}}{4k^2} + \frac{m_{B8}}{4}\right), \tag{D.3}$$

$$C_{c4} = \frac{1}{2}\left(\frac{2(k-1)m_4}{k^2} + \frac{m_7}{k^2(k-1)} + \frac{m_{B3}(k-2)^2}{2k^2(k-1)} + \frac{m_{B4}}{2} + \frac{m_{B7}(k+1)}{2k^2(k-1)} - \frac{m_{B8}}{2(k-1)}\right), \tag{D.4}$$

$$C_{c5} = \frac{1}{2}\left(\frac{4\left((k-1)\,m_4 - m_7\right) - m_{B7} + 2\,m_{B3}\,(k-2)}{2\,k^2} + \frac{m_{B4}}{2}\right), \tag{D.5}$$

$$C_{c6} = \frac{m_{B1}}{8}, \tag{D.6}$$

$$C_{c7} = \frac{m_{B1}}{4\,k}, \tag{D.7}$$

$$C_{c8} = \frac{m_{B10}\,L_{B10}^2}{8}, \tag{D.8}$$

$$C_{c9} = \frac{I_{YY}^{(B4)} + I_{YY}^{(B7)}}{2}, \tag{D.9}$$

$$C_{c10} = \frac{I_{XX}^{(B4)} + I_{XX}^{(B7)}}{2}, \tag{D.10}$$

$$C_{c11} = \frac{I_{YY}^{(B3)} + I_{YY}^{(B8)}}{2}, \tag{D.11}$$

$$C_{c12} = \frac{I_{XX}^{(B3)} + I_{XX}^{(B8)}}{2}, \tag{D.12}$$

$$C_{c13} = \frac{I_{B2} + I_{B10}}{2}. \tag{D.13}$$

So the input efforts can be deduced from equation (5.40) using the expression (5.6). After simplifications, it is possible to see that they can be written under the form:

$$\tau = \mathbf{W_b} + \mathbf{J}^T\mathbf{W_p} \tag{D.14}$$

where $\mathbf{J} = -\mathbf{A^{-1}B}$ is the global Jacobian matrix (the expression of matrix $\mathbf{A}$ is given at relation (3.6)) and:

$$\mathbf{B} = \begin{bmatrix} \rho_1 & 0 & 0 & 0 \\ 0 & \rho_2 & 0 & 0 \\ 0 & 0 & \rho_3 & 0 \\ 0 & 0 & 0 & k \\ 0 & 0 & 0 & k \\ 0 & 0 & 0 & k \end{bmatrix} \tag{D.15}$$

$$\begin{aligned} \mathbf{W_b} = \sum_{i=1}^{3} (&\mathbf{J}_{\mathbf{Q}3i}^T \mathbf{F}_{3i} + \mathbf{J}_{\mathbf{Q}4i}^T \mathbf{F}_{4i} + \mathbf{J}_{\mathbf{Q}9i}^T \mathbf{F}_{9i} + \mathbf{J}_{\mathbf{Q}7i}^T \mathbf{F}_{7i} + \mathbf{J}_{\mathbf{Q}2i}^T \mathbf{F}_{2i} + \mathbf{J}_{\mathbf{Q}S4i}^T \mathbf{F}_{S4i} + \\ &\mathbf{J}_{\mathbf{Q}S3i}^T \mathbf{F}_{S3i} + \mathbf{J}_{\mathbf{Q}S8i}^T \mathbf{F}_{S8i} + \mathbf{J}_{\mathbf{Q}S7i}^T \mathbf{F}_{S7i} + \mathbf{J}_{\mathbf{Q}S10i}^T \mathbf{F}_{S10i} + \mathbf{J}_{\mathbf{Q}S2i}^T \mathbf{F}_{S2i}) \end{aligned} \tag{D.16}$$

$$\begin{aligned} \mathbf{W_p} = \mathbf{F_P} + \sum_{i=1}^{3} (&\mathbf{J}_{\mathbf{X}8i}^T \mathbf{F}_{8i} + \mathbf{J}_{\mathbf{X}5i}^T \mathbf{F}_{5i} + \mathbf{J}_{\mathbf{X}9i}^T \mathbf{F}_{9i} + \mathbf{J}_{\mathbf{X}4i}^T \mathbf{F}_{4i} + \mathbf{J}_{\mathbf{X}7i}^T \mathbf{F}_{7i} + \\ &+ \mathbf{J}_{\mathbf{X}S4i}^T \mathbf{F}_{S4i} + \mathbf{J}_{\mathbf{X}S3i}^T \mathbf{F}_{S3i} + \mathbf{J}_{\mathbf{X}S8i}^T \mathbf{F}_{S8i} + \mathbf{J}_{\mathbf{X}S7i}^T \mathbf{F}_{S7i}) \end{aligned} \tag{D.17}$$

In equations (D.16) and (D.17), vectors $\mathbf{F_P}$, $\mathbf{F}_{ji}$ and $\mathbf{F}_{Sji}$ represents respectively the wrenches due to both gravity and inertia effects applied on the platform, the joints and the links of the pantograph linkage. Moreover, matrices $\mathbf{J}_{\mathbf{X}ji}$, $\mathbf{J}_{\mathbf{X}Sji}$, $\mathbf{J}_{\mathbf{Q}ji}$ and $\mathbf{J}_{\mathbf{Q}Sji}$ represents the Jacobian matrices between the coordinates of the points j_i, S_{ji} (position and orientation) and the variables $\mathbf{x} = [x,\ y,\ z,\ \phi]^T$ and $\mathbf{q} = [q_1,\ q_2,\ q_3,\ q_v]^T$ respectively. Their expressions are detailed below. In these expressions, δ_{ij} represents the Kronecker symbol ($\delta_{ij} = 1$ if $j = i$ and $\delta_{ij} = 0$ if $j \neq i$).

$$\mathbf{J}_{\mathbf{X}5i} = \begin{bmatrix} \left(\dfrac{\partial [x_{5i}, y_{5i}, z_{5i}]^T}{\partial [x, y, z]^T} \right)_{\mathbf{3\times 3}} & \mathbf{0_{3\times 3}} & \left(\dfrac{\partial [x_{5i}, y_{5i}, z_{5i}]^T}{\partial \phi} \right)_{\mathbf{3\times 1}} \\ \mathbf{0_{3\times 3}} & \mathbf{0_{3\times 3}} & \mathbf{0_{3\times 1}} \end{bmatrix}, \tag{D.18}$$

$$\mathbf{J}_{\mathbf{X}8i} = \frac{1}{1-k} \begin{bmatrix} 1 & 0 & \mathbf{0_{1\times 4}} \\ 0 & 1 & \mathbf{0_{1\times 4}} \\ \mathbf{0_{4\times 1}} & \mathbf{0_{4\times 1}} & \mathbf{0_{4\times 4}} \end{bmatrix} \mathbf{J}_{\mathbf{X}5i}, \tag{D.19}$$

$$\mathbf{J}_{\mathbf{Q}3i} = \begin{bmatrix} \mathbf{0_{2\times3}} & \mathbf{0_{2\times1}} \\ \mathbf{0_{1\times3}} & 1 \\ \mathbf{0_{3\times3}} & \mathbf{0_{3\times1}} \end{bmatrix}, \tag{D.20}$$

$$\mathbf{J}_{\mathbf{Q}2i} = \mathbf{J}_{\mathbf{Q}3i}, \tag{D.21}$$

$$\mathbf{J}_{\mathbf{Q}9i} = \begin{bmatrix} \mathbf{0_{1\times3}} & \delta_{1i}\left(\mathbf{R}_{\mathbf{P}qi}\,\mathbf{Rot}(\varepsilon_i,\boldsymbol{y})\begin{bmatrix} L_{B3} \\ \mathbf{0_{2\times1}} \end{bmatrix}\right)^T \\ \mathbf{0_{1\times3}} & \delta_{2i}\left(\mathbf{R}_{\mathbf{P}qi}\,\mathbf{Rot}(\varepsilon_i,\boldsymbol{y})\begin{bmatrix} L_{B3} \\ \mathbf{0_{2\times1}} \end{bmatrix}\right)^T \\ \mathbf{0_{1\times3}} & \delta_{3i}\left(\mathbf{R}_{\mathbf{P}qi}\,\mathbf{Rot}(\varepsilon_i,\boldsymbol{y})\begin{bmatrix} L_{B3} \\ \mathbf{0_{2\times1}} \end{bmatrix}\right)^T \\ \mathbf{0_{1\times3}} & \mathbf{0_{1\times3}} \end{bmatrix}^T, \tag{D.22}$$

with

$$\mathbf{R}_{\mathbf{P}qi} = \begin{bmatrix} -\sin q_i & -\cos q_i & 0 \\ \cos q_i & -\sin q_i & 0 \\ 0 & 0 & 0 \end{bmatrix}, \tag{D.23}$$

$$\mathbf{J}_{\mathbf{X}9i} = \begin{bmatrix} \mathbf{Rot}(q_i,\boldsymbol{z})\,\mathbf{R}_{\mathbf{P}\varepsilon i}\begin{bmatrix} L_{B3} \\ \mathbf{0_{2\times1}} \end{bmatrix} & \mathbf{0_{3\times1}} \\ \mathbf{0_{3\times1}} & \mathbf{0_{3\times1}} \end{bmatrix}\mathbf{J}_{\mathbf{X}\zeta i\varepsilon i} + \mathbf{J}_{\mathbf{X}8i}, \tag{D.24}$$

$$\mathbf{R}_{\mathbf{P}\varepsilon i} = \begin{bmatrix} -\sin\varepsilon_i & 0 & \cos\varepsilon_i \\ 0 & 0 & 0 \\ -\cos\varepsilon_i & 0 & -\sin\varepsilon_i \end{bmatrix}, \tag{D.25}$$

with

$$\mathbf{J}_{\mathbf{X}\zeta i\varepsilon i} = -\begin{bmatrix} L_{B3}\sin\varepsilon_i & L_{B4}\sin\zeta_i \\ L_{B3}\cos\varepsilon_i & L_{B4}\cos\zeta_i \end{bmatrix}^{-1}\begin{bmatrix} \dfrac{k}{k-1}\mathbf{J}_{\mathbf{X}\rho i} \\ [\mathbf{0_{1\times2}}\ 1\ \mathbf{0_{1\times3}}]\mathbf{J}_{\mathbf{X}5i} \end{bmatrix}, \tag{D.26}$$

$$\mathbf{J}_{\mathbf{X}\rho i} = \begin{bmatrix} \dfrac{\partial\rho_i}{\partial x} & \dfrac{\partial\rho_i}{\partial y} & \dfrac{\partial\rho_i}{\partial z} & 0 & 0 & \dfrac{\partial\rho_i}{\partial\phi} \end{bmatrix}, \tag{D.27}$$

$$\mathbf{J}_{\mathbf{Q}4i} = \begin{bmatrix} \mathbf{0_{1\times 3}} & \delta_{1i}\left(\mathbf{R}_{\mathbf{P}qi}\,\mathbf{Rot}(\zeta_i,\boldsymbol{y})\begin{bmatrix} L_{B4}/k \\ \mathbf{0_{2\times 1}} \end{bmatrix}\right)^T \\ \mathbf{0_{1\times 3}} & \delta_{2i}\left(\mathbf{R}_{\mathbf{P}qi}\,\mathbf{Rot}(\zeta_i,\boldsymbol{y})\begin{bmatrix} L_{B4}/k \\ \mathbf{0_{2\times 1}} \end{bmatrix}\right)^T \\ \mathbf{0_{1\times 3}} & \delta_{3i}\left(\mathbf{R}_{\mathbf{P}qi}\,\mathbf{Rot}(\zeta_i,\boldsymbol{y})\begin{bmatrix} L_{B4}/k \\ \mathbf{0_{2\times 1}} \end{bmatrix}\right)^T \\ \mathbf{0_{1\times 3}} & \mathbf{0_{1\times 3}} \end{bmatrix}^T + \mathbf{J}_{\mathbf{Q}9i}, \tag{D.28}$$

$$\mathbf{J}_{\mathbf{X}4i} = \begin{bmatrix} \mathbf{0_{3\times 1}} & \mathbf{Rot}(q_i,\boldsymbol{z})\,\mathbf{R}_{\mathbf{P}\zeta i}\begin{bmatrix} L_{B4}/k \\ \mathbf{0_{2\times 1}} \end{bmatrix} \\ \mathbf{0_{3\times 1}} & \mathbf{0_{3\times 1}} \end{bmatrix}\mathbf{J}_{\mathbf{X}\zeta i\varepsilon i} + \mathbf{J}_{\mathbf{X}9i}, \tag{D.29}$$

$$\mathbf{R}_{\mathbf{P}\zeta i} = \begin{bmatrix} -\sin\zeta_i & 0 & \cos\zeta_i \\ 0 & 0 & 0 \\ -\cos\zeta_i & 0 & -\sin\zeta_i \end{bmatrix}, \tag{D.30}$$

$$\mathbf{J}_{\mathbf{Q}7i} = \begin{bmatrix} \mathbf{0_{1\times 3}} & \delta_{1i}\left(\mathbf{R}_{\mathbf{P}qi}\,\mathbf{Rot}(\zeta_i,\boldsymbol{y})\begin{bmatrix} L_{B4}/k \\ \mathbf{0_{2\times 1}} \end{bmatrix}\right)^T \\ \mathbf{0_{1\times 3}} & \delta_{2i}\left(\mathbf{R}_{\mathbf{P}qi}\,\mathbf{Rot}(\zeta_i,\boldsymbol{y})\begin{bmatrix} L_{B4}/k \\ \mathbf{0_{2\times 1}} \end{bmatrix}\right)^T \\ \mathbf{0_{1\times 3}} & \delta_{3i}\left(\mathbf{R}_{\mathbf{P}qi}\,\mathbf{Rot}(\zeta_i,\boldsymbol{y})\begin{bmatrix} L_{B4}/k \\ \mathbf{0_{2\times 1}} \end{bmatrix}\right)^T \\ \mathbf{0_{1\times 3}} & \mathbf{0_{1\times 3}} \end{bmatrix}^T, \tag{D.31}$$

$$\mathbf{J}_{\mathbf{X}7i} = \begin{bmatrix} \mathbf{0_{3\times 1}} & \mathbf{Rot}(q_i,\boldsymbol{z})\,\mathbf{R}_{\mathbf{P}\zeta i}\begin{bmatrix} L_{B4}/k \\ \mathbf{0_{2\times 1}} \end{bmatrix} \\ \mathbf{0_{3\times 1}} & \mathbf{0_{3\times 1}} \end{bmatrix}\mathbf{J}_{\mathbf{X}\zeta i\varepsilon i} + \mathbf{J}_{\mathbf{X}8i}, \tag{D.32}$$

$$\mathbf{J}_{\mathbf{Q}S4i} = 0.5\left(\mathbf{J}_{\mathbf{Q}5i} + \mathbf{J}_{\mathbf{Q}9i}\right) + \begin{bmatrix} \mathbf{0_{3\times 4}} \\ \mathbf{J}_{\mathbf{Q}\Omega\mathbf{1}i} \end{bmatrix}, \tag{D.33}$$

$$\mathbf{J}_{\mathbf{Q}\Omega\mathbf{1}i} = \begin{bmatrix} \mathbf{0_{2\times1}} & \mathbf{0_{2\times1}} & \mathbf{0_{2\times1}} & \mathbf{0_{2\times1}} \\ \delta_{1i} & \delta_{2i} & \delta_{3i} & 0 \end{bmatrix}, \tag{D.34}$$

$$\mathbf{J}_{\mathbf{X}S4i} = 0.5\left(\mathbf{J}_{\mathbf{X}5i} + \mathbf{J}_{\mathbf{X}9i}\right) + \begin{bmatrix} \mathbf{0_{3\times6}} \\ \mathbf{J}_{\mathbf{X}\Omega1i} \end{bmatrix}, \tag{D.35}$$

$$\mathbf{J}_{\mathbf{X}\Omega\mathbf{1}i} = \begin{bmatrix} 0 & -\sin q_i \\ 0 & \cos q_i \\ 0 & 0 \end{bmatrix} \mathbf{J}_{\mathbf{X}\zeta i\varepsilon i}, \tag{D.36}$$

$$\mathbf{J}_{\mathbf{Q}S3i} = 0.5\left(\mathbf{J}_{\mathbf{Q}4i} + \mathbf{J}_{\mathbf{Q}7i}\right) + \begin{bmatrix} \mathbf{0_{3\times4}} \\ \mathbf{J}_{\mathbf{Q}\Omega2i} \end{bmatrix}, \tag{D.37}$$

$$\mathbf{J}_{\mathbf{Q}\Omega2i} = \begin{bmatrix} \mathbf{0_{2\times1}} & \mathbf{0_{2\times1}} & \mathbf{0_{2\times1}} & \mathbf{0_{2\times1}} \\ \delta_{1i} & \delta_{2i} & \delta_{3i} & 0 \end{bmatrix}, \tag{D.38}$$

$$\mathbf{J}_{\mathbf{X}S3i} = 0.5\left(\mathbf{J}_{\mathbf{X}4i} + \mathbf{J}_{\mathbf{X}7i}\right) + \begin{bmatrix} \mathbf{0_{3\times6}} \\ \mathbf{J}_{\mathbf{X}\Omega2i} \end{bmatrix}, \tag{D.39}$$

$$\mathbf{J}_{\mathbf{X}\Omega2i} = \begin{bmatrix} -\sin q_i & 0 \\ \cos q_i & 0 \\ 0 & 0 \end{bmatrix} \mathbf{J}_{\mathbf{X}\zeta i\varepsilon i}, \tag{D.40}$$

$$\mathbf{J}_{\mathbf{Q}S8i} = 0.5\left(\mathbf{J}_{\mathbf{Q}8i} + \mathbf{J}_{\mathbf{Q}9i}\right) + \begin{bmatrix} \mathbf{0_{3\times4}} \\ \mathbf{J}_{\mathbf{Q}\Omega2i} \end{bmatrix}, \tag{D.41}$$

$$\mathbf{J}_{\mathbf{X}S8i} = 0.5\left(\mathbf{J}_{\mathbf{X}8i} + \mathbf{J}_{\mathbf{X}9i}\right) + \begin{bmatrix} \mathbf{0_{3\times6}} \\ \mathbf{J}_{\mathbf{X}\Omega2i} \end{bmatrix}, \tag{D.42}$$

$$\mathbf{J}_{\mathbf{Q}S7i} = 0.5\left(\mathbf{J}_{\mathbf{Q}8i} + \mathbf{J}_{\mathbf{Q}7i}\right) + \begin{bmatrix} \mathbf{0_{3\times4}} \\ \mathbf{J}_{\mathbf{Q}\Omega1i} \end{bmatrix}, \tag{D.43}$$

$$\mathbf{J}_{\mathbf{X}S7i} = 0.5\left(\mathbf{J}_{\mathbf{X}8i} + \mathbf{J}_{\mathbf{X}7i}\right) + \begin{bmatrix} \mathbf{0}_{\mathbf{3\times 6}} \\ \mathbf{J}_{\mathbf{X}\Omega 1i} \end{bmatrix}, \tag{D.44}$$

$$\mathbf{J}_{\mathbf{Q}S10i} = \begin{bmatrix} \dfrac{\partial\left[x_{S10i}, y_{S10i}, z_{S10i}\right]^T}{\partial \mathbf{q}} \\ \mathbf{J}_{\mathbf{Q}\Omega 1i} \end{bmatrix}, \tag{D.45}$$

$$\mathbf{J}_{\mathbf{Q}S2i} = \begin{bmatrix} \begin{bmatrix} 1 & 0 & 0 & 0 \\ 0 & 1 & 0 & 0 \\ 0 & 0 & 1 & 0 \end{bmatrix} \mathbf{J}_{\mathbf{Q}3i} \\ \mathbf{J}_{\mathbf{Q}\Omega 1i} \end{bmatrix}, \tag{D.46}$$

$$\mathbf{F}_{\mathbf{P}} = \begin{bmatrix} m_{pl}\,\ddot{x} & m_{pl}\,\ddot{y} & m_{pl}\,\ddot{z} & 0 & 0 & I_{pl}\,\ddot{\phi} \end{bmatrix}^T, \tag{D.47}$$

$$\mathbf{F}_{ji} = m_j \begin{bmatrix} \ddot{x}_{ji} & \ddot{y}_{ji} & \ddot{z}_{ji} & 0 & 0 & 0 \end{bmatrix}^T, \text{ for } j = 2,\ 3,\ 4,\ 5,\ 7,\ 8,\ 9 \tag{D.48}$$

$$\mathbf{F}_{B1i} = \begin{bmatrix} 0 & 0 & m_{B1}\ddot{q}_v & 0 & 0 & 0 \end{bmatrix}^T, \tag{D.49}$$

$$\mathbf{F}_{Bji} = \begin{bmatrix} m_{Bj}\ddot{x}_{Sji} & m_{Bj}\ddot{y}_{Sji} & m_{B2}\ddot{z}_{Sji} & 0 & 0 & I_{Bj}\ddot{q}_i \end{bmatrix}^T, \text{ for } j = 2,\ 10 \tag{D.50}$$

$$\mathbf{F}_{Bji} = \begin{bmatrix} m_{Bj}\ddot{x}_{Sji} & m_{Bj}\ddot{y}_{Sji} & m_{B2}\ddot{z}_{Sji} & \mathbf{C}_{Sji}^T \end{bmatrix}^T, \text{ for } j = 3,\ 4,\ 7,\ 8 \tag{D.51}$$

where

$$\begin{aligned} \mathbf{C}_{Sji} = {} & \left(\mathbf{R}_{\mathbf{P}qi}\,\mathbf{Rot}(\alpha_i, \boldsymbol{y}) + \mathbf{Rot}(q_i, \boldsymbol{z})\,\mathbf{R}_{\mathbf{P}\alpha i}\right)\mathbf{I}_{Bj}\left(\mathbf{Rot}(q_i, \boldsymbol{z})\,\mathbf{Rot}(\alpha_i, \boldsymbol{y})\right)^T \boldsymbol{\Omega}_{Bji} \\ & + \mathbf{Rot}(q_i, \boldsymbol{z})\,\mathbf{Rot}(\alpha_i, \boldsymbol{y})\,\mathbf{I}_{Bj}\left(\mathbf{R}_{\mathbf{P}qi}\,\mathbf{Rot}(\alpha_i, \boldsymbol{y}) + \mathbf{Rot}(q_i, \boldsymbol{z})\,\mathbf{R}_{\mathbf{P}\alpha i}\right)^T \boldsymbol{\Omega}_{Bji} \\ & + \mathbf{Rot}(q_i, \boldsymbol{z})\,\mathbf{Rot}(\alpha_i, \boldsymbol{y})\,\mathbf{I}_{Bj}\left(\mathbf{Rot}(q_i, \boldsymbol{z})\,\mathbf{Rot}(\alpha_i, \boldsymbol{y})\right)^T \dot{\boldsymbol{\Omega}}_{Bji} \end{aligned} \tag{D.52}$$

with $\alpha_i = \zeta_i$ if $j = 4,\ 7$, $\alpha_i = \varepsilon_i$ if $j = 3,\ 8$ and

$$\boldsymbol{\Omega}_{Bji} = \begin{bmatrix} -\dot{\alpha}_i \sin q_i & \dot{\alpha}_i \cos q_i & \dot{q}_i \end{bmatrix}^T. \tag{D.53}$$

Appendix E

Characteristics of the PAMINSA Used for the Numerical Simulations

For the numerical simulations, we used the following characteristics:

- the radii of the circles circumscribed to the base and platform triangles are respectively equal to $R_b = 0.35$ m and $R_{pl} = 0.1$ m;
- magnification factor of the pantograph: $k = 3$;
- the gravitational acceleration g is equal to 9.81 m/s^2.
- lengths of the links of the pantograph linkages: $L_{B1} = 0.308$ m, $L_{B2} = 0.442$ m, $L_{B3} = L_{B8} = 0.42$ m, $L_{B4} = k\, L_{B7} = 0.63$ m, $L_{B5} = 0.0275$ m, $L_{B10} = 0.3635$ m;
- masses of the joints of the pantograph linkages: $m_2 = 0.214$ kg, $m_3 = 0.338$ kg, $m_4 = 0.262$ kg, $m_5 = 0.233$ kg, $m_7 = 0.28$ kg, $m_8 = 0.305$ kg, $m_9 = 0.259$ kg;
- mass of the platform: $m_{pl} = 2.301$ kg;
- masses of the links of the pantograph linkages: $m_{B1} = 1.221$ kg, $m_{B2} = 0.921$ kg, $m_{B3} = 0.406$ kg, $m_{B4} = 0.672$ kg, $m_{B7} = 0.107$ kg, $m_{B8} = 0.403$ kg, $m_{B10} = 0.436$ kg;
- mass of 2.8 kg added on point 7_p for the simulations of figure 2.8.
- axial moment of inertia of the platform: $I_{pl} = 0.015 \text{kg/m}^2$.
- axial moments of inertia of the links of pantograph linkages:

$$I_{XX}^{(B3)} = 0.0038\,\text{kg/m}^2,\ I_{YY}^{(B3)} = 0.02\,\text{kg/m}^2,\ I_{XX}^{(B4)} = 0.0012\,\text{kg/m}^2,$$

$$I_{YY}^{(B4)} = 0.048\,\text{kg/m}^2,\ I_{XX}^{(B7)} = 8\cdot 10^{-4}\,\text{kg/m}^2,\ I_{YY}^{(B7)} = 0.003\,\text{kg/m}^2,$$

$$I_{XX}^{(B8)} = 0.0024\,\text{kg/m}^2,\ I_{YY}^{(B8)} = 0.02\,\text{kg/m}^2,\ I_{B2} = 0.003\,\text{kg/m}^2,\ I_{B10} = 0.02\,\text{kg/m}^2.$$

Appendix F

List of Publications about Presented Works

International patent

[Arakelian 2006a] V. Arakelian, P. Maurine, S. Briot and E. Pion, 2006, "Parallel robots comprising means for setting in motion a mobile element split in two separate subassemblies," Patent FR No. 2873317, WO No. 2006/021629, January 27.

Publications in international journals.

[Briot 2007a] S. Briot and I.A. Bonev, "Accuracy analysis of 3-DOF planar parallel robots," Mechanism and Machine Theory, Elsevier, accepted for publication, in press.

[Arakelian 2006b] V. Arakelian, S. Briot and V. Glazunov, 2006, "Singular Position of a PAMINSA Parallel Manipulator," Journal of Machinery, Manufacture and Reliability, Allerton Press Inc., No. 1, pp. 62-69.

[Arakelian 2007a] V. Arakelian, S. Briot and V. Glazunov, "Increase of singularity-free zones in the workspace of parallel

manipulators using mechanisms of variable structure," Mechanism and Machine Theory, Elsevier.

Articles submitted to international journals.

[Briot 2007b] S. Briot and V. Arakelian, "Optimal Force Generation in Parallel Manipulators for Passing through the Singular Positions," The International Journal of Robotic Research.

[Briot 2007c] S. Briot, V. Arakelian, and S. Guegan, "PAMINSA: a new family of partially decoupled parallel manipulators," Mechanism and Machine Theory, Elsevier.

[Briot 2007d] S. Briot, I.A. Bonev, D. Chablat, P. Wenger and V. Arakelian, "Self motions of general 3-RPR planar parallel robots," The International Journal of Robotic Research.

Publications in international congress.

[Briot 2007e] S. Briot, S. Guegan, E. Courteille and V. Arakelian, 2007, "PAMINSA: new classes of decoupled parallel manipulators for high-load carrying," to appear in Proceedings of the 2007 ASME International Design Engineering Technical Conferences (DETC 2007), Las Vegas, Nevada, USA, September 4-7.

[Arakelian 2007b] V. Arakelian, S. Briot and V. Glazunov, 2007, "Improvement of functional performance of spatial parallel manipulators using mechanisms of variable structure," Proceedings of the 12th IFToMM World Congress, Besancon, France, June 18-21.

[Briot 2007f] S. Briot and V. Arakelian, 2007, "Singularity analysis of PAMINSA manipulators," Proceedings of the 12th IFToMM World Congress, Besancon, France, June 18-21.

[Briot 2006] S. Briot, V. Arakelian and V. Glazunov, 2006, "Analysis and synthesis of parallel-variable structure manipulators," Proceedings of the 18th International Conference on Modern Problems of Mechanical Design, Moscow, Russia, December 27-29.

[Arakelian 2006c] V. Arakelian, S. Briot, C. Baradat and V. Glazunov, 2006, "Kinematic and dynamic decoupling methods of parallel manipulators," Proceedings of the International Conference on Mechanism Theory and Mechanics of Machines, Krasnodar, Russia, October 9-15.

[Arakelian 2006d] V. Arakelian and S. Briot, 2006, "Improvement of positioning accuracy of PAMINSA (Parallel Manipulator of the I.N.S.A.)" Proceedings of the ROMANSY, Warsaw, Poland, June 20-24.

[Arakelian 2006e] V. Arakelian, S. Briot and V. Glazunov, 2006, "Kinematic decoupling of parallel manipulators," Proceedings of the Conference of Young Scientists on Artificial Intellect, Moscow, Russia, April 6-8.

[Arakelian 2005a] V. Arakelian, S. Briot and V. Glazunov, 2005, "Elaboration of parallel structure robot based on pantographs," Proceedings of the 17th International Internet Conference of Young Scientists and Students on Modern Problems of Machinery, Moscow, Russia.

[Arakelian 2005b] V. Arakelian, S. Briot, S. Guegan and J. Le Flecher, 2005, "Design and prototyping of new 4, 5 and 6 degrees of freedom parallel manipulators based on the copying properties of the pantograph linkage," Proceedings of the 36th International

Symposium on Robotics (ISR), Tokyo, Japan, November 29 – December 1st.

[Arakelian 2005c] V. Arakelian, S. Briot and S. Guegan, 2005, "Static and dynamic analysis of the PAMINSA," Proceedings of ASME 2005 International Design Engineering Technical Conferences & Computers and Information in Engineering Conference (IDETC/CIE), Long Beach, California, USA, September 24-28.

Articles submitted to international congress.

[Briot 2008] S. Briot and V. Arakelian, "On the Dynamic Properties and Optimum Control of Parallel Manipulators in the Presence of Singularity," Proceedings of the 2008 IEEE International Conference on Robotics and Automation (ICRA), Pasadena, California, USA, May 19 – 23.

Publications in national congress.

[Briot 2005a] S. Briot, P. Maurine, S. Guegan and V. Arakelian, 2005, "Le PAMINSA: un nouveau manipulateur d'architecture parallele aux mouvements decouples," Actes du 17eme Congres Francais de Mecanique, Universite de Technologie, Troyes, France, September.

[Arakelian 2005d] V. Arakelian and S. Briot, 2005, "A new decoupled parallel manipulator with four degrees of freedom," Proceedings of the 20th Canadian Congress of Applied Mechanics (CANCAM), Montreal, Quebec, Canada, May 30 – June 2.

Appendix G

Patent of PAMINSA Manipulators

(12) DEMANDE INTERNATIONALE PUBLIÉE EN VERTU DU TRAITÉ DE COOPÉRATION EN MATIÈRE DE BREVETS (PCT)

(19) Organisation Mondiale de la Propriété Intellectuelle
Bureau international

(43) Date de la publication internationale
2 mars 2006 (02.03.2006)

PCT

(10) Numéro de publication internationale
WO 2006/021629 A1

(51) Classification internationale des brevets[7] : B25J 17/02

(21) Numéro de la demande internationale :
PCT/FR2005/001326

(22) Date de dépôt international : 30 mai 2005 (30.05.2005)

(25) Langue de dépôt : français

(26) Langue de publication : français

(30) Données relatives à la priorité :
0408151 22 juillet 2004 (22.07.2004) FR

(71) Déposant *(pour tous les États désignés sauf US)* : **INSTITUT NATIONAL DES SCIENCES APPLIQUEES DE RENNES** [FR/FR]; 20, avenue des Buttes de Coësmes, CS 14315, F-35043 Rennes Cedex (FR).

(72) Inventeurs; et

(75) Inventeurs/Déposants *(pour US seulement)* : **ARAKELYAN, Vigen** [FR/FR]; 21, boulevard Franklin Roosevelt, F-35200 Rennes (FR). **MAURINE, Patrick** [FR/FR]; 14, rue Pierre Sauvaget, F-35230 Orgeres (FR). **BRIOT, Sébastien** [FR/FR]; 57, route de Redon, F-35580 Pont-Rean (FR). **PION, Emmanuel** [FR/FR]; Ruguellou, F-29400 Saint-Sauveur (FR).

(74) Mandataire : **LARCHER, Dominique**; Cabinet Vidon, 16B, rue de Jouanet, Boîte postale 90333, F-35703 Rennes Cedex 7 (FR).

(81) États désignés *(sauf indication contraire, pour tout titre de protection nationale disponible)* : AE, AG, AL, AM, AT, AU, AZ, BA, BB, BG, BR, BW, BY, BZ, CA, CH, CN, CO, CR, CU, CZ, DE, DK, DM, DZ, EC, EE, EG, ES, FI, GB, GD, GE, GH, GM, HR, HU, ID, IL, IN, IS, JP, KE, KG, KM, KP, KR, KZ, LC, LK, LR, LS, LT, LU, LV, MA, MD, MG, MK, MN, MW, MX, MZ, NA, NG, NI, NO, NZ, OM, PG, PH, PL, PT, RO, RU, SC, SD, SE, SG, SK, SL, SM, SY, TJ, TM, TN, TR, TT, TZ, UA, UG, US, UZ, VC, VN, YU, ZA, ZM, ZW.

(84) États désignés *(sauf indication contraire, pour tout titre de protection régionale disponible)* : ARIPO (BW, GH,

[Suite sur la page suivante]

(54) Title: PARALLEL ROBOT COMPRISING MEANS FOR SETTING IN MOTION A MOBILE ELEMENT SPLIT IN TWO SEPARATE SUBASSEMBLIES

(54) Titre : ROBOT PARALLELE COMPRENANT DES MOYENS DE MISE EN MOUVEMENT D'UN ELEMENT MOBILE DECOMPOSES EN DEUX SOUS-ENSEMBLES

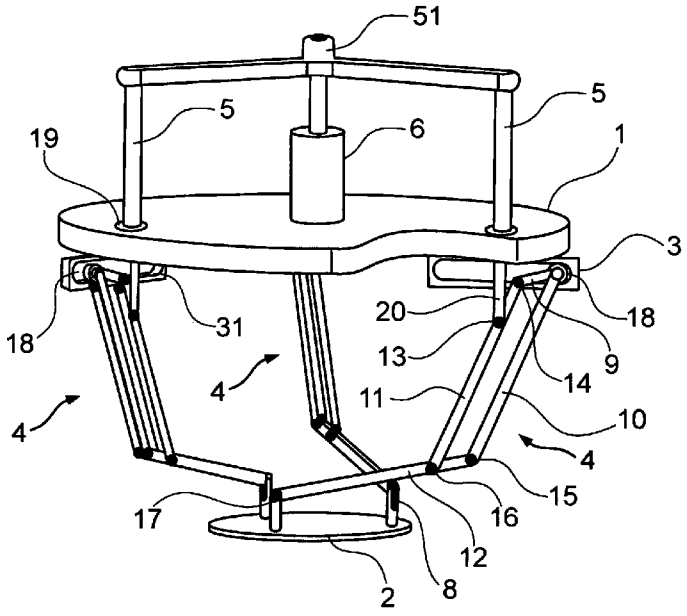

(57) Abstract: The invention concerns a robot of the type comprising a base element (1) and a mobile element (2) coupled to said base element through means for triggering movement, characterized in that said movement-triggering means comprise first and second subassemblies, said first assembly being designed to move said mobile element (2) along a substantially vertical direction, said second subassembly connecting said first subassembly to said mobile element (2) and including at least three actuators (4) capable of acting in parallel to move said mobile element (2) in a substantially horizontal plane independently of said first subassembly.

[Suite sur la page suivante]

WO 2006/021629 A1

GM, KE, LS, MW, MZ, NA, SD, SL, SZ, TZ, UG, ZM, ZW), eurasien (AM, AZ, BY, KG, KZ, MD, RU, TJ, TM), européen (AT, BE, BG, CH, CY, CZ, DE, DK, EE, ES, FI, FR, GB, GR, HU, IE, IS, IT, LT, LU, MC, NL, PL, PT, RO, SE, SI, SK, TR), OAPI (BF, BJ, CF, CG, CI, CM, GA, GN, GQ, GW, ML, MR, NE, SN, TD, TG).

Publiée :

— *avec rapport de recherche internationale*

En ce qui concerne les codes à deux lettres et autres abréviations, se référer aux "Notes explicatives relatives aux codes et abréviations" figurant au début de chaque numéro ordinaire de la Gazette du PCT.

(57) Abrégé : L'invention a pour objet un robot du type comprenant un élément de base (1) et un élément mobile (2) couplé audit élément de base par des moyens de mise en mouvement, caractérisé en ce que lesdits moyens de mise en mouvement comprennent un premier et un deuxième sous-ensembles, ledit premier sous-ensemble étant destiné à déplacer ledit élément mobile (2) selon une direction sensiblement verticale, ledit deuxième sous-ensemble reliant ledit premier sous ensemble audit élément mobile (2) et incluant au moins trois actionneurs (4) susceptibles d'agir en parallèle pour déplacer ledit élément mobile (2) dans un plan sensiblement horizontal indépendamment dudit premier sous-ensemble

ROBOT PARALLELE COMPRENANT DES MOYENS DE MISE EN MOUVEMENT D'UN ELEMENT MOBILE DECOMPOSES EN DEUX SOUS-ENSEMBLES

Le domaine de l'invention est celui des manipulateurs automatiques. Plus précisément, l'invention concerne un robot dit parallèle.

Les robots industriels sont classés par deux groupes principaux : robots sériels et robots parallèles.

La structure mobile des robots sériels est une chaîne ouverte formée d'une succession de segments reliés entre eux par des liaisons à un degré de liberté. Chaque articulation est commandée par un actionneur situé à l'endroit de l'articulation ou sur un des segments précédents. Dans ce dernier cas, un mécanisme assure la transmission entre l'actionneur et l'articulation considérée.

Une telle configuration implique une structure lourde car des masses importantes doivent être mises en mouvement, même dans le cas du déplacement d'une petite charge.

Les robots parallèles peuvent être définis comme étant des systèmes mécaniques à plusieurs degrés de liberté composés de deux corps rigides interconnectés par une ou plusieurs boucles formant un polygone plan.

Les robots parallèles présentent de multiples avantages par rapport aux robots sériels : des mouvements à hautes cadences et surtout des accélérations importantes, la répartition plus régulière des charges sur les actionneurs, une grande rigidité mécanique et peu de masse en mouvement qui améliore notablement la capacité dynamique du robot.

Parmi les inconvénients des robots parallèles on peut constater un volume de travail restreint imposé par la conception même du robot, la présence de singularités dans le volume de travail et un fort couplage entre le mouvement des différentes chaînes cinématiques. Le couplage de mouvements soulevait des difficultés à déterminer les modèles différentiels. Par exemple, l'incrément du moteur dépend de la position du robot, il va être plus petit au fur et à mesure que le robot va se rapprocher du centre, ce phénomène introduit une inertie variable

qui est difficile à gérer en conservant des vitesses importantes de fonctionnement.

En vingt ans, les applications des robots parallèles se sont succédées : on peut trouver ces robots dans l'industrie agro-alimentaire, pharmaceutique, aéronautique, etc. Ils sont de plus en plus utilisés dans l'industrie pour la conception des nouvelles générations de machines outils.

La plupart des robots du type ci-dessus que l'on connaît, tels que par exemple le robot Delta (marque déposée) décrit dans le document de brevet publié sous le numéro US-4976582, comporte un élément de base et un élément mobile, ainsi que trois bras de commande montés de façon rigide à leur première extrémité sur trois axes qui peuvent être mis en rotation. L'autre extrémité de chaque bras de commande est rendue solidaire de l'élément mobile par l'intermédiaire de deux barres de liaison montées en articulation, d'une part, sur la seconde extrémité du bras de commande et, d'autre part, sur l'élément mobile.

Selon cette technique, l'inclinaison et l'orientation dans l'espace de l'élément mobile restent inchangés, quels que soient les mouvements des trois bras de commande.

L'élément mobile supporte un élément de travail dont la rotation est commandée par un moteur fixe situé sur l'élément de base. Un bras télescopique relie le moteur à l'élément de travail.

Un tel robot a quatre degrés de liberté. Il assure les trois mouvements de l'élément mobile et la rotation de l'élément de travail.

Toutefois, un robot de ce type est mal adapté pour le transfert précis des pièces lourdes car les commandes de l'élément mobile sont couplées.

Cela signifie que pour déplacer l'élément mobile selon une direction, il est nécessaire d'actionner tous les moteurs simultanément et de lier les commandes du robot.

En d'autres termes, il n'est pas possible pour un tel robot d'actionner un seul moteur pour déplacer l'élément mobile dans une seule direction. Il advient que le contrôle d'un tel système est difficile car il demande la synchronisation

des commandes. Aussi, la représentation dynamique du robot relève d'un système d'équations différentielles couplées et non-linéaires. Il en résulte que les commandes n'intègrent pas les phénomènes non-linéaires liés à la dynamique du système et conduisent par conséquent à d'importantes difficultés de contrôle.

Un inconvénient majeur de ce type de robot réside donc dans la perte du niveau de précision au cours des déplacements des charges importantes conditionnée par l'inertie variable et le couplage des commandes.

L'invention a notamment pour objectif de pallier les inconvénients de l'art antérieur.

Plus précisément, l'invention a pour objectif de proposer un robot parallèle qui permette d'exécuter des déplacements selon une relation entrée/sortie linéaire.

L'invention a également pour objectif de fournir un tel robot qui soit adapté tant à l'exécution de mouvements relativement importants qu'à celle de microdéplacements.

L'invention a aussi pour objectif de fournir un tel robot qui permette la manipulation de charges importantes, y compris avec une grande précision.

Un autre objectif de l'invention est de fournir un tel robot qui évite la nécessité de synchroniser systématiquement les commandes comme c'est le cas avec l'art antérieur.

Un autre objectif de l'invention est de fournir un tel robot qui soit simple de conception et facile à mettre en œuvre.

Ces objectifs, ainsi que d'autres qui apparaîtront par la suite, sont atteints grâce à l'invention qui a pour objet un robot du type comprenant un élément de base et un élément mobile couplé audit élément de base par des moyens de mise en mouvement, caractérisé en ce que lesdits moyens de mise en mouvement comprennent un premier et un deuxième sous-ensembles, ledit premier sous-ensemble étant destiné à déplacer ledit élément mobile selon une direction sensiblement verticale, ledit deuxième sous-ensemble reliant ledit premier sous-ensemble audit élément mobile et incluant au moins trois actionneurs

susceptibles d'agir en parallèle pour déplacer ledit élément mobile dans un plan sensiblement horizontal indépendamment dudit premier sous-ensemble.

Un robot parallèle selon l'invention présente de multiples avantages.

Un des avantages principaux de ce robot est que les mouvements dans les plans horizontaux et selon l'axe vertical sont découplés, ceci grâce à la présence des premier et deuxième sous-ensembles.

En effet, le découplage des mouvements entraîne le découplage des puissances.

Or, on sait que, pour soulever une charge, il faut dépenser beaucoup d'énergie car la force de gravité a la même direction que le déplacement. Par contre pour déplacer la même charge dans le plan horizontal la dépense d'énergie est considérablement réduite car la force de gravité est perpendiculaire au déplacement. L'invention permet donc d'introduire dans la construction du robot des moteurs de capacité adaptée au déplacement considéré, par exemple un moteur puissant pour soulever une charge à une altitude donnée, et des moteurs moins puissants mais beaucoup plus précis pour les manipulations dans le plan horizontal.

On comprend donc que l'invention permet de créer des robots à grande capacité de charge exécutant des déplacements précis.

De plus, le découplage des mouvements simplifie la commande du robot dans la mesure où l'exécution du déplacement vertical permet une relation entrée - sortie linéaire.

En outre, comme cela va apparaître plus clairement par la suite, l'invention donne la possibilité de copier proportionnellement le mouvement vertical par un rapport de similitude, ce qui permet d'utiliser le robot selon l'invention pour la mise en œuvre de systèmes micromécaniques (système à grande précision).

Par ailleurs, les trois actionneurs mécaniques sont constitués chacun, comme cela va apparaître plus clairement par la suite, par un système à chaîne cinématique plane et fermée agissant en parallèle de façon que l'élément mobile

reste toujours parallèle à l'élément de base. Cette architecture assure une augmentation de la raideur de la mécanique d'ensemble qui est très favorable à l'obtention d'une meilleure précision du positionnement de l'élément mobile. Ainsi celui-ci ne peut présenter d'erreur d'inclinaison horizontale si les éléments constitutifs des chaînes cinématiques fermées sont géométriquement parfaits.

Un robot d'une telle conception est également avantageux en ce qu'il présente une architecture mécanique réalisable à faible coût, notamment en ce que cette architecture peut être composée d'éléments de construction standardisés.

Selon un premier mode de réalisation, ledit premier sous-ensemble comprend, pour chacun desdits actionneurs, un support, lesdits supports étant couplés à des premiers moyens moteurs communs à chacun desdits supports.

Le déplacement du robot selon un axe vertical est ainsi obtenu par un moteur unique, ce qui assure une grande simplicité du robot en termes de conception et évite la nécessité, pour ce déplacement, de synchroniser plusieurs moteurs.

Selon un deuxième mode de réalisation, ledit premier sous-ensemble comprend, pour chacun desdits actionneurs, un support couplé à des moyens moteurs qui lui sont propres.

Ainsi, on augmente le nombre de degré de liberté du manipulateur, en portant ce nombre à six.

Selon une solution avantageuse, lesdits premiers moyens moteurs sont portés par ledit élément de base.

De cette façon, ces moyens moteurs sont portés par un élément fixe et ne constituent pas une charge susceptible de nuire à la précision du robot, notamment lorsque celui-ci manipule les pièces légères.

On comprend donc que le robot ainsi conçu est adapté tant à la manipulation de charges importantes qu'à celle de petites pièces.

Avantageusement, chaque support est guidé en translation sur ledit élément de base.

Préférentiellement, lesdits moyens moteurs comprennent au moins un vérin hydraulique.

Un tel vérin assure au robot la capacité de transporter des charges relativement importantes, ceci sans nuire à sa précision, le vérin en lui-même n'étant pas une charge à déplacer.

Toutefois, d'autres systèmes cinématiquement équivalents pourront être mis en oeuvre dans d'autres modes de réalisation envisageables, par exemple des moteurs électriques linéaires.

Selon une solution préférée, le robot comprend, pour chaque actionneur, un support secondaire monté mobile en rotation sur ledit élément de base.

Selon une première variante, un moyen moteur secondaire peut être associé à chaque support secondaire pour entraîner celui-ci.

Selon une autre caractéristique, chaque actionneur comprend un ensemble de barres articulées entre elles de façon à former un pantographe.

De cette façon, on assure la relation entrée/sortie selon une fonction linéaire, cette fonction présentant un coefficient constant qui est le rapport de similitude du pantographe.

Une telle structure en pantographe procure un système de copiage des déplacements du premier sous-ensemble autorisant en sortie des déplacements importants ou des micro-déplacements.

Selon une solution avantageuse, lesdits supports secondaires présentent chacun des moyens de guidage en translation d'un élément porté par l'une desdites barres d'un desdits pantographes.

Dans ce cas, lesdits supports secondaires présentent chacun préférentiellement une glissière dans laquelle un galet porté par l'une desdites barres d'un desdits pantographes est susceptible de coulisser.

Selon une seconde variante, le dispositif comprend un moyen moteur secondaire associé à chaque moyen de guidage en translation (au lieu de moyens moteurs associés à chaque support secondaire tel qu'indiqué ci-dessus).

D'autres solutions pour le guidage en translation sur les supports peuvent être envisagées, par exemple en faisant coopérer une glissière avec un roulement à billes, ou en déplaçant un chariot sur un rail, etc...

De plus, le pantographe peut être remplacé par un autre système mécanique équivalent, permettant un copiage de mouvement.

Préférentiellement, ledit moyen moteur associé à chaque support secondaire comprend un moteur électrique.

De tels moteurs sont relativement peu puissants mais permettent l'exécution de mouvements avec une grande précision.

Le découplage des mouvements verticaux et horizontaux selon le principe de l'invention permet le recours à de tels moteurs dans la mesure où ceux-ci agissent par rapport à des charges déplacées horizontalement qui impliquent des dépenses d'énergie peu importantes par rapport aux dépenses d'énergie liées aux déplacements verticaux.

Bien entendu, d'autres actionneurs motorisés pourront être envisagés sans sortir du cadre de l'invention.

Ainsi, on évite la nécessité d'une synchronisation des commandes.

De plus, on peut gérer des actionneurs fonctionnant avec des sources d'énergie distinctes, ces moteurs ayant éventuellement des temps de réponse différents.

D'autres caractéristiques et avantages de l'invention apparaîtront plus clairement à la lecture de la description suivante d'un mode de réalisation préférentiel de l'invention, donné à titre d'exemple illustratif et non limitatif, et des dessins parmi lesquels :

- la figure 1 est une vue en perspective d'un robot selon un premier mode de réalisation de l'invention ;
- la figure 2 est une représentation cinématique d'un robot selon le mode de réalisation illustré par la figure 1 ;
- la figure 3 est une représentation cinématique d'un robot selon un deuxième mode de réalisation de l'invention ;

- la figure 4 est une vue en perspective d'un robot selon un troisième mode de réalisation.

Tel que déjà mentionné précédemment, le principe de l'invention réside dans le fait de prévoir, dans un robot de type parallèle, un découplage des moyens assurant les déplacements verticaux de ceux assurant les déplacements horizontaux.

En référence aux figures 1 et 2 relatifs à un premier mode de réalisation de la présente invention, un robot parallèle comporte un élément de base 1, un élément mobile 2 relié à l'élément de base par des moyens de mise en mouvement constitués par des chaînes cinématiques détaillées ci-après.

Selon le principe de l'invention, ces moyens de mise en mouvement comprennent :

- un premier sous-ensemble 5, 6 destiné à déplacer l'élément mobile 2 verticalement ;
- un deuxième sous-ensemble reliant le premier sous-ensemble à l'élément mobile 2 et comprenant trois actionneurs 4 susceptibles d'agir en parallèle pour déplacer l'élément mobile 2 horizontalement, indépendamment du premier sous-ensemble.

Tel que cela apparaît sur la figure 1, le premier sous-ensemble comprend trois supports 5 s'étendant verticalement et reliés chacun à un actionneur 4 d'une part, et à un croisillon 51 couplé à des moyens moteurs électriques 6.(On notera que dans un autre mode de réalisation, ce moyens moteurs pourront inclure un vérin hydraulique.)

Comme il apparaît sur la figure 2, l'élément de base 1 porte trois modules rotatifs 21 destinés chacun à entraîner en rotation un support secondaire 3 monté sur l'élément de base 1 par une articulation 19. Ces modules rotatifs 21 incluent chacun un moteur électrique.

On note que chaque articulation 19 constitue à la fois une liaison pivot d'un support secondaire 3 par rapport à l'élément de base 1, et un moyen de guidage en translation verticale d'un support 5 sur l'élément de base 1.

Chaque support secondaire 3 est solidaire en rotation d'un actionneur mécanique 4 qui est monté par l'intermédiaire d'une liaison pivotante 52 sur le support 5 d'une part, et monté d'autre part par l'intermédiaire d'une articulation 8 sur l'élément mobile 2.

Tel qu'illustré par la figure 1, chaque actionneur mécanique 4 comprend un mécanisme de pantographe constitué de barres 9, 10, 11 et 12, liées entre elles par les articulations 13, 14, 16, 17.

Chaque actionneur 4 est rendu solidaire en rotation du support secondaire 3 correspondant par l'intermédiaire d'un galet 18, ce galet étant monté à coulissement dans une rainure 31 du support secondaire 3 (une telle liaison peut être réalisée aussi par une glissière avec un roulement à billes ou par une autre liaison de translation selon d'autres modes de réalisation envisageables).

Chaque galet 18 est monté à l'intersection des barres 9 et 10 de chaque mécanisme de pantographe, c'est à dire au niveau de l'articulation 13.

Les trois modules rotatifs 21 sont connectés par l'intermédiaire d'amplificateurs appropriés à une unité de pilotage 22 (un ordinateur ou un automate) destinée à contrôler les mouvements en rotation des actionneurs 4 dans le plan horizontal.

Cette unité de pilotage 22 est également connectée au moteur 6 pour commander celui-ci.

Ainsi, le mouvement vertical du moteur 6 entraîne le mouvement vertical du support 5 qui se traduit par le mouvement de l'articulation 13. Le mouvement vertical de l'articulation 13 provoque un mouvement vertical de l'articulation 17 par l'intermédiaire de l'actionneur mécanique 4.

Les actionneurs mécaniques réalisés sous forme de pantographes permettent une relation entre l'entrée 6 et la sortie 2 sous forme d'une fonction

linéaire avec un coefficient constant qui est le rapport de similitude du pantographe.

Par ailleurs, les rotations des modules rotatifs 21 sont transformées en rotations des supports secondaires 3 qui se transforment à leur tour, par l'intermédiaire des actionneurs mécaniques 4, en mouvements de l'élément mobile 2 dans le plan horizontal.

On note que les trois degrés de liberté dans le plan horizontal se décomposent en deux translations de directions perpendiculaires dans le plan horizontal et en une rotation autour d'un axe vertical.

On comprend que le blocage du moteur 6 fixe l'altitude de l'élément mobile 2, ce qui permet de conserver l'élément mobile 2 dans un plan horizontal lors des rotations des actionneurs 4.

Un deuxième mode de réalisation schématisé à la figure 3 ne diffère du mode de réalisation décrit ci-dessus en référence aux figures 1 et 2 que par la position du support secondaire 3 et du galet 18 et par le point de fixation de l'extrémité inférieure du support 5.

Dans ce mode de réalisation, le support secondaire 3 et le galet 18 sont prévus sur la barre 11 tandis que l'extrémité inférieure du support 5 est montée pivotante sur l'articulation 13.

Un troisième mode de réalisation est représenté à la figure 4 .

Selon ce troisième mode de réalisation, chacun des supports 5 est associé à un moteur 32 qui lui est propre. Par ailleurs, des rotules 33 sont prévues pour reliées les barres 12 des mécanisme de pantographe à l'élément mobile. Le robot manipulateur selon l'invention dispose ainsi de six degrés de liberté.

Les trois modes de réalisation de robot parallèle selon la présente invention décrits ci-dessus présentent trois bras montrant :

- une liaison rotoïde motorisée correspondant à la liaison entre la base 1 et le support 3 ;
- une liaison prismatique passive correspondant à la liaison glissière entre le galet 18 et le support secondaire 3 ;

- une liaison rotoïde passive par l'articulation 8 sur le l'élément mobile 2.

Toutefois, on notera que dans d'autres modes de réalisation, ce sont les liaison prismatiques qui pourront être motorisées et non les liaisons rotoïdes et ce, sans sortir du cadre de la présente invention.

Le robot selon l'invention peut être utilisé dans des domaines d'applications très variés, notamment celui de la robotique médicale dans lequel il est nécessaire de positionner des appareils avec une grande précision (imagerie médicale, générateurs de rayons, ustensiles chirurgicaux).

D'autres applications concernent de nouvelles machines, notamment des machine-outils à capacité de charge importante devant exécuter des mouvements très précis, surtout dans le plan horizontal et suivant l'axe vertical.

REVENDICATIONS

1. Robot du type comprenant un élément de base (1) et un élément mobile (2) couplé audit élément de base par des moyens de mise en mouvement, caractérisé en ce que lesdits moyens de mise en mouvement comprennent un premier et un deuxième sous-ensembles, ledit premier sous-ensemble étant destiné à déplacer ledit élément mobile (2) selon une direction sensiblement verticale, ledit deuxième sous-ensemble reliant ledit premier sous-ensemble audit élément mobile (2) et incluant au moins trois actionneurs (4) susceptibles d'agir en parallèle pour déplacer ledit élément mobile (2) dans un plan sensiblement horizontal indépendamment dudit premier sous-ensemble.

2. Robot selon la revendication 1, caractérisé en ce que ledit premier sous-ensemble comprend, pour chacun desdits actionneurs (4), un support (5), lesdits supports (5) étant couplés à des premiers moyens moteurs (6) communs à chacun desdits supports (5).

3. Robot selon la revendication 1, caractérisé en ce que ledit premier sous-ensemble comprend, pour chacun desdits actionneurs (4), un support couplé à des premiers moyens moteurs (32) qui lui sont propres.

4. Robot selon l'une des revendications 2 ou 3, caractérisé en ce que lesdits premiers moyens moteurs (6), (32) sont portés par ledit élément de base (1).

5. Robot selon l'une des revendications 2 à 4 caractérisé en ce que lesdits moyens moteurs (6) (32) coopèrent avec des supports (5) reliés auxdits actionneurs et montés coulissant sur ledit élément de base (1).

6. Robot selon l'une quelconque des revendications 1 à 5, caractérisé en ce qu'il comprend, pour chaque actionneur (4), un support secondaire (3) monté mobile en rotation sur ledit élément de base (1).

7. Robot selon la revendication 6 caractérisé en ce qu'il comprend un moyen moteur secondaire (21) associé à chaque support secondaire (3) pour entraîner celui-ci.

8. Robot selon l'une quelconque des revendications 1 à 7, caractérisé en ce que chaque actionneur (4) comprend un ensemble de barre (9), (10), (11), (12) articulées entre elles de façon à former un pantographe.

9. Robot selon la revendication 8, caractérisé en ce que lesdits supports secondaires (3) présentent chacun des moyens de guidage en translation d'un élément porté par l'une desdites barres d'un desdits pantographes.

10. Robot selon la revendication 9, caractérisé en ce que lesdits supports secondaires (3) présentent chacun une glissière (31) dans laquelle un galet (18) porté par l'une desdites barres (11) d'un desdits pantographes est susceptible de coulisser.

11. Robot selon la revendication 9 ou 10 sauf lorsqu'elles dépendent de la revendication 9 caractérisé en ce qu'il comprend un moyen moteur secondaire associé à chaque moyen de guidage en translation.

1/2

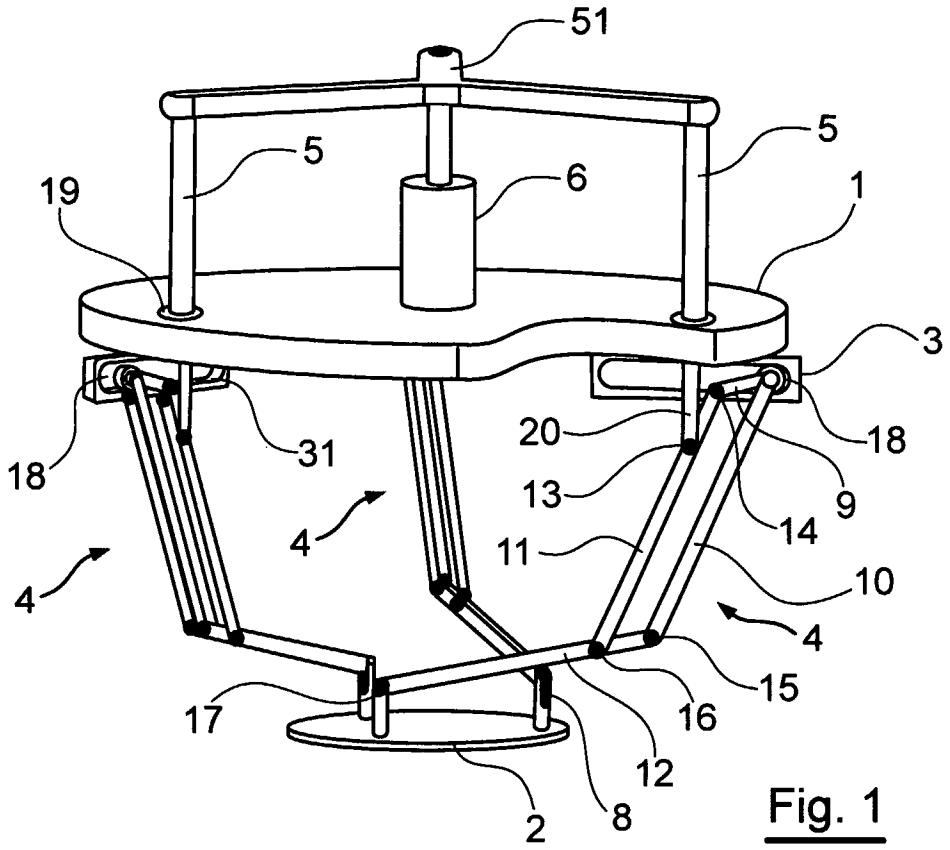
51
5
5
19
6
1
3
18
31
20
18
13
9
14
4
11
10
4
4
15
17
16
12
2
8

Fig. 1

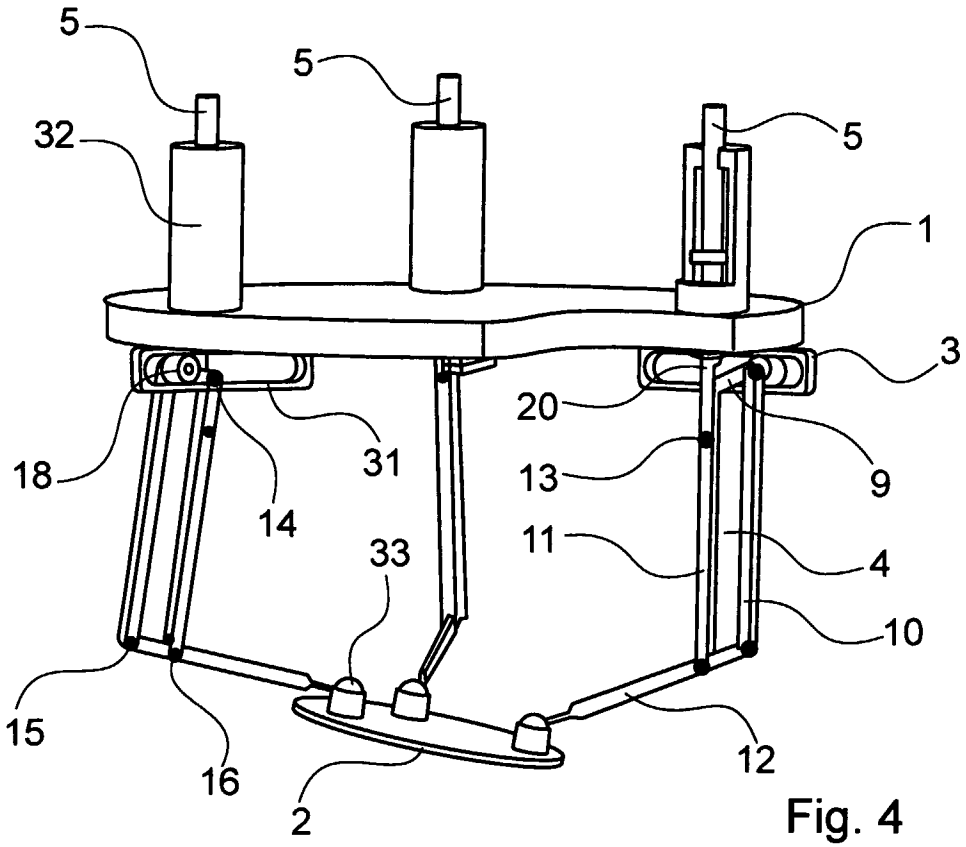
5
5
32
5
1
3
20
18
31
9
13
14
11
4
33
10
15
16
12
2

Fig. 4

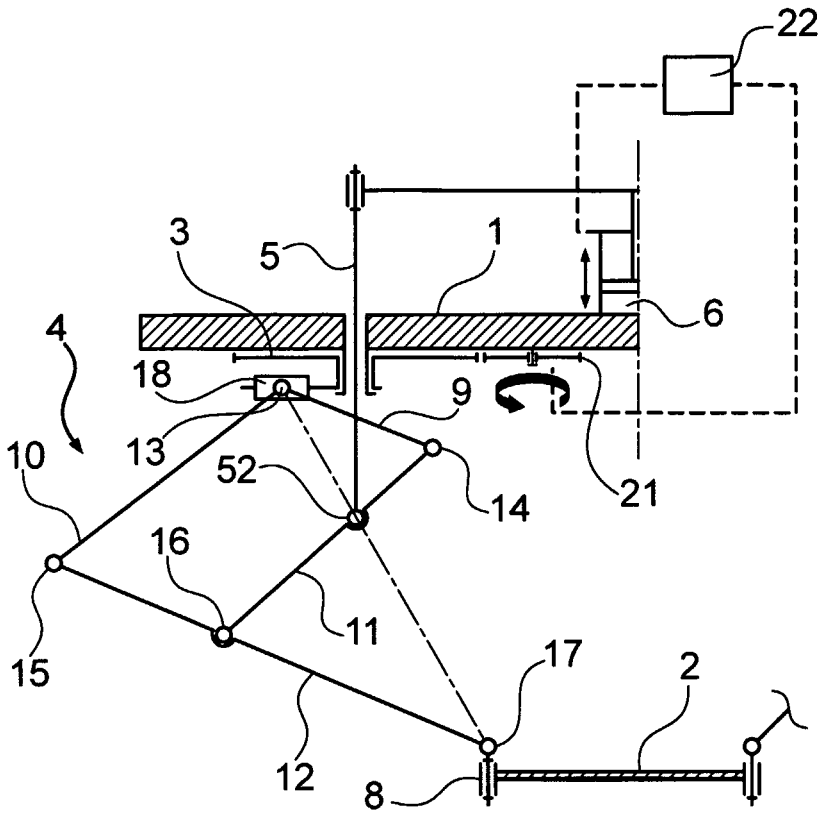
22
3
5
1
6
4
18
9
10
13
52
14
21
16
11
15
17
2
12
8

Fig. 2

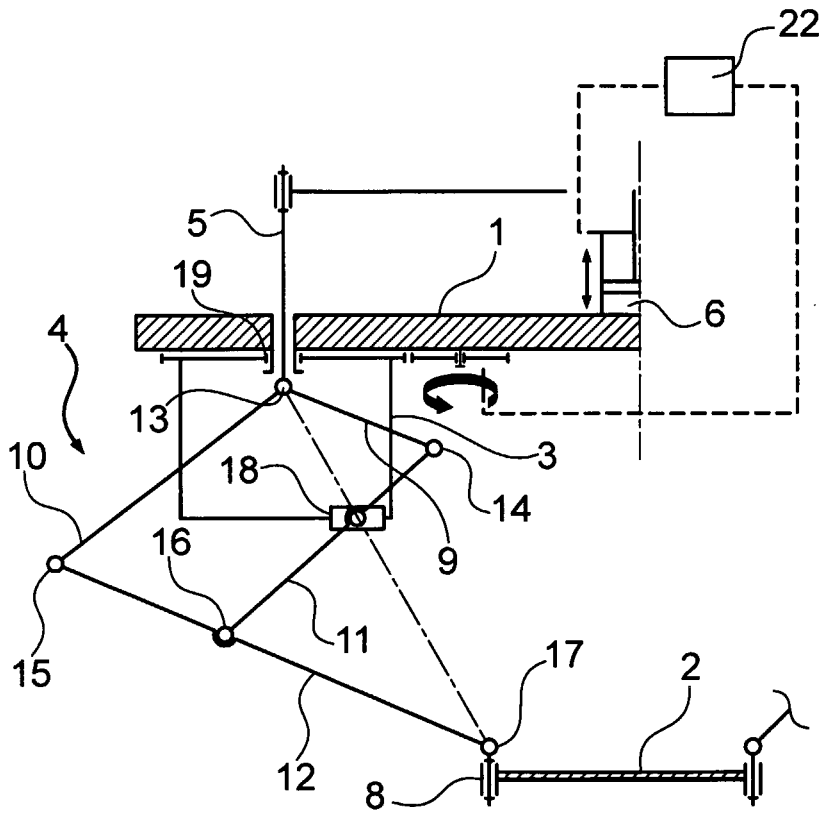
22
5
1
19
6
4
13
3
10
18
14
16
9
11
15
17
2
12
8

Fig. 3

INTERNATIONAL SEARCH REPORT

International Application No
PCT/FR2005/001326

A. CLASSIFICATION OF SUBJECT MATTER
B25J17/02

According to International Patent Classification (IPC) or to both national classification and IPC

B. FIELDS SEARCHED

Minimum documentation searched (classification system followed by classification symbols)
B25J B23Q

Documentation searched other than minimum documentation to the extent that such documents are included in the fields searched

Electronic data base consulted during the international search (name of data base and, where practical, search terms used)
EPO-Internal

C. DOCUMENTS CONSIDERED TO BE RELEVANT

Category °	Citation of document, with indication, where appropriate, of the relevant passages	Relevant to claim No.
P,X	WO 2004/076132 A (FAUDE DIETER) 10 September 2004 (2004-09-10) page 11, lines 11-18 claim 2 figure 4	1
A	US 2003/121351 A1 (KONG XIANWEN ET AL) 3 July 2003 (2003-07-03) paragraphs '0049!, '0050! figure 4	1
A	US 4 976 582 A (CLAVEL REYMOND) 11 December 1990 (1990-12-11) cited in the application the whole document	1

☐ Further documents are listed in the continuation of box C.

☒ Patent family members are listed in annex.

° Special categories of cited documents:

"A" document defining the general state of the art which is not considered to be of particular relevance

"E" earlier document but published on or after the international filing date

"L" document which may throw doubts on priority claim(s) or which is cited to establish the publication date of another citation or other special reason (as specified)

"O" document referring to an oral disclosure, use, exhibition or other means

"P" document published prior to the international filing date but later than the priority date claimed

"T" later document published after the international filing date or priority date and not in conflict with the application but cited to understand the principle or theory underlying the invention

"X" document of particular relevance; the claimed invention cannot be considered novel or cannot be considered to involve an inventive step when the document is taken alone

"Y" document of particular relevance; the claimed invention cannot be considered to involve an inventive step when the document is combined with one or more other such documents, such combination being obvious to a person skilled in the art.

"&" document member of the same patent family

Date of the actual completion of the international search	Date of mailing of the international search report
28 October 2005	28/11/2005

Name and mailing address of the ISA	Authorized officer
European Patent Office, P.B. 5818 Patentlaan 2 NL – 2280 HV Rijswijk Tel. (+31–70) 340–2040, Tx. 31 651 epo nl, Fax: (+31–70) 340–3016	Grenier, A

Form PCT/ISA/210 (second sheet) (January 2004)

INTERNATIONAL SEARCH REPORT

ormation on patent family members

Int onal Application No
PCT/FR2005/001326

Patent document cited in search report	Publication date	Patent family member(s)	Publication date
WO 2004076132 A	10-09-2004	DE 20303367 U1	24-07-2003
		DE 102004010826 A1	14-10-2004
US 2003121351 A1	03-07-2003	WO 02096605 A1	05-12-2002
		EP 1395399 A1	10-03-2004
US 4976582 A	11-12-1990	CA 1298806 C	14-04-1992
		CH 672089 A5	31-10-1989
		WO 8703528 A1	18-06-1987
		EP 0250470 A1	07-01-1988
		JP 4045310 B	24-07-1992
		JP 63501860 T	28-07-1988

RAPPORT DE RECHERCHE INTERNATIONALE

Dem: Internationale No
PCT/FR2005/001326

A. CLASSEMENT DE L'OBJET DE LA DEMANDE
B25J17/02

Selon la classification internationale des brevets (CIB) ou à la fois selon la classification nationale et la CIB

B. DOMAINES SUR LESQUELS LA RECHERCHE A PORTE

Documentation minimale consultée (système de classification suivi des symboles de classement)
B25J B23Q

Documentation consultée autre que la documentation minimale dans la mesure où ces documents relèvent des domaines sur lesquels a porté la recherche

Base de données électronique consultée au cours de la recherche internationale (nom de la base de données, et si réalisable, termes de recherche utilisés)
EPO-Internal

C. DOCUMENTS CONSIDERES COMME PERTINENTS

Catégorie °	Identification des documents cités, avec, le cas échéant, l'indication des passages pertinents	no. des revendications visées
P,X	WO 2004/076132 A (FAUDE DIETER) 10 septembre 2004 (2004-09-10) page 11, ligne 11-18 revendication 2 figure 4	1
A	US 2003/121351 A1 (KONG XIANWEN ET AL) 3 juillet 2003 (2003-07-03) alinéas '0049!, '0050! figure 4	1
A	US 4 976 582 A (CLAVEL REYMOND) 11 décembre 1990 (1990-12-11) cité dans la demande le document en entier	1

☐ Voir la suite du cadre C pour la fin de la liste des documents

☒ Les documents de familles de brevets sont indiqués en annexe

° Catégories spéciales de documents cités:

'A' document définissant l'état général de la technique, non considéré comme particulièrement pertinent

'E' document antérieur, mais publié à la date de dépôt international ou après cette date

'L' document pouvant jeter un doute sur une revendication de priorité ou cité pour déterminer la date de publication d'une autre citation ou pour une raison spéciale (telle qu'indiquée)

'O' document se référant à une divulgation orale, à un usage, à une exposition ou tous autres moyens

'P' document publié avant la date de dépôt international, mais postérieurement à la date de priorité revendiquée

'T' document ultérieur publié après la date de dépôt international ou la date de priorité et n'appartenenant pas à l'état de la technique pertinent, mais cité pour comprendre le principe ou la théorie constituant la base de l'invention

'X' document particulièrement pertinent; l'invention revendiquée ne peut être considérée comme nouvelle ou comme impliquant une activité inventive par rapport au document considéré isolément

'Y' document particulièrement pertinent; l'invention revendiquée ne peut être considérée comme impliquant une activité inventive lorsque le document est associé à un ou plusieurs autres documents de même nature, cette combinaison étant évidente pour une personne du métier

'&' document qui fait partie de la même famille de brevets

Date à laquelle la recherche internationale a été effectivement achevée	Date d'expédition du présent rapport de recherche internationale
28 octobre 2005	28/11/2005

Nom et adresse postale de l'administration chargée de la recherche internationale	Fonctionnaire autorisé
Office Européen des Brevets, P.B. 5818 Patentlaan 2 NL – 2280 HV Rijswijk Tel. (+31–70) 340–2040, Tx. 31 651 epo nl, Fax: (+31–70) 340–3016	Grenier, A

RAPPORT DE RECHERCHE INTERNATIONALE

Renseignements relatifs aux membres de familles de brevets

Demande internationale No
PCT/FR2005/001326

Document brevet cité au rapport de recherche	Date de publication	Membre(s) de la famille de brevet(s)	Date de publication
WO 2004076132 A	10-09-2004	DE 20303367 U1	24-07-2003
		DE 102004010826 A1	14-10-2004
US 2003121351 A1	03-07-2003	WO 02096605 A1	05-12-2002
		EP 1395399 A1	10-03-2004
US 4976582 A	11-12-1990	CA 1298806 C	14-04-1992
		CH 672089 A5	31-10-1989
		WO 8703528 A1	18-06-1987
		EP 0250470 A1	07-01-1988
		JP 4045310 B	24-07-1992
		JP 63501860 T	28-07-1988

TITRE :
« Analyse et Optimisation d'une Nouvelle Famille de Manipulateurs Parallèles aux Mouvements Découplés »

RÉSUMÉ :
Il est bien connu que, parmi les nombreux avantages des manipulateurs parallèles par rapport aux robots sériels, on peut citer des vitesses et accélérations plus élevées, et une plus grande capacité de charge. Cependant, il existe des inconvénients, comme un volume de travail restreint, de forts couplages cinématiques et des singularités plus contraignantes. Afin d'améliorer leurs performances, des travaux ont été menés concernant le découplage des mouvements des robots parallèles. Le projet de thèse porte sur la conception, l'optimisation et l'amélioration d'une nouvelle famille de manipulateurs parallèles de 3 à 6 degrés de libertés partiellement découplés appelés PAMINSA (PArallel Manipulator of the I.N.S.A.). La deuxième partie de ce manuscrit présente la particularité de ces architectures qui est le découplage entre les mouvements de la plate-forme dans le plan horizontal et les translations suivant l'axe vertical. Dans une troisième partie, nous faisons l'analyse des singularités de ces manipulateurs. Cette analyse est nécessaire pour choisir le manipulateur qui a le plus grand espace de travail sans singularité. Dans les parties 4 et 5, nous proposons des méthodes permettant d'augmenter la taille de leur espace de travail sans singularité. La première solution est basée sur l'utilisation de mécanismes à structure variable, c'est-à-dire des mécanismes dont les paramètres structurels peuvent être changés. Cette solution permet d'augmenter l'espace de travail sans singularité jusqu'à 100% de l'espace de travail total. La deuxième solution porte sur une optimisation des paramètres dynamiques des manipulateurs qui permet de traverser les singularités lors de déplacements de la plate-forme. Enfin, dans une sixième partie, une nouvelle méthode performante et rapide permettant de calculer la précision des manipulateurs PAMINSA ainsi que des solutions pour améliorer leurs caractéristiques fonctionnelles sont proposées.

MOTS-CLÉS :
Manipulateurs parallèles, PAMINSA, découplage, singularités, augmentation de l'espace de travail sans singularité, réduction des efforts moteurs, précision.

TITLE:
"Analysis and Optimization of a New Family of Parallel Manipulators with Decoupled Motions"

ABSTRACT:
It is well known that, amongst the numerous advantages of parallel manipulators when compared with their serial counterparts, one can notice better velocities and dynamic characteristics, as well as higher payload capacities. However, there are some drawbacks, such as a smaller workspace, a high coupling in the kinematic relationships and more constraining singularities. In order to overcome these disadvantages, the decoupling of the movements of parallel robots has been proposed. Thus, the research project deals with the design, the optimization and the improvement of a new family of parallel manipulators from 3 to 6 degrees of freedom named PAMINSA (PArallel Manipulator of the I.N.S.A.). The second part of this manuscript presents the characteristics of these architectures, namely the decoupling between the movements of the platform in the horizontal plane from its translations along the vertical axis. In a third section, we analyse the singular configurations of these manipulators. This analysis is necessary in order to choose the manipulator which has the largest singularity-free workspace. In sections 4 and 5, we propose novel methods allowing an increase in the size of their singularity-free workspace. The first solution is based on the use of mechanisms with variable structures, i.e. mechanisms of which structural parameters can be altered. Such a solution makes it possible to increase the singularity-free workspace to 100% of the maximal workspace. The second solution deals with the optimization of the dynamic parameters of the manipulators, which makes it possible to pass through the singularities during the displacements of the manipulator. Finally, in a sixth section, a new, fast and efficient method of computing the accuracy of PAMINSA manipulators is described. In addition, solutions for the improvement of functional characteristics of PAMINSA manipulators are proposed.

KEYWORDS:
Parallel manipulators, PAMINSA, decoupling, singularities, increase of the singularity-free zones of the workspace, input effort reduction, accuracy.

DISCIPLINE : Génie Mécanique

LABORATOIRE : Laboratoire de Génie Civil et Génie Mécanique (L.G.C.G.M.), E.A. 3913 / I.N.S.A.
20 avenue des buttes de Coësmes, CS 14315, 35043 RENNES, Cedex – FRANCE.